Systems pharmacology of the amyloid cascade : unfolding oligomer modulation in Alzheimer's disease

Maanen, E.M.T. van

Cover Page

Universiteit Leiden

Author: Maanen, E.M.T. van
Title: Systems pharmacology of the amyloid cascade : unfolding oligomer modulation in Alzheimer's disease
Issue Date: 2017-11-23

Systems pharmacology of the amyloid cascade

Unfolding oligomer modulation in Alzheimer's disease

Eline M.T. van Maanen

Systems pharmacology of the amyloid cascade

Unfolding oligomer modulation in Alzheimer's disease

Proefschrift

ter verkrijging van
de graad van Doctor aan de Universiteit Leiden,
op gezag van Rector Magnificus prof.mr. C.J.J.M. Stolker,
volgens besluit van het College voor Promoties
te verdedigen op donderdag 23 november 2017
klokke 15.00 uur

door

Eline M.T. van Maanen

geboren te Hoogezand-Sappemeer
in 1978

Doof uw inspiratie en verbeeldingskracht niet uit, wordt geen slaaf van 't model.

Don't snuff out your inspiration and power of imagination, don't become a slave to the model.

Vincent van Gogh

Letter to Theo van Gogh, November 1882

Dutch post-impressionist painter

1853-1890

TABLE OF CONTENTS

Section I

Systems pharmacology of the amyloid cascade

General introduction
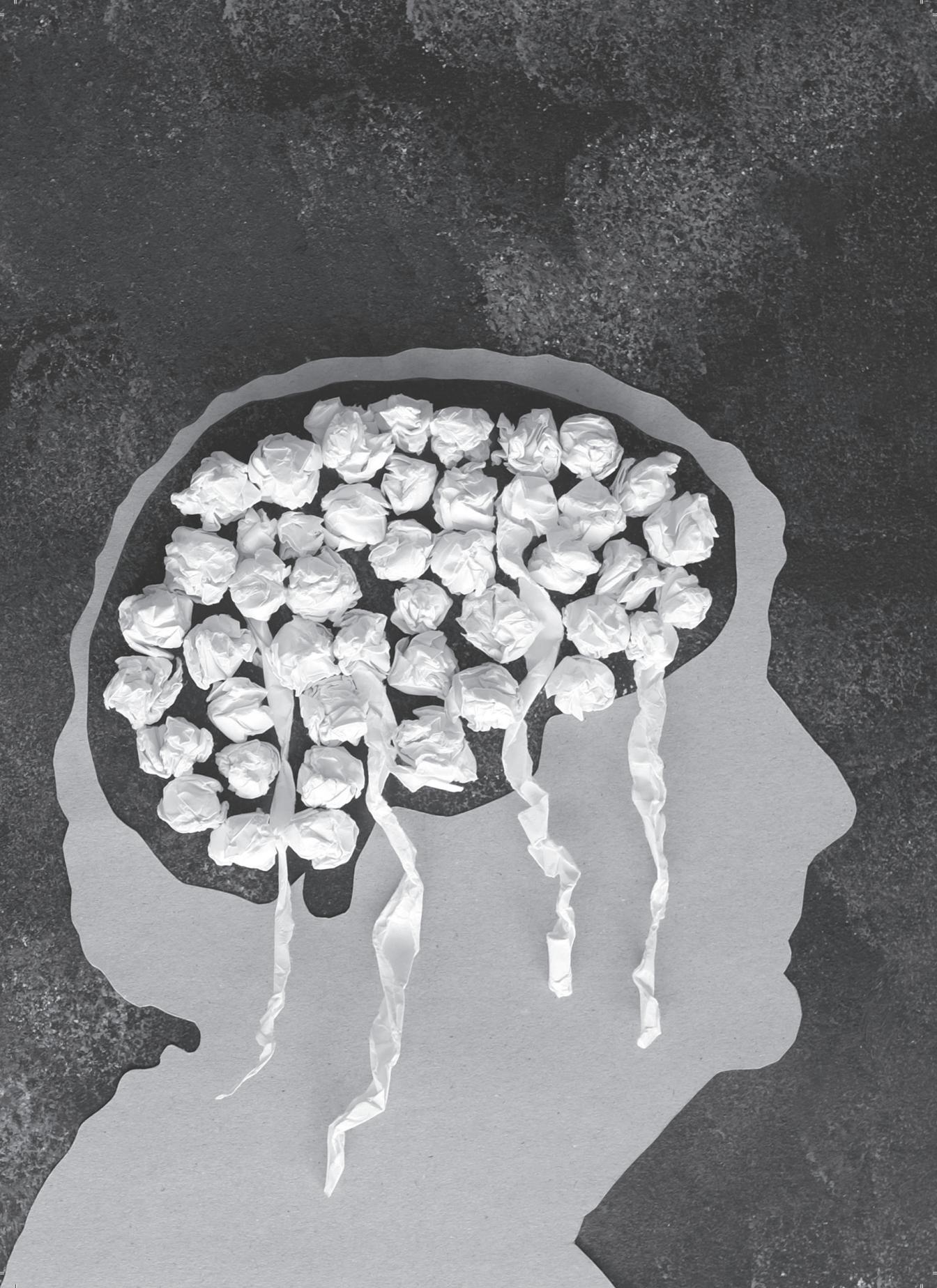
Chapter 1

Systems pharmacology of the amyloid cascade

Scope and outline of investigations

Scope

The misfolding and abnormal assembly of proteins is the hallmark of various pathologies, including neurodegenerative diseases such as Alzheimer's Disease (AD)[1]. The amyloid cascade hypothesis posits that abnormal amyloid-β (Aβ) peptide processing, resulting in the deposition of Aβ in the brain parenchyma, initiates a sequence of events ultimately leading to the development of AD dementia[2]. The amyloid hypothesis provides a framework for all amyloid disorders, in which protein misfolding and different stages of aggregation are the drivers of pathological changes.

Aβ is believed to exist as a mixture of monomers, oligomers and fibrils, which are in a constant equilibrium[3]. Within this mixture, toxic soluble Aβ oligomers (Aβ_O) are considered to be the primary drivers of the neurodegeneration in AD brain[3,4]. One of the main therapeutic strategies for AD aims at Aβ reduction in the central nervous system (i.e. CSF and brain) through the inhibition of secretases responsible for its production[5]. Therapeutic strategies aimed at reducing the Aβ burden have the potential for eliciting a disease modifying effect, inhibiting disease progression and subsequently the prevention of the development of Aβ associated pathologies. When targeting the disease in its earliest stages, a biomarker related to the pathophysiology is needed to detect AD before symptoms as mental decline and brain damage occur. Aβ_O is a potential biomarker for disease progression of AD.

To date, despite decades of research, there is no treatment that halts or slows progression of the pathological cascade in AD. The development of disease-modifying therapies, such as anti-Aβ treatments, has lead to several failures. Multiple studies on the pharmacokinetics (PK) and the pharmacodynamics (PD) of Aβ production inhibitors have been reported[6,7,8,9,10,11,12]. A limitation of these studies is that they focused on the behaviour of monomeric Aβ and not at the pathologically relevant species Aβ_O. Moreover, these investigations focused on specific aspects of the pathology without considering the functional behaviour of the system as a whole. In this respect it is important that the amyloid cascade has the structure of a biochemical network as the rate of formation of Aβ_O is not determined by the activity of a single enzyme. This complicates the prediction of the behaviour of a single component, without considering the dynamic equilibrium of multiple pathways in the system, where all kinds of mechanisms contribute to the resilience of the system. Further, it may be necessary to deploy combination therapy which targets multiple parts of the biochemical network to obtain sufficient suppression of Aβ_O. In this respect, systems analysis is essential in order to gain insight into the expected response of

such a therapeutic intervention.

Biological and preclinical research are constantly adding new pieces of the puzzle of the amyloid cascade. The integration of pharmacological and biological information through a systems pharmacology approach has the potential to bring us closer to optimizing the therapeutic intervention to reduce $A\beta_O$ burden. A further advantage of a systems approach is that the model can be extended when new information becomes available, thereby building up and integrating the knowledge available for the β-amyloid precursor protein (APP) pathway. Such an approach will provide an adequate, mechanistic understanding of the behaviour of the APP pathway as a whole and its resilience, as opposed to the behaviour of its individual attributes, which is imperative to improve the prediction of therapeutic effects on $A\beta$ and their reflection on $A\beta_O$ levels.

The aim of the proposed investigation is the development of a systems pharmacology model describing the functioning of the APP processing pathway, with emphasis on the dynamics of the $A\beta_O$ during pharmacotherapy aimed at reduction of $A\beta$ monomers. Therefore, the objectives of the proposed investigation are:

[1] To establish a systems pharmacology model to describe in a strictly quantitative manner the biochemical network of APP processing.

[2] To predict and evaluate the effect of $A\beta$ production inhibitors, acting at different sequence in the APP processing pathway, on $A\beta_O$ concentrations.

[3] To explore other therapeutic strategies which may aid the reduction of $A\beta_O$ burden.

Outline

In **section I** the amyloid cascade hypothesis for Alzheimer's disease is presented as a theoretical framework for the modeling of drug effects in protein misfolding neurodegenerative diseases. Moreover, the use of Aβ as biomarker for disease progression and as the scientific basis of therapy leading to a decrease in Aβ production is considered. In addition, the use of systems pharmacology modeling to provide a quantitative understanding of the modulation of the amyloid cascade is discussed (**Chapter 2**).

In **section II** a systems pharmacology model is presented describing the changes of the β-amyloid precursor protein (APP) pathway in response to relevant β- and γ-secretase inhibitors, in cisterna magna ported rhesus monkeys[13]. In (**Chapter 3**) a systems pharmacology model is presented that describes the changes in APP metabolites to β-secretase (BACE1) inhibition[14]. Based on monomeric APP metabolite data an Aβ oligomer pool was identified through modeling, suggesting that Aβ production inhibition may have the ability to reduce Aβ oligomeric forms as well.

Next, the systems pharmacology model was extended to account for tracer dynamics in response to BACE1 inhibition throughout the APP pathway (**Chapter 4**). In the past, a stable isotope labeling kinetic (SILK) platform to measure Aβ was developed by Bateman and colleagues[15]. As both SILK data and absolute concentration measurements of APP metabolites from an enzyme linked immunosorbant assay (ELISA) were available from the same study, and both were measurements of the same biological system, it was of interest to compare these. The systems model was able to integrate the two types of data and describe seven biomarkers successfully, which facilitated a comparison of absolute concentrations of APP metabolites with the tracer kinetic data. In addition, the combined analysis confirmed the biological system that was identified based on absolute concentrations of APP metabolites only.

Concurrently, the systems pharmacology model was extended to describe the Aβ responses to include γ-secretase (GS) inhibition (**Chapter 5**)[16]. This extension is considered to be an essential addition as it enabled the separation of BACE1 and GS sequential cleavage steps. Furthermore, differences in Aβ response and anticipated effect on Aβ oligomers (Aβ_{O}) between BACE1 and GS inhibition were assessed. The predicted effect on Aβ_{O} was explored which was quantified at a later stage *(vide infra)*.

In **section III** the developed systems pharmacology model was applied to Aβ oligomer data. In a cross-over study, changes in Aβ oligomer levels in CSF were quantified in response to BACE1 and GS inhibition. This enabled the verification of the systems

model predictions of $A\beta_O$ response to BACE1 (**Chapter 6**) and GS inhibition (**Chapter 7**). Using this data, it could be determined that BACE1 inhibition is equivalent to GS inhibition with regards to oligomer response. In addition, in this study, for the first time APP metabolite responses to GS inhibition upstream of the GS cleavage step were measured. This facilitated the identification of a homeostatic feedback mechanism in the APP pathway (**Chapter 7**).

In **section IV** the summary and general discussion are provided. In **Chapter 8** the results of the presented research are summarized. The systems pharmacology model was used to simulate the effects of $A\beta$ elimination enhancers on $A\beta_O$, as well as combination therapy. In addition, future perspectives are addressed. The final goal would be to utilize the systems pharmacology model in translational pharmacology to anticipate $A\beta$ response of new drug candidates in human. Hence, the scaling-up of the systems pharmacology model developed in rhesus monkeys for application in humans is discussed. Additionally, a number of potential applications of the model in the design and development of therapeutic interventions for AD are considered.

References

1. Eisele, Y.S., *et al.* Targeting protein aggregation for the treatment of degenerative diseases.. Nat Rev Drug Discov. 2015;14 (11):759–80.

2. Hardy, J. & Selkoe, D.J. The amyloid hypothesis of Alzheimer's disease: progress and problems on the road to therapeutics.. Science. 2002;297(5580):353–6.

3. Benilova, I., Karran, E., & De Strooper, B. The toxic Aβ oligomer and Alzheimer's disease: an emperor in need of clothes. Nat Neurosci. 2012;15(3):349–357.

4. Klein, W.L. Synaptotoxic amyloid-β oligomers: a molecular basis for the cause, diagnosis, and treatment of Alzheimer's disease? J Alzheimer's Dis. 2013;33:S49–S65.

5. Mangialasche, F., Solomon, A., Winblad, B., Mecocci, P., & Kivipelto, M. Alzheimer's disease: clinical trials and drug development.. Lancet Neurol. 2010;9(7):702–16.

6. Das, R., *et al.* Modeling effect of a γ-secretase inhibitor on amyloid-β dynamics reveals significant role of an amyloid clearance mechanism. Bull Math Biol. 2011;73 (1):230–47.

7. Lu, Y., *et al.* Cerebrospinal fluid β-amyloid turnover in the mouse, dog, monkey and human evaluated by systematic quantitative analyses. Neurodegener Dis. 2013;12(1): 36–50.

8. Lu, Y., *et al.* Cerebrospinal fluid amyloid-β (Aβ) as an effect biomarker for brain Aβ lowering verified by quantitative preclinical analyses. J Pharmacol Exp Ther. 2012;342 (2):366–75.

9. Niva, C., Parkinson, J., Olsson, F., van Schaick, E., Lundkvist, J., & Visser, S.a.G. Has inhibition of Aβ production adequately been tested as therapeutic approach in mild AD? A model-based meta-analysis of γ-secretase inhibitor data. Eur J Clin Pharmacol. 2013;69(6):1247–60.

10. Tai, L.M., *et al.* The dynamics of Aβ distribution after γ-secretase inhibitor treatment, as determined by experimental and modelling approaches in a wild type rat. J Pharmacokinet Pharmacodyn. 2012;39(3):227–37.

11. Janson, J., *et al.* Population PKPD modeling of BACE1 inhibitor-induced reduction in Aβ levels in vivo and correlation to in vitro potency in primary cortical neurons from mouse and guinea pig. Pharm Res. 2014;31 (3):670–83.

12. Parkinson, J., *et al.* Modeling of age-dependent amyloid accumulation and γ-secretase inhibition of soluble and insoluble Aβ in a transgenic mouse model of amyloid deposition. Pharmacol Res Perspect. 2013;1 (2):e00012.

13. Gilberto, D.B., *et al.* An alternative method of chronic cerebrospinal fluid collection via the cisterna magna in conscious rhesus monkeys. Contemp Top Lab Anim Sci. 2003;42 (4):53–59.

14. van Maanen, E.M.T., *et al.* Systems pharmacology analysis of the amyloid cascade after

β-secretase inhibition enables the identification of an Aβ42 oligomer pool. J Pharmacol Exp Ther. 2016;357(1):205–16.

15. Bateman, R.J., Munsell, L.Y., Chen, X., Holtzman, D.M., & Yarasheski, K.E. Stable isotope labeling tandem mass spectrometry (SILT) to quantify protein production and clearance rates. J Am Soc Mass Spectrom.

2007;18(6):997–1006.

16. Cook, J.J., *et al.* Acute γ-secretase inhibition of nonhuman primate CNS shifts amyloid precursor protein (APP) metabolism from amyloid-β production to alternative APP fragments without amyloid-β rebound. J Neurosci. 2010;30(19):6743–50.
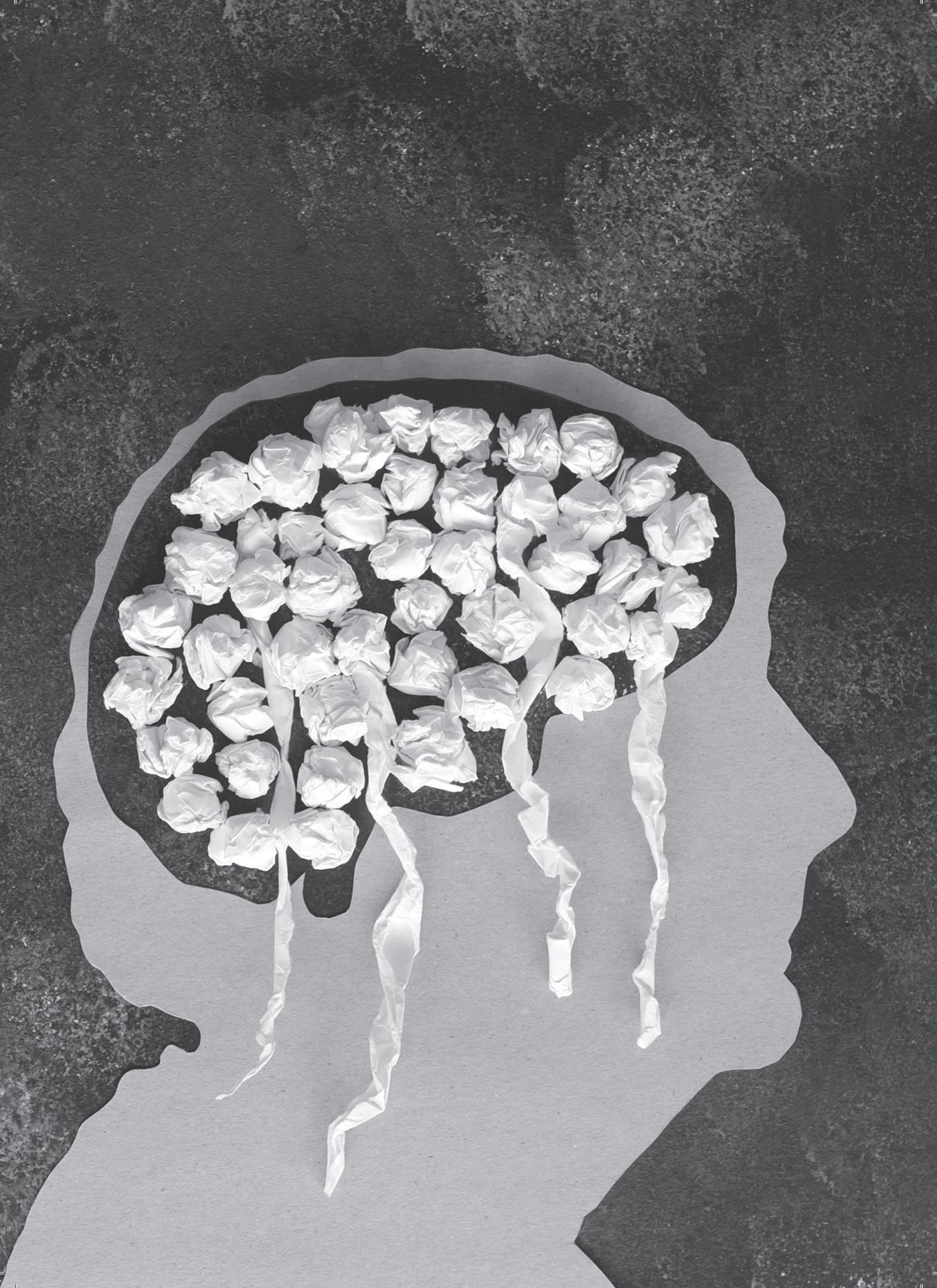
Chapter 2

Systems pharmacology approach
to the modulation of oligomers in protein
misfolding neurodegenerative disorders

Accumulation of protein aggregates inside or outside of neurons is the leading cause of cellular dysfunction in neurodegenerative disorders. The common cause of protein deposition and the trigger of degenerative signals in the neurons is an unusual folding of proteins, such as α-synuclein in Parkinson's disease (PD) and Huntingtin in Huntington's disease (HD) (Table 2.1). Through folding, proteins obtain a tertiary structure needed to take on their biological functions. To ensure correct folding, multiple chaperone systems are required as well as degradation pathways to destroy misfolded proteins[1]. Due to the complexity of this process, an error can disrupt protein folding causing the protein not to achieve its functional conformation, and the misfolded protein may be toxic or aggregation-prone. These early aggregates are believed to instigate toxicity in neurodegenerative disorders. The phenotypically different but biochemically similar aggregates across protein misfolding neurodegenerative diseases indicate a highly conserved molecular mechanism of pathogenesis[2]. Moreover, the same progression of neuronal death, nervous system deterioration and cognitive impairment is presented in Alzheimer's disease (AD), PD, HD, Prion disease and motor disorders, such as amyotrophic lateral sclerosis[3]. Even though major progress has been made in the unraveling of the pathogenesis of protein misfolding neurodegenerative diseases, effective treatments are still lacking.

Table 2.1: Examples of protein misfolding neurodegenerative diseases and their disease specific proteins

DISEASE	PROTEIN FEATURED	Reference
Alzheimer's disease	Amyloid-β	[4]
Parkinson's disease	α-Synuclein	[5]
Parkinson's disease dementia	α-Synuclein, Amyloid-β	[6]
Transmissible spongiform encephalopathy (Prion disease)	Scrapie prion protein (PrP^{Sc})	[7]
Huntington's disease	Huntingtin	[8]
Familial amyloid polyneuropathy	Transthyretin	[9]
Cerebral amyloid angiopathy	Amyloid-β	[10]
Amyotrophic lateral sclerosis	Superoxide dismutase 1 (SOD1)	[11]

One of the most studied protein misfolding neurodegenerative disorders is AD *(vide infra)*. Amyloid-β peptide (Aβ) is the main component of the amyloid plaques in the brain of AD patients. Soluble monomeric Aβ does not cause the reduced neuroviability; the issue begins when the Aβ peptide self-aggregates. The 'amyloid cascade hypothesis'

poses that this Aβ aggregation is the initiating mechanistic event, in which the different stages of aggregation, from soluble Aβ oligomers (Aβ_O) to insoluble fibrils in plaques, are believed to impair synaptic function and ultimately damage neurons, resulting in chronic neurodegeneration leading to cognitive impairment and finally dementia[12]. The amyloid cascade hypothesis provides a framework for other protein misfolding neurodegenerative diseases, in which pathological changes are driven by an error in protein conformation followed by abnormal assemblies.

One of the main therapeutic strategies for AD aims at Aβ reduction through either inhibition of Aβ production or enhancing of Aβ clearance. Due to the complexity of the underlying biochemical network, the effects of these interventions on the individual attributes of the APP processing pathways are difficult to predict. Furthermore, the effect on Aβ_O after inhibiting Aβ production or enhancing Aβ clearance is not fully understood. This step is essential in view of the development of disease-modifying treatments: Aβ_O concentrations in cerebrospinal fluid (CSF) may be considered as tool to monitor the effects of disease-modifying drugs.

This thesis focuses on drugs aimed at Aβ production inhibition and the potential for subsequent reduction of Aβ_O levels. In this chapter, the pathophysiology of AD is described first. Next, the amyloid cascade hypothesis and the production of Aβ through the amyloid-β precursor protein (APP) pathway are outlined. Then, the diagnosis and pharmacological treatment of AD is discussed. After that, generally used methods to detect and quantify Aβ are summarized. Finally, the use of systems pharmacology modelling to provide a quantitative understanding of the effects of drugs on the APP pathway is outlined.

Alzheimer's Disease

AD is the most prevalent form of dementia. The World Health Organization estimates that in 2015 46.8 million people worldwide were living with AD, or related dementia, and that this number will almost double every 20 years, making it the major chronic health issue of this century[13]. The prevalence of AD is rising due to the 'double ageing' process: there are relatively more and more elderly who are individually living longer.

Although AD mainly affects older people, it is not a normal part of ageing It is a chronic and progressive neurodegenerative disorder, impairing higher brain functions such as memory, thinking and personality. The neuropathology of AD involves massive neuronal cell loss and atrophy, which is especially prevalent in the cortex and hippocam-
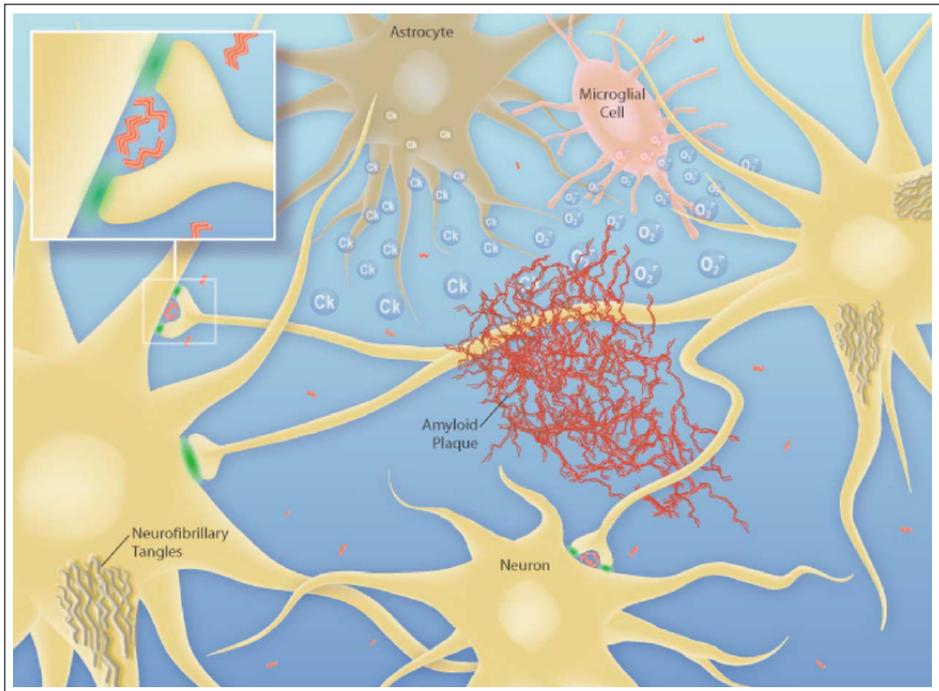
Figure 2.1: Illustration of neurofibrillary tangles within neurons and amyloid plaques [14].
Green cloud: Disruption of synaptic efficacy by diffusible, low-n $A\beta_O$, depicted as a decrease in normal transmission at synapses; *Red*: $A\beta$ species; *Ck*: Cytokines, released as result of activation of astrocytes; O_2: Superoxide radicals, generated by microglia.

pus, and ventricle enlargement [15,16]. Pathologically, the disease is characterized by the misfolding and abnormal assembly of two proteins, tau and a short fragment of APP, the 42-amino acid long peptide $A\beta42$, causing abnormal structures that cover the brains of AD patients. Hyperphosphorylated tau protein appears in neurofibrillary tangles within neurons, whereas $A\beta$ is deposited in extracellular neuritic plaques that consist of neuron fragments surrounding a core of $A\beta$ (Figure 2.1) [17,18,19]. The progressive accumulation of neurofibrillary tangles in neurons and amyloid fibers in neuritic plaques are two of several brain changes believed to contribute to the development of AD.

The two basic types of AD are sporadic and familial. AD generally occurs sporadic in patients over the age of 60, but there is also an early-onset phenotype afflicting patients in the 4th or 5th decade of life that develops as result of autosomal dominant inheritance [21]. Both forms of AD show similar neuropathology and altered $A\beta42$ kinetic rates (Figure 2.2).
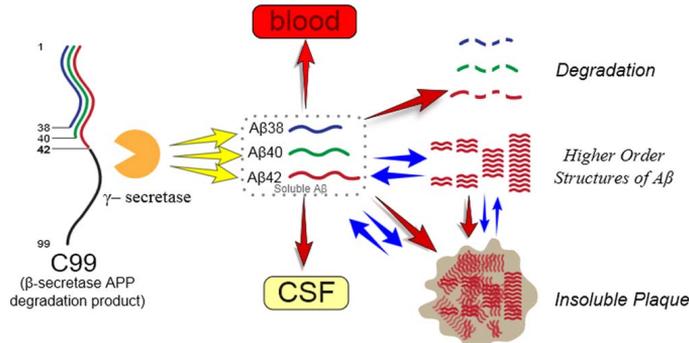
Figure 2.2: Biological model for increased Aβ42 exchange and increased irreversible loss in the presents of amyloidosis [20].
Faster irreversible loss *(red arrows)* and exchange *(blue arrows)* are present in amyloidosis.

Familial AD (FAD) mutations are found in APP as well as in the presenilin genes PS1 and PS2, genes encoding for the catalytic subunit of γ-secretase, a protease that cleaves APP and generates the Aβ peptides[22]. The FAD mutations increase the production of Aβ42, which is more neurotoxic compared to the shorter Aβ40, leading to elevated total amounts of Aβ and altering Aβ peptide ratios[23,24,22]. No mutations in the tau gene have been linked to AD[18].

In AD patients, decreased CSF Aβ42 concentrations have been consistently found. Postmortem investigations have established inverse correlations between CSF Aβ42 and neuritic plaque burden indicating that low concentrations of CSF Aβ42 are resulting from its deposition in brain parenchyma [25,26].

There are three recognized disease stages of AD: preclinical, mild cognitive impairment (MCI) and AD dementia[27] (Figure 2.3). In the preclinical stage subjects are asymptomatic and cognitively normal, but some have AD pathological changes such as Aβ accumulation and neuronal injury and dysfunction. This will eventually lead to clinical symptoms, but accumulation of Aβ begins years before the onset of clinical symptoms. The second, prodromal, stage of AD, MCI, is defined by noticeable dysfunction in memory and impairments related to cognitive function that do not meet the criteria for dementia. The patients have elevated CSF tau or signs of neuronal injury on imaging methods (positron emission tomography [PET] imaging, magnetic resonance imaging [MRI] of the brain). The final stage, dementia, is characterized by unresponsiveness, loss of mobility and control of body functions. The disease course can last 2-20 years, leading to death.
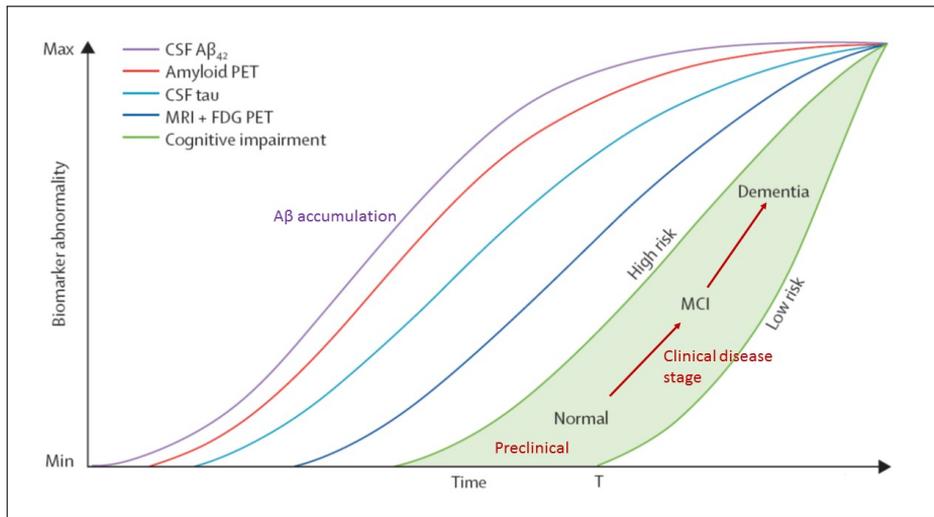
Figure 2.3: Schematic of biomarkers of the pathological cascade and clinical disease stages in AD. Adapted from Jack et al. (2013).
Cognitive impairment is illustrated as a green area with low-risk and high-risk borders.

The amyloid cascade hypothesis

The amyloid cascade hypothesis poses that Aβ levels are increased early in the disease process, forming toxic oligomers and plaques (Figure 2.4)[30,31,32,33,12,34]. These accumulate over time, interfering with the neuron-to-neuron communication at synapses and contributing to cell death, ultimately leading to cognitive and functional decline. It is generally believed that aggregated Aβ is the primary influence that is responsible for disease progression[12]. Soluble toxic Aβ oligomers have been proposed to account for the neurotoxicity of Aβ peptide[29]. Tau protein, aggregating to tangles, accumulate later than Aβ[35,36]. The AD biomarkers become abnormal sequentially, while people remain clinically asymptomatic (Figure 2.3). The amyloid cascade hypothesis is a framework for all amyloid disorders, in which protein misfolding and different stages of aggregates are the drivers of pathological changes.

APP processing pathway

Aβ exists in both soluble and fibrillar forms. Soluble Aβ is a normal metabolic product, present in cerebrospinal fluid (CSF), sera of normal individuals and patients with AD. Aβ peptide is the final product of proteolytic cleavage of the transmembrane protein APP, which is synthesized in the brain as well as in the periphery. The physiological role of
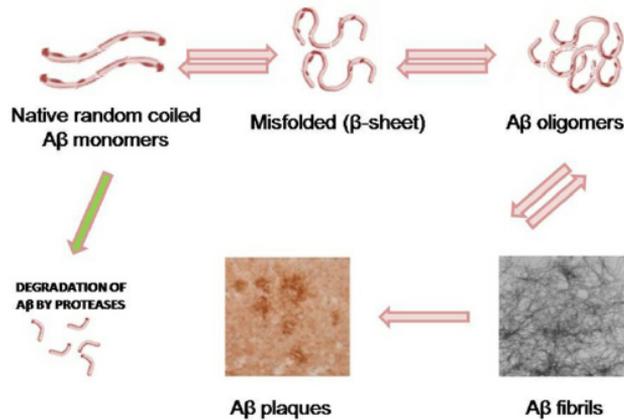
Figure 2.4: Aβ exists in various aggregation states [28].
Aβ monomers can misfold to form β-sheet structures. From the misfolded Aβ, soluble Aβ_O and insoluble amyloid fibrils are generated. These form amyloid plaques and cerebrovascular deposits in the AD brain. Aβ monomers, Aβ_O and fibrils exist in a complex equilibrium [29].

Aβ is yet to be fully elucidated. Aβ fragments have been associated with neurogenesis, anti-viral functions and pro-inflammatory response [37,38,39].

In the APP processing pathway, APP is cleaved sequentially by β-secretase (BACE1) and γ-secretase (GS) resulting in Aβ (Figure 2.5). A third secretase, α-secretase cleaves APP within the Aβ sequence generating non-amyloidogenic sAPPα and precluding Aβ generation.

In the non-amyloidogenic pathway, γ-secretase releases the so called P3 peptide. At the γ-site, APP can be cleaved at different positions, creating Aβ peptides of different amino acid forms (Aβ38-42), of which the 40-residue β peptide (Aβ40) accounts for 80-90% of the total. Aβ42 appears to be the most pathogenic, as it is more prone to aggregation and the predominant Aβ form found in amyloid plaques.

A new APP processing pathway was recently reported by Willem et al. (2015), in which sequential cleavage of APP by η-secretase and BACE1 or α-secretase leads to the formation of A$\eta - \alpha$ and A$\eta - \beta$, respectively. There may be other alternate pathways unknown at this time.
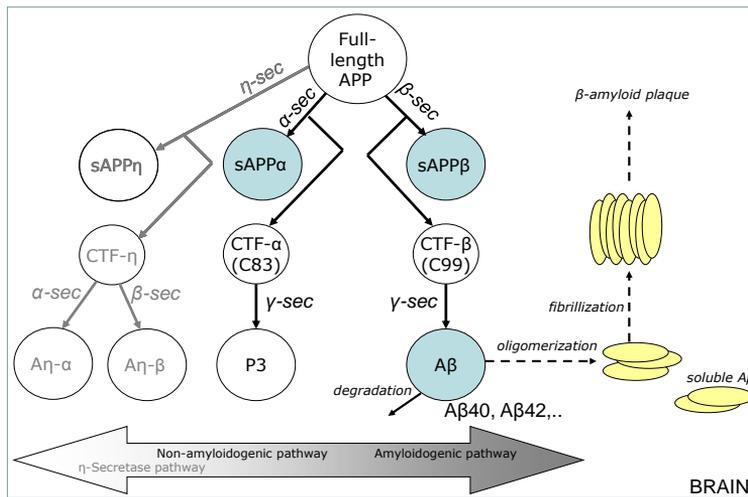
Figure 2.5: Schematic of the APP processing pathway.
In the APP processing pathway, full length APP is cleaved by BACE1 (β-sec) or α-secretase (α-sec) to form sAPPβ and C99 or sAPPα and C83. C99 is then cleaved by γ-secretase (γ-sec) to form Aβ. The amyloid hypothesis states that an imbalance in production and clearance of Aβ can result in aggregation of Aβ42 fragments into amyloid plaque. In an alternative path, APP is sequentially cleaved by η-secretase (η-sec) and BACE1 or α-secretase leading to the formation of A$\eta - \alpha$ and A$\eta - \beta$.
blue circles: APP metabolites measured in CSF.

Pharmacological treatment of AD

AD is presently incurable, as the loss of neurons is irreversible and none of the currently available treatments slow down the progression of the pathologic cascade let alone halt the disease. The FDA has only approved a few drugs to alleviate the symptoms associated with AD. The primary treatment goals of these symptomatic treatments are to enhance the quality of life and to maximize function by improving cognition, mood and behaviour. These treatments are aimed at improving processes at the end of AD's pathologic cascade. FDA approved AD medications include antidepressants, antipsychotics, cholinesterase inhibitors (e.g. Exelon (rivastigmine[41]), weak NMDA receptor antagonists (e.g. memantine), acethylcholinesterase inhibitors (e.g. Aricept (donepezil)) and other cognitive enhancers such as estrogen and vitamin E[42]. None of the treatments available slows or stops the damage to neurons that causes AD symptoms and ultimately makes the disease fatal.

Brain changes associated with AD begin before symptoms such as memory loss appear.

The dementia phase in AD may be prevented from ever developing, by treating AD early with disease modifying treatments. Disease modifying treatments are expected to be most effective during preclinical and MCI stages of AD. It is theorized that all downstream pathological processes may be prevented by lowering the levels of Aβ peptides prone to toxic aggregation, e.g. Aβ42.

Lower Aβ42 levels can be achieved by increasing Aβ42 clearance and/or decreasing Aβ42 production. The latter requires modulation of the APP processing pathway. Examples of such are immune-based therapies, designed to remove Aβ peptide from the brain[21] and inhibitors of secretases of the APP processing pathway, designed to decrease Aβ42 production[42].

To date, no disease-modifying treatment has demonstrated therapeutic benefit and to be safe[43]. Several promising BACE1 inhibitors (BACEi) have recently entered human clinical trials[44]. Given the complex pathophysiology of AD, combination disease-modifying treatment, targeting more than one pathophysiological pathway, may be necessary for effective intervention[45]. Furthermore, the appropriate target(s) may depend on the disease stage.

Diagnosing AD

Presently, AD is diagnosed after the onset of clinical manifestations. There is no single test that can verify whether a person has AD. It may be difficult to determine the exact cause of a person's dementia. Current diagnosis of AD relies on a combination of a thorough medical history, mental status checking, a physical and neurological exam, CSF biomarkers and imaging techniques such as positron emission tomography (PET) and magnetic resonance imaging (MRI)[46]. Blood tests and brain imaging are also used to eliminate other causes of dementia-like symptoms. However, the definite diagnosis of AD can only be made after the patient has died, by histological examination of brain tissue at autopsy to confirm the presence of plaques and tangles.

Three cerebrospinal fluid (CSF) biomarkers have been well established and validated: Aβ42, total Tau and phospho-Tau-181 [47]. The diagnostic validity significantly increases by the combination of these three CSF biomarkers [4]. CSF biomarkers have the potential to improve the diagnostic accuracy at the early stages of AD [48]. This is essential when treating AD early with disease-modifying treatments, to monitor the effects of drugs before clinical symptoms occur. Novel biomarkers to monitor important pathological mechanisms in AD are constantly sought. CSF Aβ_O has the potential to be a biomarker

of disease pathogenesis of AD, as it is related to toxicity and synaptic dysfunction.

Aβ as a biomarker

As Aβ is a central factor in AD pathogenesis, reliable detection and quantification of this peptide in biological samples is important for understanding disease progression as well as for the evaluation of therapeutic intervention targeting Aβ. Clinically and generally in *in vivo* animal work we can only measure the response in CSF. CSF is in contact with the brain and by that provides a reflection of cerebral processes. Thus, CSF Aβ serves as key biomarker for disease progression and Aβ targeted therapy.

Concentrations of Aβ peptides are typically determined using direct or sandwich enzyme linked immunosorbant assay (ELISA) systems[49]. Some of these assays are specifically constructed to measure both the first and last amino acid of the Aβ isoform of interest (e.g., Aβ1-40, Aβ1-42)[50]. There are also assays that are C-terminally end-specific but use N-terminal antibodies to capture the N-terminally truncated Aβ fragments, in addition to the full Aβ peptide[51,52].

Bateman et al. (2007) reported a method to quantify Aβ protein production and clearance rates in the CNS based on *in vivo* stable isotope labelling kinetics (SILK), immunoprecipitation of Aβ from cerebrospinal fluid, and quantitative liquid chromatography electrospray-ionization tandem mass spectrometry (LC-ESI-tandem MS). The SILK protocol has also been used to assess the effect of drugs on Aβ production. However, questions have been raised about the interpretation of the findings of the SILK protocol[54].

Modeling in Alzheimer's disease

The relationship between Aβ concentrations in CSF and the pharmacokinetics (PK) of Aβ lowering agents is complex. Preclinical selection of AD's drug candidates is based on an evaluation of the PK, pharmacodynamics (PD) and safety in *in vitro* assays and preclinical animal models. This requires a understanding of the *in vivo* pharmacology and the relevant biological system. In that respect drug development efforts for AD can benefit from modelling approaches.

PKPD modelling
PKPD modelling can be used to describe and understand the time-course of drug exposure and response after the administration of different doses or formulations of a drug

to individuals, based on the use of mathematical and statistical models. A PK model describes the relationship between the dose of a drug and the time profile of drug concentration. A PD model describes the relationship between the drug concentration and the pharmacological efficacy. An PKPD model describes the dynamics of exposure-response relationship(s) of a drug. The PD variable(s) in a PKPD model is usually a biomarker related to either efficacy or toxicity of the drug. Several studies on the PK and the PD of BACE1 and GS secretase inhibitors have been reported,[55,56,57,58,59,60,61]. Liu et al. (2013) proposed a mechanistic PKPD model of BACE1 inhibition in monkeys. They identified the β-secretase cleavage step as the rate limiting step for Aβ formation. However, their model is a simplification of the underlying system as no distinction is made between the β-secretase and γ-secretase steps and Aβ was modelled as a direct product of APP. Also, the transport of APP metabolites from brain to CSF, which may differ per species, was not taken into account. Therefore, their identified β-secretase cleavage rate reflects both transport and cleavage by sequentially β-secretase and γ-secretase. What's more, all parameters were estimated by fitting the PK and PD models to the average of the observed data at each time point, not taking into account the variability in drug concentrations and drug effects among individuals. Das et al. (2011) reported a two-compartment model describing Aβ response to GS inhibition, as observed in plasma and CSF in rhesus monkeys. Their model postulates an inhibitory mechanism of Aβ clearance by GS inhibition. However, in their model aspects of the Aβ production, transport and clearance processes were simplified. A model-based meta-analysis of published and in-house (pre-)clinical GS inhibitors data was performed by Niva et al. (2013). The production and clearance of Aβ was described with a turnover model, with a drug effect on the production rate. Tai et al.[59] also used turnover models to describe Aβ levels following GS inhibition in brain, CSF and plasma in wild type rat. They propose a quasi-static Aβ pool in the brain which does not change after short drug exposure.

It has been demonstrated that mechanism-based PKPD models have much improved properties for extrapolation and prediction[62,63]. However, the mechanistic detail of most PKPD models remains relatively limited compared to full systems biology models.

Systems biology

Systems biology is the study of biological systems, based on the understanding that these are composed of interacting parts, resulting in characteristics not found in the individual parts alone. These systems include signalling, gene regulatory, and metabolic networks[64]. An example of a signalling network is the AlzPathway, reported by Mizuno

et al. (2012). The AlzPathway is a comprehensive map of intra-, inter- and extracellular signalling pathways in AD, consisting of 1347 molecules and 1070 reactions in neuron, brain blood barrier, presynaptic, postsynaptic, astrocyte, and microglial cells and their cellular localizations (Figure 2.6). It was based on a collection of 123 review articles involving AD. The key molecules of the AlzPathway are presented in Figure 2.7, in which each reaction is decomposed into a binary relation between reactant(s) and product(s), and modifier(s) and product(s). The molecules Aβ, apolipoprotein-E, microtubule-associated protein-τ and γ-secretase were considered central in the AD-signalling network. The model was developed for both clarification of the pathogenic mechanisms of AD and identifying drug targets. In general, these type of models are used to explore and identify drug targets and potential biomarkers of disease and drug response.

Figure 2.6: Overview of the AlzPathway map[65]

Figure 2.7: Key molecules in the AlzPathway in binary-relation notation[65].

Systems pharmacology modelling

The above mentioned reported PKPD models looked solely at the behaviour of Aβ and not at the behaviour of the APP system as a whole. The intricacy of the underlying biochemical network makes it difficult to predict the effects of drug interventions on the individual attributes of the APP processing pathway. Therefore, the understanding of the APP system is imperative to translate drug concentrations to APP pathway inhibition and to improve the prediction of drug effects on Aβ levels. Systems biology models are not concerned with pharmacology and general principles of PKPD modelling.

Systems pharmacology (SP) models integrate the best available understanding of the biology and pharmacology of the system responses. This involves computational analysis of the time course of the changes in treatment associated biomarkers on the basis of a structural mathematical model that describes the underlying biological processes, while making a strict distinction between drug-specific and systems specific parameters. In essence, SP models are mechanism-based models embedded in a systems biology

Increased understanding of the system

1. **Objectives**

Progress

- *(follow-up)* Questions
- Assumptions
- *(novel)* Hypothesis

4. **Challenge SP model**

- Verify SP model can capture key data
- Validation

START

- Exploring knowledge gaps
- Prioritize data needs
- *Emerging data*

- Define scope of model
- Data integration

2. **Information collection**

3. **Build/extend SP model**
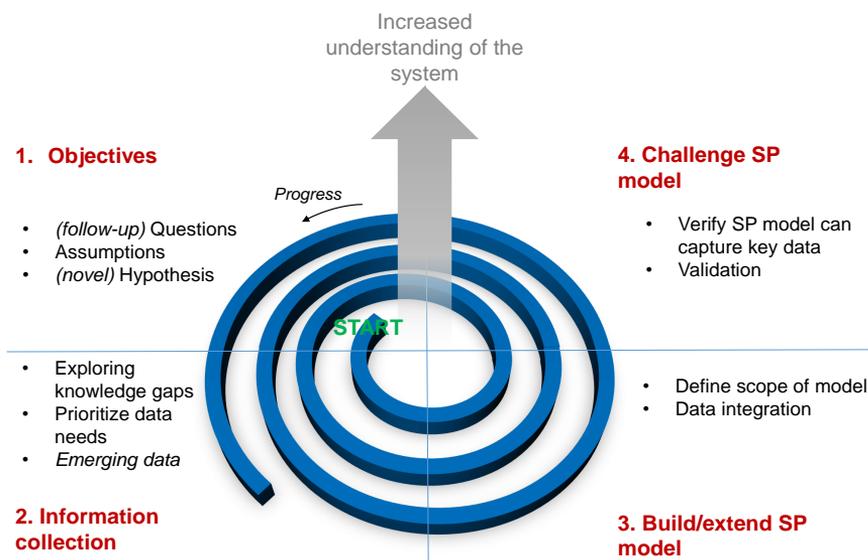
Figure 2.8: Schematic of the evolutionary process of systems pharmacology (SP) model building

framework. No SP models have been developed or applied to the pharmacological action of drugs in the APP processing pathway.

The development and implementation of a SP model is an evolutionary process, as presented in Figure 2.8. The model facilitates the integration of prior knowledge of biological systems, assumptions about the pathology and pharmacology with emerging data. In Figure 2.8, the spiral represents the iterative approach of model development. An iterative model development approach has the benefit that model updates are foreseen: before going into the first cycle of model building, it is know that another round will follow, but on a higher level, in terms of more knowledge and understanding of the system than the first time. Thus, we obtain an evolutionary improvement of the SP model and consequently of the (model based) understanding of the system.

By recognizing that building a SP model is an evolutionary process, it acknowledges the fact that at the beginning, there are knowledge gaps and that the specifications and requirements of the final SP model are not known. There could be hidden behaviours

of the systems, e.g. feedback loops, which cannot be predicted until the SP model is assembled together and parametrized. It could also be that, presuming a mechanism of action, the systems model does not fit the data. In case the model does not capture the data adequately, we can learn something. Then, the only question we need to ask is *why?* As such, a SP model is a hypothesis generating tool.

How many iteration cycles are necessary depends on how long one cycle takes, and how much time is available in order to set the SP model up to answer relevant questions that are as concise and directed as possible. A SP model is a framework for asking questions about the pharmacology of the drug in the context of the system and the disease. The scope of the model must be tailored to answering the question at hand. For some questions, it may be enough to capture the main trend of the behaviour of the system, but for other situations a more detailed model is needed. SP models can also identify the data needs and be reapplied to follow-up questions. Thus, SP models act as a central repository of (novel) hypotheses, knowledge and data.

A SP model of the APP pathway will provide a quantitative understanding of the effects of drugs on the APP processing pathway to improve the prediction and magnitude of $A\beta$ reducing effects. Perturbing the APP system through drug interactions acting at different sequence in the APP pathway *(BACE1 and GS inhibition)* and not looking solely at the behaviour of a single biomarker, but in the context of the system, is expected to provide valuable biological insights into the APP pathway and the chances to modify AD. By using a systems model, we can learn more on the biological complexity of the APP system (e.g. resilience), and by understanding its complexity make more informed decisions concerning pharmacological intervention and support challenges in drug development.

References

1. Valastyan, J.S. & Lindquist, S. Mechanisms of protein-folding diseases at a glance. Dis Model Mech. 2014;7(1):9–14.

2. Hekmatimoghaddam, S., Zare-Khormizi, M.R., & Pourrajab, F. Underlying mechanisms and chemical/biochemical therapeutic approaches to ameliorate protein misfolding neurodegenerative diseases. Biofactors. 2016.

3. Majd, S., Power, J.H., & Grantham, H.J.M. Neuronal response in Alzheimer's and Parkinson's disease: the effect of toxic proteins on intracellular pathways. BMC Neurosci. 2015;16:69.

4. Di Carlo, M., Giacomazza, D., & San Biagio, P.L. Alzheimer's disease: biological aspects, therapeutic perspectives and diagnostic tools. J physics Condens matter an Inst Phys J. 2012;24(24):244102.

5. Sivanesam, K. & Andersen, N. Modulating the Amyloidogenesis of α-Synuclein.. Curr Neuropharmacol. 2015.

6. Irwin, D.J., Lee, V.M.Y., & Trojanowski, J.Q. Parkinson's disease dementia: convergence of α-synuclein, tau and amyloid-β pathologies. Nat Rev Neurosci. 2013;14(9): 626–36.

7. Kupfer, L., Hinrichs, W., & Groschup, M.H. Prion protein misfolding.. Curr Mol Med. 2009;9(7):826–35.

8. Trepte, P., Strempel, N., & Wanker, E.E. Spontaneous self-assembly of pathogenic huntingtin exon 1 protein into amyloid structures.. Essays Biochem. 2014;56:167–80.

9. Adams, D. Recent advances in the treatment of familial amyloid polyneuropathy. Ther Adv Neurol Disord. 2013;6(2):129–39.

10. Boulouis, G., Charidimou, A., & Greenberg, S.M. Sporadic Cerebral Amyloid Angiopathy: Pathophysiology, Neuroimaging Features, and Clinical Implications. Semin Neurol. 2016;36(3):233–43.

11. Silverman, J.M., *et al.* Disease Mechanisms in ALS: Misfolded SOD1 Transferred Through Exosome-Dependent and Exosome-Independent Pathways. Cell Mol Neurobiol. 2016;36(3):377–81.

12. Selkoe, D.J. & Hardy, J. The amyloid hypothesis of Alzheimer's disease at 25 years. EMBO Mol Med. 2016;8(6):595–608.

13. Prince, M., Wimo, A., Guerchet, M., Gemma-Claire, A., Wu, Y.T., & Prina, M. World Alzheimer Report 2015: The Global Impact of Dementia - An analysis of prevalence, incidence, cost and trends. Alzheimer's Dis Int. 2015;page 84.

14. Walsh, D.M. & Selkoe, D.J. Deciphering the molecular basis of memory failure in Alzheimer's disease. Neuron. 2004;44(1): 181–193.

15. Serrano-Pozo, A., Frosch, M.P., Masliah, E., & Hyman, B.T. Neuropathological alterations in Alzheimer disease. Cold Spring Harb Perspect Med. 2011;1(1):a006189.

16. Schott, J.M., Price, S.L., Frost, C., Whitwell, J.L., Rossor, M.N., & Fox, N.C. Measuring atrophy in Alzheimer disease:

a serial MRI study over 6 and 12 months. Neurology. 2005;65(1):119–24.

17. Iqbal, K., Liu, F., Gong, C.X., & Grundke-Iqbal, I. Tau in Alzheimer disease and related tauopathies. Curr Alzheimer Res. 2010;7(8):656–64.

18. Marx, J. ALZHEIMER'S DISEASE A New Take on Tau. Science. 2007;316:1416–1417.

19. Selkoe, D.J. Translating cell biology into therapeutic advances in Alzheimer's disease. Nature. 1999;399(6738 Suppl):A23–31.

20. Patterson, B.W., *et al.* Age and amyloid effects on human central nervous system amyloid-beta kinetics. Ann Neurol. 2015;78(3):439–453.

21. Weiner, H.L. & Frenkel, D. Immunology and immunotherapy of Alzheimer's disease. Nat Rev Immunol. 2006;6(5):404–16.

22. Chávez-Gutiérrez, L., *et al.* The mechanism of γ-Secretase dysfunction in familial Alzheimer disease. EMBO J. 2012;31(10):2261–74.

23. Wisniewski, T., Ghiso, J., & Frangione, B. Peptides homologous to the amyloid protein of Alzheimer's disease containing a glutamine for glutamic acid substitution have accelerated amyloid fibril formation. Biochem Biophys Res Commun. 1991;179(3):1247–54.

24. Pimplikar, S.W. Reassessing the amyloid cascade hypothesis of Alzheimer's disease. Int J Biochem Cell Biol. 2009;41(6):1261–8.

25. Tapiola, T., *et al.* Cerebrospinal Fluid β-Amyloid 42 and Tau Proteins as Biomarkers of Alzheimer-Type Pathologic Changes in the Brain. Arch Neurol. 2009;66(3):382–389.

26. Janelidze, S., *et al.* CSF Aβ42/Aβ40 and Aβ42/Aβ38 ratios: better diagnostic markers of Alzheimer disease. Ann Clin Transl Neurol. 2016;3(3):154–65.

27. Sperling, R.a., *et al.* Toward defining the preclinical stages of Alzheimer's disease: recommendations from the National Institute on Aging-Alzheimer's Association workgroups on diagnostic guidelines for Alzheimer's disease. Alzheimers Dement. 2011;7(3):280–92.

28. Bentham Science Publisher, B.S.P. Role of Nanotechnology in the Diagnosis and Treatment of Alzheimer's Disease In Selvin, M.E. editor *Curr Adv Med Appl Nanotechnol*,;chapter 9, pages 107–124. Bentham Science Publishers;Manchester;1 ed.;2012 ISBN 9781608051311.

29. Benilova, I., Karran, E., & De Strooper, B. The toxic Aβ oligomer and Alzheimer's disease: an emperor in need of clothes. Nat Neurosci. 2012;15(3):349–357.

30. Hardy, J. & Allsop, D. Amyloid deposition as the central event in the aetiology of Alzheimer's disease. Trends Pharmacol Sci. 1991;12(10):383–8.

31. Selkoe, D.J. Alzheimer's disease. In the beginning.... Nature. 1991;354(6353):432–3.

32. Masters, C.L. & Beyreuther, K. Alzheimer's disease: molecular basis of structural lesions. Brain Pathol. 1991;1(4):226–7.

33. Hardy, J.A. & Higgins, G.A. Alzheimer's disease: the amyloid cascade hypothesis. Science. 1992;256(5054):184–5.

34. Karran, E. & De Strooper, B. The amyloid cascade hypothesis: are we poised for success or failure? J Neurochem. 2016.

35. Jack, C.R., *et al.* Hypothetical model of dynamic biomarkers of the Alzheimer's pathological cascade. Lancet Neurol. 2010;9(1):119–28.

36. Jack, C.R., *et al.* Tracking pathophysiological processes in Alzheimer's disease: an updated hypothetical model of dynamic biomarkers. Lancet Neurol. 2013;12(2):207–16.

37. Chen, Y. & Dong, C. Abeta40 promotes neuronal cell fate in neural progenitor cells. Cell Death Differ. 2009;16(3):386–94.

38. Bourgade, K., *et al.* Protective Effect of Amyloid-β Peptides Against Herpes Simplex Virus-1 Infection in a Neuronal Cell Culture Model. J Alzheimer's Dis. 2016;50(4):1227–1241.

39. Struble, R.G., Ala, T., Patrylo, P.R., Brewer, G.J., & Yan, X.X. Is brain amyloid production a cause or a result of dementia of the Alzheimer's type? J Alzheimer's Dis. 2010;22(2):393–399.

40. Willem, M., *et al.* η-Secretase processing of APP inhibits neuronal activity in the hippocampus. Nature. 2015;526(7573):443–7.

41. Gabelli, C. Rivastigmine: an update on therapeutic efficacy in Alzheimer's disease and other conditions. Curr Med Res Opin. 2003;19(2):69–82.

42. Husain, M.M., Kenneth, T., Siddique, H., & McClintock, S.M. Present and prospective clinical therapeutic regimens for Alzheimer's disease. Neuropsychiatr Dis Treat. 2008;4(4):765–777.

43. Strittmatter, W.J. Medicine. Old drug, new hope for Alzheimer's disease. Science. 2012;335(6075):1447–8.

44. Yan, R. & Vassar, R. Targeting the β secretase BACE1 for Alzheimer's disease therapy. Lancet Neurol. 2014;13(3):319–329.

45. Hendrix, J.A., *et al.* Challenges, solutions, and recommendations for Alzheimer's disease combination therapy. Alzheimer's Dement. 2016;12(5):623–630.

46. Alzheimer Association Alzheimer's disease facts and figures 2013.

47. Lewczuk, P., Mroczko, B., Fagan, A., & Kornhuber, J. Biomarkers of Alzheimer's disease and mild cognitive impairment: A current perspective. Adv Med Sci. 2015;60(1):76–82.

48. Blennow, K., Biscetti, L., Eusebi, P., & Parnetti, L. Cerebrospinal fluid biomarkers in Alzheimer's and Parkinson's diseases-From pathophysiology to clinical practice. Mov Disord. 2016;31(6):836–847.

49. Jensen, M., *et al.* Quantification of Alzheimer amyloid beta peptides ending at residues 40 and 42 by novel ELISA systems. Mol Med. 2000;6:291–302.

50. Andreasen, N., *et al.* Cerebrospinal fluid beta-amyloid(1-42) in Alzheimer disease: differences between early- and late-onset Alzheimer disease and stability during the course of disease. Arch Neurol. 1999;56(6):673–80.

51. Cirrito, J.R., *et al.* In vivo assessment of brain interstitial fluid with microdialysis reveals plaque-associated changes in amyloid-beta metabolism and half-life. J Neurosci. 2003;23(26):8844–53.

52. Sankaranarayanan, S., *et al.* First demonstration of cerebrospinal fluid and plasma Aβ lowering with oral administration of a β-site amyloid precursor protein-cleaving enzyme 1 inhibitor in nonhuman primates. J Pharmacol Exp Ther. 2009;328(1):131–140.

53. Bateman, R.J., Munsell, L.Y., Chen, X., Holtzman, D.M., & Yarasheski, K.E. Stable isotope labeling tandem mass spectrometry (SILT) to quantify protein production and clearance rates. J Am Soc Mass Spectrom. 2007;18(6):997–1006.

54. Edland, S.D. correspondence Fractional synthesis and clearance rates for amyloid β. Nat Med. 2011;17(10):3–5.

55. Das, R., *et al.* Modeling effect of a γ-secretase inhibitor on amyloid-β dynamics reveals significant role of an amyloid clearance mechanism. Bull Math Biol. 2011;73(1):230–47.

56. Lu, Y., *et al.* Cerebrospinal fluid β-amyloid turnover in the mouse, dog, monkey and human evaluated by systematic quantitative analyses. Neurodegener Dis. 2013;12(1):36–50.

57. Lu, Y., *et al.* Cerebrospinal fluid amyloid-β (Aβ) as an effect biomarker for brain Aβ lowering verified by quantitative preclinical analyses. J Pharmacol Exp Ther. 2012;342(2):366–75.

58. Niva, C., Parkinson, J., Olsson, F., van Schaick, E., Lundkvist, J., & Visser, S.a.G. Has inhibition of Aβ production adequately been tested as therapeutic approach in mild AD? A model-based meta-analysis of γ-secretase inhibitor data. Eur J Clin Pharmacol. 2013;69(6):1247–60.

59. Tai, L.M., *et al.* The dynamics of Aβ distribution after γ-secretase inhibitor treatment, as determined by experimental and modelling approaches in a wild type rat. J Pharmacokinet Pharmacodyn. 2012;39(3):227–37.

60. Janson, J., *et al.* Population PKPD modeling of BACE1 inhibitor-induced reduction in Aβ levels in vivo and correlation to in vitro potency in primary cortical neurons from mouse and guinea pig. Pharm Res. 2014;31(3):670–83.

61. Parkinson, J., *et al.* Modeling of age-dependent amyloid accumulation and γ-secretase inhibition of soluble and insoluble Aβ in a transgenic mouse model of amyloid deposition. Pharmacol Res Perspect. 2013;1(2):e00012.

62. Danhof, M., Alvan, G., Dahl, S.G., Kuhlmann, J., & Paintaud, G. Mechanism-based pharmacokinetic-pharmacodynamic modeling - A new classification of biomarkers. Pharm Res. 2005;22(9):1432–7.

63. Danhof, M., De Jongh, J., De Lange, E.C., Della Pasqua, O., Ploeger, B.A., & Voskuyl, R.A. Mechanism-based pharmacokinetic-pharmacodynamic modeling: biophase distribution, receptor theory, and dynamical systems analysis. Annu Rev Pharmacol Toxicol. 2007;47:357–400.

64. Machado, D., Costa, R.S., Rocha, M., Ferreira, E.C., Tidor, B., & Rocha, I. Modeling formalisms in Systems Biology. AMB Express. 2011;1(1):45.

65. Mizuno, S., *et al.* AlzPathway: a comprehensive map of signaling pathways of Alzheimer's disease. BMC Syst Biol. 2012;6(1):52.
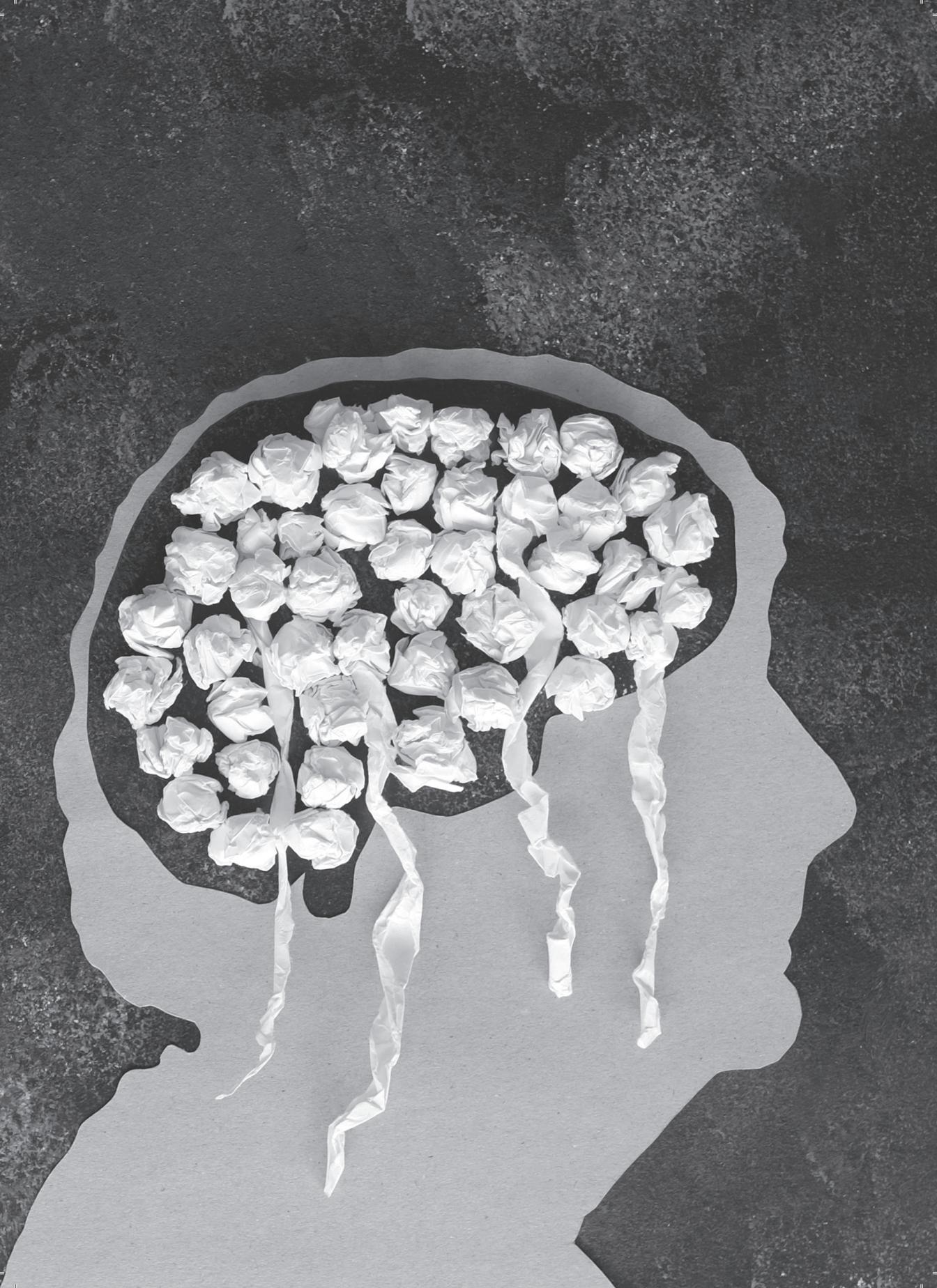
Section II

Development of a systems pharmacology model
to predict oligomer response following
secretase inhibition
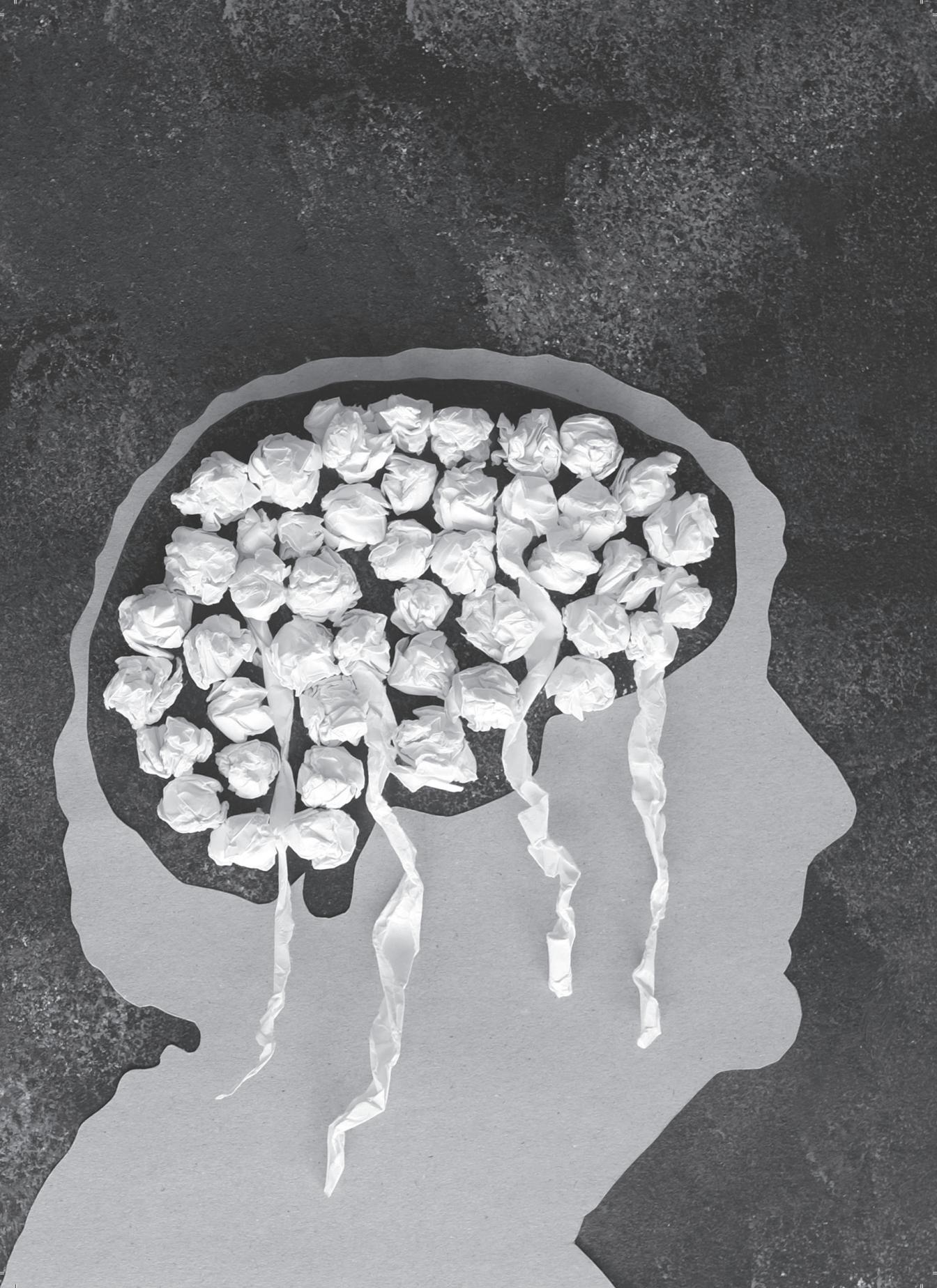
Chapter 3

Systems pharmacology analysis of the amyloid cascade following β-secretase inhibition enables the identification of an Aβ42 oligomer pool

E.M.T. van Maanen, T.J. van Steeg, M.S. Michener, M.J. Savage, M.E. Kennedy, H.J. Kleijn, J.A. Stone, M. Danhof

Visual Abstract
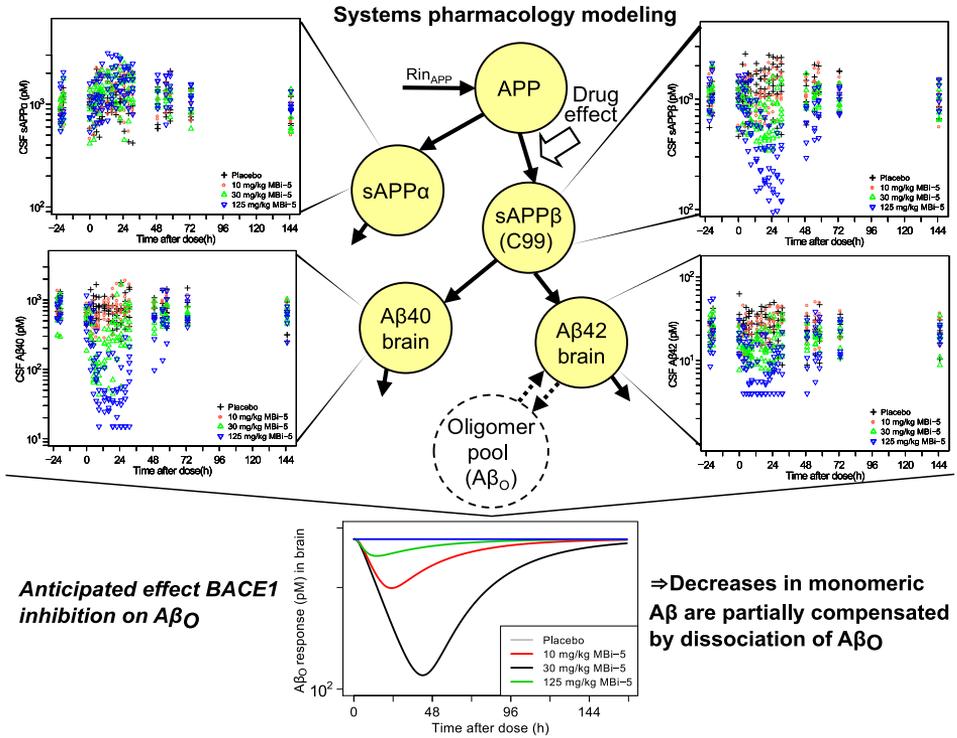
Abstract

The deposition of amyloid-β oligomers in brain parenchyma has been implicated in the pathophysiology of Alzheimer's disease. Here we present a systems pharmacology model describing the changes in the amyloid precursor protein (APP) pathway following administration of three different doses (10, 30 and 125 mg/kg) of the β-secretase (BACE1) inhibitor MBi-5 in cisterna magna ported rhesus monkeys. The time course of the MBi-5 concentration in plasma and cerebrospinal fluid (CSF) was analysed in conjunction with the effect on the concentrations of the APP metabolites Aβ42, Aβ40, sAPPα and sAPPβ in CSF. The systems pharmacology model contained expressions to describe the production, elimination and brain-to-CSF transport for the APP metabolites. Upon the administration of MBi-5 a dose dependent increase of the metabolite sAPPα and dose dependent decreases of sAPPβ and Aβ were observed. Maximal inhibition of BACE1 was close to 100% and the value of the IC$_{50}$ was 0.0256 μM (95% CI, 0.0137-0.0375). A differential effect of BACE1 inhibition on Aβ40 and Aβ42 was observed, with the Aβ40 response being larger than the Aβ42 response. This enabled the identification of an Aβ42 oligomer pool in the systems pharmacology model. These findings indicate that decreases in monomeric Aβ responses resulting from BACE1 inhibition are partially compensated by dissociation of Aβ oligomers and suggest that BACE1 inhibition may also reduce the putatively neurotoxic oligomer pool.

Introduction

The amyloid cascade hypothesis posits that amyloid-β protein (Aβ) peptide levels are increased early in Alzheimer's Disease (AD) leading to the formation of toxic soluble Aβ oligomers (Aβ_O) and plaques[1]. According to this hypothesis, a series of causal events initiated by abnormal Aβ levels leads to neuronal cell death and cognitive and functional decline over time[2]. Toxic Aβ_O are considered to be the drivers of the neurode-generation[3,4]. Such soluble forms of multimeric Aβ peptides are intermediate of soluble Aβ monomers and insoluble Aβ fibrils and likely consist of a mixture of oligomeric species. Aβ dimers, trimers, larger Aβ_O and structures such as soluble protofibrils have been isolated from AD brain[5,6,7,8]. Aβ_O are in a constant equilibrium with Aβ monomers and other Aβ aggregates[3].

Formation of Aβ requires proteolytic cleavage of the transmembrane protein 'β-amyloid precursor protein' (APP). Sequential cleavage of APP by the enzymes β-secretase (BACE1) and γ-secretase leads to the formation of Aβ[9], as schematically depicted in 3.1. Here cleavage by BACE1 leads to the formation of both the N-terminal secreted fragment soluble APPβ (sAPPβ) and the C-terminal membrane-bound 99-amino acid fragment (C99). C99 is subsequent subject to cleavage by γ-secretase yielding Aβ species of different chain length. The most common Aβ isoforms have 38 (Aβ38), 40 (Aβ40) or 42 (Aβ42) amino acids[10]. In parallel full length APP is also cleaved by α-secretase leading to the formation of soluble APPα (sAPPα), which is non-amyloidogenic[11].

Aβ production in brain is a target for AD therapy, with the potential for a disease modifying effect by reducing Aβ levels[12]. Several BACE1 inhibitors (BACEi) are being tested in human clinical trials, but the optimum level of BACE1 inhibition required for the treatment of AD remains to be determined[13]. A quantitative understanding of the effects of secretase inhibitors on the APP pathway may provide greater insights into dose-response pharmacology relationships.

Generally, measures of Aβ response in humans and primates can only be obtained in CSF and not in brain. However, it is believed that changes in Aβ concentrations in CSF reflect changes in brain Aβ[14]. Thus, CSF Aβ serves as key biomarker for Aβ production targeted therapies[15]. The cisterna magna ported (CMP) rhesus monkey model enables longitudinal sampling in the CSF outflow from the cisterna magna in conscious rhesus. As APP is completely homologous between human and rhesus, the CMP rhesus monkey model is used to study the effects of secretase inhibitors[16,17,18].

Several studies on the pharmacokinetics (PK) and the pharmacodynamics (PD) of
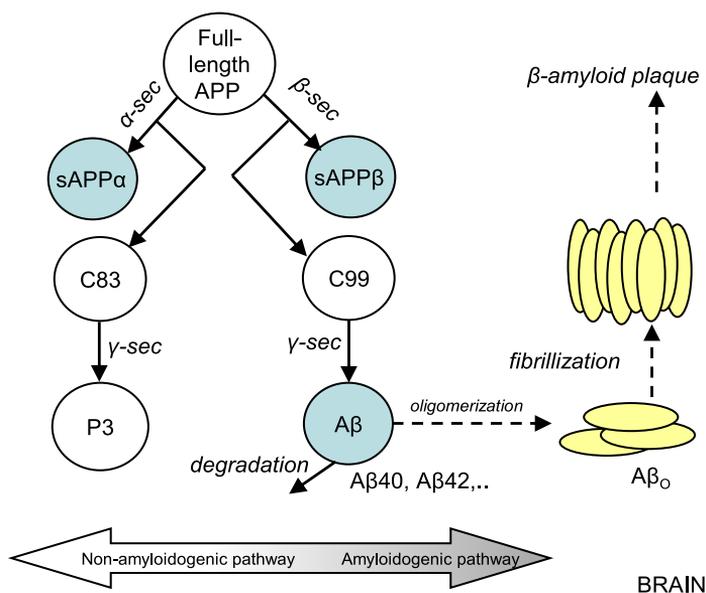
Figure 3.1: Schematic representation of the amyloid hypothesis of AD.
In the APP processing pathway, full length APP is cleaved by BACE1 (β-sec) or
α-secretase (α-sec) to form sAPPβ and C99 or sAPPα and C83. C99 is then cleaved by
γ-secretase (γ-sec) to form Aβ. The amyloid hypothesis states that an imbalance in production
and clearance of Aβ can result in aggregation of Aβ42 fragments into amyloid plaque.
blue circles: APP metabolites measured in CSF.

BACE1 and γ-secretase inhibitors have been reported [19,14,20,21]. Liu et al. 2013 proposed
a mechanistic PK-PD model of BACE1 inhibition in monkeys. They identified the β-
secretase cleavage step as the rate limiting step for Aβ formation. However, their model
is a simplification of the underlying system as no distinction is made between the β-
secretase and γ-secretase cleavage steps and Aβ was modelled as a direct product of
APP. Potter et al. 2013 used compartmental modelling to investigate the APP processing
pathway based on the results from a metabolic tracer study in humans with rare autosomal
dominant AD (ADAD). A model with 18 compartments accounting for the kinetics of
Aβ38, Aβ40 and Aβ42 enrichments, including compartments representing APP and C99
was proposed. However, the reported model is structurally and numerically unidentifiable,
considering that not all APP metabolites were measured.

No systems pharmacology model has been reported that provides an integrated de-
scription of the effects of drugs on the APP metabolites. Systems pharmacology modelling
is an extension of traditional mechanism-based PK-PD modelling, linking the system that

is affected by the drug to its treatment associated measured biomarkers. This involves computational analysis of the time course of the changes in biomarkers on the basis of a structural mathematical model that describes the underlying biological processes, while making a strict distinction between drug-specific and systems specific parameters. It has been demonstrated that such mechanism-based PK-PD models have much improved properties for extrapolation and prediction[24,25]. Systems pharmacology modelling will provide a quantitative understanding of the effects of drugs on the APP processing pathway to improve the prediction and magnitude of Aβ reducing effects.

The objective of this investigation was to characterize the multi-step production of Aβ in brain and its disposition into CSF in rhesus and obtain an indirect impression of Aβ_O using information from the monomeric Aβ species. To this end, CSF Aβ dynamic data from CMP monkeys treated with the BACEi MBi-5 were analysed. APP metabolites inter-relationships and their responses to MBi-5 were each measured by ELISA and metabolite responses were then integrated by means of a systems pharmacology modelling approach. Comprehensive, model-based information from MBi-5 PK and PD is integrated across time points, doses and endpoints, yielding information on dose response and APP metabolite (sAPPβ, sAPPα and Aβ) responses and interrelationships. In this manner invaluable information is obtained on the functioning of the integrated biological system. The effect of BACE1 inhibition on Aβ_O is anticipated which will be measured in future studies.

Materials and Methods

Animals

Animal use procedures were conform to the Guide for the Care and Use of Laboratory Animals (Institute of Laboratory Animal Resources, National Research Council, 1996) and reviewed and approved by the Institutional Animal Care and Use Committee at Merck Research Laboratories. The CMP rhesus monkey model was described by [17]. The rhesus monkeys are chronically implanted with catheters in the cisterna magna, allowing repeated sampling of CSF and plasma in conscious rhesus. Six male animals, weighing between 5.2 and 11.7 kg (average, 8.7 kg), age 2 to 10 years (average, 8 years), were included in the study. These monkeys were captive-bred in a closed colony and individually housed.

Drug administration and sampling

The study protocol and pharmacological profile of MBi-5 was described previously by Dobrowolska et al. [26]. The study protocol is summarized here. In a single dose, four-way, full crossover study, MBi-5 was administrated at 10, 30, 125 mg/kg (5 ml/kg), or vehicle (0.4% methylcellulose) p.o., with at least two weeks washout between each period. Plasma and CSF drug concentrations were collected at 0 (predose) and 3, 5, 7, 9, 13, 16, 19, 22, 25, 28, 31, 49, 55, 58, 73 and 145 h postdose, resulting in 17 plasma and CSF PK samples for each monkey per treatment group. 2 mL of blood and 1 mL of CSF were collected at each time point. The concentration of MBi-5 in the plasma and CSF samples was determined using LC-MS/MS.

The concentrations of Aβ40, Aβ42, sAPPα and sAPPβ were determined from CSF samples collected at -22, -20 and -1 h (predose) and 2, 4, 6, 8, 12, 15, 18, 21, 24, 27, 30, 48, 54, 57, 72 and 144 h postdose, giving 19 measurements of each biomarker for each monkey per treatment group. 1 mL of CSF were collected at each time point. The assays used for the concentration measurements were described previously [27,28].

PK-PD analysis

The PK-PD model was developed and fitted to the data by means of non-linear mixed effects modelling using the NONMEM software package version VI level 2 [29]. This approach takes into account structural (fixed) effects and both intra- and interindividual variability. The following parameters are estimated: typical values of structural model parameters (population parameters, which define the average value for a parameter in a population) (θ), the variance and covariance of the interindividual variability (ω^2) and the variance of the residual error (σ^2). A step-wise procedure was used to find the model that best fitted the data. A convergence criterion of three significant digits in the parameter estimates was used. The obtained minimum value of the objective function was used for the comparison of nested models. A decrease of 10.8 points in the minimum value of the objective function by adding an additional parameter, corresponding to p<0.001 in a χ-squared distribution, was considered significant. The first-order conditional estimation approximation with η-ϵ interaction (FOCE interaction) was used for parameter estimation. Random effects at the individual level were included as exponential (e$^\eta$), reflecting lognormal distributions of the individual model parameters:

$$\theta_i = \theta \times e^{(\eta_i)} \tag{3.1}$$

in which θ_i is the value for the ith individual; θ is the typical value for the parameter, and η is an interindividual random effect, which is assumed to follow a normal distribution with mean zero and variance ω^2.

The residual variability was explored with additive (Eq. 3.2) and proportional (Eq. 3.3) error models or a combination of both (Eq. 3.4) .

$$y_{ijk} = f(\theta_{ij}) + \epsilon_{ijk} \tag{3.2}$$

$$y_{ijk} = f(\theta_{ij}) \times (1 + \epsilon_{ijk}) \tag{3.3}$$

$$y_{ijk} = f(\theta_{ij}) \times (1 + \epsilon_{ijk1}) + \epsilon_{ijk2} \tag{3.4}$$

where y_{ijk} is the kth observation on the jth occasion for the ith individual; $f(\theta_{ij})$ is the corresponding model predicted observation and ϵ represents the residual departure of the observed concentration from the predicted concentration, which is assumed to follow a normal distribution with mean zero and variance σ^2.

To evaluate the prediction of the central tendency and distribution of the observed data by the model a visual predictive check (VPC) was performed in which the median and the 90% inter-quantile range of the data simulated with the developed model were plotted together with the observations. A validated result would have close agreement of median observed and predicted line with ∼90% of the observations falling within the 90% prediction interval.

The NONMEM software package was implemented on an Intel QuadCore (Intel®Core[TM] i7 CPU860, 2.80 GHz, 3.24 GB RAM) and Compaq Visual Fortran (version 6.6, Compaq Computer Corporation, Houston, Texas, USA) was used as compiler. Data management and model assessment was done using the statistical software package S-PLUS for Windows (version 8.0 Professional, Insightful Corp., Seattle, USA).

Model description

The systems pharmacology model of MBi-5 was developed by sequential analysis of PK and PD data. The PK model of MBi-5 was based on simultaneous analysis of plasma and CSF PK data. The results of the PK data analysis is provided in the Supplemental Material. The PK profiles of MBi-5 observed in plasma and CSF were adequately described by a three-compartmental model (Supplemental Figure S3.2) and the PK parameters were estimated with good precision (Supplemental Table S3.1), thus the model could serve as input for PD model analysis.

The biomarker response profiles of MBi-5 measured in CSF were adequately described

by a model containing compartments for five variables: APP, sAPPβ, sAPPα, Aβ40 and Aβ42 (Figure 3.2). The production of APP was believed to be zero order, i.e. a constant production of APP. It was assumed that there is no alternative proteolytic enzyme cleaving full length APP other than α-secretase and BACE1. As both sAPPβ and C99 are products of APP cleavage by BACE1, sAPPβ and C99 were presumed to follow the same kinetics and therefore sAPPβ could be used in the model as surrogate precursor for Aβ. The production of sAPPα, sAPPβ and Aβ were assumed to be first order, i.e. dependent on the concentration of its precursor. The interaction between APP, sAPPβ, sAPPα, Aβ40 and Aβ42 is described by Eq. 3.5 - Eq. 3.9:

$$\frac{d}{dt}APP = Rin_{APP} - (Rin\beta \times EFF + Rin\alpha) \times APP \tag{3.5}$$

$$\frac{d}{dt}sAPP\alpha = Rin\alpha \times APP - Rout_a \times sAPP\alpha \tag{3.6}$$

$$\frac{d}{dt}sAPP\beta = Rin\beta \times EFF \times APP - (Kin_{40} + Kin_{42}) \times sAPP\beta \tag{3.7}$$

$$\frac{d}{dt}A\beta_{40} = Kin_{40} \times sAPP\beta - Kout \times A\beta_{40} \tag{3.8}$$

$$\frac{d}{dt}A\beta_{42} = Kin_{42} \times sAPP\beta - Kout \times A\beta_{42} \tag{3.9}$$

The rate of change of APP with respect to time in the presence of the inhibitor is described by Eq. 3.5, in which the BACE1 cleavage inhibition is incorporated by the factor *EFF*. *EFF* is the degree of inhibition caused by MBi-5, expressed as shown in Eq. 3.10.

$$EFF = 1 - \frac{C_{\text{target}}^{\text{GAM}} \times Imax}{C_{\text{target}}^{\text{GAM}} + IC50^{\text{GAM}}} \tag{3.10}$$

Where C_{target} is the target site concentration of MBi-5 , *IC50* the C_{target} that results in 50% inhibition of BACE1, *Imax* is the maximum response and *GAM* is the Hill coefficient. C_{target} was derived from the PK model as:

$$C_{\text{target}} = C_{\text{plasma}} \times \frac{AUC_{\text{CSF}}}{AUC_{\text{plasma}}} \tag{3.11}$$

Where AUC_{CSF} and AUC_{plasma} are the areas under the CSF and plasma concentration time curves, respectively. Here, C_{target} is assumed to follow the same profile as C_{plasma}, but at a level between C_{CSF} and C_{plasma}.

It is assumed that the system is in steady state when no treatment is given *(EFF=1)*. At the treatment free-state, the change of the variables with respect to time is:

$$\frac{d}{dt}APP = 0 \quad \frac{d}{dt}sAPP\alpha = 0 \quad \frac{d}{dt}sAPP\beta = 0 \quad \frac{d}{dt}A\beta_{40} = 0 \quad \frac{d}{dt}A\beta_{42} = 0 \tag{3.12}$$

These steady state conditions were used to derive part of the system parameters. From Eq. 3.12 and Eq. 3.5 it follows that the source of APP *(Rin$_{\text{APP}}$)* is:

$$Rin_{APP} = (Rin\alpha + Rin\beta) \times APP_{base} \tag{3.13}$$

Where APP_{base} is the baseline level of APP, which is assumed to be equal to the sum of the baseline levels of sAPPα and sAPPβ, as it was assumed that there is no alternative proteolytic enzyme cleaving full length APP other than α-secretase and BACE1.

Using Eq. 3.12 and Eq. 3.6 the sAPPα formation rate *(Rinα)*, equivalent to the α-secretase cleavage step, can be derived:

$$Rin\alpha = Rout_a \times \frac{sAPP\alpha_{base}}{APP_{base}} \tag{3.14}$$

Where sAPPα_{base} is the baseline level of sAPPα.

The sAPPβ formation rate *(Rinβ)*, equivalent to the BACE1 cleavage step, follows from Eq. 3.12 and Eq. 3.7:

$$Rin\beta = (Kin_{40} + Kin_{42}) \times \frac{sAPP\beta_{base}}{APP_{base}} \tag{3.15}$$

Where $sAPP\beta_{\text{base}}$ is the baseline level of sAPPβ.

From Eq. 3.12 and Eq. 3.8 the Aβ40 formation rate (*Kin40*), equivalent to a γ-secretase cleavage step can be calculated:

$$Kin_{40} = Kout \times \frac{A\beta 40_{base}}{sAPP\beta_{base}} \qquad (3.16)$$

Where $A\beta 40_{\text{base}}$ is the baseline level of Aβ40. sAPPβ_{base} is the baseline level of sAPPβ, used here as surrogate for the baseline level of C99.

From Eq. 3.9 and Eq. 3.12, with substitution of *Kout* from Eq.3.16, the Aβ42 formation rate (*Kin42*), equivalent to a γ-secretase cleavage step, is deduced:

$$Kin_{42} = Kin_{40} \times \frac{A\beta 42_{base}}{A\beta 40_{base}} \qquad (3.17)$$

Where $A\beta 42_{\text{base}}$ is the baseline level of Aβ42.

The model structure includes four transit compartments (Fig. 3.2), one for each biomarker measured in CSF (sAPPα, sAPPβ, Aβ40, Aβ42), to account for transport from the target site in the brain to CSF. These transit processes are described, in general, by Eq. 3.18:

$$\frac{d}{dt}species_{CSF} = Kt \times (species - species_{CSF}) \qquad (3.18)$$

Where *Kt* is the transit rate for the particular species (*KtAP* for sAPPα and sAPPβ and *KtAB* for Aβ40 and Aβ42).

The system defined above can now be extended to incorporate an Aβ_{O} pool for Aβ42 oligomerization. The addition of the Aβ_{O} pool to the model structure requires adaptation of Eq. 3.9, describing Aβ42 dynamics. The exchange between the Aβ_{O} pool and the Aβ42 compartment is described by Eq. 3.19 and Eq. 3.20:

$$\frac{d}{dt}A\beta_{42} = Kin_{42} \times sAPP\beta - Kout_{42} \times A\beta_{42} - Kpl \times A\beta_{42} + Krev \times A\beta_{O} \qquad (3.19)$$

$$\frac{d}{dt}A\beta_{O} = Kpl \times A\beta_{42} - Krev \times A\beta_{O} \qquad (3.20)$$

Where *Kpl* and *Krev* are the Aβ42 oligomerization and dissociation rate, respectively, which are dependent on the baseline values of Aβ42 and the Aβ_O pool (Aβ42$_{\text{base}}$ and A$\beta_{O\text{base}}$, resp.) according to Eq. 3.21:

$$Krev = \frac{Kpl \times A\beta_{42base}}{A\beta_{Obase}} \tag{3.21}$$

Results

Separate empiric models described response of each APP metabolite

Initially, empirical PK-PD models were developed to quantify the exposure-response relationships for each CSF APP metabolite (Aβ40, Aβ42, sAPPα and sAPPβ) of the BACEi MBi-5 in monkeys. The typical model structure of each APP metabolite-inhibitor combination consisted of a transit model with 1 or 2 compartments, with the drug effect modelled relative or subtractive to baseline using an Imax/Emax function. A summary overview of the results of these models is depicted in Table 3.1. The empirical models provided consistency of drug effects across APP metabolites (identified potencies Aβ40: 0.0254 μM (95% CI, 0.0246-0.0262); Aβ42: 0.0455 μM (95% CI, 0.0351-0.0559); sAPPβ: 0.0490 μM (95% CI, 0.0192-0.0788); sAPPα: 0.0265 μM (95% CI, 0.0135-0.0395)). The mean transit time through the compartments of the models was lower for Aβ40 and Aβ42 than for sAPPβ and sAPPα. This indicates that the response of Aβ40 and Aβ42 will appear earlier in CSF, even though sAPPβ is a sequentially earlier product of the amyloidogenic APP pathway.

A systems model to describe APP metabolite responses

A comprehensive compartmental PK-PD model, incorporating MBi-5 PK and CSF APP metabolites (Aβ40, Aβ42, sAPPα and sAPPβ) concentrations was developed to quantify APP metabolite responses to BACE1 inhibition in monkeys. The model is schematically presented in Figure 3.2. The model described production, elimination, and brain-to-CSF transport of each APP metabolite, as well as their interrelationships (Figure 3.7). The rate of APP metabolism was assumed to be close to the maximal capacity of the enzymes involved[30]. Thus, APP production was approximated to follow zero-order kinetics. sAPPβ was used in the model structure as a surrogate substrate for C99 in the

Table 3.1: Summary parameters of the separate empiric model fits for each APP metabolite

PARAMETER	DESCRIPTION	UNIT	APP METABOLITE			
			$A\beta40$	$A\beta42$	$sAPP\alpha$	$sAPP\beta$
baseline	Baseline	pM	722	24.8	1040	1190
IM/EM	Baximal inhibition / effect		100%[a]	20.4 pM	167%	100%[a]
IC_{50}/EC_{50}	median inhibition / effect concentration	μM	0.0254	0.0455	0.0265	0.0490
CV	Coefficient of variation IC_{50}/EC_{50}	%	1.63	11.6	25.0	31.0
GAM	Hill coefficient		1[a]	1[a]	1[a]	1[a]
MTT[b]	Mean transit time	h	5.155	3.597	15.873	19.417

[a] Fixed.

[b] $MTT = \frac{1}{Kt} \times (n+1)$, where n is the number of transit compartments and Kt is the transit rate.

γ-secretase cleavage step. As both sAPPβ and C99 are products of the APP cleavage by BACE1, their formation rates should be the same and thus use of sAPPβ as a surrogate for C99 was justified. To account for transport from the target site in the brain to CSF, the model included one transit compartment for each APP metabolite. The drug effect was incorporated in the model as the inhibition of loss of the APP precursor pool, equivalent to the BACE1 cleavage step.

MBi-5 increased sAPPα and decreased sAPPβ and Aβ in a dose dependent manner

APP metabolite CSF concentrations showed a dose-dependent response in the presence of the BACEi. The dose-dependent increase of sAPPα and the corresponding decreases of sAPPβ and Aβ were described by the model with a single drug effect. A potency (IC_{50}) of 0.0256 μM (95% CI, 0.0137-0.0375) was identified. This value is close to the *in vitro* inhibition constant (*Ki*) of 10 nM for MBi-5 inhibition of purified BACE1 and also close to the IC_{50} for inhibition of Aβ production in intact cells of 24±6 nM[26]. When estimated, the maximal inhibition (Imax) was close to 1. Therefore Imax could be fixed to 1, indicating 100% inhibition of BACE1 at sufficient high drug concentrations. Figures 3.3 to 3.6 show the model description of each APP metabolite for each dose group.

Aβ_{O} pool required to account for differential effect on A$\beta40$ and A$\beta42$

A differential effect of BACE1 inhibition was observed for A$\beta40$ and A$\beta42$: a higher response is observed in the data for A$\beta40$ than for A$\beta42$ (e.g. Figure 3.6E and 3.6G). This differential effect could be described by extending the model with an Aβ_{O} pool connected to the A$\beta42$ compartment, resulting in an adequate description of sAPPβ, sAPPα, A$\beta40$
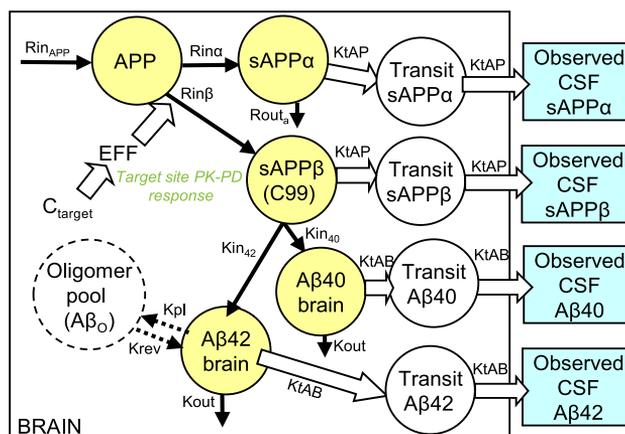
Figure 3.2: Schematic of systems model of APP processing.
The model comprised nine compartments: Five biomarker compartments in brain *(yellow circles)* and four transit compartments from brain to CSF *(white circles)*. Four biomarkers were measured in CSF (sAPPα, sAPPβ, Aβ40 and Aβ42), indicated by the blue boxes. The extended model included additionally an Aβ_O compartment *(dashed circle)*. The drug effect *(EFF)* inhibited *Rinβ*. As driver of biomarker response C_{target} was used, which was derived from the PK model (see Supplemental Material). sAPPβ was used in the model structure as a surrogate substrate of C99 in the γ-secretase cleavage step.
APP: Aβ-precursor protein; *Aβ*: amyloid-β-peptide; C_{target}: drug concentration target site; *Kin$_{40}$*: Aβ40 formation rate; *Kin$_{42}$*: Aβ42 formation rate; *Kout*: Aβ degradation rate; *Kpl*: Oligomerization rate; *Krev*: Aβ_O dissociation rate; *KtAB*: transit rate Aβ from brain to CSF; *KtAP*: transit rate sAPPα and sAPPβ from brain to CSF; *RinAPP*: zero order input constant for APP; *Rinα*: sAPPα formation rate; *Rinβ*: sAPPβ formation rate; *Rout*: sAPPβ degradation rate; *Routa*: sAPPα degradation rate.

and Aβ42 CSF concentration time profiles for each dose group (Figures 3.3, 3.4, 3.5 and 3.6, respectively). Incorporating the Aβ_O pool in the model improved the description of Aβ40 response for the 30 and 125 mg/kg dose group (compare Figure 3.5E to Figure 3.5F and Figure 3.6E to Figure 3.6F), as well as the description of the 125 mg/kg dose for Aβ42 response (compare Figure 3.6G to Figure 3.6H). Furthermore, the description of sAPPβ response for 125 mg/kg dose (compare Figure 3.6C to Figure 3.6D) was improved. Exchange of an Aβ40 monomer pool with an Aβ_O pool was evaluated, but could not be identified.
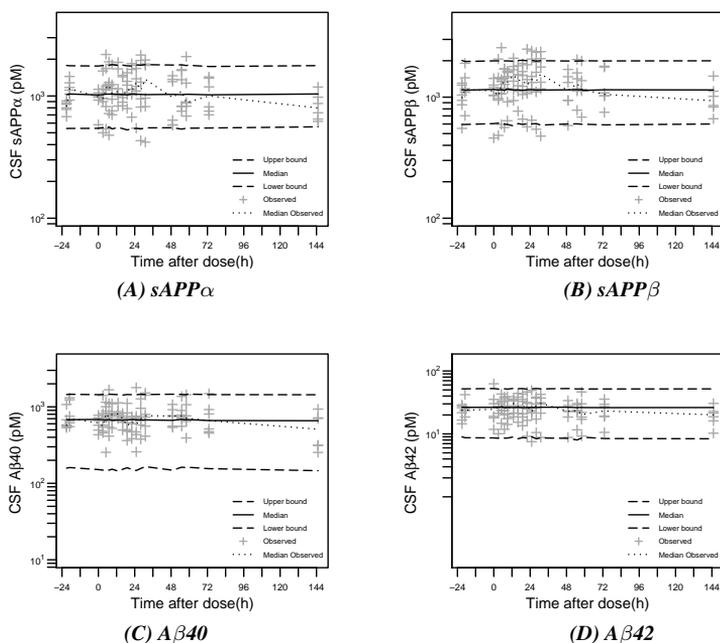
*Figure 3.3: Placebo. Visual predictive check of biomarker response **vs**. time profile of placebo in the rhesus with 90% confidence interval.* Predictions were performed with model without $A\beta_O$ compartment ((A), (B), (C), (D)). Predictions performed with model with $A\beta_O$ pool had identical results (not shown). Observation sample size: n=114 for each APP metabolite from 6 monkeys collected over 7 days.

Plus-symbols represent observed measurements. Dotted line corresponds to the median observed profile. Solid lines show the median simulated profiles. The longs-dashed lines correspond to the 90% prediction intervals obtained from 1000 individual simulated profiles.

(A) sAPPα

(B) sAPPα (With Aβ$_O$)

(C) sAPPβ

(D) sAPPβ (With Aβ$_O$)

(E) Aβ40

(F) Aβ40 (With Aβ$_O$)

(G) Aβ42

(H) Aβ42 (With Aβ$_O$)
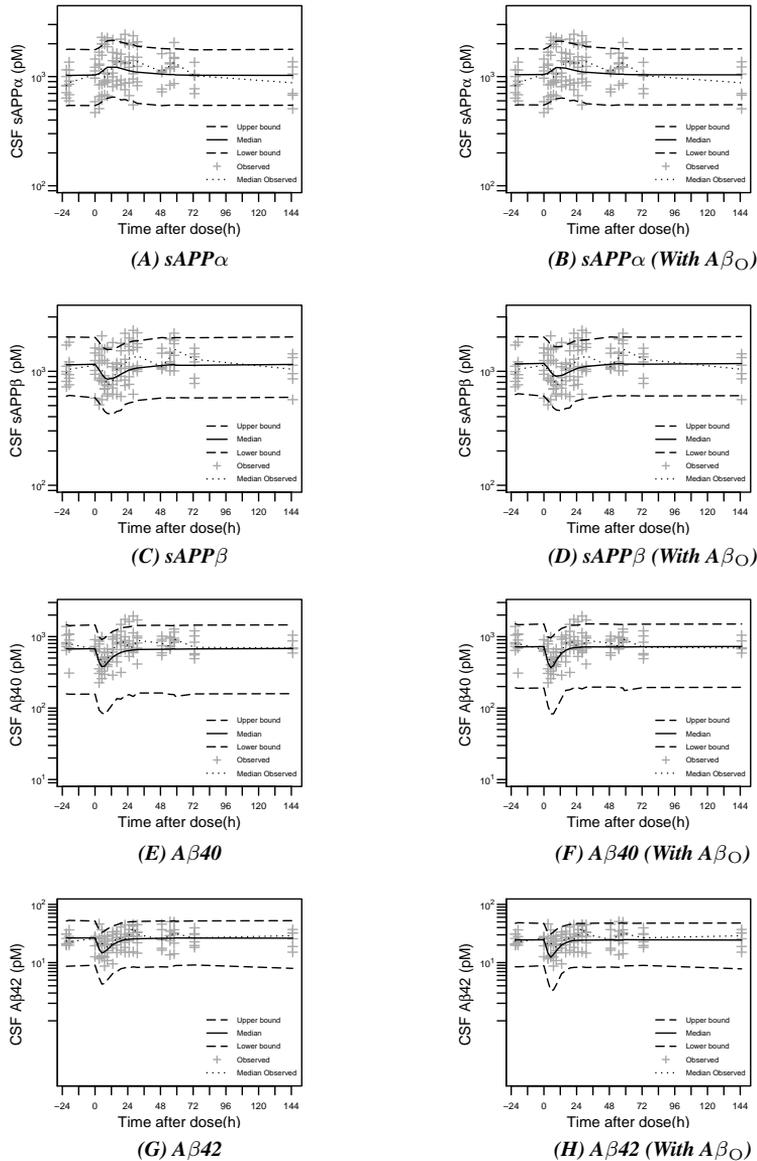
Figure 3.4: Dose 10 mg/kg. Visual predictive check of biomarker response vs. time profile of MBi-5 in the rhesus with 90% confidence interval. Predictions were performed with model with ((B), (D), (F), (H)) and without ((A), (C), (E), (G)) Aβ$_O$ compartment. Observation sample size: n=114 for each APP metabolite from 6 monkeys collected over 7 days.
Plus-symbols represent observed measurements. Dotted line corresponds to the median observed profile. Solid lines show the median simulated profiles. The longs-dashed lines correspond to the 90% prediction intervals obtained from 1000 individual simulated profiles.

Figure 3.5: Dose 30 mg/kg. Visual predictive check of biomarker response* vs. *time profile of MBi-5 in the rhesus with 90% confidence interval. Predictions were performed with model with ((B), (D), (F), (H)) and without ((A), (C), (E), (G)) $A\beta_O$ compartment. Observation sample size: n=114 for each APP metabolite from 6 monkeys collected over 7 days.
Plus-symbols represent observed measurements. Dotted line corresponds to the median observed profile. Solid lines show the median simulated profiles. The longs-dashed lines correspond to the 90% prediction intervals obtained from 1000 individual simulated profiles.

(A) sAPPα

(B) sAPPα (With Aβ$_O$)

(C) sAPPβ

(D) sAPPβ (With Aβ$_O$)

(E) Aβ40

(F) Aβ40 (With Aβ$_O$)

(G) Aβ42

(H) Aβ42 (With Aβ$_O$)
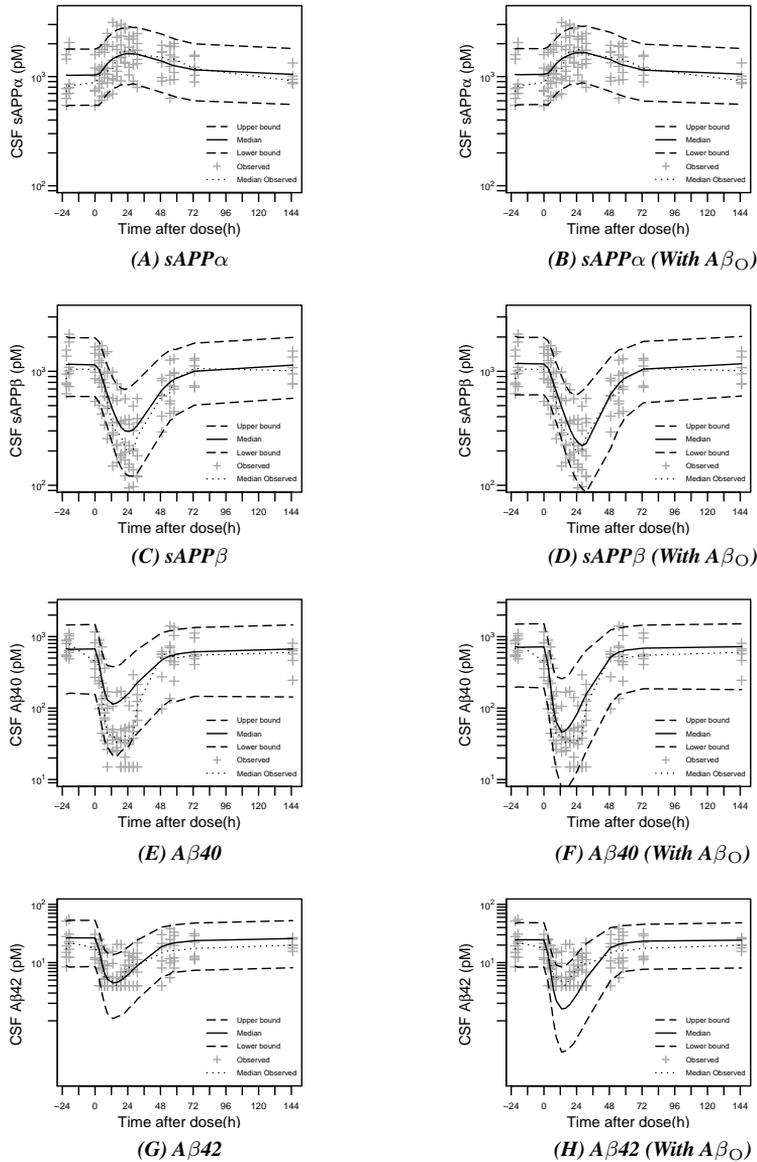
Figure 3.6: Dose 125 mg/kg. Visual predictive check of biomarker response vs. time profile of MBi-5 in the rhesus with 90% confidence interval. Predictions were performed with model with ((B), (D), (F), (H)) and without ((A), (C), (E), (G)) Aβ$_O$ compartment. Observation sample size: n=114 for each APP metabolite from 6 monkeys collected over 7 days.
Plus-symbols represent observed measurements. Dotted line corresponds to the median observed profile. Solid lines show the median simulated profiles. The longs-dashed lines correspond to the 90% prediction intervals obtained from 1000 individual simulated profiles.

Model parameters

The population parameters and intra- and interanimal variability were optimized for the study population and are depicted in Table 3.2. A sequence of models with interanimal variability on different parameters was tested and the results compared, in order to select the best random effects model structure. The final model included interanimal variability for the baseline of sAPPβ and the IC$_{50}$ of MBi-5. Both were included as exponential in nature, reflecting lognormal distributions of the individual model parameters. As the baselines of the other APP metabolites were modelled as function of the baseline of sAPPβ, its interanimal variability reflects also on the other baselines. Residual variability was included for each APP metabolite (sAPPβ, sAPPα, Aβ40, Aβ42), as proportional error models, assuming that the residual errors are normally distributed. The identified residual variability was higher for Aβ40 and Aβ42 than for sAPPβ and sAPPα. System specific parameters could be distinguished from drug specific parameters (all correlations <0.95).

Incorporating the Aβ_{O} pool in the model improved the description and did not affect the parameter estimate of the IC$_{50}$ significantly: With Aβ_{O} pool an IC$_{50}$ of 0.0269 μM (95% CI, 0.0154-0.0384) was identified and without Aβ_{O} pool the IC$_{50}$ was 0.0256 μM (95% CI, 0.0137-0.0375). The incorporation of the Aβ_{O} pool affected the Hill coefficient of the sigmoidal Imax concentration response relationship. The Aβ_{O} pool resulted in a Hill coefficient slightly deviating from unity: With the Aβ_{O} pool a Hill coefficient of 1.53 (95% CI, 1.14-1.92) was identified and without Aβ_{O} pool the Hill coefficient was 1 (fixed). This mainly improved the description of the APP metabolite concentration response curves for the higher dose groups (Figure 3.6).

Higher brain-to-CSF transport of Aβ

It was not possible to separate the rate of the γ-secretase cleavage from the brain-to-CSF transport. The transit rate for Aβ40 and Aβ42 was assumed to be equal and fast. Therefore, the transit rate from brain to CSF for Aβ40 and Aβ42 was fixed to an arbitrary high value (10 h^{-1}). Then, the Aβ half-life of 0.7 h reflects delays due to the γ-secretase cleavage step and brain-to-CSF transfer. For sAPPβ and sAPPα the transit rate was estimated to be 0.0985 h^{-1}. This value should be interpreted relative to the Aβ transit from brain-to-CSF. For sAPPα the brain-turnover (0.8 h) could be distinguished from the half-life of brain-to-CSF transfer (7.0 h). Aβ is transported from brain to CSF approximately 10^2-fold faster than sAPPα. As a result, the response of Aβ to drug treatment will appear earlier in CSF than the response of sAPPα, even though sAPPα is a sequentially earlier product of the

Table 3.2: Population parameter estimates including coefficient of variation (CV%) for the extended model with $A\beta_O$ pool

PARAMETER	DESCRIPTION	VALUE	UNIT	CV%
Structural parameters				
$sAPP\beta_{base}$	baseline $sAPP\beta$	1.19×10^3	pM	11.6
$Fbase_{A\beta40}$[b]	$A\beta40$ baseline as fraction of $sAPP\beta_{base}$	0.611		12.3
$Fbase_{A\beta42}$[c]	$A\beta42$ baseline as fraction of $sAPP\beta_{base}$	0.0210		8.38
$Fbase_{sAPP\alpha}$[d]	$sAPP\alpha$ baseline as fraction of $sAPP\beta_{base}$	0.894		2.84
Kout	degradation rate $A\beta40$ and $A\beta42$	0.940	h^{-1}	13.6
$Rout_a$	degradation rate $sAPP\alpha$	0.856	h^{-1}	30.8
KtAP	transit rate $sAPP\alpha$ and $sAPP\beta$	0.0985	h^{-1}	2.82
KtAB[a]	transit rate $A\beta$	10	h^{-1}	
IM[a]	maximal inhibition (Imax)	1		
IC_{50}	median inhibition concentration	0.0269	μM	21.8
GAM	Hill coefficient	1.53		13.1
Kpl	oligomerization rate	0.524	h^{-1}	20.0
$A\beta_{Obase}$	baseline $A\beta_O$	278	pM	41.0
Interanimal variability				
ω^2_{BSAPb}[e]	Interanimal variability $sAPP\beta$ baseline	0.0568		30.1
$\omega^2_{IC_{50}}$[e]	Interanimal variability IC50	0.279		35.5
Residual error				
$\sigma^2_{A\beta40}$[f]	Residual variability $A\beta40$	0.240		12.7
$\sigma^2_{A\beta42}$[f]	Residual variability $A\beta42$	0.161		12.4
$\sigma^2_{sAPP\beta}$[f]	Residual analysed $sAPP\beta$	0.0621		23.5
$\sigma^2_{sAPP\alpha}$[f]	Residual variability $sAPP\alpha$	0.0634		10.6

[a] Fixed.
[b] $A\beta40_{base}=Fbase_{A\beta40} \times sAPP\beta_{base}$.
[c] $A\beta42_{base}=Fbase_{A\beta42} \times sAPP\beta_{base}$.
[d] $sAPP\alpha_{base}=Fbase_{sAPP\alpha} \times sAPP\beta_{base}$.
[e] Interanimal variability is assumed to follow a normal distribution with mean zero and variance ω^2.
[f] Residual variability is assumed to follow a normal distribution with mean zero and variance σ^2.

APP pathway.

It was not possible to identify the brain-turnover of $sAPP\beta$ as a separate parameter. In the model structure, $sAPP\beta$ was used as a surrogate substrate for C99 in the γ-secretase cleavage step, driving the response of $A\beta$. Therefore, the γ-secretase cleavage step could not be separated from $sAPP\beta$ elimination.

APP metabolites interrelationships

The proteolytic cleavage rates of APP through the action of BACE1 (*Rinβ*) and α-secretase (*Rinα*) were calculated from the model parameters according to Eq. 5.12 and Eq. 5.11 to be 0.314 h^{-1} and 0.404 h^{-1} indicating that 56% of full length APP is cleaved
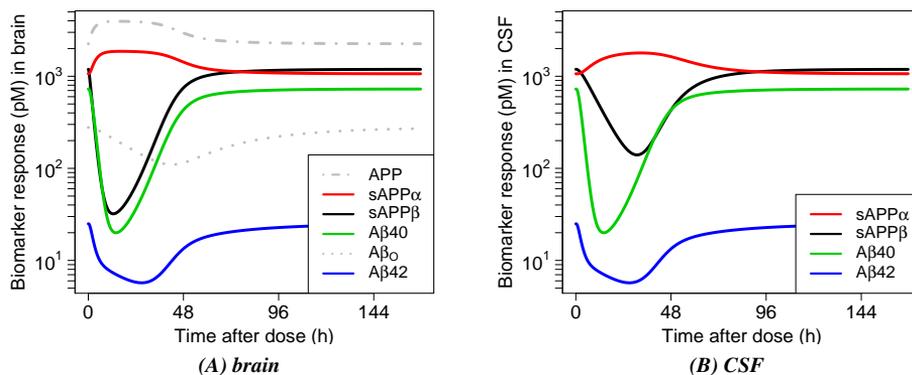
Figure 3.7: Graphical insight into the biomarker responses in brain and CSF, using the identified systems model of the APP processing pathway.
The biomarker responses in brain and CSF are predicted after a single dose of 125 mg MBi-5, using the typical parameter estimates.
APP grey dotdashed line; sAPPα red solid line; sAPPβ black solid line; Aβ40 green solid line; Aβ_O grey dotted line; Aβ42 blue solid line.

by α-secretase and 44% by BACE1. The formation rates of Aβ40 and Aβ42 were calculated according to S4.27 and 5.15. The higher Kin_{40} (0.574 h^{-1}) than Kin_{42} (0.020 h^{-1}) is in line with previously reported findings of the ratio between Aβ42 and Aβ40 of about 1:10 in non-Alzheimer brain[31]. A difference in Aβ40 and Aβ42 degradation rate (*Kout*) was also evaluated during the model development process, but this could not adequately capture the response profile of Aβ42.

The developed model could be used to predict biomarker interrelationships in response to BACE1 inhibition and visualize the response of APP and Aβ_O (3.7A) in brain. APP increases after BACE1 inhibition and appears to be shunted down the α-secretase pathway, resulting in an increase of sAPPα product. The elevation in sAPPα in the data drives the modelling conclusion that there is some increase in APP in the setting of BACE1 inhibition but it is fairly modest. The Aβ_O level decreases after BACE1 inhibition, indicating that there is reduced formation of Aβ_O by reduced levels of monomeric Aβ42 and that Aβ_O dissociates to monomeric Aβ42. The latter influences the shape of the Aβ42 response curve, which is different than the shape of the Aβ40 response curve.

For sAPPβ, sAPPβ, Aβ40 and Aβ42 the time courses of brain *versus* CSF responses were predicted (Figure 3.7A and 3.7B, respectively), showing that the earlier appearance of Aβ response in CSF relative to sAPPα and sAPPβ arises from the slower brain to CSF transfer.

Discussion

A systems model of the APP processing pathway was developed describing the interrelationships of Aβ40, Aβ42, sAPPα, and sAPPβ upon inhibition of BACE1 with MBi-5. All four APP metabolites provided consistent information regarding drug potency. The MBi-5 concentration-dependent decrease of the APP metabolites could be described by incorporating a single drug effect in the model: inhibition of the formation rate of sAPPβ, equivalent to the BACE1 cleavage step. The model supported the notion that MBi-5 can provide 100% inhibition of BACE1, consistent with a complete blockage of Aβ production at high drug concentrations. The fact that MBi-5 can provide 100% inhibition of BACE1, implies that there are no inherent mechanistic limitations of the APP pathway to blocking Aβ production. Therefore, reaching complete inhibition largely depends on drug properties such as having sufficient potency, bioavailability and tolerability.

The relatively large interanimal variability identified on the baseline level of sAPPβ (also reflecting on the baseline levels of the other APP metabolites) and the IC$_{50}$ probably denotes the large intrinsic biological differences in APP processing between subjects. Residual variability was higher for Aβ40 and Aβ42 than for sAPPβ and sAPPα. Residual variability represents the uncertainty in the relationship between the concentrations predicted by the model and the observed concentration and includes any model misspecification error. The higher residual variability for Aβ could be related to the second cleavage step by γ-secretase, yielding Aβ. In the current analysis, no direct information was available regarding the γ-secretase cleavage step. This would require data from a γ-secretase inhibitor study. Such data may explain some of the residual variability identified for Aβ.

The systems model identified a higher brain-to-CSF transport of Aβ compared to sAPPα. This results is consistent with the identified lower mean transit time for Aβ40 and Aβ42 compared to sAPPα in the separate empirical models for each APP metabolite. The potencies identified in the empirical models were consistent with the single potency of 0.0256 μM (95% CI, 0.0137-0.0375) identified using the systems model.

In the systems model, the APP production was approximated to follow zero-order kinetics. In reality, APP production is regulated by various factors, above all the synaptic activity[32]. In the current analysis, no quantitative data on the factors involved in APP production was available. It was assumed that the APP production was close to the maximum. Consequently, subtle changes in APP regulation would have little impact on APP metabolites formation.

Our modelling results imply that 56% of full length APP is cleaved by α-secretase and 44% by BACE1. There is no quantitative data available from literature on the ratio of APP moving down the α-secretase pathway and BACE1 pathway. Dobrowlska et al. (2014) compared sAPPα and sAPPβ levels in human CSF from the lumbar region from cognitively normal and AD participants[33]. They identified a sAPPβ/sAPPα ratio of 0.59 $\pm$0.4 (n=15) in cognitively normal healthy controls. Wu et al. (2011) reported sAPPα and sAPPβ levels in human brain cortex samples from elderly subjects without AD (n=16) of 37.1 pmol/g and 50.8 pmol/g, respectively[27], resulting in a ratio of 0.73. However, both ratios do not directly reflect the ratio of APP cleaved by α-secretase and BACE1, as the steady state sAPPβ and sAPPα levels in brain are the result of multiple processes such as production, degradation and transfer from brain-to-CSF. Levels in CSF are also affected by transfer through the lumbar region. In the current analysis, the developed model facilitated the separation of the different processes involved.

The systems analysis points to a difference in biology of Aβ40 and Aβ42. Firstly, a lower formation rate for Aβ42 than for Aβ40 was identified. This is consistent with the composition of Aβ species reported for human CSF where the Aβ40 is the dominant isoform[34]. The relative production of Aβ40 and Aβ42 is probably regulated through changes in the γ-secretase cleavage site[35,34]. Secondly, the model included an Aβ_O pool in brain for Aβ42 but not Aβ40. Inclusion of exchange of an Aβ42 monomer pool with an Aβ_O pool could account for the differential effect of MBi-5 on Aβ40 and Aβ42 response observed in the data, in which the response for Aβ40 was higher than for Aβ42. Without incorporation of the Aβ_O pool in the model, the Aβ40 and Aβ42 response could not both be described adequately by a single drug effect. The identification of this Aβ_O constitutes the scientific basis for the identification of BACE1 inhibitor effects on higher ordered amyloid species. Due to the dissociation of Aβ42 oligomers to Aβ42 monomers during BACE1 inhibition the response for Aβ42 was lower than for Aβ40. The differential effect of the Aβ_O pool on Aβ42 is consistent with the biology of oligomer- and plaque formation where Aβ42 plays a more significant role than Aβ40[1]. Aβ42 is the major constituent of plaque and other species such as oligomers[31,36].

The baseline level of the Aβ_O pool estimated by the model of 278 pM (1,255 pg/mL) should be interpreted as the level of Aβ42 monomers that is incorporated in the 'oligomer soup' in the brain, i.e. Aβ dimers, trimers and high molecular weight species[3]. Here, no distinction is made between oligomeric species, as the Aβ_O pool is modelled as a pool in equilibrium with monomeric Aβ42 without correction for the number of subunits in multimeric species comprising the Aβ_O pool.

The $A\beta_O$ dissociation rate (*Krev*) of 1.308×10^{-5} s^{-1} identified here is relatively slow compared to the dissociation of $A\beta$ aggregates acquired from *in vitro* analysis techniques. Gruning et al. (2013) detected the appearance of monomers from $A\beta 42$ and $A\beta 40$ protofibrils: the dissociation rate was 1.4×10^{-4} and 1.2×10^{-4} s^{-1} for $A\beta 42$ and $A\beta 40$, respectively. Narayan et al. (2012) reported $A\beta 40$ fibrils releasing soluble $A\beta 40$ species at a rate of 9.3×10^{-5} s^{-1}. Sánchez et al. (2011) identified $A\beta$ monomer off-rates of 0.6×10^{-2} and 1.0×10^{-2} s^{-1} for $A\beta 40$ and $A\beta 42$ fibrils. It is difficult to compare rates obtained *in vivo* to those determined using *in vitro* approaches, as the *in vitro* experimental settings can have major impact. Moreover, the comparability of the dissociation rates to the value obtained in the current analysis is limited, because no particular oligomeric species was characterized in the systems pharmacology approach.

Quantitative measurements of the response of $A\beta_O$ to drugs targeting the APP pathway, such as BACE1 inhibition, is of interest. Initial results of a new sensitive $A\beta$ oligomer assay[5] suggest an $A\beta_O$ baseline level of ~1.5 pg/mL in rhesus CSF from the cisterna magna, which constitutes different oligomeric species (Mary Savage, Juliya Kalinina, unpublished observations). This number cannot be compared directly to the model derived $A\beta_O$ baseline of 1,255 pg/mL representing $A\beta$ subunits in the 'oligomer soup' in the brain. Also, the $A\beta$-oligomer assay may not pick up all oligomeric species or $A\beta_O$ may dissociate to monomers during sample preparation. Furthermore, it remains to be seen if CSF $A\beta_O$ measurements accurately reflect the brain $A\beta_O$ concentrations[40]. The hydrophobicity of oligomers may make them very low or absent in aqueous fluids as CSF[8]. Recent data suggest that human CSF $A\beta_O$ range between 0.1 and 10 pg/mL and human brain $A\beta_O$ levels are 252 pg/mL in AD and 87 pg/mL in control brain[5]. Other data suggest 1,000-fold higher concentrations of $A\beta_O$ than monomers in the soluble fraction of human AD cerebral cortex[8]. Relative concentrations in CSF will not necessary reflect the relative concentrations in brain as oligomers are likely cleared to CSF much more slowly than monomeric $A\beta$. Additional dose-ranging studies of BACE1 inhibition in rhesus in which $A\beta_O$ response is quantified, are ongoing. It is anticipated that including such data in the systems pharmacology model analysis will elucidate the relationship between the $A\beta_O$ pool in the model and measurements of $A\beta_O$.

The identified $A\beta_O$ pool should be interpreted with caution as an $A\beta_O$ pool in rhesus may differ from an $A\beta_O$ pool in AD patients with plaque burden. Rhesus do not develop dementia and neurodegenerative changes that characterize AD[41]. It is almost certain that the rhesus used in this study had far less amyloid deposition than a human AD patient. Therefore, the most crucial question is the nature of the identified $A\beta_O$ pool in rhesus and

its pathological relevance to AD in human. Aβ oligomerization is a separate aggregation event. Certain oligomers are off-pathway species that do not further aggregate to amyloid fibrils. Coexistence of several oligomeric populations that do or do not propagate into fibrils is possible. If it can be demonstrated that there is a relationship between the soluble Aβ_O identified in rhesus and the AD brain-derived soluble Aβ_O and this could be correlated with neurotoxicity, then the relevance of Aβ_O in rhesus would be indisputable.

The lack of success of clinical trials targeting the APP pathway has been ascribed to the failure to reduce the level of toxic Aβ_O [40]. Plaques, toxic Aβ_O and Aβ peptides should be targeted to significantly reduce soluble Aβ load because of the relationship between these three. It has been hypothesized that by decreasing Aβ levels, soluble Aβ_O amounts are also reduced, in turn inducing the release of Aβ_O from plaques to restore the balance between Aβ_O in the plaques and the extracellular environment [40].

The ability to identify and estimate the oligomerization effect through modelling suggested that these efforts to model the monomer pathway may also provide information on the higher ordered amyloid species. The ability to see this effect suggested that Aβ production inhibition by MBi-5 may also have the ability to draw down these forms as well as inhibit Aβ *de novo* production. In an APP transgenic mice study it has been demonstrated that BACE1 inhibition reduces amyloid plaque load (Kennedy and Hide, unpublished observations). This implies that if monomeric Aβ levels decrease as result of blocked Aβ production, Aβ_O dissociate to restore the equilibrium between monomeric Aβ and Aβ_O. To confirm this, incorporation of Aβ_O data into the model using rhesus data is ongoing.

A comprehensive model of the APP pathway describing the effects the BACEi MBi-5 has been established, taking into account the kinetics and interrelationships of sAPPα, sAPPβ, Aβ40 and Aβ42. The effect of BACE1 inhibition was incorporated in the model as inhibition of the formation rate of sAPPβ. As sAPPβ and C99 are both products of the same BACE1 cleavage step, the response of sAPPβ could be used as driver of Aβ response. However, sAPPβ and C99 could be subjected to different elimination processes as C99 remains membrane bound [42]. The fact that the Hill coefficient of the concentration response relationship slightly deviates from unity may be a reflection of this simplification of the underlying biological system. To adequately separate the sequential cleavage steps of BACE1 and γ-secretase from other processes involved, data from a γ-secretase inhibitor study in CMP rhesus [18] will be added to inform the model further (ongoing).

As BACE1 is the initiating enzyme in Aβ production, its inhibition has been proposed

to decrease the amount of cerebral $A\beta$ and to subsequently prevent the development of $A\beta$-associated pathologies[43]. With the developed systems pharmacology model a deeper comprehension of the effects of BACEi on the APP processing pathway and the anticipated effect on $A\beta_O$ was gained. Understanding these effects early in preclinical development could improve the anticipation of the magnitude of $A\beta$ reducing effects in humans. The model forms the first step in developing a translational systems model to predict possible $A\beta$ response of new drug candidates in human, based on their estimated potency in rhesus.

References

1. Di Carlo, M., Giacomazza, D., & San Biagio, P.L. Alzheimer's disease: biological aspects, therapeutic perspectives and diagnostic tools. J physics Condens matter an Inst Phys J. 2012;24(24):244102.

2. Hardy, J. & Selkoe, D.J. The amyloid hypothesis of Alzheimer's disease: progress and problems on the road to therapeutics. Science. 2002;297(5580):353–6.

3. Benilova, I., Karran, E., & De Strooper, B. The toxic Aβ oligomer and Alzheimer's disease: an emperor in need of clothes. Nat Neurosci. 2012;15(3):349–357.

4. Klein, W.L. Synaptotoxic amyloid-β oligomers: a molecular basis for the cause, diagnosis, and treatment of Alzheimer's disease? J Alzheimer's Dis. 2013;33:S49–S65.

5. Savage, M.J., *et al.* A sensitive Aβ oligomer assay discriminates Alzheimer's and aged control cerebrospinal fluid. J Neurosci. 2014;34(8):2884–97.

6. Esparza, T.J., *et al.* Amyloid-beta oligomerization in Alzheimer dementia vs. high pathology controls. Ann Neurol. 2013;73(1):104–119.

7. Mc Donald, J.M., *et al.* The presence of sodium dodecyl sulphate-stable Aβ dimers is strongly associated with Alzheimer-type dementia. Brain. 2010;133:1328–41.

8. Yang, T., Hong, S., O'Malley, T., Sperling, R.A., Walsh, D.M., & Selkoe, D.J. New ELISAs with high specificity for soluble oligomers of amyloid β-protein detect natural Aβ oligomers in human brain but not

CSF. Alzheimer's Dement. 2013;9(2):99–112.

9. Esler, W.P. & Wolfe, M.S. A portrait of Alzheimer secretases - New features and familiar faces. Science. 2001;293(5534):1449–54.

10. Wiltfang, J., *et al.* Higly conserved and disease-specific patterns of carboxyterminally truncated Aβ peptides 1-37/38/39 in addition to 1-40/42 in Alzheimer's disease and in patients with chronic neuroinflammation. J Neurochem. 2002;81(3):481–496.

11. Portelius, E., Mattsson, N., Andreasson, U., Blennow, K., & Zetterberg, H. Novel A Isoforms in Alzheimer's Disease - Their Role in Diagnosis and Treatment. Curr Pharm Des. 2011;17(25):2594–2602.

12. Husain, M.M., Kenneth, T., Siddique, H., & McClintock, S.M. Present and prospective clinical therapeutic regimens for Alzheimer's disease. Neuropsychiatr Dis Treat. 2008;4(4):765–777.

13. Yan, R. & Vassar, R. Targeting the β secretase BACE1 for Alzheimer's disease therapy. Lancet Neurol. 2014;13(3):319–329.

14. Lu, Y., *et al.* Cerebrospinal fluid amyloid-β (Aβ) as an effect biomarker for brain Aβ lowering verified by quantitative preclinical analyses. J Pharmacol Exp Ther. 2012;342(2):366–75.

15. Jack, C.R. & Holtzman, D.M. Biomarker modeling of Alzheimer's disease. Neuron. 2013;80(6):1347–1358.

16. Podlisny, M.B., Tolan, D.R., & Selkoe, D.J. Homology of the amyloid beta protein precursor in monkey and human supports a primate model for beta amyloidosis in Alzheimer's disease. Am J Pathol. 1991;138 (6):1423–1435.

17. Gilberto, D.B., *et al.* An alternative method of chronic cerebrospinal fluid collection via the cisterna magna in conscious rhesus monkeys. Contemp Top Lab Anim Sci. 2003;42 (4):53–59.

18. Cook, J.J., *et al.* Acute γ-secretase inhibition of nonhuman primate CNS shifts amyloid precursor protein (APP) metabolism from amyloid-β production to alternative APP fragments without amyloid-β rebound. J Neurosci. 2010;30(19):6743–50.

19. Lu, Y., *et al.* Cerebrospinal fluid β-amyloid turnover in the mouse, dog, monkey and human evaluated by systematic quantitative analyses. Neurodegener Dis. 2013;12(1): 36–50.

20. Janson, J., *et al.* Population PKPD modeling of BACE1 inhibitor-induced reduction in Aβ levels in vivo and correlation to in vitro potency in primary cortical neurons from mouse and guinea pig. Pharm Res. 2014;31 (3):670–83.

21. Parkinson, J., *et al.* Modeling of age-dependent amyloid accumulation and γ-secretase inhibition of soluble and insoluble Aβ in a transgenic mouse model of amyloid deposition. Pharmacol Res Perspect. 2013;1 (2):e00012.

22. Liu, X., *et al.* Mechanistic pharmacokinetic-pharmacodynamic modeling of BACE1 inhibition in monkeys: development of a pre-dictive model for amyloid precursor protein processing. Drug Metab Dispos. 2013;41 (7):1319–28.

23. Potter, R., *et al.* Increased in vivo Amyloid-β42 production, exchange, and irreversible loss in Presenilin Mutations Carriers. Sci Transl Med. 2013;5(189):189ra77.

24. Danhof, M., Alvan, G., Dahl, S.G., Kuhlmann, J., & Paintaud, G. Mechanism-based pharmacokinetic-pharmacodynamic modeling - A new classification of biomarkers. Pharm Res. 2005;22(9):1432–7.

25. Danhof, M., De Jongh, J., De Lange, E.C., Della Pasqua, O., Ploeger, B.A., & Voskuyl, R.A. Mechanism-based pharmacokinetic-pharmacodynamic modeling: biophase distribution, receptor theory, and dynamical systems analysis. Annu Rev Pharmacol Toxicol. 2007;47:357–400.

26. Dobrowolska, J.A., *et al.* CNS amyloid-β, soluble APP-α and -β kinetics during BACE inhibition. J Neurosci. 2014;34(24): 8336–8346.

27. Wu, G., Sankaranarayanan, S., Hsieh, S.H.K., Simon, A.J., & Savage, M.J. Decrease in brain soluble amyloid precursor protein β (sAPPβ) in Alzheimer's disease cortex. J Neurosci Res. 2011;89(6):822–32.

28. Sankaranarayanan, S., *et al.* First demonstration of cerebrospinal fluid and plasma Aβ lowering with oral administration of a β-site amyloid precursor protein-cleaving enzyme 1 inhibitor in nonhuman primates. J Pharmacol Exp Ther. 2009;328(1):131–140.

29. Beal, S.L. NONMEM Users Guide: Introduction to Version VI GloboMax

ICON Development Solutions;Ellicott City, MD;2008.

30. Nelson, D.L. & Cox, M.M. Lehninger Principles of Biochemistry 3rd ed. Worth Publishers;New York;2000.

31. Iwatsubo, T., Odaka, A., Suzuki, N., Mizusawa, H., Nukina, N., & Ihara, Y. Visualization of Aβ42(43) and Aβ40 in senile plaques with end-specific Aβ monoclonals: evidence that an initially deposited species is Aβ42(43). Neuron. 1994;13(1):45–53.

32. Cheng, X., Wu, J., Geng, M., & Xiong, J. The role of synaptic activity in the regulation of amyloid beta levels in Alzheimer's disease. Neurobiol Aging. 2014;35(6):1217–1232.

33. Dobrowolska, J.A., *et al.* Diurnal patterns of soluble amyloid precursor protein metabolites in the human central nervous system. PLoS One. 2014;9(3):e89998.

34. Murphy, M.P., Hickman, L.J., Eckman, C.B., Uljon, S.N., Wang, R., & Golde, E.T. γ-Secretase, evidence for multiple proteolytic activities and influence of membrane positioning of substrate on generation of amyloid β peptides of varying length. J Biol Chem. 1999;274(17):11914–11923.

35. Dolev, I., *et al.* Spike bursts increase amyloid-β 40/42 ratio by inducing a presenilin-1 conformational change. Nat Neurosci. 2013;16(5):587–95.

36. Jarrett, J.T., Berger, E.P., & Lansbury, P.T. The carboxy terminus of the β amyloid protein is critical for the seeding of amyloid formation: Implications for the pathogenesis of Alzheimer's disease. Biochemistry. 1993;32(18):4693–4697.

37. Grüning, C.S.R., *et al.* The off-rate of monomers dissociating from amyloid-β protofibrils. J Biol Chem. 2013;288(52): 37104–11.

38. Narayan, P., *et al.* The extracellular chaperone clusterin sequesters oligomeric forms of the amyloid-β1-40 peptide. Nat Struct Mol Biol. 2012;19(1):79–83.

39. Sánchez, L., *et al.* Aβ40 and Aβ42 amyloid fibrils exhibit distinct molecular recycling properties. J Am Chem Soc. 2011;133(17): 6505–6508.

40. Rosenblum, W.I. Why Alzheimer trials fail: removing soluble oligomeric beta amyloid is essential, inconsistent, and difficult. Neurobiol Aging. 2014;35(5):969–974.

41. Heuer, E., Rosen, R.F., Cintron, A., & Walker, L.C. Nonhuman primate models of Alzheimer-like cerebral proteopathy. Curr Pharm Des. 2012;18(8):1159–1169.

42. Selkoe, D.J. Translating cell biology into therapeutic advances in Alzheimer's disease. Nature. 1999;399(6738 Suppl):A23–31.

43. Cole, S.L. & Vassar, R. The basic biology of BACE1: A key therapeutic target for Alzheimer's disease. Curr Genomics. 2007;8(8):509–530.

Chapter 3

Supplemental Material

E.M.T. van Maanen, T.J. van Steeg, M.S. Michener, M.J. Savage, M.E. Kennedy, H.J. Kleijn, J.A. Stone, M. Danhof

Pharmacokinetic Data Analysis MBi-5

The exposure at the target site in the brain can rarely be quantified directly. In the cisterna magna ported (CMP) rhesus monkey model exposure can be measured in cerebrospinal fluid (CSF) in addition to plasma. The pharmacokinetics (PK) in plasma and CSF can be used to derive a measure of exposure at the target site. Therefore, a population PK model was developed that describes the PK of MBi-5 in plasma and CSF in CMP rhesus monkeys. The results of the PK analysis of MBi-5 were included in the subsequent PK-PD analysis.

The PK model was developed and fitted to the data by means of non-linear mixed effects modelling using the NONMEM software package version VI level 2 (see the Materials and Methods section in chapter 3).
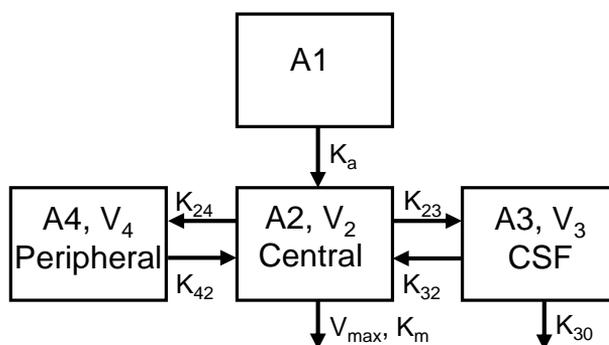
Figure S3.1: Schematic of the population PK model for MBi-5, that comprised of a dose, central, peripheral and CSF compartment.
Rate constants for the individual compartments are K_a (absorption), K_{24} (rate constant from central to peripheral), K_{42} (rate constant from peripheral to central), K_{23} (rate constant from central to CSF), K_{32} (rate constant from CSF to central). *A1*, *A2*, *A3*, *A4*, V_2, V_3 and V_4 are amounts (A) and volume of distribution (V) of MBi-5 in dose, central, CSF and peripheral compartments, respectively. K_{30} is the elimination rate in CSF compartment. V_{max} is the maximum velocity; K_m is the Michaelis-Menten constant.

The compartmental PK model of MBi-5 was based on simultaneous analysis of plasma and CSF PK data. The PK profiles of MBi-5 in plasma and CSF were adequately described by a model containing three compartments: a central, peripheral and CSF compartment (Supplemental Figure S3.1). The CSF compartment is linked to the central compartment, with exchange determined by rate constants K_{32} and K_{23}. The model

considered elimination from the central and CSF compartment, where the elimination from the central compartment (K_{20}) is described by the Michaelis-Menten equation (Equation S3.1).

$$K_{20} = \frac{V_{MAX}}{K_M + \frac{A_2}{V_2}} \tag{S3.1}$$

The rate of change in each compartment can be expresses as:

$$\frac{d}{dt}A_1 = -K_a \times A_1 \tag{S3.2}$$

$$\begin{aligned}\frac{d}{dt}A_2 =& K_a \times A_1 - K_{24} \times A_2 + K_{42} \times A_4 - K_{23} \times A_2 + K_{32} \times A_3 \\ & - \frac{V_{MAX} \times A_2}{K_M + \frac{A_2}{V_2}}\end{aligned} \tag{S3.3}$$

$$\frac{d}{dt}A_3 = K_{23} \times A_2 - K_{32} \times A_3 - K_{30} \times A_3 \tag{S3.4}$$

$$\frac{d}{dt}A_4 = K_{24} \times A_2 - K_{42} \times A_4 \tag{S3.5}$$

MBi-5 displayed nonlinear PK at different kinetic levels. The extent of the absorption decreased with an increase in dose (K_a, from 10.0 to 0.144 h^{-1} for 10 and 125 mg/kg, respectively). The distribution to the CSF compartment appeared to be saturable, reflected in a decrease in the rate constant from the central to CSF compartment for the 125 mg/kg dose (K_{23}, from 0.000488 to 0.000116 h^{-1}). Elimination was identified from the central and CSF compartment. As the elimination of MBi-5 from the central compartment followed Michaelis-Menten kinetics (Supplemental Equation S3.1) the clearance in the central compartment changed as function of time and concentration ($CL_2 = K_{20}(t,Cp) \times V_2$). At the doses included in the current investigation, clearance in the CSF compartment ($CL_3 = K_{30}{}^*V_3$) was approximately 10^6-fold greater than clearance from the central

compartment, indicating that the CSF clearance route contributes remarkably.

Table S3.1 shows all PK parameter estimates. The volume of the CSF compartment could not be estimated and was fixed to a small value (0.0250 L). Interanimial variability was quantified for the volume of the central compartment (V_2). Residual variability (proportional error) was higher for the CSF than for the plasma concentration (0.628 and 0.188 for CSF and plasma, respectively).

The developed PK model gives an adequate description of plasma and CSF concentration-time profiles, as can be seen from plots of the simulated and observed concentrations *versus* time profiles with 90% confidence interval (Figure S3.2).

PK data from the CMP rhesus monkey show that there is substantial CSF exposure after oral dosing (10 fold lower than in plasma). The data suggest that MBi-5 concentrations in brain, expected to be in between plasma and CSF levels, are sufficient to adequately inhibit β-secretase activity in brain. The plasma and CSF concentrations *versus* time profiles predicted from the model had a good fit to the values observed in the rhesus monkeys. Thus, the model could serve as input for PD model analysis.

Table S3.1: Population parameter estimates including coefficient of variation (CV%) for the PK model of MBi-5

PARAMETER	DESCRIPTION	VALUE	UNIT	CV%
Structural parameters				
V_2	central volume	122	L	18.9
Q_4	intercompartmental clearance	2.01	$L.h^{-1}$	53.2
FV_4[a]	peripheral volume as fraction of central volume	0.488		42.8
K_m	Michaelis-Menten constant	6.24	μM	24.4
V_{max}	maximum velocity	1.04	$\mu M.h^{-1}$	25.7
K_a dose10[b]	absorption rate dose10	10.0	h^{-1}	-
K_a dose30	absorption rate dose30	0.250	h^{-1}	47.6
FK_a[c]	absorption rate dose125 as fraction of K_a dose30	0.579		37.0
K_{23}	rate constant from central to CSF	0.000488	h^{-1}	37.7
FK_{23} dose 125[d]	K_{23} for dose125 as fraction	0.239		23.5
K_{30}	elimination rate CSF compartment	34.5	h^{-1}	21.2
V_3[b]	volume CSF compartment	0.0250	L	-
Interanimal variability				
ω^2_{V2}	Interanimal variability central volume	0.0612		27.0
Residual error				
σ^2_{plasma}	Residual variabiliy plasma	0.188		10.5
σ^2_{CSF}	Residual variabiliy CSF	0.628		26.4

[a] $V_4 = V_2 \times FV_4$.

[b] Fixed.

[c] K_a dose125 = K_a dose30 $\times FK_a$.

[d] K_{23} dose125 = $K_{23} \times FK_{23}$.
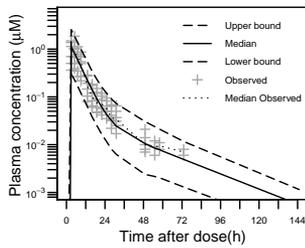
(A) 10 mg/kg MBi-5 plasma
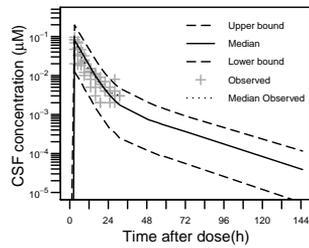
(B) 10 mg/kg MBi-5 CSF
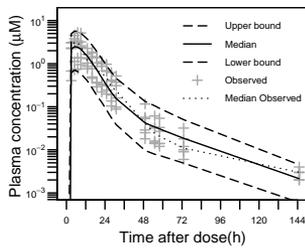
(C) 30 mg/kg MBi-5 plasma
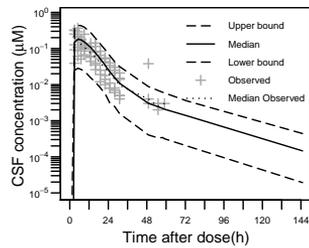
(D) 30 mg/kg MBi-5 CSF
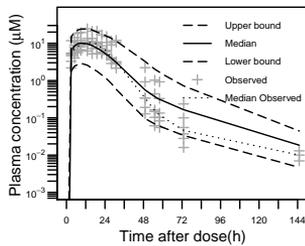
(E) 125 mg/kg MBi-5 plasma
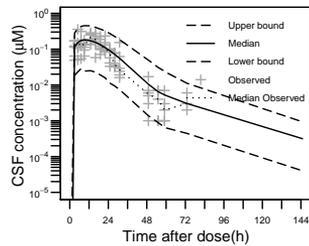
(F) 125 mg/kg MBi-5 CSF

Figure S3.2: Visual predictive check of plasma* (left panels) *and CSF* (right panels) *concentration time profile of MBi-5 in the rhesus with 90% confidence interval.
The rhesus were administered with 10 mg/kg (A) (B), 30 mg/kg (C) (D) and 125 mg/kg (E) (F) MBi-5. Observation sample size: n=102 for plasma and CSF per dose from 6 monkeys collected over 7 days.
Plus-symbols represent observed measurements. Dotted line corresponds to the median observed profile. Solid lines show the median simulated profiles. The longs-dashed lines correspond to the 90% prediction intervals obtained from 1000 individual simulated profiles.
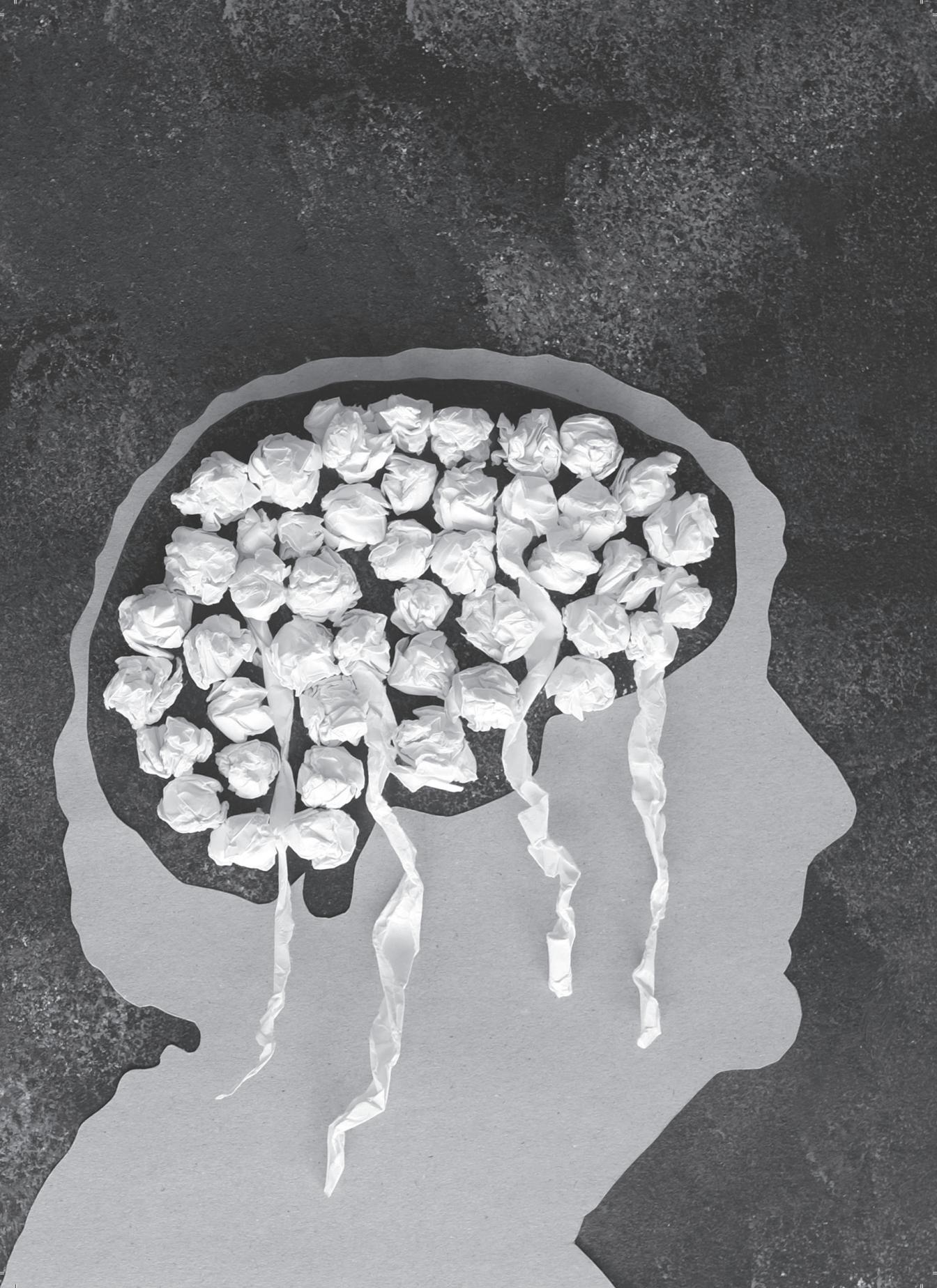
Chapter 4

Integrating tracer kinetic data in a systems
pharmacology model of the amyloid precursor
pathway: effect of a β-secretase inhibitor

E.M.T. van Maanen, T.J. van Steeg, J.A. Dobrowolska Zakaria,
M.S. Michener, M.J. Savage, M.E. Kennedy, R.J. Bateman,
H.J. Kleijn, J.A. Stone, M. Danhof

Abstract

Purpose: To assess the ability of a recently developed systems pharmacology model of the β-amyloid precursor protein (APP) pathway to predict the tracer kinetics of APP metabolites following administration of a β-secretase inhibitor.

Methods: A stable isotope tracer $^{13}C_6$-labelled Leucine was administered to cisterna magna ported (CMP) rhesus monkeys in conjunction with the β-secretase (BACE1) inhibitor MBi-5. The fraction labelled APP metabolites (total Aβ, sAPPα , sAPPβ) were measured over 145 hours. A systems pharmacology model of the APP pathway, recently developed using information on CSF absolute concentrations of the APP metabolites (Aβ40, Aβ42, sAPPβ and sAPPα), was used as the basis for the prediction of the tracer kinetic data.

Results: BACE1 inhibition by MBi-5 resulted in a concentration driven saturable effect on the APP pathway as reflected in the absolute concentrations of the metabolites, fraction labelled Aβ and sAPPβ. In contrast, this MBi-5 concentration dependency was not observed in the fraction labelled sAPPα because similar drug effects on both the labelled and unlabelled pools for this marker yield a lack of dose-differentiation in this relative biomarker. The recent APP systems model and absolute concentrations of the APP metabolites support a dose-dependent response. The current results indicate that interpretation of fraction labelled data is complex and best achieved with a kinetic model. Aβ40 and Aβ42 dynamics did not fully explain the measured fraction labelled Aβ. The model was used to demonstrate that a contribution of other Aβ isoforms with altered dynamics from Aβ40 and Aβ42 is a potential explanation.

Conclusions: This analysis demonstrated that using a systems pharmacology model to integrate tracer kinetic data with absolute protein concentrations enables a more accurate interpretation of the tracer kinetic data.

Key words

81

Introduction

The accumulation of amyloid-β (Aβ) peptide in the brain parenchyma as result of over-production and/or decreased clearance has been implicated in the pathophysiology of Alzheimer's disease (AD)[1]. Toxic soluble Aβ oligomers (Aβ_O) are considered to be the drivers of the neurodegeneration in the brains of patients with AD[2]. Modulation of Aβ is a therapeutic target for AD, with the potential for eliciting a disease modifying effect by reducing high levels of Aβ peptides and subsequently preventing the development of Aβ associated pathologies[3,4]. One of the main therapeutic strategies aims at Aβ reduction through the inhibition of secretases responsible for their production.

Aβ peptides are generated by two sequential proteolytic cleavages of the β-amyloid precursor protein (APP)[5]. The first step is catalyzed by β-site APP-cleaving enzyme (BACE1, also called β-secretase) to yield the N-terminal fragment soluble APPβ (sAPPβ) and the C-terminal membrane-bound 99-aminoacid fragment (C99). C99 undergoes further cleavage by a second protease known as γ-secretase to generate Aβ species of different chain lengths, the major variants having 38 (Aβ38), 40 (Aβ40) or 42 (Aβ42) amino acids[6]. A third protease, α-secretase, cleaves APP within the Aβ sequence generating non-amyloidogenic soluble APPα (sAPPα) and precluding the formation of the major Aβ variants[7]. A new APP processing pathway was recently reported by Willem et al. (2015), in which sequential cleavage of APP by η-secretase and BACE1 or ADAM10 leads to the formation of A$\eta - \beta$ and A$\eta - \alpha$, respectively. There may be other alternate pathways unknown at this time.

To improve the prediction of therapeutic effects on Aβ burden, an understanding of the behaviour of the APP system as a whole, as opposed to the behaviour of its individual components, is imperative. This requires a quantitative analysis of the dynamic interactions between drugs and the APP processing pathway. To this end, a systems pharmacology model of the APP processing pathway was reported recently[9].

The model was based on the absolute concentrations of APP metabolites sAPPα, sAPPβ, Aβ40 and Aβ42 and described their kinetics and interrelationships following β-secretase inhibition. In the current analysis, we evaluated whether the systems pharmacology model could adequately describe the tracer kinetic data of the APP metabolites following β-secretase inhibition.

Tracer kinetic studies have been introduced to gain understanding of the dynamics of the APP pathway following secretase inhibition. In 2007 Bateman et al.[10] published a stable isotope labeling kinetics (SILK) protocol for quantification of Aβ production

and clearance rates in the brain. In short, a tracer is infused intravenously after drug administration and the proportion of synthesized labelled APP metabolites is monitored for 145 hours. The SILK protocol measures the fraction of APP metabolites labelled with tracer. In addition, many of the SILK studies used liquid chromatography/MS or enzyme linked immunosorbant assay (ELISA) to measure absolute APP metabolite concentrations[11,12,13]. Integrating the tracer kinetic data with absolute protein concentration measurements yields detailed insights in the functioning of the underlying biological system. For example, tracer kinetics combined with absolute protein concentrations have led to observations such as increased rates of the production of Aβ in carriers of the PSEN1 mutation and a reported dose-dependent decrease in Aβ production with γ-secretase inhibitors in humans[11,14]. The technique has also been applied to define a clear related change in slowed Aβ half-life and increasing age[12].

The objective of the current investigation is to compare the findings of the novel systems pharmacology model of the APP pathway to the tracer kinetic data. To this end, we extended the recently developed systems pharmacology model, by accounting for tracer dynamics throughout the APP pathway. Such an approach involves a quantitative analysis of the drug concentrations, plasma tracer enrichment and biomarker responses (absolute and fraction labelled proteins) using a comprehensive mathematical model that describes the underlying biological processes, while making a strict distinction between drug-specific and systems specific parameters. This allows for detailed interpretation of the biomarker responses by accounting for interdependencies among biomarkers as well as allowing for separation of rate *versus* extent of effects on the system. In this manner invaluable information is obtained on the functioning of the integrated biological system.

Dose ranging, biomarker, plasma tracer enrichment and pharmacokinetic data obtained from cisterna magna ported (CMP) rhesus monkeys receiving single doses of the BACE1 inhibitor MBi-5 and an infusion of the stable isotope tracer $^{13}C_6$-labelled Leucine ($^{13}C_6$-L) were available. The biomarkers measured were APP metabolites (Aβ40, Aβ42, sAPPβ and sAPPα); their concentrations were determined by ELISA. SILK was utilized to determine plasma enrichment $^{13}C_6$-L and fraction $^{13}C_6$-L labelled APP metabolites (fraction labeled sAPPβ, fraction labeled sAPPα, fraction labeled total Aβ).

The application of a systems pharmacology model based analysis accounting for tracer dynamics throughout the APP pathway revealed the similarities and differences in response measurements to BACE1 inhibition as determined by ELISA and SILK and these are discussed in this manuscript.

Materials and Methods

Animals

The CMP rhesus monkey model was described by Gilberto et al. (2003). The rhesus monkeys are chronically implanted with catheters in the cisterna magna, allowing repeated sampling of CSF and plasma. Six male animals, weighing between 5.2 and 11.7 kg (average, 8.7 kg), age 2 to 10 years (average, 8 years), were included in the study. Data from one animal was excluded from the analysis because of problems with the GS-MS.

These monkeys were captive-bred in a closed colony and individually housed. Animal use procedures were conform to the Guide for the Care and Use of Laboratory Animals[16].

In vivo labeling protocol

The $^{13}C_6$-Leucine infusion protocol was previously described by Cook et al. (2010). In brief, the monkeys were administered $^{13}C_6$-labelled Leucine ($^{13}C_6$-L) intravenously, with a primed infusion of 4 mg/kg bolus over 10 minutes, followed by 12 h of continuous infusion at a rate of 4 mg/kg/h. The primed 12 h $^{13}C_6$-L infusion was administered 1 hour post drug administration. The study protocol was described previously by Dobrowolska et al. (2014). CSF was sampled at -21, -19, 0 (pre-drug dose) and 3, 5, 7, 9, 13, 16, 19, 22, 25, 28, 31, 49, 55, 58, 73 and 145 h post drug administration, resulting in 19 samples for each monkey per treatment group to determine fraction labeled total $A\beta$, fraction labeled sAPPα and fraction labeled sAPPβ. Blood was sampled at 0 (pre-drug dose) and 3, 5, 7, 9, 13, 16, 19, 22, 25, 28, 31 and 49 h post drug administration resulting in 13 samples for each monkey per treatment group to assess the $^{13}C_6$-L enrichment in plasma.

GC-MS was used to quantify plasma $^{13}C_6$-L enrichment as previously described by Bateman et al. (2007) and Cook et al. (2010). $^{13}C_6$-L enrichment was quantified as a tracer-to-tracee ratio (TTR).

$A\beta$, sAPPα and sAPPβ were isolated by immunoprecipitation. To isolate $A\beta$ a combination of the antibodies W0-2, directed against $A\beta$5-8, and HJ5.1, raised against $A\beta$13-28, was used. The proteins were proteolytically cleaved into smaller peptide fragments. LC-ESI-tandem MS was used to quantify the amount of $^{13}C_6$-L labeling in total $A\beta$, sAPPα and sAPPβ at each time point. Fraction $^{13}C_6$-L labelled protein was calculated as the fraction of the signal intensities for labelled peptide fragments over the sum of the signal intensities for labelled and unlabelled peptide fragments[17]. For $A\beta$, the peptide quantified was $A\beta_{16-27}$.

Drug administration and sampling

In a single dose, four-way, full crossover study, MBi-5 was administered at 10, 30, 125 mg/kg (5 mL/kg), or vehicle (0.4% methylcellulose) PO, with at least two weeks washout between each period. In conjunction $^{13}C_6$-L was administered as described above. Plasma and CSF drug concentrations were collected at 0 (pre-drug dose) and 3, 5, 7, 9, 13, 16, 19, 22, 25, 28, 31, 49, 55, 58, 73 and 145 h post-drug dose, resulting in 17 plasma and CSF PK samples for each monkey per treatment group. 2 mL of blood and 1 mL of CSF were collected at each time point. The concentration of MBi-5 in the plasma and CSF samples was determined using LC-MS/MS. The pharmacological profile of MBi-5 was summarized by Dobrowolska et al. (2014).

The concentrations of Aβ40, Aβ42, sAPPα and sAPPβ were collected at -22, -20 and -1 h (pre-drug dose) and 2, 4, 6, 8, 12, 15, 18, 21, 24, 27, 30, 48, 54, 57, 72 and 144 h post-drug dose, giving 19 measurements of each biomarker for each monkey per treatment. 1 mL of CSF were collected at each time point. The assays used for the protein concentration measurements were described previously [18,19,20]. Neoepitope-specific antibodies were used to detect Aβ40 and Aβ42, directed against Aβ1-40 and Aβ1-42.

PK-PD analysis

The PK-PD model has been developed and fitted to the data by means of non-linear mixed effects modelling using the NONMEM software package version 7 level 2[21]. The NONMEM software package was implemented on an Intel QuadCore (Intel® Core™ i7-3370 CPU, 3.40 GHz, 4.00 GB RAM) and Compaq Visual Fortran (version 6.6, Compaq Computer Corporation, Houston, Texas, USA) was used as compiler.

Modeling techniques were detailed by Van Maanen et al[9]. A decrease of 10.8 points in the minimum value of the objective function by adding an additional parameter, corresponding to p<0.001 in a χ-squared distribution, was considered significant. Data management and model assessment were done using the statistical software package S-PLUS for Windows (TIBCO Spotfire S+® 8.2, TIBCO Software Inc.).

To validate the model a visual predictive check (VPC) was performed in which the median and the 90% inter-quantile range of the data simulated with the developed model were plotted together with the observations. A validated result is close agreement of median observed and predicted line with ∼90% of the observations falling within the 90% prediction interval.

Model description

The systems pharmacology model of MBi-5 was based on sequential analysis of plasma tracer enrichment, PK and PD data. For the description of plasma enrichment over time a model that considers two pools for both $^{13}C_6$-L and $^{12}C_6$-L was developed (see Supplemental Material 1). The model related tracer input ($^{13}C_6$-Leucine infusion, in mg/kg/hr) to the measured enrichment (tracer to tracee ratio, TTR in%) in plasma. The PK model of MBi-5 was based on simultaneous analysis of plasma and CSF PK data (see van Maanen et al. (2016)). The PK profiles of MBi-5 observed in plasma and CSF were adequately described, thus the model could serve as input for PD model analysis.

The PKPD model accounting for labelled and unlabelled species is an extension of the model presented in van Maanen et al. (2016). For each individual monkey, the PK of MBi-5 and kinetics of plasma tracer enrichment were utilized as two independent inputs, by using individual parameter estimates of the respective kinetic models. The biomarker response profiles of MBi-5 measured in CSF were adequately described by a model containing expressions to describe the time courses of APP, sAPPβ, sAPPα, Aβ40, Aβ42, Aβ_O, FactorX (Fig. 4.1). sAPPβ, sAPPα, Aβ40 and Aβ42 were informed by data, whereas APP, Aβ_O and FactorX were inferred based on the model and the data of aforementioned biomarkers. FactorX represents other (unknown) analytes quantified in fraction labelled Aβ *(vide infra)*.

The production of APP was believed to be zero order, i.e. a constant production of APP. It was assumed that there is no alternative proteolytic enzyme cleaving full length APP other than α-secretase and BACE1. As both sAPPβ and C99 are products of APP cleavage by BACE1, sAPPβ and C99 were assumed to follow the same kinetics and therefore sAPPβ could be used in the model as surrogate precursor for Aβ. The production of sAPPα, sAPPβ and Aβ were assumed to be first order, i.e. dependent on the concentration of its precursor. To keep track of tracer dynamics throughout the pathway, two differential equations were implemented for each variable to account for labelled and unlabelled species, in which the tracer is assumed to be metabolically indistinguishable from the tracee. The system of differential equations is presented in Supplemental Material 4. The label incorporation in the APP pathway is driven by the kinetic model of plasma enrichment (Supplemental Material 4, Eq. S4.8 and S4.9). The inhibition of the BACE1 cleavage by MBi-5 was described by a sigmoidal Imax function (Supplemental Material 4, Eq. S4.22) using the individual predicted target site concentration of MBi-5, derived from the PK model (Supplemental Material 4, Eq. S4.23), as driver of the response.
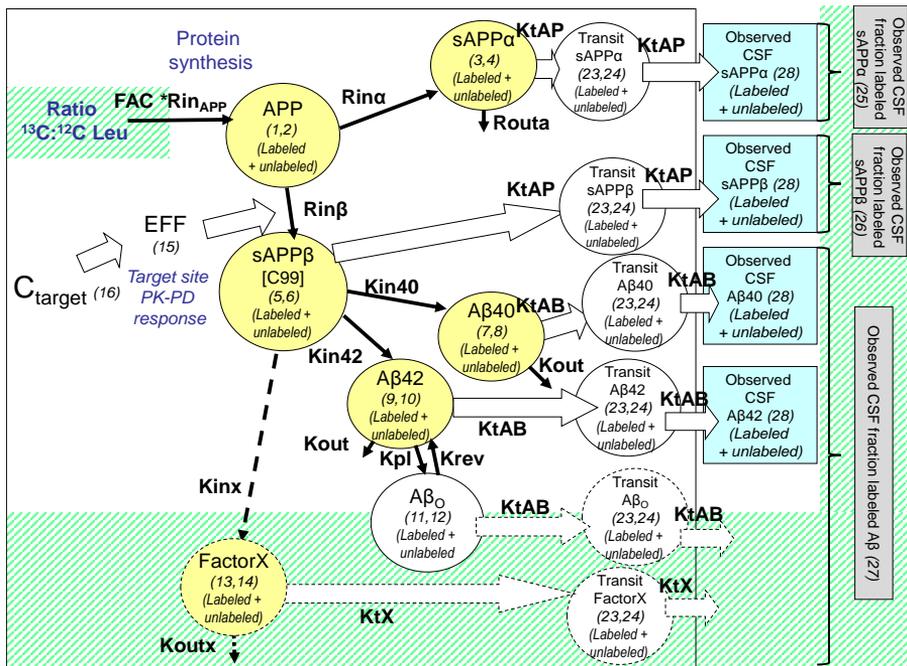
Figure 4.1: Schematic of systems model of APP processing.
The model comprised two times thirteen compartments: Six biomarker compartments in brain *(yellow circles)*, one oligomer compartment and six transit compartments from brain to CSF *(white circles)*, where each compartment was duplicated to track labelled and unlabelled species. Four biomarkers were measured in CSF (sAPPα, sAPPβ, Aβ40 and Aβ42), indicated by the blue boxes. Total concentrations (labelled plus unlabelled) of sAPPα, sAPPβ, Aβ40 and Aβ42 were measured using ELISA. Using SILK, fraction labelled sAPPα, fraction labelled sAPPβ and fraction labelled total Aβ were determined where fraction labelled total Aβ is labelled over total Aβ species. The drug effect *(EFF)* inhibited *Rinβ*. C_{target}, derived from the PK model, was used as driver of the biomarker response in the model[9]. sAPPβ was used in the model structure as a surrogate substrate for C99 in the γ-secretase cleavage step. The tracer PK model of label enrichment of the Leucine pool (see Supplemental Material 1) informed label incorporation into the APP pathway.

Dashed arrows and compartments are additions to the model structure compared to the model based on ELISA data only[9]. Model extensions are indicated with the green shaded area. Equation numbers for each compartment have been included inside parentheses in order to facilitate their identification (see Supplemental Material 4).

APP: Aβ-precursor protein; *Aβ*: amyloid-β-peptide; C_{target}: drug concentration target site; *Kin$_{40}$*: Aβ40 formation rate; *Kin$_{42}$*: Aβ42 formation rate; *Kin$_{x}$*: FactorX formation rate; *Kout*: Aβ40 and Aβ42 degradation rate; *Koutx*: FactorX degradation rate; *Krev*: Oligomer dissociation rate; *KtAP*: transit rate sAPPα and sAPPβ from brain to CSF; *Kpl*: Oligomerization rate; *KtAB*: transit rate Aβ from brain to CSF; *RinAPP*: source of APP; *Rinβ*: sAPPβ formation rate; *Rinα*: sAPPα formation rate; *Rout*: sAPPβ degradation rate; *Routa*: sAPPα degradation rate.

Results

Tracer enrichment in the brain

A kinetic model was used to describe the time course of the tracer enrichment in plasma during and after the infusion of the tracer. The model described tracer ($^{13}C_6$-L) and tracee (endogenous $^{12}C_6$-L) kinetics (see Supplemental Material 1).

Individual parameters from the kinetic tracer enrichment model were used to derive the enrichment at the target site in the brain. For this, the following assumptions were made: (1) there is no significant time delay between when the tracer is measured in plasma and when the tracer enters the brain. Any modest time delays in tracer entering the brain would be accounted for by later delay functions such as transit to CSF as the model could not independently assess this component of delay; (2) the shape of the enrichment-time profile in the brain is similar to that in plasma; (3) the probability of the incorporation of $^{13}C_6$-L into protein is the same as the probability that endogenous $^{12}C_6$-L is incorporated into protein; (4) none of the tracer incorporated into protein reappears as a consequence of protein breakdown in the time course of the tracer infusion. In the initial phase of tracer infusion the $^{13}C_6$-L incorporation in the APP metabolites is so small, that it is unlikely that $^{13}C_6$-L would be recycled by protein breakdown. Furthermore, protein turnover is assumed to be slow relative to the tracer infusion time.

No distinction can be made between the relative uptake of $^{13}C_6$-L in the APP pool and the transport of tracer from plasma to the brain. The blood-brain barrier transport is assumed not to be the rate-limiting step for $^{13}C_6$-L uptake in the APP pool. The relative formation of labelled and unlabelled APP species is related to the brain enrichment. Therefore, brain enrichment refers to the tracer ($^{13}C_6$-L) to tracee (endogenous $^{12}C_6$-L) ratio (TTR [%]) at the target site in the brain accessible for precursor (APP) formation. Consequently, brain enrichment can be derived using information from the placebo groups: if no inhibitor is given, and hence the system is in steady state, the sum of the labelled and unlabelled species is constant. A scale correction factor (*FAC*, see Supplement Material 4 Eq. S4.9) was applied to the plasma tracer enrichment, representing the relative uptake of tracer in the precursor (APP) pool. *FAC* was estimated to be 0.764 indicating that enrichment in the precursor pool was 76.4% of the level of plasma tracer enrichment.

Extension of the APP pathway model to account for tracer dynamics

Previously, a comprehensive systems model, incorporating the pharmacokinetics of MBi-5 and APP metabolites (Aβ40, Aβ42, sAPPα and sAPPβ) concentrations was developed[9].

The model quantified APP metabolite concentrations response to BACE1 inhibition and included an $A\beta_O$ compartment that could account for the differential effect of MBi-5 on $A\beta40$ and $A\beta42$ response. $sAPP\beta$ was used in the model structure as a surrogate substrate for C99 in the γ-secretase cleavage step. As $sAPP\beta$ and C99 are both products of the same cleavage step, their formation rates should be the same. Modeling efforts to separately account for $sAPP\beta$ and C99 did not improve the model description of the data and, therefore, demonstrated adequacy of the surrogate assumption.

For the current analysis, this model was extended to account for tracer dynamics throughout the APP pathway (Figure 4.1). The $^{13}C_6$-L label incorporation into the APP pathway is determined from the derived brain tracer enrichment. To account for labelled and unlabelled species, two compartments were implemented for each variable (APP, $sAPP\beta$, $sAPP\alpha$, $A\beta40$, $A\beta42$, $A\beta_O$). Accordingly, the absolute amount of each APP metabolite is the sum of its labelled and unlabelled species and the fraction labelled APP metabolite is the ratio of labelled over the sum of its labelled and unlabelled species, with the exception of $A\beta$ (Supplemental Material 4, Eq. S4.32-S4.34). In the SILK protocol no distinction was made between $A\beta40$ and $A\beta42$. Therefore, fraction labelled $A\beta$ was initially assumed to be equal to the fraction labelled of total $A\beta40$ and $A\beta42$.

At first, the model structure and parameter values were fixed to those identified recently on absolute APP metabolite concentration data[9]. The model was then used to predict the fraction labelled proteins (SILK). Here, underprediction was observed for fraction labeled $sAPP\beta$ (placebo, dose 30 and dose 125 mg/kg, Fig. 4.4C, 4.4O, 4.4U) and fraction labeled $sAPP\alpha$ (placebo, 10 mg/kg, 30 mg/kg, Fig. 4.4A, 4.4G, 4.4M). Overprediction was observed for fraction labeled $A\beta$ for all dose groups (Fig. 4.4E, 4.4K, 4.4Q, 4.4W). As the response measurements to BACE1 inhibition by ELISA and SILK were the result of inhibiting the same pathway step, difference in effects of BACE1 inhibition on the biomarkers was not expected. Therefore, the flawed model fit indicated that there was additional information content to be gained from the SILK data beyond that from the ELISA. As such this additional data helped to better refine the true mechanistic representation of the APP system.

Accounting for differences in APP metabolite response measurements by ELISA and SILK

Integrating kinetic modelling of labelled and absolute data allows for the inconsistency of the results to be more robustly evaluated beyond comparison of observed response measurements. The results indicated a inconsistency between response magnitudes by

ELISA and SILK within the framework of the previously established kinetic model. Likely, aspects misspecified would be related to how the label is incorporated into the pathway or in how the two quantitative measures related to each other.

It was hypothesized that differences in APP metabolite responses as measured by ELISA and SILK may be caused by some deeper compartment in the APP pathway that could not be identified based on ELISA data only. This could be an additional APP pool causing a release of labelled APP that feeds slowly into the system, or an C99 pool that gives a slow release of labelled C99 that feeds into the system. Inclusion of the additional APP pool in the model worsened the description of fraction labeled sAPPα (results not shown). This indicated that the cause of the discrepancy in measurements should be sought further down the APP pathway. It was not possible to identify an C99 model component based on the current dataset, with which it was not feasible to separate the γ-secretase cleavage step from sAPPβ elimination[9].

An understanding of the assay differences between SILK and ELISA could suggest another alternate explanation of the disconnect, as one technique may have measured analytes which the other did not. Possibilities include ELISA cross-reactivity to species which were not measured by the SILK method, e.g. η-secretase products[8], or SILK measured alternative APP fragments in addition to sAPPα, sAPPβ, Aβ40 or Aβ42. If the same analytes were measured in both methods, then fraction labeled Aβ (SILK) would be composed of labelled over total Aβ40 and Aβ42 species and absolute Aβ40 and Aβ42 protein concentrations (ELISA) would be the sum of its labelled and unlabelled species. If the analytes as measured in SILK differ from those in ELISA this assumption will not hold. Fraction labelled Aβ (SILK) is then composed of labelled over total Aβ40, Aβ42 and other analytes. Absolute Aβ40 and Aβ42 protein concentrations (ELISA) remain the sum of their labelled and unlabelled species. To address this, a FactorX compartment was incorporated in the model representing these other analytes.

It was investigated if the other analytes represented by FactorX have a similar degradation rate (*Koutx*) as Aβ40 and Aβ42 (*Kout*). The formation rate of FactorX (*Kinx*) was defined by steady state conditions and derived from the other parameters (Supplement Material 4 Eq. S4.29). As a result, *Kinx* had a different value than *Kin40* and *Kin42*. With the similar degradation rate and the derived formation rate of FactorX, the inclusion of FactorX in the calculation of fraction labeled Aβ had no impact on the fraction labeled Aβ curve (not shown). Because mathematically terms were canceled out in the calculation of fraction labeled Aβ including FactorX, the same fraction labeled Aβ as

based on only labelled over total Aβ40 and Aβ42 species was obtained. This indicated
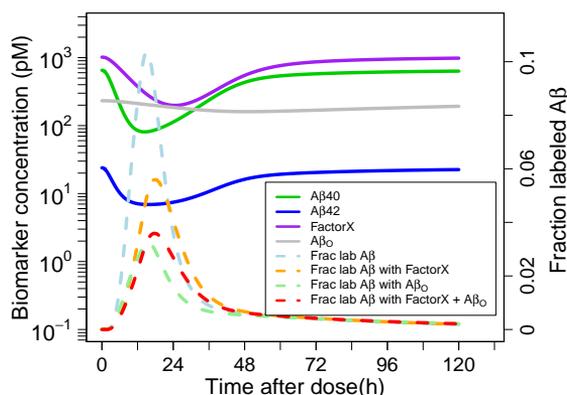
Figure 4.2: Graphical insight into the Aβ biomarker responses in CSF, using the identified systems model of the APP processing pathway.
The biomarker responses in CSF are predicted after a single dose of 125 mg MBi-5, using the typical parameter estimates.
Aβ40 green solid line; *Aβ42* blue solid line; *FactorX* purple solid line; $A\beta_O$ grey solid line; *fraction labeled Aβ* light blue dashed line; *fraction labeled Aβ with FactorX* orange dashed line; *fraction labeled Aβ with $A\beta_O$* light green dashed line; *fraction labeled Aβ with FactorX and $A\beta_O$* red dashed line.

that the analytes that were hypothesized to be additionally measured in SILK had to have different kinetics. Therefore, a different degradation rate for the analytes represented by FactorX was included in the model. The transit rate from brain-to-CSF for FactorX (*KtX*) was assumed to be similar to the transit rate for Aβ species (Aβ40 and Aβ42). The model including FactorX labelled and unlabelled species, with different kinetics for FactorX than for Aβ40 and Aβ42, improved the description of the SILK data (results not shown). Description was further improved by also including labelled over total $A\beta_O$ in fraction labelled Aβ as determined in CSF. For this, the transit of $A\beta_O$ from brain to CSF needed to be added to the model structure. This facilitated the identification of the $A\beta_O$ transit rate. When estimated the $A\beta_O$ transit rate was similar to the Aβ transit rate from brain to CSF (*KtAB*) and could therefore be fixed to the same high value $(10\,\text{h}^{-1})$[9]. It was not possible to identify the brain-turnover of $A\beta_O$ as a separate parameter. Therefore, the $A\beta_O$ half-life of 0.07 h reflects delays due to the brain-turnover and brain-to-CSF transfer. The value of the transit rate for sAPPα and sAPPβ *(KtAPP)* should be interpreted relative to the Aβ transit rate. By fixing *KtAB* all possible delay is lumped in *KtAPP*.

The right panels in Fig. 4.4 show the description of the SILK data for the model with FactorX and $A\beta_O$ included in the calculation of fraction labelled Aβ. A prediction was performed with the model to investigate the contribution of FactorX and $A\beta_O$ to

the fraction labeled $A\beta$ curve (Fig. 4.2). The FactorX level was slightly higher than $A\beta40$ and the shape of the FactorX response curve was different from the $A\beta40$ and $A\beta42$ responses due to the different degradation rate of FactorX (*Koutx*). Inclusion of FactorX and $A\beta_O$ in fraction labeled $A\beta$ had a lowering effect on the fraction labelled $A\beta$ curve and slightly altered its shape.

Comparison results based on ELISA and SILK *versus* ELISA only

Administration of MBi-5 increased $sAPP\alpha$ and decreased $sAPP\beta$, $A\beta40$ and $A\beta42$ concentrations in a concentration driven saturable effect as measured by ELISA (Fig. 4.5). A concentration-dependent response was also identified for the fraction labeled profiles of $A\beta$ and $sAPP\beta$. For the fraction labeled profile of $sAPP\alpha$, the drug effect was almost absent (Fig. 4.4). One single drug effect could describe the concentration-dependent response of all biomarkers, including the lack of response for fraction labeled $sAPP\alpha$.

Predictions from the systems model (Fig. 4.3) show that BACE1 inhibition resulted in a MBi-5 concentration driven accumulation of APP, leading to an increased production of $sAPP\alpha$ as APP is shunted down the α-secretase pathway. Both labelled and unlabelled species accumulate in a dose-dependent manner as result of BACE1 inhibition, but as the tracer infusion starts one hour post drug administration, the relatively more unlabelled species than labelled species accumulate. Due to the fractional nature of the fraction labeled measurement, these unlabelled species dilute the apparent response, from the start of drug treatment. Therefore, although there is a MBi-5 concentration driven increase in APP, this is not reflected in the 'fraction labeled APP' curve. The fraction labelled $sAPP\alpha$ is dependent on labelled APP and dilution by the accumulation of unlabelled $sAPP\alpha$. Consequently, minimal drug concentration-dependent increase appeared from the fraction labelled $sAPP\alpha$ curve, even though there is drug concentration driven increase in $sAPP\alpha$ formation. The same effect does not occur for fraction labeled $sAPP\beta$. The labeling process is continuous during the tracer infusion and washout, as is the APP accumulation during BACE1 inhibition. However, during the one hour time period between drug administration and start of tracer infusion there is no accumulation of unlabelled $sAPP\beta$, as $sAPP\beta$ levels are reducing as result of BACE1 inhibition. Therefore, there is no dilution of the apparent fraction labeled $sAPP\beta$ response by unlabelled $sAPP\beta$ species.

The drug potency (IC_{50}) identified in the combined analysis of ELISA and SILK data was 0.0267 μM (95% CI, 0.0201-0.0333), comparable to the IC_{50} identified on ELISA data only (0.0269 μM (95% CI, 0.0154-0.0384))[9]. This value is also close to the *in vitro* inhibition constant (Ki) of 10 nM for MBI-5 inhibition of purified BACE1[17]. The Hill

(A) APP brain

(B) sAPPα CSF

(C) sAPPβ CSF
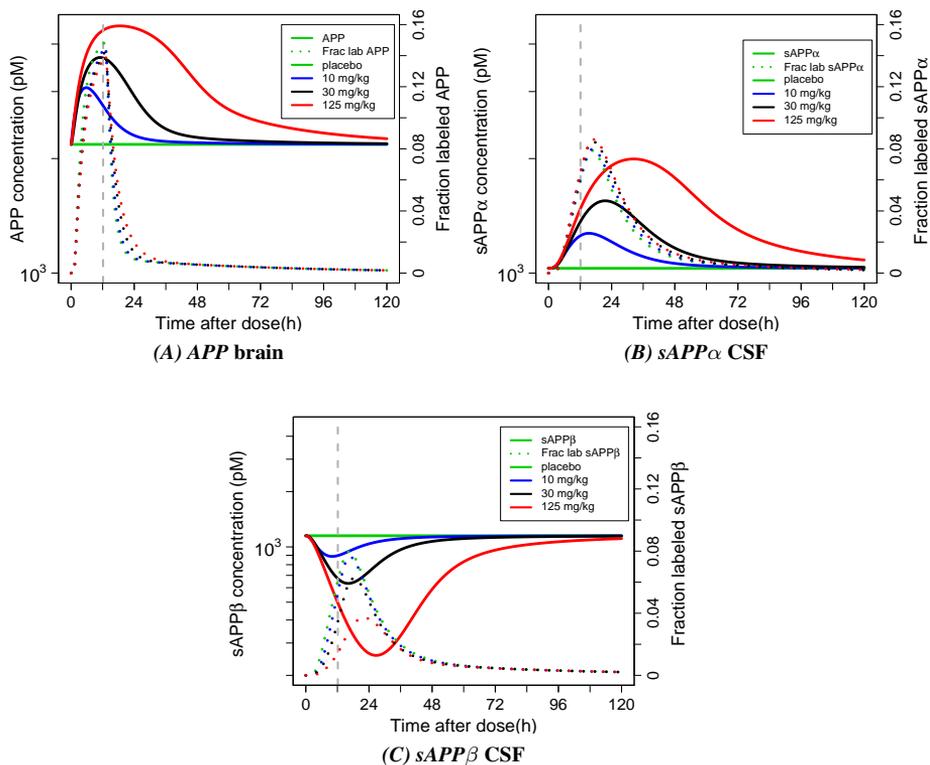
Figure 4.3: Predicted APP in brain (A), sAPPα in CSF (B) and sAPPβ in CSF (C) responses, using the identified systems model of APP processing.
The biomarker responses are predicted after a dose range of MBi-5, using typical parameter estimates.
Absolute protein concentrations: solid line; *Fraction labelled proteins:* dotted line; *Placebo:* green; *Dose 10 mg/kg:* blue; *Dose 30 mg/kg:* black; *Dose 125 mg/kg:* red; *End time of tracer infusion:* vertical grey line.

coefficient of the concentration response relationship significantly changed from 1.53 (95% CI, 1.44-1.92) based on ELISA data to 0.986 (95% CI, 0.963-1.01) based on ELISA and SILK data. As the Hill coefficient was not significantly different from 1, the sigmoid-emax concentration response relationship could be reduced to an Emax relationship by fixing the Hill coefficient to 1. A Hill coefficient of 1 is the theoretical value for a simple receptor-target interaction. The shift to this value based on the ELISA and SILK data suggested that a more distinct representation of the inhibitor interaction with the target was achieved.

The Hill coefficient of unity based on ELISA and SILK data indicated a less steep

concentration response relationship than was identified on ELISA data only. Based on the ELISA and SILK data, inhibition rises much less quickly with concentration than expected based on the recent result. This mainly affected the description of the APP metabolite concentration response curves for the higher dose groups (Fig. 4.5)[9].

The brain-turnover of sAPPα was slower based on the combined analysis (1.6 h) compared to based on ELISA data only (0.8 h). The identified proteolytic cleavage rates of APP by BACE1 and α-secretase imply that 49.1% of endogenous full length APP is cleaved by BACE1 and 50.9% by alternate pathways represented by the terms for α-secretase. These results are similar to the percentages APP identified to go down each path based on ELISA data only (44% and 56%, respectively)[9].

A sequence of models with interanimal variability on different parameters was tested and the results compared, in order to select the best random effects model structure. The final model included interanimal variability on the baseline level of sAPPβ and FAC. The identified interanimal variability on the baseline level of sAPPβ also reflects on the baseline levels of the other APP metabolites, because of their interrelationships. Interanimal variability could not be identified for the drug effect parameters, indicating that the variation in drug effect was small relative to the underlying biologic variation in the system. Residual variability for absolute protein concentrations were implemented as proportional error models. Residual variability was higher for Aβ40 and Aβ42 than for sAPPβ and sAPPα. Residual variability for fraction labelled proteins was implemented as an additive error model.

Table 4.1: Population parameter estimates including coefficient of variation (CV%) for updated model based on ELISA and SILK data.

PARAMETER	DESCRIPTION	VALUE	UNIT	CV%
Structural parameters				
sAPPβ_{base}	baseline sAPPβ	1.15e+003	pM	6.23
Fbase$_{A\beta40}$	Aβ40 baseline as fraction of sAPPβ_{base}	0.566		7.83
Fbase$_{A\beta42}$	Aβ42 baseline as fraction of sAPPβ_{base}	0.0208		5.58
Fbase$_{\text{sAPP}\alpha}$	sAPPα baseline as fraction of sAPPβ_{base}	0.895		2.20
Fbase$_{\text{X}}$	FactorX baseline as fraction of sAPPβ_{base}	0.883		26.6
Rout$_a$	degradation rate sAPPα	0.427	h^{-1}	5.53
Kout	degradation rate Aβ40 and Aβ42	0.603	h^{-1}	7.05
Kout$_x$	degradation rate FactorX	0.138	h^{-1}	9.78
KtAP	transit rate sAPPα and sAPPβ	0.110	h^{-1}	5.04
KtAB[a]	transit rate Aβ	10	h^{-1}	
FAC	scale correction factor	0.764		2.50
Kpl	oligomerization rate	0.164	h^{-1}	42.0
Krev	oligomer dissociation rate	0.0169	h^{-1}	35.4
IM[a]	Imax	1		
IC50	IC50	0.0267	μM	12.5
Interanimal variability				
ω^2_{BSAPb} [b]	Interanimal variability sAPPβ baseline	0.0670		22.5
ω^2_{FAC} [b]	Interanimal variability scale correction factor (FAC)	0.0127		44.7
Residual error				
$\sigma^2_{A\beta40}$ [c]	Residual variability Aβ40	0.266		15.4
$\sigma^2_{A\beta42}$ [c]	Residual variability Aβ42	0.126		10.6
$\sigma^2_{\text{sAPP}\beta}$ [c]	Residual variability sAPPβ	0.0548		14.6
$\sigma^2_{\text{sAPP}\alpha}$ [c]	Residual variability sAPPα	0.0625		8.19
$\sigma^2_{\text{FracLab}}$ [c]	Residual variability fraction labelled	4.62e-005		7.40

[a] Fixed.

[b] Interanimal variability is assumed to follow a normal distribution with mean zero and variance ω^2.

[c] Residual variability is assumed to follow a normal distribution with mean zero and variance σ^2.

(A) fraction labeled sAPPα

(B) fraction labeled sAPPα updated

(C) fraction labeled sAPPβ

(D) fraction labeled sAPPβ updated

(E) fraction labeled Aβ

(F) fraction labeled Aβ updated
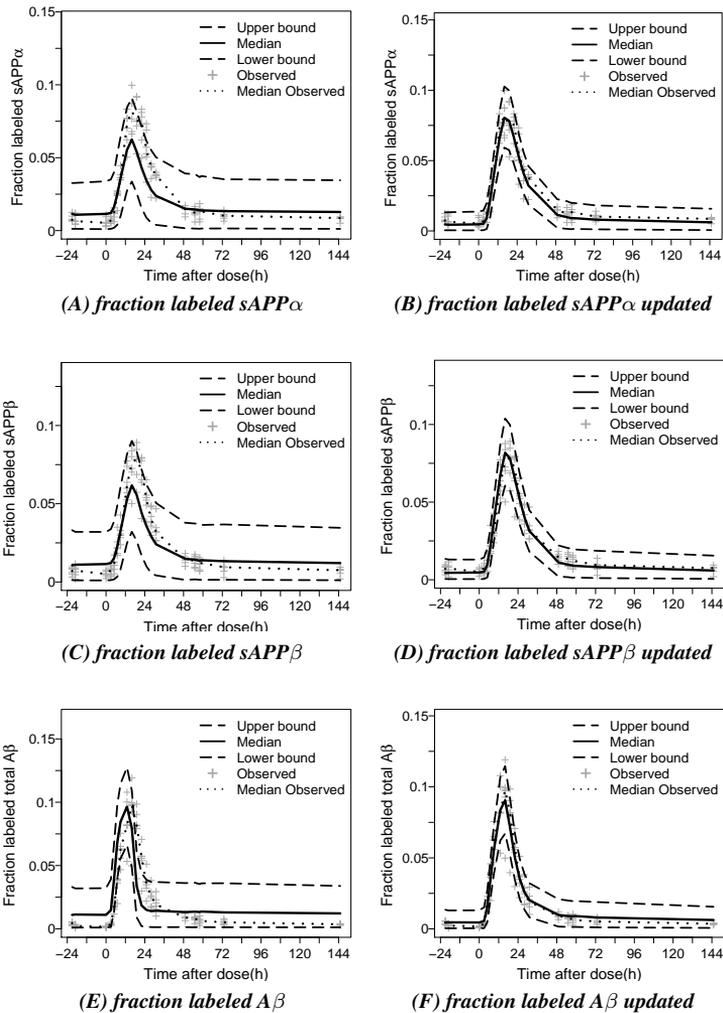
Figure 4.4: Visual predictive check of fraction labeled protein response vs. time profile of MBi-5 in the rhesus with 90% confidence interval.
Predictions were performed with model based on ELISA data only (*left*) and updated model based on ELISA and SILK data (*right*). Placebo (*A-F*), dose 10 mg/kg (*G-L*), dose 30 mg/kg (*M-R*) and dose 125 mg/kg (*S-X*). Observation sample size: n=95 for each SILK biomarker from 5 monkeys collected over 7 days at 4 occasions.
Solid line: Median model predicted fraction labeled protein response-time profile; *Long-dashed line:* 90 % prediction interval; *Dotted line:* Median observed fraction labeled protein response-time profile; + *symbol:* Observations.

(G) fraction labeled sAPPα

(H) fraction labeled sAPPα updated

(I) fraction labeled sAPPβ

(J) fraction labeled sAPPβ updated

(K) fraction labeled Aβ

(L) fraction labeled Aβ updated

Figure 4.4: **(Continued)**

(M) fraction labeled sAPPα

(N) fraction labeled sAPPα updated

(O) fraction labeled sAPPβ

(P) fraction labeled sAPPβ updated

(Q) fraction labeled Aβ

(R) fraction labeled Aβ updated

Figure 4.4: (Continued)

(S) fraction labeled sAPPα

(T) fraction labeled sAPPα updated

(U) fraction labeled sAPPβ

(V) fraction labeled sAPPβ updated

(W) fraction labeled Aβ

(X) fraction labeled Aβ updated

Figure 4.4: (Continued)

(A) sAPPα Placebo

(B) sAPPβ Placebo

(C) sAPPα 10 mg/kg

(D) sAPPβ 10 mg/kg

(E) sAPPα 30 mg/kg

(F) sAPPβ 30 mg/kg

(G) sAPPα 125 mg/kg

(H) sAPPβ 125 mg/kg

Figure 4.5: Visual predictive check of sAPPα (left: A,C,E,G), sAPPβ (right: B,D,F,H), Aβ40 (left: I,K,M,O) and Aβ42 (right: J,L,N,P) concentration response vs. time profile of MBi-5 in the rhesus with 90% confidence interval. Predictions were performed with updated model based on ELISA and SILK. Observation sample size: n=95 for each APP metabolite from 5 monkeys collected over 7 days at 4 occasions. *Solid line:* Median model predicted concentration-time profile *Long-dashed line:* 90 % prediction interval. *Dotted line:* Median observed concentration-time profile + *symbol:* Observations.

100

(I) Aβ40 Placebo

(J) Aβ42 Placebo

(K) Aβ40 10 mg/kg

(L) Aβ42 10 mg/kg

(M) Aβ40 30 mg/kg

(N) Aβ42 30 mg/kg

(O) Aβ40 125 mg/kg

(P) Aβ42 125 mg/kg
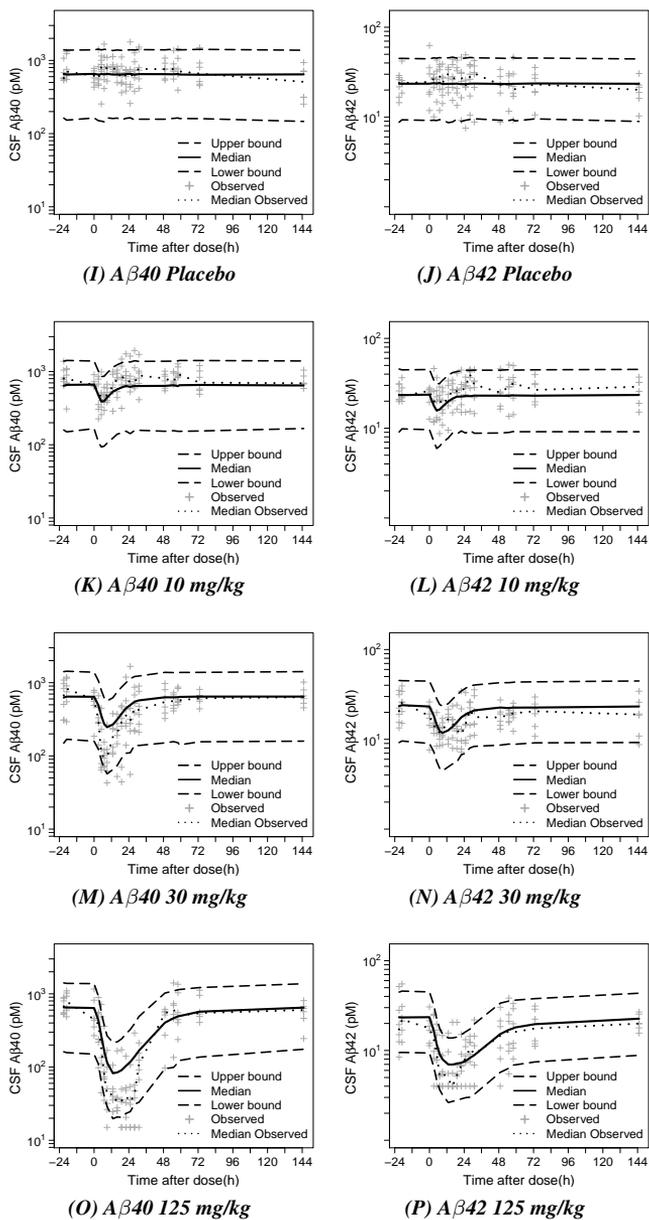
Figure 4.5: (Continued)

Discussion

Tracer kinetic studies are widely used to determine the influence of enzyme inducers or inhibitors on the rates of production and degradation of proteins. Traditionally, a non-compartmental analysis of the tracer enrichments versus time curve is used to estimate their effects on the rates of protein production and/or degradation. The rate of protein production being estimated from the upswing of the curve and the rate of degradation from the downswing. It has been demonstrated that the use of non-compartmental tracer kinetic data analysis where the enrichment is not in steady state could lead to inaccurate quantification of kinetic parameters [22].

Alternatively, compartmental models have been used for this purpose [23,24]. Here typically a standard two stage is followed in which each individuals PD parameters are estimated and then population mean and variance of each parameter are derived [25]. A limitation of this approach is that the effect on protein disposition is related to the dose rather than to measures of drug concentrations.

To our knowledge, we are the first to utilize a population PK-PD modelling approach to the analysis of tracer kinetic data. The approach utilized here, in which the time course of the plasma tracer enrichment is analysed in conjunction with the time course of the plasma and CSF concentrations of the BACE1 inhibitor MBi-5, is novel for this type of data. The individual values of the (pharmaco)kinetic parameters obtained in these models serve as input for the modelling of the time course of the tracer enrichment of the APP metabolites. This enabled characterization of the concentration-enrichment-effect relationship of the BACE1 inhibitor, while taking into account the variability in PK, enrichment and PD in the study population.

We have recently been able to propose a systems pharmacology model for the APP processing pathway based on absolute concentrations of APP metabolites in rhesus monkeys [9]. This model provided a unique opportunity to further evaluate our understanding of the APP processing pathway while including tracer kinetic data in addition to absolute protein measurements. To this end we have simultaneously analysed the effects of a BACE1 inhibitor on the APP processing pathway, by analyzing the effects on tracer kinetic parameters (fraction labelled of various peptide species) as well as absolute protein concentrations. This has yielded invaluable information on the nature of measurements used in both techniques and on the underlying physiology.

The application of the existing systems pharmacology model to the combined dataset was generally consistent with our understanding of the APP processing pathway and

the existence of the oligomer pool. Moreover, the parameters describing the formation and degradation of the APP metabolites were comparable thereby strengthening our understanding of the relative contribution of the different analytes to the observed responses.

In the presence of the BACE1 inhibitor MBi-5 a concentration dependent saturable decrease in Aβ40, Aβ42 and sAPPβ concentrations was observed in combination with an increase in sAPPα absolute protein concentrations. In the SILK assay fraction labelled profiles for Aβ and sAPPβ were reduced in a similar MBi-5 concentration-dependent manner. However, the effect on the fraction labelled profile of sAPPα was negligible. This is explained by the fact that the effect on sAPPα is an indirect effect through the accumulation of APP, secondary to the inhibition of BACE1. As the concentrations of both unlabelled and labelled sAPPα change in the same direction, there is no clear effect on the ratio labelled over total sAPPα (= the fraction labelled). This is further augmented by the fact that the tracer infusion starts one hour after MBi-5 administration. In this first hour after the administration of the BACE1 inhibitor unlabelled sAPPα starts to accumulate while there is no accumulation of labelled sAPPα. This further dampens the effect on the fraction labelled sAPPα. Finally, after a single dose of the BACE1 inhibitor, the observed dose response relationship also depends on the end time of the tracer infusion relative to the time of the maximal PD response.

In contrast to the attenuated effects of BACE1 inhibition on parameters characterizing the α-secretase pathway (fraction labelled sAPPα), clear effects on the parameters of BACE1 pathway (fraction labelled sAPPβ, fraction labelled Aβ) were observed, which is explained by the fact that these parameters are all downstream of BACE1, so that there is no accumulation of unlabelled protein in the time between drug administration and start of tracer infusion. These observations show, that due the complexity of the underlying biochemical network, lack of concentration dependent effect of an enzyme inhibitor on certain parameters, does not exclude the possibility that there is indeed such an effect.

We found a lower brain tracer enrichment relative to plasma tracer enrichment during $^{13}C_6$-L infusion (Supplemental Material 3, Figure S4.4). The discrepancy between plasma tracer enrichment and target site enrichment may be explained by a lower amount of tracer at the target site, due to dilution of tracer. This may be the result of a higher amount of endogenous Leucine at the target site than in plasma. Also, kinetics of Leucine into and out of the cells, as well as into and out of the corresponding protein pools can differ across tissues [22].

The lower relative enrichment at the target site indicates that $^{13}C_6$-L does not achieve

an isotopic equilibrium throughout all free pools of Leucine in the time frame of tracer infusion. This is also observed in the plasma tracer enrichment data, where plasma TTR is still rising during the 12 h infusion. This was confirmed by simulations using the developed model, indicating that it takes approximately 52 days of infusion to reach steady state with the primed-constant infusion technique as used in SILK (see Supplemental Material 1, Figure S4.3). With the primed 12 h infusion used in the current study, 62% of the steady state level of plasma tracer enrichment was reached. Therefore, the plateau observed in plasma tracer enrichment is a pseudo steady-state. The absence of steady state in tracer enrichment requires an analysis which takes into account the dynamics of the system, such as a comprehensive model based analysis performed currently.

The extension of the systems pharmacology model to include tracer kinetic data provides additional insights into the underlying APP processing pathway. Our modelling results indicate that 49.1% of APP is cleaved by BACE1 and 50.9% by α-secretase. It was assumed that all alternate pathways were represented by the terms for α-secretase. The reported percentage of APP to go down the α-secretase path should be interpreted as capturing the contribution of alternate pathways in general, as it acts to mediate the increase in APP which drives the α-secretase response and any other alternate pathway response. Increases in APP due to BACE1 inhibition result in more substrate being available to alternate pathways in general and α-secretase as an alternate path well represents this phenomena. It is expected that all alternate paths will behave dynamically as α-secretase does as all drug effects on alternate paths will be driven by the APP increase under BACE1 inhibition. The increases seen with α-secretase and captured in this model should also reflect the relative changes to be expected for any alternate pathway that may be present. Therefore, it is expected that sAPP-η would build-up in response to BACE1 inhibition similar to sAPPα build-up. An accumulation of the cleavage products of η-secretase after BACE1 inhibition was also reported by Willem et al 2015 in mice.

The simultaneous analysis of the combined data revealed differences in Aβresponses after BACE1 inhibition in rhesus monkeys as determined by ELISA and SILK. In a model-based analysis, in which knowledge of the biological system and analytical methods was integrated, various hypotheses to align APP metabolite response measurements in ELISA and SILK were tested. A possible explanation of the disconnect may be that an unknown process or analytes other than Aβ40 (Aβ1-40) and Aβ42 (Aβ1-42) were measured in SILK and not ELISA. The incorporation of the FactorX compartment in the model accounted for this (Fig. 4.1). The disconnect in measurements between both methods may be explained by the use of different measurement techniques. The antibodies

used in the ELISA where neoepitope-specific antibodies (N-terminal antibodies), directed against Aβ1-40 and Aβ1-42. The antibodies used to isolate Aβ in the SILK protocol were not end-specific for the N- or C-terminus, but directed against Aβ5-27. As the antibodies used to isolate Aβ were raised against Aβ5-27, these analytes that were detected in this assay must include this amino acid sequence.

A new APP processing pathway was recently reported by Willem et al 2015, in which sequential cleavage of APP by η-secretase and BACE1 or ADAM10 leads to the formation of Aη-β and Aη-α, respectively. Several Aη peptides were reported by Willem et al 2015, that could have been captured by antibody W0-2, but not by HJ5.1, as used in the SILK protocol. Therefore, this does not explain the disconnect.

In an alternative path, BACE1 can cleave full length APP at the β-prime site (GLU11 in the Aβ sequence) leading to the production of Aβ11-40 and Aβ11-42. These are major cleavage products of BACE1, as reported by[26]. Both Aβ11-40 and Aβ11-42 could not have been captured by the antibody W0-2 used in the SILK protocol, nor the neoepitope-specific antibodies used in the ELISA. Thus, β-prime site cleavage products cannot explain a difference in measurements between both methods.

It could be that ELISA does not detect the full complement of Aβ42, as it is either tied up in Aβ_O or bound to a carrier protein[27]. The methods used to detect the fraction labelled Aβ in the SILK protocol should also capture Aβ_O. How rapidly newly synthesized Aβ becomes an oligomeric species and how rapidly Aβ_O would move from brain to CSF is not known, but they are likely cleared to CSF much more slowly than the monomer due to their biophysical properties. It could also be that there is active transport of soluble toxic Aβ_O out of the brain, resulting in faster brain-to-CSF transport than for monomeric species. It was not possible to identify the brain-turnover of Aβ_O and turnover over brain-to-CSF transport as separate parameters. Therefore, the half-life of Aβ_O of 0.07 h reflects delays due to both brain-to-CSF transfer and turnover in the brain. Therefore, the rate of appearance of Aβ_O response in CSF relative to Aβ cannot be appointed to one of these processes.

Remarkably, different kinetics were identified for the process or analytes represented by FactorX, compared to Aβ40 and Aβ42. It was not possible to separate the rate of the γ-secretasecleavage from the brain-to-CSF transport. Therefore, the transit rates from brain-to-CSF for Aβ40, Aβ42 (KtAB) and FactorX (KtX) were fixed to an arbitrary high value (10 h-1) and assumed to be equal.

Consequently, the Aβ40 and Aβ42 half-life of 1.1 h reflects delays due to the γ-secretase cleavage step and brain-to-CSF transfer. The current model structure in which

Aβ40 and Aβ42 are directly formed is a simplification of the underlying system. γ-secretase cleaves C99 through interactive pathways for stepwise successive processing to generate different Aβ isoforms, with Aβ40 and Aβ42 as the major products[28]. The initial γ-secretase cleavages are followed sequentially by γ-secretase cleavages after every three or four residues. The systems model was able to combine two types of data and describe seven biomarkers successfully. Adding the tracer kinetic data (SILK) to the model based on absolute protein concentrations (ELISA)[9] confirmed the system that was identified on ELISA data only. This is one utility of the biomarkers of the SILK protocol. Our understanding of the relationships among the absolute APP metabolite concentrations did not change compared to the recent analysis based on ELISA data only. However, the combined analysis allowed for more hypotheses to be tested. Vice versa, including absolute protein concentrations in the interpretation of the tracer kinetic data had added value. This facilitated the correct interpretation of drug concentration dependencies in the tracer kinetic data and led to the investigation of a disconnect in the two type of measurements of the same system, which was accounted for by the FactorX model component.

If dedicated measurements of Aβ1-40 and Aβ1-42 were used in the SILK protocol, it is expected that Aβ40, Aβ42, fraction labelled Aβ could have been described by a model without inclusion of the FactorX model component. However, even then, matrix components in the CSF may affect the measurement reproducibility across different immunoassays[27].

In a follow-up study, dedicated measures of Aβ40, Aβ42 and Aβ38 will be performed in the same samples in both labelled and absolute quantification. In addition, Aβ will be quantified using an antibody directed at the mid-domain Aβ17-28. If FactorX is an Aβ isoform, it would then be possible to determine if it has different half-lifes from Aβ40, Aβ42 and Aβ38 and how much FactorX accounts for total of Aβ species compared to Aβ40, Aβ42 and Aβ38.

Conclusion

This investigation demonstrated that the simultaneous analysis of absolute protein concentrations and tracer kinetic data using a systems pharmacology model will elucidate the underlying biological system and will thereby facilitate the interpretation of the tracer kinetic data in the light of the system. The model-based analysis distinguished labelled and unlabelled species, as well as separated steps in the APP pathway and distribution to CSF. This enabled and improved understanding of the (lack-of) dose-dependent response in kinetic data.

Different hypotheses to align APP metabolite response measurements in ELISA and SILK were tested. A possible explanation of the disconnect may be that an unknown APP fragment with differing kinetics or an unknown process was picked up in SILK assay. This requires further investigation.

The developed comprehensive model can be used to perform simulations to investigate study design features that may influence the magnitude of biomarker responses, such as dose and degree of Aβ production inhibition. To maximize information on the APP pathway from the tracer protocol, simulations can be performed to investigate how the $^{13}C_6$-L infusion time and length affects the fraction labelled curves (ongoing). It is anticipated that adding information on APP metabolite responses (absolute and fraction labelled proteins) following γ-secretase inhibition will provide more information on the biological system as well as the discrepancies between absolute protein concentrations and tracer kinetic data.

References

1. Jack, C.R., *et al.* Hypothetical model of dynamic biomarkers of the Alzheimer's pathological cascade. Lancet Neurol. 2010;9(1): 119–28.

2. Benilova, I., Karran, E., & De Strooper, B. The toxic Aβ oligomer and Alzheimer's disease: an emperor in need of clothes. Nat Neurosci. 2012;15(3):349–357.

3. Husain, M.M., Kenneth, T., Siddique, H., & McClintock, S.M. Present and prospective clinical therapeutic regimens for Alzheimer's disease. Neuropsychiatr Dis Treat. 2008;4(4):765–777.

4. Cole, S.L. & Vassar, R. The basic biology of BACE1: A key therapeutic target for Alzheimer's disease. Curr Genomics. 2007;8(8):509–530.

5. Dawkins, E. & Small, D.H. Insights into the physiological function of the β-amyloid precursor protein: beyond Alzheimer's disease. J Neurochem. 2014;129(5):756–69.

6. Wiltfang, J., *et al.* Higly conserved and disease-specific patterns of carboxyterminally truncated Aβ peptides 1-37/38/39 in addition to 1-40/42 in Alzheimer's disease and in patients with chronic neuroinflammation. J Neurochem. 2002;81(3):481–496.

7. Vingtdeux, V. & Marambaud, P. Identification and biology of α-secretase. J Neurochem. 2012;120 (Suppl. 1):34–45.

8. Willem, M., *et al.* η-Secretase processing of APP inhibits neuronal activity in the hippocampus. Nature. 2015;526(7573):443–7.

9. van Maanen, E.M.T., *et al.* Systems pharmacology analysis of the amyloid cascade after β-secretase inhibition enables the identification of an Aβ42 oligomer pool. J Pharmacol Exp Ther. 2016;357(1):205–16.

10. Bateman, R.J., Munsell, L.Y., Chen, X., Holtzman, D.M., & Yarasheski, K.E. Stable isotope labeling tandem mass spectrometry (SILT) to quantify protein production and clearance rates. J Am Soc Mass Spectrom. 2007;18(6):997–1006.

11. Potter, R., *et al.* Increased in vivo Amyloid-β42 production, exchange, and irreversible loss in Presenilin Mutations Carriers. Sci Transl Med. 2013;5(189):189ra77.

12. Patterson, B.W., *et al.* Age and amyloid effects on human central nervous system amyloid-beta kinetics. Ann Neurol. 2015;78 (3):439–453.

13. Cook, J.J., *et al.* Acute γ-secretase inhibition of nonhuman primate CNS shifts amyloid precursor protein (APP) metabolism from amyloid-β production to alternative APP fragments without amyloid-β rebound. J Neurosci. 2010;30(19):6743–50.

14. Bateman, R.J., *et al.* A gamma-secretase inhibitor decreases amyloid-beta production in the central nervous system. Ann Neurol. 2010;66(1):48–54.

15. Gilberto, D.B., *et al.* An alternative method of chronic cerebrospinal fluid collection via the cisterna magna in conscious rhesus monkeys. Contemp Top Lab Anim Sci. 2003;42 (4):53–59.

16. National Research Council. Guide for the Care and Use of Laboratory Animals The National Academies Press;Washington DC;1996.

17. Dobrowolska, J.A., *et al.* CNS amyloid-β, soluble APP-α and -β kinetics during BACE inhibition. J Neurosci. 2014;34(24): 8336–8346.

18. Wu, G., Sankaranarayanan, S., Hsieh, S.H.K., Simon, A.J., & Savage, M.J. Decrease in brain soluble amyloid precursor protein β (sAPPβ) in Alzheimer's disease cortex. J Neurosci Res. 2011;89(6):822–32.

19. Sankaranarayanan, S., *et al.* First demonstration of cerebrospinal fluid and plasma Aβ lowering with oral administration of a β-site amyloid precursor protein-cleaving enzyme 1 inhibitor in nonhuman primates. J Pharmacol Exp Ther. 2009;328(1):131–140.

20. Nubuo, I. & Hartmann, T. Analysis of Heterogeneous beta A4 Peptides in Human Cerebrospinal Fluid and Blood by a Newly Developed Sensitive Western Blot Assay. J Biol Chem. 1996;271(37):22908–22914.

21. Bauer, R.J. 2011 NONMEM users guide. Introduction to NONMEM 7.2.0 Technical report;ICON Development Solutions, Ellicott City, MD.

22. Wolfe, R.R. & Chinkes, D.L. Isotope tracers in metabolic research: principles and practice of kinetic analysis. 2nd ed. John Wiley & Sons;Hoboken, New Jersey;2005.

23. Gowrie, I., Roudsari, A., Umpleby, A., & Hovorka, R. Estimating Protein Turnover with a [15 N , 13 C] Leucine Tracer : a Study Using Simulated Data. J Theor Biol. 1999;198:165–172.

24. Cobelli, C., Saccomani, M.P., Tessari, P., Biolo, G., Luzi, L., & Matthews, D.E. Compartmental model of leucine kinetics in humans. Am J Physiol. 1991;261(4 Pt 1):E539–50.

25. Bonate, P.L. Pharmacokinetic-Pharmacodynamic Modeling and Simulation Springer;New York;2006.

26. Liu, K., Doms, R.W., & Lee, V.M.Y. Glu11 site cleavage and N-terminally truncated A beta production upon BACE overexpression. Biochemistry. 2002;41(9):3128–36.

27. Slemmon, J.R., *et al.* Measurement of Aβ1-42 in cerebrospinal fluid is influenced by matrix effects. J Neurochem. 2012;120(2): 325–33.

28. Matsumura, N., *et al.* γ-Secretase associated with lipid rafts: multiple interactive pathways in the stepwise processing of β-carboxyl-terminal fragment. J Biol Chem. 2014;289(8):5109–21.

Chapter 4

Supplemental Material

E.M.T. van Maanen, T.J. van Steeg, J.A. Dobrowolska Zakaria, M.S. Michener, M.J. Savage, M.E. Kennedy, R.J. Bateman, H.J. Kleijn, J.A. Stone, M. Danhof

SUPPLEMENTAL MATERIAL (1)

Kinetic Data Analysis of Plasma Enrichment

A kinetic model was developed to quantify plasma $^{13}C_6$-L enrichment in CMP rhesus monkeys. The results of the plasma enrichment analysis were included in the subsequent PK-tracer-PD analysis.

The kinetic model was developed and fitted to the data by means of non-linear mixed effects modeling using the NONMEM software package version 7 level 2 (see the Materials and Methods section in Chapter 4).
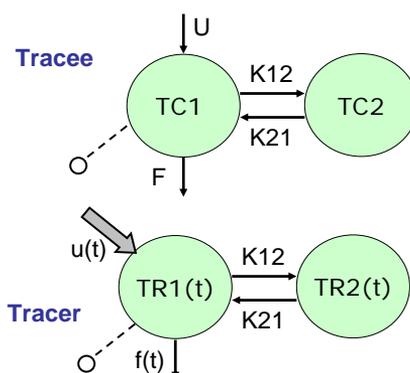
Figure S4.1: Model structure of kinetic model describing plasma tracer enrichment.
The model relates tracer input [mg/kg/hr] to the tracer-to-tracee ratio (TTR[%]). The model includes two tracee ($^{12}C_6$-Leucine) and two tracer ($^{13}C_6$-Leucine) compartments, representing extra- (pool 1) and intra-cellular (pool 2) tracee and tracer, respectively. Measurements are assumed to be taken from the extracellular compartment.
Dashed line: sampling. *Arrow*: tracer infusion. *U*: production of tracee in pool 1. *u(t)*: tracer infusion into pool 1. *F*: disposal of tracee from pool 1. *f(t)*: disposal of tracer from pool 1. *K12*: Transit rate from pool 1 to pool 2. *K21*: Transit rate from pool 2 to pool 1.

The compartmental model related the tracer infusion [mg/kg/h] to the measured enrichment, quantified as tracer ($^{13}C_6$-Leucine) to tracee (endogenous $^{12}C_6$-Leucine) ratio (TTR [%]), by describing tracee and tracer kinetics.

The model included two tracee ($^{12}C_6$-Leucine) and two tracer ($^{13}C_6$-Leucine) compartments (Supplemental Figure S4.1), representing extra- and intra-cellular tracee and

tracer. Measurements are assumed to be taken from the extracellular compartment.

Tracee is produced and disposed from tracee pool 1. Tracer is disposed from tracer pool 1. It is assumed that the natural production of tracer is negligible within the time frame of the experiment. The tracer coming into the system comes from the tracer infusion. The rate of disposal of tracer (f(t)) equals the rate of disposal of the tracee (*F*). The tracer and tracee kinetics is described by Eqs. S4.1 - Eqs. S4.4:

Tracee pool 1 (TC_1):

$$\frac{d}{dt}TC_1 = -K_{12} * TC_1 + K_{21} * TC_2 - F * TC_1 + U \tag{S4.1}$$

Tracee pool 2 (TC_2):

$$\frac{d}{dt}TC_2 = K_{12} * TC_1 - K_{21} * TC_2 \tag{S4.2}$$

Tracer pool 1 (TR_1):

$$\frac{d}{dt}TR_1(t) = -K_{12} * TR_1(t) + K_{21} * TR_2(t) - f(t) * TR_1(t) + u(t) \tag{S4.3}$$

Tracer pool 2 (TR_2):

$$\frac{d}{dt}TR_2(t) = K_{12} * TR_1(t) - K_{21} * TR_2(t) \tag{S4.4}$$

The TTR in plasma can then be calculated as described by Eqs. S4.5: Tracer to tracee ratio (*TTR*):

$$\frac{d}{dt}TTR = \frac{\frac{TR_1(t)}{TC_1} - TTR_{base}}{1 + 0.0111 * 6} * 100\% \tag{S4.5}$$

Here, TTR_{base} is the observed ratio of $^{13}C_6$-Leucine to $^{12}C_6$-Leucine prior to the addition of tracer.

The value $1/(1+0.0111*6)$ is the skew correction factor, accounting for the natural abundance of $^{13}C_6$-Leucine[1]. The spectrum of $^{13}C_6$-Leucine does not have the same mass abundance distribution as natural $^{12}C_6$-Leucine. In the calculation of TTR, this skew in

isotopomer distribution must be accounted for. The correction factor can be approximated by the value $1/(1+An)$, where A is the natural isotopic abundance of ^{13}C carbon atoms and n is the number of atoms labelled[2]. 1.11% of the naturally occurring carbon atoms are ^{13}C atoms and Leucine has six carbon atoms ($C_6H_{13}NO_2$), therefore $1/(1+0.0111*6)$.

The baseline of tracee pool 2 (TC_{2base}) and production of tracee (U) follow from steady state conditions.

$$TC_{2base} = TC_{1base} * \frac{K_{12}}{K_{21}} \qquad (S4.6)$$

$$U = F * TC_{1base} \qquad (S4.7)$$

Supplemental Table S4.1 shows all kinetic parameter estimates. All parameters could be estimated with good precision. For the baseline of the tracee pool 1 (TR_{1base}) interanimal variability was quantified. The model included a proportional error to describe the residual variability.

The measured plasma tracer enrichment was adequately described by the model, as can been seen from the visual predictive check (Supplemental Figure S4.2). Thus, the model could serve as input for PK-tracer-PD model analysis.

Table S4.1: Population parameter estimates including coefficient of variation (CV%) for kinetic model of plasma tracer enrichment.

PARAMETER	DESCRIPTION	VALUE	UNIT	CV%
F	Disposal	0.931	h^{-1}	25.5
K12	Transit rate from pool 1 to pool 2	0.644	h^{-1}	16.5
K21	Transit rate from pool 1 to pool 2	0.0154	h^{-1}	33.4
TC_{1base}	Baseline tracee pool 1	141	mg	15.1
$\omega^2_{TC_{1base}}$	Interanimal variability baseline tracee pool 1	0.0166		20.0
σ^2	Residual variability	0.722		20.4

Time to steady state

A simulation was performed with the kinetic model to investigate if plasma tracer enrichment reached steady state with the primed 12 h $^{13}C_6$-L infusion as used in the current SILK study (Supplemental Figure S4.3). To that end, the continuous infusion time was extended and the time to steady state derived. It takes approximately 52 days of infusion to reach steady state with the primed infusion technique. After approximately 10 and 17 days respectively 95% and 99% of the steady state level is reached. In the current study,

with the primed 12 h infusion, 62% of the steady state level of plasma tracer enrichment was reached.
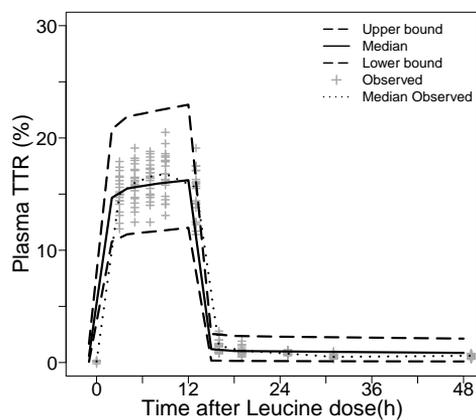
Figure S4.2: Visual predictive check of plasma tracer enrichment (TTR) time profile of
$^{13}C_6$-Leucine in the rhesus with 90% confidence interval.
Observation sample size: n=260 from 5 monkeys collected over 2 days at four occasions.
Solid line: Median model predicted plasma TTR-time profile *Long-dashed line:* 90% prediction interval.
Dotted line: Median observed plasma TTR-time profile *Plus-symbols:* Observations.
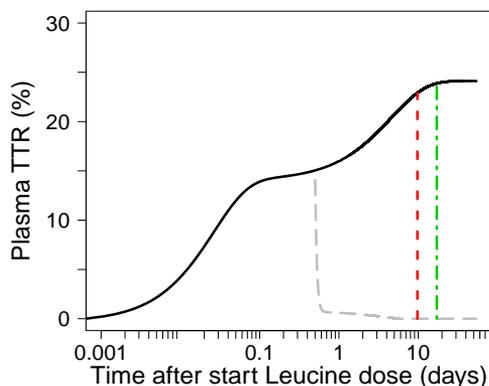
Figure S4.3: Simulation of plasma tracer enrichment (TTR) time profile using the identified kinetic model.

The plasma TTR is predicted after a primed infusion of 4 mg/kg bolus over 10 minutes, followed by 1300 h continuous infusion at a rate of 4 mg/kg/h, using the typical parameter estimates. Steady state plasma TTR is reached after $\sim$ 52 days of infusion.

Solid line: Model predicted plasma TTR-time profile after primed 1300 h infusion. *Long-dashed grey line:* Model predicted plasma TTR-time profile after primed 12 h infusion. *Dashed vertical red line:* Time of 95% steady state plasma TTR. *Dot-dashed vertical green line:* Time of 99% steady state plasma TTR.

References

1. Wolfe, R.R. & Chinkes, D.L. Isotope tracers in metabolic research: principles and practice of kinetic analysis 2nd ed. John Wiley & Sons;Hoboken, New Jersey;2005.

2. Rosenblatt, J., Chinkes, D., Wolfe, M., & Wolfe, R.R. Stable isotope tracer analysis by GC-MS, including quantification of isotopomer effects. Am J Physiol. 1992;263(3 Pt 1):E584–96.

SUPPLEMENTAL MATERIAL (2)

Table S4.2: Population parameters derived from model parameters for updated model based on ELISA and SILK data.

PARAMETER	DESCRIPTION	VALUE	UNIT
$A\beta40_{base}$[a]	$A\beta40$ baseline	650.9	pM
$A\beta42_{base}$[b]	$A\beta42$ baseline	23.92	pM
$FactorX_{base}$[c]	FactorX baseline	1,015	pM
$sAPP\alpha_{base}$[d]	$sAPP\alpha$ baseline	1,029	pM
$A\beta_{O\,base}$[e]	$A\beta_O$ baseline	232.12	pM
APP_{base}[f]	APP baseline	2,179	pM
Rin_{APP}[g]	source of APP	$9.25*10^{-7}$	$L^{-1}h^{-1}$
Rin_{α}[h]	$sAPP\alpha$ formation rate	0.202	h^{-1}
Rin_{β}[i]	$sAPP\beta$ formation rate	0.209	h^{-1}
Kin_{40}[j]	$A\beta40$ formation rate	0.341	h^{-1}
Kin_{42}[k]	$A\beta42$ formation rate	0.0125	h^{-1}
Kin_x[l]	$A\beta x$ formation rate	0.122	h^{-1}

[a] $A\beta40_{base}=Fbase_{A\beta40}*sAPP\beta_{base}$.

[b] $A\beta42_{base}=Fbase_{A\beta42}*sAPP\beta_{base}$.

[c] $FactorX_{base}=Fbase_{FactorX}*sAPP\beta_{base}$.

[d] $sAPP\alpha_{base}=Fbase_{sAPP\alpha}*sAPP\beta_{base}$.

[e] $A\beta_{O\,base}=Kpl*A\beta42_{base}/Krev$.

[f] $APP_{base}=sAPP\beta_{base}+sAPP\beta_{base}$

[g] $Rin_{APP}=(Rin_{\alpha}+Rin_{\beta})*APP_{base}*MW_{LeuL}/(TC_{1base}*10^9)$

[h] $Rin_{\alpha}=Rout_a*sAPP\alpha_{base}/APP_{base}$

[i] $Rin_{\beta}=(Kin_{40}+Kin_{42}+Kin_x)*sAPP\beta_{base}/APP_{base}$

[j] $Kin_{40}=Kout*A\beta40_{base}/sAPP\beta_{base}$

[k] $Kin_{42}=Kin_{40}*A\beta42_{base}/A\beta40_{base}$

[l] $Kin_x=Kout_x*FactorX_{base}/sAPP\beta_{base}$

SUPPLEMENTAL MATERIAL (3)

Simulation scale correction factor

In the PKPD model the plasma tracer enrichment was scaled to the level of tracer enrichment in the brain using a scale correction factor *FAC*. *FAC* represents the relative uptake of tracer in the precursor APP pool and was estimated to be 0.764. $^{13}C_6$-Leu does not achieve an isotopic equilibrium throughout all free pools of Leucine within the timeframe of the tracer infusion. Therefore, the tracer enrichment in the brain differs from plasma enrichment.

If isotopic equilibrium is assumed, and hence FAC=1, the fraction labelled protein is overestimated for fraction labeled total $A\beta$, sAPPβ and sAPPα, as is demonstrated in Supplemental Figure S4.4 for the placebo group.

(A) fraction labeled total $A\beta$ *(B) fraction labeled sAPPβ*   *(C) fraction labeled sAPPα*
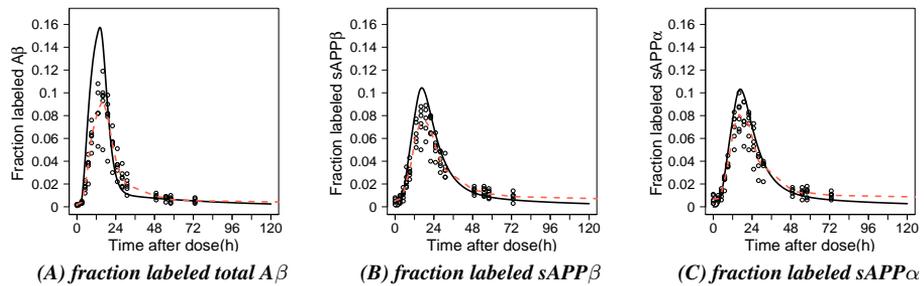
Figure S4.4: Simulation fraction labelled protein response* vs. *time profile for the placebo group with scale correction factor (FAC) equals 1.
Solid line: Predicted fraction labelled protein response-time profile; *Dashed line:* Smoother through the observations of the placebo group; *Symbols:* Observations placebo group.

SUPPLEMENTAL MATERIAL (4)

Equations

The interaction between labeled and unlabelled APP, sAPPβ, sAPPα, Aβ40, Aβ42, Aβ_O and FactorX is described by Eq. S4.8 - Eq. S4.21:

$$
\begin{aligned}
\frac{d}{dt}APP^{unlab} =& Rin_{APP} * \frac{TC_1 * 10^9}{MW_{LeuU}} - (Rin\beta * EFF + Rin\alpha) * APP^{unlab} \\
& - Rin_{APP} * \frac{TR_1 * 10^9 * FAC}{MW_{LeuL}}
\end{aligned} \tag{S4.8}
$$

$$
\begin{aligned}
\frac{d}{dt}APP^{lab} =& Rin_{APP} * \frac{TR_1 * 10^9 * FAC}{MW_{LeuL}} \\
& - (Rin\beta * EFF + Rin\alpha) * APP^{lab}
\end{aligned} \tag{S4.9}
$$

$$
\frac{d}{dt}sAPP\alpha^{unlab} = Rin\alpha * APP^{unlab} - Rout_a * sAPP\alpha^{unlab} \tag{S4.10}
$$

$$
\frac{d}{dt}sAPP\alpha^{lab} = Rin\alpha * APP^{lab} - Rout_a * sAPP\alpha^{lab} \tag{S4.11}
$$

$$
\begin{aligned}
\frac{d}{dt}sAPP\beta^{unlab} =& Rin\beta * EFF * APP^{unlab} \\
& - (Kin_{40} + Kin_{42} + Kin_x) * sAPP\beta^{unlab}
\end{aligned} \tag{S4.12}
$$

$$
\begin{aligned}
\frac{d}{dt}sAPP\beta^{lab} =& Rin\beta * EFF * APP^{lab} \\
& - (Kin_{40} + Kin_{42} + Kin_x) * sAPP\beta^{lab}
\end{aligned} \tag{S4.13}
$$

$$
\frac{d}{dt}A\beta_{40}^{unlab} = Kin_{40} * sAPP\beta^{unlab} - Kout * A\beta_{40}^{unlab} \tag{S4.14}
$$

$$
\frac{d}{dt}A\beta_{40}^{lab} = Kin_{40} * sAPP\beta^{lab} - Kout * A\beta_{40}^{lab} \tag{S4.15}
$$

$$\frac{d}{dt}A\beta_{42}^{unlab} = Kin_{42} * sAPP\beta^{unlab} - Kout * A\beta_{42}^{unlab}$$
$$- Kpl * A\beta_{42}^{unlab} + Krev * A\beta_{O}^{unlab} \tag{S4.16}$$

$$\frac{d}{dt}A\beta_{42}^{lab} = Kin_{42} * sAPP\beta^{lab} - Kout * A\beta_{42}^{lab} - Kpl * A\beta_{42}^{lab}$$
$$+ Krev * A\beta_{O}^{lab} \tag{S4.17}$$

$$\frac{d}{dt}A\beta_{O}^{unlab} = Kpl * A\beta_{42}^{unlab} - Krev * A\beta_{O}^{unlab} \tag{S4.18}$$

$$\frac{d}{dt}A\beta_{O}^{lab} = Kpl * A\beta_{42}^{lab} - Krev * A\beta_{O}^{lab} \tag{S4.19}$$

$$\frac{d}{dt}FactorX^{unlab} = Kin_x * sAPP\beta^{unlab} - Kout_x * FactorX^{unlab} \tag{S4.20}$$

$$\frac{d}{dt}FactorX^{lab} = Kin_x * sAPP\beta^{lab} - Kout_x * FactorX^{lab} \tag{S4.21}$$

The label incorporation in the APP pathway is informed from the kinetic model of plasma tracer enrichment. In Eqs. S4.8 and S4.9 this is imputed by TC_1 and TR_1, converted from mg to pM by $10^9/MW_{Leu}$. FAC in Eqs. S4.9 is a scale correction factor, used to scale the plasma tracer enrichment to the level of tracer enrichment in the brain.

The rate of change of APP with respect to time in the presence of the inhibitor is described by Eqs. S4.8 and S4.9, in which the BACE1 cleavage inhibition is incorporated by the factor *EFF*. *EFF* is the degree of inhibition caused by MBi-5, expressed as shown in Eqs. 5.8.

$$EFF = 1 - \frac{C_{target}^{GAM} * Imax}{C_{target}^{GAM} + IC50^{GAM}} \tag{S4.22}$$

Where C_{target} is the target site concentration of MBi-5 , *IC50* the C_{target} that results in 50% inhibition of BACE1, *Imax* is the maximum inhibition and *GAM* is the Hill coefficient. C_{target} was derived from the PK model as:

$$C_{target} = C_{plasma} * \frac{AUC_{CSF}}{AUC_{plasma}} \tag{S4.23}$$

Where AUC_{CSF} and AUC_{plasma} are the areas under the CSF and plasma concentration time curves, respectively. Here, C_{target} is assumed to follow the same profile as C_{plasma}, with the ratio

between the two concentrations being equal to the ratio between AUC_{CSF} and AUC_{plasma}.

It is assumed that the system is in steady state when no tracer and no treatment is given *(EFF=1)*. In addition, it is assumed that prior to tracer infusion, there are no labelled species. These steady state conditions were used to derive part of the system parameters.

From the steady state conditions and Eqs. S4.8 it follows that the source of APP *(Rin_APP)* was:

$$Rin_{APP} = (Rin\beta + Rin\alpha) * \frac{APP_{base} * MW_{LeuL}}{TC_{1base} * 10^9} \qquad \text{(S4.24)}$$

Where APP_{base} is the baseline level of APP (*unlabelled, prior to tracer infusion*), which is assumed to be equal to the sum of the baseline levels of sAPPα and sAPPβ, as all alternate pathways are represented by the terms for α-secretase. BTC_1 is the baseline of tracee pool 1.

Using the steady state conditions and Eqs. S4.10 the sAPPα formation rate (*Rinα*), equivalent to the α-secretase cleavage step, can be derived:

$$Rin\alpha = Rout_a * \frac{sAPP\alpha_{base}}{APP_{base}} \qquad \text{(S4.25)}$$

Where sAPPα_{base} is the baseline level of sAPPα.

The sAPPβ formation rate (*Rinβ*), equivalent to the BACE1 cleavage step, follows from steady state conditions and Eqs. S4.12:

$$Rin\beta = (Kin_{40} + Kin_{42} + Kin_x) * \frac{sAPP\beta_{base}}{APP_{base}} \qquad \text{(S4.26)}$$

Where *sAPPβ*$_{\text{base}}$ is the baseline level of sAPPβ.

From steady state conditions and Eqs. S4.14 the Aβ40 formation rate (*Kin40*), equivalent to a γ-secretase cleavage step can be calculated:

$$Kin_{40} = Kout * \frac{A\beta40_{base}}{sAPP\beta_{base}} \qquad \text{(S4.27)}$$

Where *Aβ40*$_{\text{base}}$ is the baseline level of Aβ40. *sAPPβ*$_{\text{base}}$ is the baseline level of sAPPβ, used here as surrogate for the baseline level of C99.

From Eqs. S4.16 and steady state conditions, with substitution of *Kout* from Eqs. S4.27, the Aβ42 formation rate (*Kin42*), equivalent to a γ-secretase cleavage step, is deduced:

$$Kin_{42} = Kin_{40} * \frac{A\beta42_{base}}{A\beta40_{base}} \qquad \text{(S4.28)}$$

Where *Aβ42*$_{\text{base}}$ is the baseline level of Aβ42.

From Eqs. S4.20 and steady state conditions, the FactorX formation rate (*Kinx*) is deduced:

$$Kin_x = Kout_x * \frac{FactorX_{base}}{sAPP\beta_{base}} \qquad \text{(S4.29)}$$

Where *FactorX*$_{\text{base}}$ is the baseline level of FactorX.

The model structure includes two times six transit compartments, two for each biomarker (labelled and unlabelled) (sAPPα, sAPPβ, Aβ40, Aβ42, Aβ_O, FactorX), to account for transport from the target site in the brain to CSF. These transit processes are described, in general, by Eqs. S4.30 and S4.31:

$$\frac{d}{dt} species_{CSF}^{lab} = Kt * (species^{lab} - species_{CSF}^{lab}) \tag{S4.30}$$

$$\frac{d}{dt} species_{CSF}^{unlab} = Kt * (species^{unlab} - species_{CSF}^{unlab}) \tag{S4.31}$$

Where *Kt* is the transit rate for the particular species (*KtAP* for sAPPα and sAPPβ; *KtAB* for Aβ40, Aβ42 and Aβ_O; *KtX* for FactorX).

The fraction labelled species (FracLab) for each APP metabolite in CSF are calculated as labelled over total species (Eq. S4.32-S4.34).

$$FracLab_{sAPP\alpha_{CSF}} = \frac{sAPP\alpha_{CSF}^{lab}}{sAPP\alpha_{CSF}^{Total}} \tag{S4.32}$$

$$FracLab_{sAPP\beta_{CSF}} = \frac{sAPP\beta_{CSF}^{lab}}{sAPP\beta_{CSF}^{Total}} \tag{S4.33}$$

$$FracLab_{A\beta_{CSF}} = \frac{A\beta_{40CSF}^{lab} + A\beta_{42CSF}^{lab} + A\beta_{O_{CSF}}^{lab} + FactorX_{CSF}^{lab}}{A\beta_{40CSF}^{Total} + A\beta_{42CSF}^{Total} + A\beta_{O_{CSF}}^{Total} + FactorX_{CSF}^{Total}} \tag{S4.34}$$

The total concentrations for each APP fragment in CSF are calculated as:

$$Total_{species_{CSF}} = species_{CSF}^{lab} + species_{CSF}^{unlab} \tag{S4.35}$$
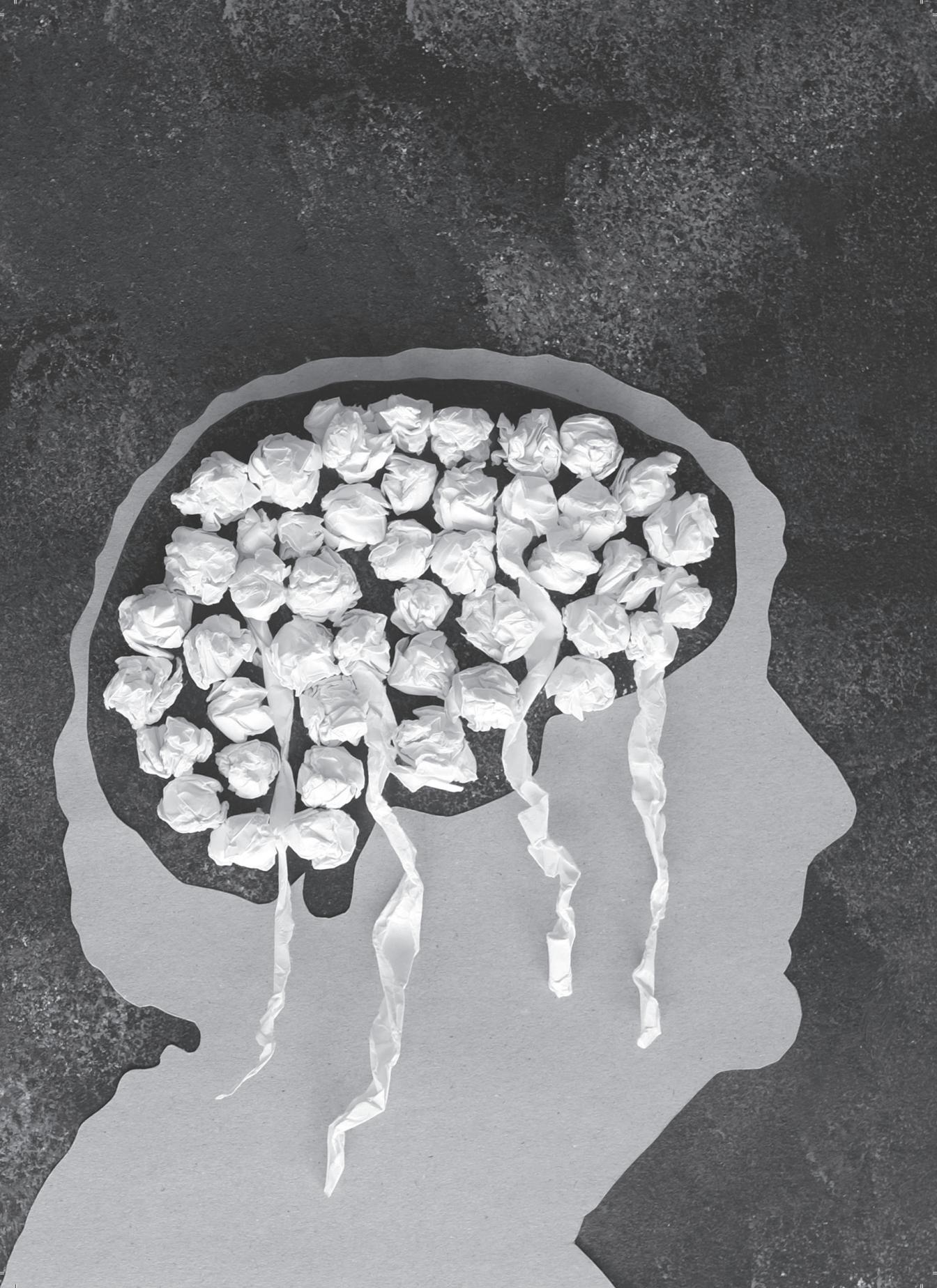
Chapter 5

Extending a systems model of the APP pathway:
Separation of β- and γ-secretase sequential cleavage
steps of APP

E.M.T. van Maanen, T.J. van Steeg, M.J. Ahsman, M.S. Michener,
M.J. Savage, M.E. Kennedy, H.J. Kleijn, J.A. Stone, M. Danhof

Visual Abstract
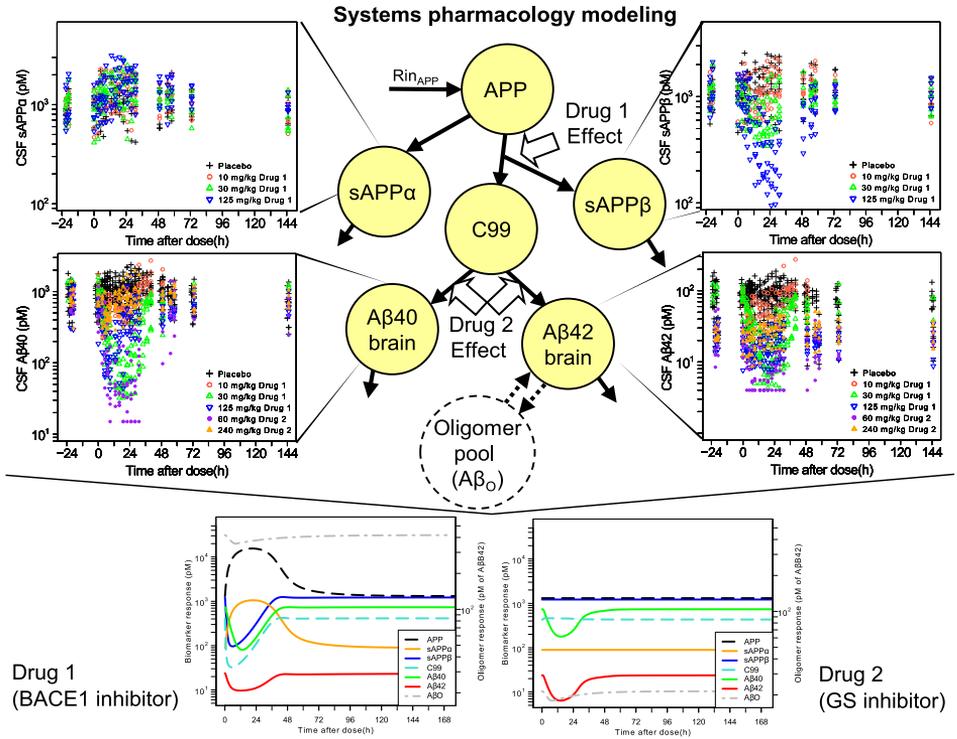
Abstract

The abnormal accumulation of amyloid-β (Aβ) in the brain parenchyma has been posited as a central event in the pathophysiology of Alzheimer's disease. Recently, we have proposed a systems pharmacology model of the APP pathway, describing the Aβ precursor protein (APP) metabolite responses (Aβ40, Aβ42, sAPPα and sAPPβ) to β-secretase 1 (BACE1) inhibition [1]. In this investigation this model was challenged to describe Aβ dynamics following γ-secretase (GS) inhibition. This led an extended systems pharmacology model, with separate descriptions to characterize the sequential cleavage steps of APP by BACE1 and GS, to describe the differences in Aβ response to their respective inhibition. Following GS inhibition a lower Aβ40 formation rate constant was observed, compared to BACE1 inhibition. Both BACE1 and GS inhibition were predicted to lower Aβ_O levels. Further model refinement and new data may be helpful to fully understand the difference in Aβ dynamics following BACE1 *versus* GS inhibition.

Introduction

The amyloid cascade hypothesis posits that the pathological cascade leading to Alzheimer's Disease (AD) is triggered by abnormal accumulation of amyloid-β protein (Aβ) in the brain parenchyma[2]. Inhibition of Aβ production in the brain is therefore a therapeutic target for treating AD with a potentially disease-modifying effect[3,4].

Aβ is generated through sequential proteolytic cleavage of β-amyloid precursor protein (APP) by β-secretase (BACE1) and γ-secretase (GS)[5], as schematically depicted in Figure 5.1. In the first cleavage step, the N-terminal secreted fragment soluble APPβ (sAPPβ) and the C-terminal membrane-bound 99-amino acid fragment (βCTF or C99) are formed by BACE1. Subsequently, C99 is cleaved by GS yielding Aβ species of different chain length of which Aβ38, Aβ40 and Aβ42 are the most common isoforms. In an alternative pathway, cleavage of APP by α-secretase leads to the formation of soluble APPα (sAPPα) and the C-terminal membrane-bound 83-amino acid fragment (αCTF or C83). α-secretase cleavage precludes Aβ formation. Recently, a new APP processing pathway was reported by Willem et al.[6], in which sequential cleavage of APP by η-secretase and BACE1 or ADAM10 produces Aη-β and Aη-α, respectively. There may be other alternate processing of APP unidentified at this moment.

These observations show that the accumulation of Aβ species is governed by a biochemical network, in which there are multiple enzymes that may serve as a target to modify the exposure to distinct Aβ peptide species. The network structure complicates the prediction of the effect of inhibitors of the various enzymes on the exposure to the various Aβ species. This may explain the mixed observations in some of the early clinical trials with enzyme inhibitors. Against this background we have recently proposed a systems pharmacology model to describe the effect of BACE1 inhibition on multiple Aβ species[1].

Inhibitors of the two secretases that generate Aβ from APP, BACE1 and GS inhibitors, have been proposed as potential disease-modifying approaches in the treatment of AD[3]. Several BACE1 inhibitors are presently in clinical trials. The BACE1 inhibitor E2609 (Eisai) is currently in Phase II clinical development, MK-8931 (MSD) has advanced to Phase III and AZD 3293 (Eli Lilly and AstraZenica) recently progressed to Phase III. Various GS inhibitors, acting downstream on the APP pathway compared to BACE1 inhibitors, have also been pursued in the pharmaceutical industry. The GS inhibitor MK-0752 was progressed to Phase I, but then discontinued due to tolerability issues. The GS inhibitor avagecestat (BMS-708163) was discontinued after Phase II because of lack of efficacy and adverse effects of the gastrointestinal and dermatological system[7]. The

development of the GS inhibitor begacestat (GSI953) was discontinued after several Phase I trials. Begacestat reduced plasma Aβ40 levels but not CSF Aβ40[8]. The Phase III trial of the GS inhibitor semagacestat (LY450139) was terminated before completion, because semagacestat was associated with worsening of cognition and function, as well as adverse events such as skin cancers[9]. As yet, no GS inhibitor demonstrated therapeutic success in AD patients.
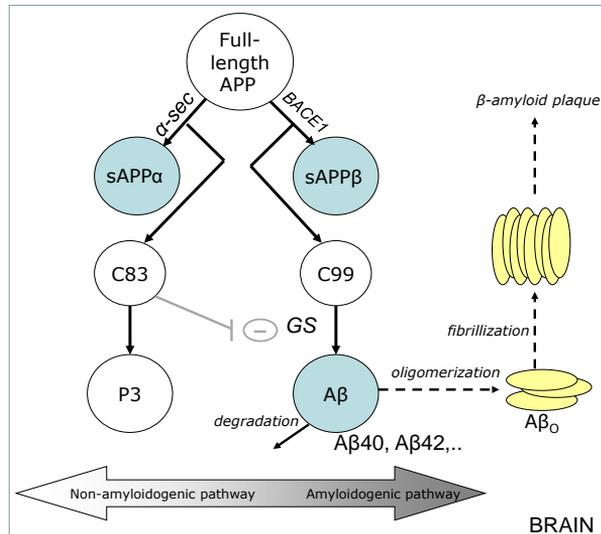
Figure 5.1: The amyloid hypothesis of AD.
In the APP processing pathway, full length APP is cleaved by β-secretase (β-sec) or α-secretase (α-sec) to form sAPPβ and C99 or sAPPα and C83. C99 is then cleaved by γ-secretase (γ-sec) to form Aβ. In a possible feedback loop C83 binds to GS γ-secretase leading to a reduction of Aβ (grey lines). The amyloid hypothesis states that an imbalance in production and clearance of Aβ can result in aggregation of Aβ42 fragments into amyloid plaque.

A better understanding of the drug-induced modulation of the APP system after GS inhibition, may be obtained through a quantitative comprehension of its concentration-response relationships. Several studies on the pharmacokinetics (PK) and the pharmacodynamics (PD) of GS inhibitors have been reported. Das et al.[10] reported a two-compartment model describing Aβ response to GS inhibition, as observed in plasma and CSF in rhesus monkeys. Their model postulates an inhibitory mechanism of Aβ clearance by GS inhibition. However, in their model aspects of the Aβ production, transport and clearance

processes were simplified. A model-based meta-analysis of published and in-house (pre-)clinical GS inhibitors data was performed by Niva et al.[11]. The production and clearance of Aβ was described with a turnover model, with a drug effect on the production rate. Tai et al.[12] also used turnover models to describe Aβ levels following GS inhibition in brain, CSF and plasma in wild type rat. They propose a quasi-static Aβ pool in the brain which does not change after short drug exposure.

The above mentioned approaches look solely at the behaviour of Aβ and not at the behaviour of the APP system as a whole. The understanding of the APP system is imperative to improve the prediction of drug effects on Aβ levels. Recently, a systems pharmacology model of the APP processing pathway was developed to characterize the APP metabolites responses to BACE1 inhibition by MBi-5[1], distinct from MSD's BACE1 inhibitor MK-8931. Throughout the article the term 'recent model' is used to refer this model. The recent model took into account the kinetics and interrelationships of sAPPβ, sAPPα, Aβ40 and Aβ42. In the model, sAPPβ was used as a surrogate substrate for C99 in the γ-secretase cleavage step, modulating the responses of Aβ40 and Aβ42 in the presence of the BACE1 inhibitor. A precursor APP pool, shared by sAPPα and sAPPβ, was included to describe the effect on all four biomarkers with a single drug effect. The effect of BACE1 inhibition was built-in the model as inhibition of the pathway mediated by BACE1. Using this model, it was demonstrated that BACE1 inhibition resulted in a larger absolute reduction of CSF levels of Aβ40 than of Aβ42, as the effect on Aβ42 was modulated by back-conversion from an oligomer (Aβ_O) pool.

There is growing evidence that Aβ_O have a central role in the pathogenesis of AD[13]. Toxic Aβ_O are considered to be the drivers of neurodegeneration. Aβ_O might exist in a complex equilibrium with Aβ monomers and fibrils[14]. Treatments that prevent Aβ production may reduce the concentration of Aβ_O and subsequently promote the release of soluble Aβ from fibrils to restore the equilibrium[15].

The objective of the current investigation was to elucidate the APP processing pathway further, by challenging the recently developed systems pharmacology model of the APP pathway to describe Aβ dynamics following GS inhibition. The aims were (i) to separate β-secretase and γ-secretase sequential cleavage steps; (ii) to investigate possible differences in Aβ response following GS versus BACE1 inhibition; and (iii) to evaluate if moderation of Aβ42 by back-conversion from an Aβ_O pool could also be identified after inhibiting GS. To this end, CSF Aβ40 and Aβ42 response data from two studies of the GS inhibitor MK-0752 in cisterna magna ported rhesus monkeys[16] were analysed simultaneously with data from a BACE1 inhibitor (MBi-5) study, using the APP systems model.

Materials and Methods

Animals

All animal studies were reviewed and approved by the MSD Institutional Animal Care and Use Committee. The NIH Guide to the care and use of Laboratory Animals and the Animal Welfare act were followed in the conduct of the animal studies (Institute of Laboratory Animal Resources, National Research Council, 1996). The CMP rhesus monkey model was reported by Gilberto et al. [17]. The rhesus monkeys are chronically implanted with catheters in the cisterna magna, facilitating repeated sampling of CSF and plasma (through a jugular vascular access point). These rhesus monkeys were individually housed and captive-bred in a closed colony.

In the first GS inhibitor study (study 1), six male animals, weighing between 6.9 kg and 9.6 kg (mean, 8.2 kg), age n=5 at 5 years to 8 years (mean, 6 years) and 1 animal aged 17 years at time of study were included. The second GS inhibitor study (study 2) included six male animals, weighing between 6.1 kg and 12.3 kg (mean, 9.1 kg), age 7 to 10 years (mean, 8 years). In the BACE1 inhibitor study (study 3), six male animals, weighing between 5.2 kg and 11.7 kg (mean, 8.7 kg), age 2 to 10 years (mean, 8 years), were included. Half of the animals in the BACE1 inhibitor study participated also in the GS inhibitor studies.

Drug administration and sampling

The effects of secretase inhibition were obtained in three studies. In study 1, information on the effect of GS inhibition on Aβ40 and Aβ42 was obtained following a single oral administration of MK-0752 (3-((1r,4s)-4-(4-chlorophenylsulfonyl)-4-(2,5-difluorophenyl)cyclohexyl)propanoic acid) at 60 and 240 mg/kg (5 mL/kg) in a vehicle controlled (sterile water) three-period crossover study. In study 2, the effect of GS inhibition on Aβ40 and Aβ42 was measured during a follow-up collection period, following a single oral dose of MK-0752 at 240 mg/kg (5 mL/kg) in a vehicle controlled (sterile water) study. In study 3, the effect of BACE1 inhibition on sAPPα, sAPPβ, Aβ40 and Aβ42 were measured, following a single, oral administration of MBi-5 at 10, 30, 125 mg/kg (5 mL/kg), or vehicle (0.4% methylcellulose) in a four-way full crossover study. The study protocols of study 1 and 2 and pharmacological profile of MK-0752 were previously described by Cook et al. [16]. The detailed study protocol of study 3 and pharmacological profile of MBi-5 were described by Dobrowolska et al. [18]. The study protocols are summarized here.

In study 1, plasma and CSF drug concentrations were collected at 0 (predose) and 3, 5, 7, 9, 13, 16, 19, 22, 25, 28, 31, 34, 37, 40 and 49 h postdose, resulting in 16 plasma and CSF PK samples for each monkey per treatment. In study 2, plasma and CSF samples were collected as described for study 1 and additional samples were taken at 73, 145, 169, 217 and 241 h postdose, resulting in 21 plasma and CSF PK samples for each monkey. 2 mL of blood and 1 mL of CSF were collected at each time point. The concentration of MK-0752 in the plasma and CSF samples was determined using LC-MS/MS. The concentrations of Aβ40 and Aβ42 were determined from CSF samples collected at the same time points as PK samples, giving 16 measurements of each biomarker for each monkey per treatment in study 1 and 21 measurements of each biomarker for each monkey in study 2. The Aβ1-40 and Aβ1-42 assays used for the concentration measurements were described previously by Cook et al. [16].

In study 3, plasma and CSF drug concentrations were collected at 0 (predose) and 3, 5, 7, 9, 13, 16, 19, 22, 25, 28, 31, 49, 55, 58, 73 and 145 h postdose, resulting in 17 plasma and CSF PK samples for each monkey per treatment group. 2 mL of blood and 1 mL of CSF were collected at each time point. The concentration of MBi-5 in the plasma and CSF samples was determined using LC-MS/MS. The concentrations of Aβ40, Aβ42, sAPPα and sAPPβ were determined from CSF samples collected at -22, -20 and -1h (predose) and 2, 4, 6, 8, 12, 15, 18, 21, 24, 27, 30, 48, 54, 57, 72 and 144 h postdose, giving 19 measurements of each biomarker for each monkey per treatment group. 1 mL of CSF were collected at each time point. The specific enzyme-linked immunosorbent assays used for the concentration measurements were described previously [19,20].

PK-PD analysis

PK-PD modelling analysis was performed by means of non-linear mixed effects modelling using the software package NONMEM (version 7.2.0[21]). In this approach, structural (fixed) effects and both intra- and interindividual variability are taken into account. Typical values of structural model parameters (population parameters, which define the average value for a parameter in a population) (θ), the variance and covariance of the interindividual variability (ω^2) and the variance of the residual error (σ^2) are estimated.

The best models were chosen based on minimum value of the objective function, the precision of parameter estimates, and visual inspection of goodness-of-fit plots. A more detailed description of the modelling procedure was described in van Maanen et al. [1].

To evaluate the performance of the model a visual predictive check (VPC) was performed in which the median and the 90% inter-quantile range of the data simulated

with the final parameter estimates were overlayed with the observations. The predictive capacity is considered sufficient when the median and 90% of predictions line up within the 5th, 50th and 95th percentiles of the observations.

The NONMEM software package was implemented on an Intel QuadCore (Intel®Core^{TM} i7 CPU860, 2.80 GHz, 3.24 GB RAM) and Compaq Visual Fortran (version 6.6, Compaq Computer Corporation, Houston, Texas, USA) was used as compiler. Data management and model assessment was done using the statistical software package S-PLUS for Windows (version 8.0 Professional, Insightful Corp., Seattle, USA).

Model description

The systems model of the APP processing pathway was developed by sequential analysis of PK and PD data following administration of MBi-5 and MK-0752. The PK models of MBi-5 and MK-0752 were based on simultaneous analysis of plasma and CSF PK data of each compound. The results of the PK data analysis of MBi-5 have been reported elsewhere by van Maanen et al.[1]. The results of the PK data analysis of MK-0752 are reported in the supplemental material.

The PK models adequately described the plasma and CSF concentration time profiles of MBi-5 and MK-0752, respectively, thus the models could serve as input for PD model analysis.

The interrelationships of APP metabolite responses to BACE1 inhibition were described recently using a comprehensive systems model of the APP processing pathway[1]. To describe the effect of the GS inhibitor, the model had to be extended.

The extended systems model of the APP processing pathway included a compartment for C99. The relation between Aβ and C99 was included in the model, representing the γ-secretase cleavage step, on which the drug effect of MK-0752 was implemented. In addition, sAPPβ was no longer used as driver of Aβ response and a sAPPβ elimination path was incorporated into the model.

The biomarker response profiles of MBi-5 and MK-0752 measured in CSF were adequately described by a model containing compartments for seven moieties: APP, sAPPβ, sAPPα, C99, Aβ40, Aβ42 and Aβ$_O$ (Fig. S5.1). The production of APP was assumed to be constant and described by a zero order input rate constant Rin_{APP}. The production of the APP metabolites was assumed to be first order, i.e. dependent on its precursor concentration. The relationship between APP and its metabolites (sAPPβ, sAPPα, C99, Aβ40 and Aβ42) and Aβ$_O$ is described by Eq. 5.1 - Eq. 5.7:

$$\frac{d}{dt}APP = Rin_{APP} - (Rin * EFFB + Rin_2) * APP \tag{5.1}$$

$$\frac{d}{dt}sAPP\alpha = Rin_2 * APP - Rout_a * sAPP\alpha \tag{5.2}$$

$$\frac{d}{dt}sAPP\beta = Rin * EFFB * APP - Rout_b * sAPP\beta \tag{5.3}$$

$$\frac{d}{dt}C99 = Rin * EFFB * APP - (Kin_{40} + Kin_{42}) * EFFG * C99$$
$$- Kout_{99} * C99 \tag{5.4}$$

$$\frac{d}{dt}A\beta_{40} = Kin_{40} * EFFG * C99 - Kout * A\beta_{40} \tag{5.5}$$

$$\frac{d}{dt}A\beta_{42} = Kin_{42} * EFFG * C99 - Kout * A\beta_{42} - Kpl \times A\beta_{42}$$
$$+ Krev \times A\beta_O \tag{5.6}$$

$$\frac{d}{dt}A\beta_O = Kpl \times A\beta_{42} - Krev \times A\beta_O \tag{5.7}$$

The rate of change of APP with respect to time in the presence of the BACE1 inhibitor is expressed by Eq. 5.1, in which the BACE1 cleavage inhibition is incorporated by the factor *EFFB*. The rate of change of C99 with respect to time in the presence of the GS inhibitor is described by Eq. 5.4, in which the GS cleavage inhibition is incorporated by the factor *EFFG*. *EFFB* and *EFFG* are the degrees of inhibition caused by MBi-5 and MK-0752, respectively. Generally, the degree of inhibition is described by a sigmoidal Imax function, as shown in Eq. 5.8.

$$EFF = 1 - \frac{C_{target}^{GAM} * Imax}{C_{target}^{GAM} + IC50^{GAM}} \qquad (5.8)$$

Where C_{target} is the target site concentration of MBi-5 or MK-0752, respectively, *IC50* the C_{target} that results in 50% inhibition of BACE1 or GS, *Imax* is the maximum response and *GAM* is the Hill coefficient. C_{target} was derived from the respective PK models as:

$$C_{target} = C_{plasma} * \frac{AUC_{CSF}}{AUC_{plasma}} \qquad (5.9)$$

Where AUC_{CSF} and AUC_{plasma} are the areas under the CSF and plasma concentration time curves, respectively. C_{target} is assumed to be in steady state with C_{plasma}.

It is assumed that the system is in steady state (SS) when no treatment is given *(EFFB=1, EFFG=1)*. These steady state conditions were used to derive part of the system parameters. From SS and Eq. 5.1 it follows that the zero order input rate constant of APP *(Rin$_{APP}$)* is:

$$Rin_{APP} = (Rin_{\alpha} + Rin_{\beta}) * APP_{base} \qquad (5.10)$$

Where *APP$_{base}$* is the baseline level of APP, assumed to be equal to the sum of the baseline levels of sAPPα and sAPPβ. All alternate pathways are represented by the terms for α-secretase.

Using SS conditions and Eq. 5.2 the sAPPα formation rate constant (Rin_{α}), equivalent to the α-secretase cleavage step, can be derived:

$$Rin_{\alpha} = Rout_a * \frac{sAPP\alpha_{base}}{APP_{base}} \qquad (5.11)$$

Where sAPPα_{base} is the baseline level of sAPPα.

The sAPPβ and C99 formation rate constant (Rin_{β}), equivalent to the BACE1 cleavage step, follows from SS conditions and Eq. 5.3:

$$Rin_{\beta} = Rout_b * \frac{sAPP\beta_{base}}{APP_{base}} \qquad (5.12)$$

Where *sAPPβ_{base}* is the baseline level of sAPPβ.

From Eq. 5.5 and SS, the Aβ degradation rate constant (*Kout*), is deduced:

$$Kout = Kin_{40} * \frac{C99_{base}}{A\beta40_{base}} \qquad (5.13)$$

Where $C99_{base}$ is the baseline level of C99. Please not that C99 is not an observed measure. From Eq. 5.4 and SS the baseline level of C99 can be calculated:

$$C99_{base} = \frac{Rout_b * sAPP\beta_{base}}{Kin_{40} + Kin_{42} + Kout_{99}} \qquad (5.14)$$

Combining Eq. 5.13 and Eq. 5.14, the Aβ42 formation rate constant (*Kin42*), equivalent to a GS cleavage step, can be written as:

$$Kin_{42} = Kout * \frac{A\beta42_{base}}{A\beta40_{base}} \qquad (5.15)$$

Kpl and *Krev* are the Aβ42 oligomerization and dissociation rate constant, respectively, which are dependent on the baseline values of Aβ42 and the Aβ_{O} pool (A$\beta42_{base}$ and A$\beta_{\mathrm{O}base}$, resp.) according to Eq. 5.16:

$$Krev = \frac{Kpl \times A\beta_{42base}}{A\beta_{Obase}} \qquad (5.16)$$

The model structure includes four transit compartments (Fig. S5.1), one for each biomarker measured in CSF (sAPPα, sAPPβ, Aβ40, Aβ42), to account for transport from the target site in the brain to CSF. These transit processes are described, in general, by Eq. 5.17:

$$\frac{d}{dt}xAx_{CSF} = Ktr * (xAx - xAx_{CSF}) \qquad (5.17)$$

Where *Ktr* is the transit rate constant for the particular APP metabolite xAx (sAPPα, sAPPβ, Aβ40, Aβ42).

Results

Aβ response to GS and BACE1 inhibition was described by separate descriptive models

Initially, empirical PK-PD models were developed to quantify the exposure-response relationships for each CSF APP metabolite of the BACE1 inhibitor MBi-5 (Aβ40, Aβ42, sAPPα and sAPPβ) and GS inhibitor MK-0752 (Aβ40 and Aβ42) in rhesus monkeys. For the BACE1 inhibitor MBi-5, the empirical PK-PD models for Aβ40, Aβ42, sAPPα and sAPPβ were discussed recently in van Maanen et al.[1]. For MBi-5 and MK-0752, we now present the empirical PK-PD models for Aβ40 and Aβ42. The exposure-response relationship for each Aβ-inhibitor combination was described by a transit model with 1 or 2 compartments, with the drug effect modelled relative or subtractive to baseline using an Imax function. Table 5.1 presents a summary overview of the results of these models. For each inhibitor, the empirical models identified similar drug effects for Aβ40 and Aβ42: for MBi-5 the identified potencies were Aβ40: 0.0254 μM (95% CI, 0.0246-0.0262) and Aβ42: 0.0455 μM (95% CI, 0.0351-0.0559) and for MK-0752 the identified potencies were Aβ40: 0.432 μM (95% CI, 0.300-0.564) and Aβ42: 0.567 μM (95% CI, 0.402-0.732).

The separate empirical models revealed potential challenges for the combined analysis. Firstly, there are study differences in Aβ baselines: Aβ40 baseline is 1.5 fold higher and the Aβ42 baseline is 3.4 fold higher in the GS inhibitor studies (study 1 and 2) compared to the BACE1 inhibitor study (study 3). Consequently, the ratio of Aβ42:Aβ40 is higher in the GS inhibitor studies: 0.078 for the GS inhibitor studies and 0.034 for the BACE1 inhibitor study, respectively. Secondly, the mean transit time through the compartments of the models was lower for Aβ42 after BACE1 inhibition than Aβ42 after GS inhibition. This indicated that the response of Aβ42 to BACE1 inhibitor will appear earlier in CSF than with GS inhibition. Sequentially, BACE1 inhibition interferes earlier in the amyloidogenic APP pathway. This suggested a temporal difference in relative response progression of Aβ42 following BACE1 *versus* GS inhibition. For Aβ40, the mean transit time was higher after BACE1 inhibition than after GS inhibition, however overlapping confidence intervals suggest insignificant differences.

A systems model to describe APP metabolite responses to GS and BACE1 inhibition

Recently, we reported a systems pharmacology model, incorporating the pharmacokinetics of MBi-5 and APP metabolites (Aβ40, Aβ42, sAPPβ and sAPPα) concentrations[1]. In

Table 5.1: Summary parameters of the separate empiric model fits for Aβ40 and Aβ42 for each inhibitor

PARAMETER	DESCRIPTION	UNIT	MBi-5		MK-0752	
			Aβ40	Aβ42	Aβ40	Aβ42
baseline	baseline	pM	722	24.8	1080	83.3
Imax	maximal inhibition		100%[a,b]	20.4 pM [c]	100%[a]	100%[a]
IC$_{50}$	median inhibition concentration	μM	0.0254	0.0455	0.432	0.567
			(CV	(CV	(CV	(CV
			1.63%)	11.6%)	15.6%)	14.8%)
GAM	Hill coefficient		1[a]	1[a]	1.70	1.48
MTT[d]	Mean transit time (MTT)	h	5.155	3.597	4.651	5.435
	95% confidence interval MTT	h	(4.23-6.60)	(2.42-7.08)	(3.72-6.21)	(4.26-7.52)

[a] Fixed.

[b] $Effect = baseline * (1 - \frac{C_{target}^{GAM}*Imax}{C_{target}^{GAM}+IC_{50}^{GAM}})$

[c] $Effect = baseline - \frac{C_{target}^{GAM}*Imax}{C_{target}^{GAM}+IC_{50}^{GAM}}$

[d] $MTT = \frac{1}{Kt} \times (n+1)$, where n is the number of transit compartments and Kt is the transit rate.

the current analysis, the model was extended to describe dynamics of Aβ responses after exposure to a GS inhibitor. To this end, the APP metabolite responses of Aβ40, Aβ42, sAPPβ and sAPPα following BACE1 inhibition and Aβ40 and Aβ42 response following GS inhibition were analysed simultaneously.

To closer match the APP processing pathway, a C99 compartment was added to the model structure. As sAPPβ and C99 are both products of the same BACE1 cleavage step, the formation rate constant of C99 was set to be equal to the formation rate constant of sAPPβ (*Rinβ*). The effect of BACE1 inhibition was incorporated in the model as inhibition of *Rinβ*. The effect of GS inhibition was modelled as inhibition of the Aβ40 and Aβ42 formation rate out off the C99 compartment, consistent with the γ-secretase cleavage step. The elimination of sAPPβ (*RoutB*) could now be described as a separate parameter.

Inclusion of a C99 compartment and the estimated GS inhibition rates implied rebound of Aβ40 and Aβ42 response after GS inhibition: Simulations indicated an excessive response above baseline upon cessation of GS inhibition (not shown). However, the data did not suggest any significant rebound. Therefore, the model was refined by adding an alternative elimination pathway of C99 (*Kout99*) and hence preventing rebound. The resulting model structure is presented in Figure 5.2.

Inter-study baseline differences were evaluated by adding baseline data from two other studies (Study A and B) (see Supplemental Material). From this, it became apparent that a correction for Aβ baseline differences between studies needed to be included. The
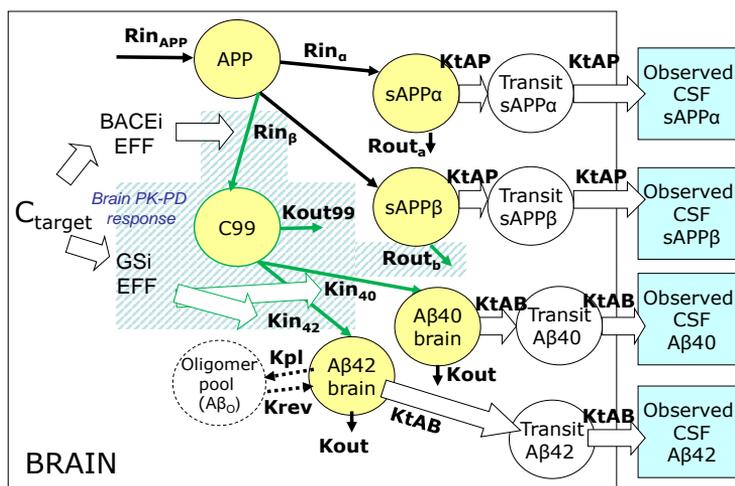
Figure 5.2: Schematic of model structure.
The model comprised eleven compartments: Six biomarker compartments in brain *(yellow)*, one oligomer pool *(blank dashed)* and four transit compartments from brain to CSF *(blank)*. Four biomarkers were measured in CSF (sAPPα, sAPPβ, Aβ40 and Aβ42), indicated by the blue boxes. The model included a C99 compartment *(dashed)*, which was not present in the model based on β-secretase inhibition data only. Model extensions are indicated with the green shaded area. The drug effect of the β-secretase inhibitor *(BACEi EFF)* inhibited *Rin*. The drug effect of the γ-secretase inhibitor *(GSi EFF)* inhibited Kin_{42} and Kin_{40}. As driver of biomarker response C_{target} was used, which was derived from the respective PK models (not shown).
APP: Aβ-precursor protein; *Aβ*: amyloid-β-peptide; C_{target}: drug concentration target site; Kin_{40}: Aβ40 formation rate; Kin_{42}: Aβ42 formation rate; *Kout*: Aβ degradation rate; $Kout_{99}$: C99 degradation rate; *KtAP*: transit rate sAPPα and sAPPβ from brain to CSF; *KtAB*: transit rate Aβ from brain to CSF; *RinAPP*: source of APP; *Rinα*: sAPPα formation rate; *Rinβ*: sAPPβ and C99 formation rate; *Routa*: sAPPα degradation rate; *Routb*: sAPPβ degradation rate. *Kpl*: Oligomerization rate; *Krev*: $Aβ_O$ dissociation rate.

underlying biological system was assumed to be the same during all studies. Therefore, scaling factors were included on the model predictions (IPRED) for Aβ40 and Aβ42 outside of the system. To improve the model description further, differences in parameter values following BACE1 or GS inhibition were investigated. The formation rate constant of Aβ40 *(Kin40)* was fixed to the value identified recently (0.574 h^{-1}) following BACE1 inhibition[1] and a significantly lower *Kin40* was identified after GS inhibition (0.349 h^{-1} (95% CI: 0.296-0.402). Also, a substantial reduction of the Aβ42 oligomerization rate constant *(Kpl)* after GS inhibition was found (95% reduction). Including these differences improved the description of all the biomarkers.

Overall, the data were adequately captured across studies (Fig.5.3-5.6). Only a slight

underprediction was observed for the baseline level of Aβ40 in study 1 (Fig. 5.3A) and the maximal Aβ42 response to 240 mg/kg MK-0752 (Fig. 5.5B and 5.5C) and 125 mg/kg MBi-5 (Fig. 5.5F).

The model separated drug-specific and system-specific parameters

The population parameters and intra- and interanimal variability were optimized for the all study populations simultaneously and are reported in Table 5.2. Interanimal variability was included as exponential in nature, reflecting lognormal distributions of the individual model parameters, for the baseline of sAPPβ, the IC50 of MBi-5 and the IC50 of MK-0752. As the baselines of other APP metabolites were modelled as function of the baseline of sAPPβ, the interanimal variability of sAPPβ is propagated in these biomarkers. Residual variability was included for each APP

(A) Aβ40 placebo St1

(B) Aβ42 placebo St1

(C) Aβ40 placebo St2

(D) Aβ42 placebo St2

(E) Aβ40 placebo St3

(F) Aβ42 placebo St3

Figure 5.3: Placebo. Aβ. Simulations of biomarker response* vs. *time profile of placebo in the rhesus with 90% confidence interval. Observation sample size: n=114 for each APP metabolite from 6 monkeys collected over 7 days. *Solid line:* Median predicted. *Long-dashed line:* 90% prediction interval. *Dotted line:* Median observed. *+ symbol:* Observations.

(A) Aβ40 Dose 60 mg/kg St1

(B) Aβ40 Dose 240 mg/kg St1

(C) Aβ40 Dose 240 mg/kg St2

(D) Aβ40 Dose 10 mg/kg St3

(E) Aβ40 Dose 30 mg/kg St3

(F) Aβ40 Dose 125 mg/kg St3

Figure 5.4: Aβ40. Simulations of biomarker response* vs. *time profile of Aβ40 in the rhesus with 90% confidence interval. Observation sample size: n=114 for each APP metabolite from 6 monkeys collected over 7 days. *Solid line:* Median predicted. *Long-dashed line:* 90% prediction interval. *Dotted line:* Median observed. *+ symbol:* Observations.

(A) *Aβ42 Dose 60 mg/kg St1* (B) *Aβ42 Dose 240 mg/kg St1*

(C) *Aβ42 Dose 240 mg/kg St2* (D) *Aβ42 Dose 10 mg/kg St3*

(E) *Aβ42 Dose 30 mg/kg St3* (F) *Aβ42 Dose 125 mg/kg St3*

Figure 5.5: Aβ42. Simulations of biomarker response **vs.** *time profile of Aβ42 in the rhesus with 90% confidence interval.* Observation sample size: n=114 for each APP metabolite from 6 monkeys collected over 7 days. *Solid line:* Median predicted. *Long-dashed line:* 90% prediction interval. *Dotted line:* Median observed. *+ symbol:* Observations.

(A) sAPPα placebo

(B) sAPPβ placebo

(C) sAPPα Dose 10 mg/kg

(D) sAPPβ Dose 10 mg/kg

(E) sAPPα Dose 30 mg/kg

(F) sAPPβ Dose 30 mg/kg

(G) sAPPα Dose 125 mg/kg

(H) sAPPβ Dose 125 mg/kg

Figure 5.6: sAPPα (left) and sAPPβ (right). Simulations of biomarker response vs. time profile of MBi-5 in the rhesus with 90% confidence interval. Observation sample size: n=114 for each APP metabolite from 6 monkeys collected over 7 days. *Solid line:* Median predicted. *Long-dashed line:* 90% prediction interval. *Dotted line:* Median observed. *+ symbol:* Observations.

metabolite (sAPPβ, sAPPα, Aβ40, Aβ42), as proportional error models, assuming a normal distribution. Drug specific parameters (*IC50, GAM, IM*) could be distinguished from system specific parameters (*Kin$_{40}$, Kout$_{99}$, Rout$_a$ Rout$_b$, KtrAP, Kpl, Krev*). The correlations between parameters were all below 0.95.

The transit rate constant from brain-to-CSF for Aβ40 and Aβ42 was assumed to be equal and fast. As the transit rate for sAPPβ and sAPPα can only be estimated relative to the transit rate of Aβ, the latter was fixed to an arbitrary high value (10 h^{-1}). The transit rate constant for sAPPβ and sAPPα was estimated to be 0.0847 h^{-1}, which should be interpreted relative to the Aβ transit rate constant.

Correction factors on Aβ42 and Aβ40 for study differences in levels compared to study 3 were 3.7 (95% CI, 3.40-4.00) and 1.37 (95% CI, 1.26-1.48), which were imputed as multipliers on the respective IPREDs of Aβ42 and Aβ40.

The *IC$_{50}$* of MBi-5 was estimated to be 0.0185 μM (95% CI, 0.0149-0.0221); the *IC$_{50}$* of MK-0752 was 0.445 μM (95% CI, 0.337-0.553). The Hill coefficients for both compounds slightly deviated from unity: MBi-5 1.49 (95% CI, 1.35-1.63) and MK-0752 1.73 (95% CI, 1.54-1.92).

Differences in APP metabolite interrelationships following BACE1 and GS inhibition

The formation rate constant of Aβ42 (*Kin$_{42}$*) was calculated according to Equation 5.15: 0.0186 h^{-1} and 0.0113 h^{-1} in the BACE1 and GS inhibition studies, respectively. *Kin$_{42}$* was higher than the formation rate constant of Aβ40 (*Kin$_{40}$*: 0.574 h^{-1} and 0.349 h^{-1}, in the BACE1 and GS inhibition studies, respectively). This is in agreement with the previously reported ratio of Aβ42 and Aβ40 of about 1:10 in non-Alzheimer brain (Iwatsubo et al. [22]).

The resulting model was used to visualize the interrelationships of the biomarkers following BACE1 and GS inhibition, respectively. Also, the behaviour of APP, C99 and Aβ_O was predicted. The relationships of the biomarker responses to BACE1 inhibition were recently discussed in van Maanen et al. [1]. The differentiation in biomarker response to inhibition of BACE1 and GS was as followed. APP increases after BACE1 but not after GS inhibition (Figure 5.7A and 5.7B, respectively). C99 decreases following BACE1 inhibition and slightly increases following GS inhibition. Both BACE1 and GS inhibition are predicted to decrease Aβ_O levels, implying that the formation of Aβ_O is reduced by decreased levels of monomeric Aβ42 and that Aβ_O is in dynamic equilibrium with monomeric Aβ42.

Table 5.2: *Population parameter estimates including coefficient of variation (CV%)*

PARAMETER	DESCRIPTION	VALUE	UNIT	CV%
Structural parameters				
sAPPβ_{base}	baseline sAPPβ	1.22e+3	pM	4.44
Fbase$^b_{A\beta40}$	Aβ40 baseline as fraction of sAPPβ_{base}	0.602		2.56
Fbase$^c_{A\beta42}$	Aβ42 baseline as fraction of sAPPβ_{base}	0.0195		2.37
Fbase$^d_{sAPP\alpha}$	sAPPα baseline as fraction of sAPPβ_{base}	0.729		2.15
Kin$_{40}$B^a	formation rate Aβ40 following BACE1 inhibition *(fixed)*	0.574	h^{-1}	
Kin$_{40}$G	formation rate Aβ40 following GS inhibition	0.349	h^{-1}	7.68
Kout$_{99}$	degradation rate C99	4.70	h^{-1}	10.1
Rout$_a$	degradation rate sAPPα	1.80	h^{-1}	13.3
Rout$_b$	degradation rate sAPPβ	1.79	h^{-1}	9.61
KtrAP	transit rate sAPPα and sAPPβ	0.0847	h^{-1}	4.17
KtrAB^a	transit rate Aβ*(fixed)*	10	h^{-1}	
IMB^a	Imax BACE *(fixed)*	1		
IC50B	IC50 BACE	0.0185	μM	9.89
GAMB^a	Hill coefficient	1.49		4.72
IMG^a	Imax GSi *(fixed)*	1		
IC50G	IC50 GSi	0.445	μM	12.4
GAMG^a	Hill coefficient	1.73		5.55
KplB	oligomerization rate following BACE1 inhibition	0.183	h^{-1}	13.3
FKplG^e	factor on oligomerization rate following GS inhibition	0.0512		21.3
Krev	oligomer dissociation rate	0.0104	h^{-1}	64.7
FAC1	correction factor for study differences Aβ42	3.70		4.16
FAC2	correction factor for study differences Aβ40	1.37		4.25
Interanimal variability				
ω^2_{BSAPb}	Interanimal variability sAPPβ baseline	0.0672		20.4
ω^2_{IC50B}	Interanimal variability IC50 BACE	0.280		39.6
ω^2_{IC50G}	Interanimal variability IC50 GSi	0.176		44.8
Residual error				
$\sigma^2_{A\beta40}$	Residual variability Aβ40	0.135		5.45
$\sigma^2_{A\beta42}$	Residual variability Aβ42	0.0911		4.97
$\sigma^2_{sAPP\beta}$	Residual variability sAPPβ	0.0732		8.09
$\sigma^2_{sAPP\alpha}$	Residual variability sAPPα	0.106		8.53

^{a} Fixed.

^{b} Aβ40$_{base}$=Fbase$_{A\beta40}$*sAPPβ_{base}.

^{c} Aβ42$_{base}$=Fbase$_{A\beta42}$*sAPPβ_{base}.

^{d} sAPPα_{base}=Fbase$_{sAPP\alpha}$*sAPPβ_{base}.

^{e} KplG=KplB*FKplG.

Figure 5.7: Simulation biomarker responses.
The biomarker responses are simulated after a single dose of 125 mg MBi-5 (A) (C) and single dose of 60 mg MK-0752 (B) (D).

APP black dashed line; *sAPPα* yellow solid line; *sAPPβ* blue solid line; *C99* light blue dashed line; *Aβ40* green solid line; *Aβ42* red solid line; *Aβ$_O$* grey twodash line.

The simulated concentration of Aβ$_O$ should be interpreted as the level if Aβ42 monomers tied in the 'oligomer soup' in the brain. The Aβ$_O$ pool was modelled as a pool in equilibrium with monomeric Aβ42 without adaptation for the number of subunits in multimeric species contained in the Aβ$_O$ pool. The simulated difference in Aβ$_O$ concentration in Figure 5.7A and 5.7B therefore reflects a difference in the the number of monomers incorporated in the Aβ$_O$ pool.

Discussion

A recently reported systems model of the APP processing pathway was extended to describe the interrelationships of Aβ40, Aβ42, sAPPβ, and sAPPα upon inhibition of BACE1 with MBi-5 and Aβ40 and Aβ42 upon inhibition of GS with MK-0752 simultaneously[1]. BACE1 acts earlier in the cascade, affecting all four biomarkers. Sequentially, GS inhibition interferes later in the amyloidogenic APP pathway and affects Aβ40 and Aβ42 only. In the recent model, sAPPβ was used as a surrogate substrate for C99 in the γ-secretase cleavage step, driving the response of Aβ. Consequently, the γ-secretase cleavage step could not be differentiated from sAPPβ elimination. Here, the combined model based analysis of BACE1 inhibitor and GS inhibitor response data facilitated the separation of the γ-secretase cleavage step from other processes involved. To that end, the extended systems model of the APP processing pathway included a compartment for C99, wherein the relationship between C99 and Aβ represents the γ-secretase cleavage step. As a result of this model extension, it was possible to identify the brain-turnover of sAPPβ as a separate parameter. Thus, the brain turnover of sAPPβ (0.39 hours) could be distinguished from the half-life of the brain-to-CSF transfer (8.2 hours).

Using the sAPPβ pool as moderator of Aβ in the recent model was a simplification of the underlying biological system. Here, the systems model structure more closely resembles the underlying APP pathway and the incorporation of the data following GS inhibition was essential for this.

The MK-0752 concentration dependent decrease of Aβ40 and Aβ42 could be described by incorporating a single drug effect in the model: inhibition of the formation rates of Aβ40 and Aβ42 out of the C99 compartment, equivalent to the GS cleavage step. The effect of BACE1 inhibition was incorporated in the model as inhibition of the formation of sAPPβ and C99 ($Rin\beta$), corresponding to the BACE1 cleavage step.

The elimination rate was higher for C99 than for sAPPβ. sAPPβ and C99 could be subjected to different elimination processes, conceivably because C99 remains membrane bound as opposed to sAPPβ, or has other biochemical/biophysical properties. The elimination rate of sAPPβ and sAPPα had similar values. Both are soluble fragments of APP, with overlapping sequence only differentiating in the 16 C-terminal amino-acids. The functions that are related to the shared domains of sAPPα and sAPPβ are identical (Chasseigneaux2012a). Therefore, it is not unlikely that sAPPα and sAPPβ also have similar elimination pathways.

The identified IC_{50} of MK-0752 in the empirical models were consistent with the

single potency identified using the systems model. Aβ is the product of GS cleavage of C99 and therefore Aβ response measurement following GS inhibition provides a direct reflection of the drug action. Hence, the IC50 values based on empirical *versus* the mechanistic systems model were similar for MK-0752. The estimated IC_{50} of MK-0752 (0.445 μM) is also similar to the brain IC_{50} in guinea-pigs of 440 nM [16].

For MBi-5, the identified IC_{50} in the empirical models were significantly higher than the single potency of 0.0185 μM identified using the systems model. As MBi-5 interferes earlier in the amyloidogenic APP pathway, inhibiting the formation of the Aβ precursor C99, Aβ response does not directly reflect the drug action. A systems model that includes key processes such as the production, elimination, and brain-to-CSF transport for the APP metabolites can more accurately describe the IC50 than an empirical model.

The identified IC_{50} of MBi-5 in the current analysis was lower 0.0185 μM (95% CI, 0.0149-0.0221) than recently identified 0.0269 μM (95% CI, 0.0154-0.0384) [1], however, confidence intervals overlap. The more complete systems model presented here, explains more fully the processes occurring in the APP pathway and therefore provides a more accurate characterization of IC50.

A significant difference in Aβ40 formation rate constant was identified following BACE1 and GS inhibition. This may reflect that the implementation of the GS cleavage step in the model is a simplification of the underlying system. Matsumura et al. [23] report multiple interactive pathways for stepwise successive processing of C99 by GS, which are hypothesized to define the Aβ isoforms and quantity of each Aβ. If Aβ40 and Aβ42 are indeed the products of consecutive GS cleavage, this may be reflected in the identified divergence in Aβ dynamics following GS inhibition *versus* BACE1 inhibition.

An alternative explanation of the differentiation in Aβ dynamics following BACE1 and GS inhibition may be that a feedback mechanism was activated. Tian et al. [24] propose that α-secretase cleavage initiates a feedback mechanism in which increased C83 may negatively modulate GS activity, thereby lowering Aβ production. As sAPPα and C83 are products of the same cleavage step by α-secretase, C83 will increase in a similar manner as sAPPα following BACE1 inhibition. The model predicts that C83 concentrations increase as result of BACE1 inhibition, but do not increase as result of GS inhibition. Therefore, we would expect this inhibitory effect on GS through C83 to occur after BACE1 inhibition, but not after GS inhibition. And this would then have to be reflected in a lower Aβ formation rate constant following BACE1 inhibition. However, a higher Aβ formation rate was found. The feedback mechanism as proposed by Tian was evaluated in the current model, but was not supported by the data.

It has been demonstrated that increased sAPPα generation is accompanied by a reduction of both β-secretase cleavage and Aβ generation [25]. The model predicts that C99 will decrease following BACE1 inhibition and slightly increases following GS inhibition. Increased C99 levels may have a stimulating effect on α-secretase. Stimulation of α-secretase will lead to enhanced production of sAPPα and C83 and reduced production of sAPPβ and C99 and, consequently, less Aβ being formed. This may be reflected in the lower Aβ formation rate constant that was identified following GS inhibition. As both sAPPα and sAPPβ levels following GS inhibition were not measured in the current study, the proposed mechanism cannot be confirmed using the current data, and will be investigated further in a follow-up study.

The interpretation of the Aβ_O pool was recently discussed in van Maanen et al. [1]. The systems analysis suggests a difference in oligomerization of Aβ42 after GS and BACE1. However, the maximal Aβ42 response to the higher dose groups of MBi-5 and MK-0752 were not adequately captured. Therefore, this should be interpreted with caution. In the recent model, inclusion of an Aβ_O pool in the model could account for the differential effect of MBi-5 on Aβ40 and Aβ42 response observed in the data. In the Supplemental Material 3, the observed change in the ratio of Aβ42:Aβ40 after GS and BACE1 inhibition is presented. After GS inhibition, there is less difference in response of Aβ40 and Aβ42 observed, and thus less change in the ratio Aβ42:Aβ40. This may be caused by differential activation of some feedback mechanism on Aβ production or oligomerization, or model simplification of successive GS cleavage, as discussed above. Once quantitative data of Aβ_O response following BACE1 and GS is added, a difference in oligomerization may be confirmed.

Correction factors on Aβ42 and Aβ40 for study differences in study 1 and 2 compared to study 3, were implemented in the model on IPRED, assuming the underlying system is the same. Because these factors were implemented outside of the system, these are assumed to not affect model derived differences following GS *versus* BACE1 inhibition. The observed study variations in Aβ42 and Aβ40 levels could result from factors related to analytical procedures, such as differences in laboratory procedures among centers and technicians, sample handling or sample storage.

When planning a new study, a cross-over study design, in which each rhesus monkey receives MBi-5 and MK-0752, should be considered. This design will facilitate an adequate separation of study differences and differences in system responses following BACE1 or GS inhibition as the first is canceled out. Also, if sAPPα and sAPPβ response to GS inhibition would additionally be measured, it is anticipated that possible feedback

mechanism in the APP pathway can be further evaluated.

By challenging the model, we can learn something: If the existing model does not capture the data, we need to ask why and understand what is going. Subsequent model refinement can then be helpful in elucidating system behaviour and identifying knowledge gaps and further experiments.

Conclusions

The development of a systems pharmacology model is an evolutionary process, integrating knowledge of the biological system with emerging data. In the current analysis, by analysing the effects of two compounds with differing method of action, i.e. a GS and BACE1 inhibitor, acting on different sequence in the APP processing pathway, the APP processing pathway could be further elucidated. As a result, the systems pharmacology model of the APP pathway could be refined. The model characterized the response and inter-relationships of the APP metabolites and gave insight into the biological mechanisms of the system. The application of such a mechanistic approach that separates drug specific and systems specific parameters provides a robust characterization of the inhibitors. A differentiation in Aβ dynamics after BACE1 *versus* GS inhibition was found, reflected in a difference in Aβ40 formation. As such, the systems pharmacology analysis also points to parts of the APP system which require further investigation, in order to fully understand the interference of secretase inhibitors on the system.

References

1. van Maanen, E.M.T., *et al.* Systems pharmacology analysis of the amyloid cascade after β-secretase inhibition enables the identification of an Aβ42 oligomer pool. J Pharmacol Exp Ther. 2016;357(1):205–16.

2. Karran, E., Mercken, M., & De Strooper, B. The amyloid cascade hypothesis for Alzheimer's disease: an appraisal for the development of therapeutics. Nat Rev Drug Discov. 2011;10(9):698–712.

3. Husain, M.M., Kenneth, T., Siddique, H., & McClintock, S.M. Present and prospective clinical therapeutic regimens for Alzheimer's disease. Neuropsychiatr Dis Treat. 2008;4(4):765–777.

4. Cole, S.L. & Vassar, R. The basic biology of BACE1: A key therapeutic target for Alzheimer's disease. Curr Genomics. 2007;8(8):509–530.

5. Esler, W.P. & Wolfe, M.S. A portrait of Alzheimer secretases - New features and familiar faces. Science. 2001;293(5534):1449–54.

6. Willem, M., *et al.* η-Secretase processing of APP inhibits neuronal activity in the hippocampus. Nature. 2015;526(7573):443–7.

7. Crump, C.J., *et al.* BMS-708,163 targets presenilin and lacks notch-sparing activity. Biochemistry. 2012;51(37):7209–11.

8. Martone, R.L., *et al.* Begacestat (GSI-953): a novel, selective thiophene sulfonamide inhibitor of amyloid precursor protein gamma-secretase for the treatment of Alzheimer's disease. J Pharmacol Exp Ther. 2009;331(2):598–608.

9. Doody, R.S., *et al.* A phase 3 trial of semagacestat for treatment of Alzheimer's disease. N Engl J Med. 2013;369(4):341–50.

10. Das, R., *et al.* Modeling effect of a γ-secretase inhibitor on amyloid-β dynamics reveals significant role of an amyloid clearance mechanism. Bull Math Biol. 2011;73(1):230–47.

11. Niva, C., Parkinson, J., Olsson, F., van Schaick, E., Lundkvist, J., & Visser, S.a.G. Has inhibition of Aβ production adequately been tested as therapeutic approach in mild AD? A model-based meta-analysis of γ-secretase inhibitor data. Eur J Clin Pharmacol. 2013;69(6):1247–60.

12. Tai, L.M., *et al.* The dynamics of Aβ distribution after γ-secretase inhibitor treatment, as determined by experimental and modelling approaches in a wild type rat. J Pharmacokinet Pharmacodyn. 2012;39(3):227–37.

13. Klein, W.L. Synaptotoxic amyloid-β oligomers: a molecular basis for the cause, diagnosis, and treatment of Alzheimer's disease? J Alzheimer's Dis. 2013;33:S49–S65.

14. Benilova, I., Karran, E., & De Strooper, B. The toxic Aβ oligomer and Alzheimer's disease: an emperor in need of clothes. Nat Neurosci. 2012;15(3):349–357.

15. Rosenblum, W.I. Why Alzheimer trials fail: removing soluble oligomeric beta amyloid

is essential, inconsistent, and difficult. Neurobiol Aging. 2014;35(5):969–974.

16. Cook, J.J., *et al.* Acute γ-secretase inhibition of nonhuman primate CNS shifts amyloid precursor protein (APP) metabolism from amyloid-β production to alternative APP fragments without amyloid-β rebound. J Neurosci. 2010;30(19):6743–50.

17. Gilberto, D.B., *et al.* An alternative method of chronic cerebrospinal fluid collection via the cisterna magna in conscious rhesus monkeys. Contemp Top Lab Anim Sci. 2003;42 (4):53–59.

18. Dobrowolska, J.A., *et al.* CNS amyloid-β, soluble APP-α and -β kinetics during BACE inhibition. J Neurosci. 2014;34(24): 8336–8346.

19. Wu, G., Sankaranarayanan, S., Hsieh, S.H.K., Simon, A.J., & Savage, M.J. Decrease in brain soluble amyloid precursor protein β (sAPPβ) in Alzheimer's disease cortex. J Neurosci Res. 2011;89(6):822–32.

20. Sankaranarayanan, S., *et al.* First demonstration of cerebrospinal fluid and plasma Aβ lowering with oral administration of a β-site amyloid precursor protein-cleaving

21. Bauer, R.J. 2011 NONMEM users guide. Introduction to NONMEM 7.2.0 Technical report;ICON Development Solutions, Ellicott City, MD.

22. Iwatsubo, T., Odaka, A., Suzuki, N., Mizusawa, H., Nukina, N., & Ihara, Y. Visualization of Aβ42(43) and Aβ40 in senile plaques with end-specific Aβ monoclonals: evidence that an initially deposited species is Aβ42(43). Neuron. 1994;13(1):45–53.

23. Matsumura, N., *et al.* γ-Secretase associated with lipid rafts: multiple interactive pathways in the stepwise processing of β-carboxyl-terminal fragment. J Biol Chem. 2014;289(8):5109–21.

24. Tian, Y., Crump, C.J., & Li, Y.M. Dual Role of α-Secretase Cleavage in the Regulation of γ-Secretase Activity for Amyloid Production. J Biol Chem. 2010;285(42): 32549–32556.

25. Lichtenthaler, S.F. Alpha-secretase in Alzheimer's disease: Molecular identity, regulation and therapeutic potential. J Neurochem. 2011;116(1):10–21.

enzyme 1 inhibitor in nonhuman primates. J Pharmacol Exp Ther. 2009;328(1):131–140.

Chapter 5

Supplemental Material

Supplement to

Extending a systems model of the APP pathway: Separation of β- and γ-secretase sequential
cleavage steps of APP

**E.M.T. van Maanen, T.J. van Steeg, M.J. Ahsman, M.S. Michener, M.J. Savage, M.E.
Kennedy, H.J. Kleijn, J.A. Stone, M. Danhof**
Submitted to JPET

SUPPLEMENTAL MATERIAL (1)

Pharmacokinetic Data Analysis MK-0752

A population PK model was developed that describes the PK of MK-0752 in plasma and CSF in cisterna magna ported (CMP) rhesus monkeys. The results of the PK analysis of MK-0752 were used to predict target site exposure for each PD observation in the subsequent PK-PD analysis.

The PK model was developed and fitted to the data by means of non-linear mixed effects modeling using the NONMEM software package version VI level 2 (see the Materials and Methods section in Chapter 5).

The compartmental PK model of MK-0752 was based on the model reported by Shou *et al.* (2005)[1]. They reported that MK-0752 exhibits enterohepatic recirculation (EHR) in rhesus monkeys. Their four-compartment PK was modified for the simultaneous analysis of plasma and CSF PK data.

The PK profiles of MK-0752 in plasma and CSF were adequately described by a model containing six compartments: GI tract, central, peripheral, gall bladder, central CSF and peripheral CSF compartment (Supplemental Figure S5.1). The CSF compartment is linked to the central compartment, with input to CSF determined by the rate constant K_{in}. A peripheral CSF compartment is linked to the central CSF compartment, with exchange determined by the rate constants K_{63} and K_{36}. The model considered EHR of MK-0752 for which the recirculation rate from the gal bladder was described by a cosine function (Supplemental Equation S5.1):

$$CS = AMP \cdot COS \left(\frac{2\pi \cdot time}{PER} + HOR \right) + VER \qquad \text{(S5.1)}$$

in which *AMP* is the amplitude of the cosine function corresponding to the maximum recirculation rate, *PER* is the period of the cosine function, *HOR* is the horizontal shift of the cosine function corresponding to a shift on the time axis and *VER* is the vertical shift of the cosine function corresponding to a shift on the rate axis.

The rate of change in each compartment can be expresses as:
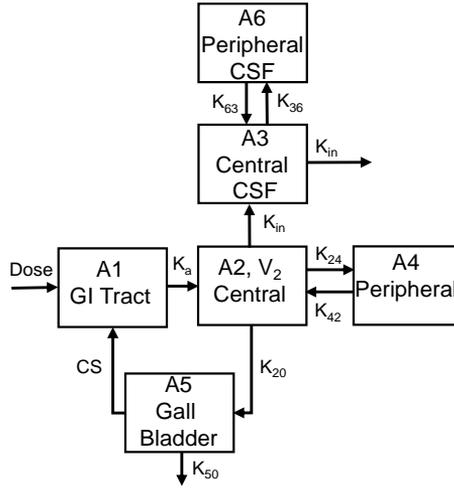
Figure S5.1: Schematic of the population PK model for MK-0752, that comprised of a GI tract, central, peripheral, gall bladder, central CSF and peripheral CSF compartment.
Rate constants for the individual compartments are K_a (absorption), K_{24} (rate constant from central to peripheral), K_{42} (rate constant from peripheral to central), K_{36} (rate constant from central CSF to peripheral CSF), K_{63} (rate constant from peripheral CSF to central CSF), K_{20} (rate constant from central to gall bladder), K_{50} (elimination rate from the gall bladder compartment), CS (rate constant recirculation via a cosine-function), K_{in} (rate constant from central to central CSF and elimination rate from the central CSF compartment). *A1*, *A2*, *A3*, *A4*, *A5* and *A6* are amounts (A) of MK-0752 in GI tract, central, central CSF, peripheral, gall bladder and peripheral CSF compartments, respectively. V_2 is the volume of the central compartment.

$$\frac{d}{dt}A_1 = -K_a \times A_1 + CS \times A_5 \tag{S5.2}$$

$$\frac{d}{dt}A_2 = K_a \times A_1 - K_{24} \times A_2 + K_{42} \times A_4 - K_{20} \times A_2 \tag{S5.3}$$

$$\frac{d}{dt}A_3 = K_{in} \times \frac{A_2}{V_2} - K_{36} \times A_3 + K_{63} \times A_6 - K_{in} \times A_3 \tag{S5.4}$$

$$\frac{d}{dt}A_4 = K_{24} \times A_2 - K_{42} \times A_4 \tag{S5.5}$$

$$\frac{d}{dt}A_5 = K_{20} \times A_2 - CS \times A_5 - K_{50} \times A_5 \qquad \text{(S5.6)}$$

$$\frac{d}{dt}A_6 = K_{36} \times A_3 - K_{63} \times A_6 \qquad \text{(S5.7)}$$

Table S5.1 shows all PK parameter estimates. The CSF input rate (K_{in}) could not be estimated with good precision. Considering the limitations of the data, this was accepted. The relative bioavailability (*F1*) was fixed to the value reported by Shou et al. (2005). The parameters *Ka* and *AMP* were fixed to parameter estimates from a preliminary analysis based on 60 mg/kg data only and a one compartmental model. In the two compartmental model based on 60 mg/kg and 240 mg/kg data, these could not be reliably estimated.

Interanimal variability was quantified for the clearance (*CL*) and volume of the central compartment (V_2). Residual variability (proportional error) was higher for the CSF than for the plasma concentration (0.173 and 0.132 for CSF and plasma, respectively).

The developed PK model gives an adequate description of plasma and CSF concentration time profiles, as can be seen from plots of the simulated and observed concentrations *versus* time profiles with 90% confidence interval (Supplemental Figure S5.2).

There is substantial CSF exposure after oral dosing, as shown by the PK data from the CMP rhesus monkeys. The data suggest that MK-0752 concentrations in brain, expected to be in between plasma and CSF levels, are sufficient to adequately inhibit γ-secretase activity in brain. The plasma and CSF concentrations *versus* time profiles predicted from the model were in good agreement with the values observed in the rhesus monkeys. Thus, the model could serve as input for PD model analysis.

Table S5.1: Population parameter estimates including coefficient of variation (CV%) for the PK model of MK-0752

PARAMETER	DESCRIPTION	VALUE	UNIT	CV%
Structural parameters				
$K_a{}^a$	absorption rate	1.13	h^{-1}	-
CL	clearance	0.774	L/h	12.3
V_2	central volume	3.68	L	17.6
K_{24}	rate constant from central to CSF	0.00745	h^{-1}	27.8
K_{42}	rate constant from central to CSF	0.0229	h^{-1}	4.89
$F1^a$	relative bioavailability	0.89	-	-
PER^a	period of cosine function	24	h	-
AMP^a	amplitude of cosine function	1.87	-	-
HOR	horizontal shift of cosine function	2.47	-	6.92
VER^a	vertical shift of cosine function	0	-	-
K_{50}	elimination rate gall bladder compartment	1.02	h^{-1}	35.8
$K_{in}CSF \times 1000$	CSF input and output rate	0.0381	h^{-1}	82.7
K_{36} as fraction of K_{in}	rate constant from central CSF to peripheral CSF as fraction of K_{in}	110	-	5.81
K_{63}	rate constant from peripheral CSF to central CSF	0.000926	h^{-1}	19.4
Interanimal variability				
ω_2^{CL}	Interanimal variability clearance	0.141		34.3
ω_2^{V2}	Interanimal variability central volume	0.381		37.3
$\omega_{(CL,V2)}$	Covariance between CL and V_2	0.195		33.3
Residual error				
σ_{plasma}^2	Residual variabiliy plasma	0.132		14.4
σ_{CSF}^2	Residual variabiliy CSF	0.173		12.2

[a] Fixed.

(A) 60 mg/kg MK-0752 plasma

(B) 60 mg/kg MK-0752 CSF

(C) 240 mg/kg MK-0752 plasma

(D) 240 mg/kg MK-0752 CSF
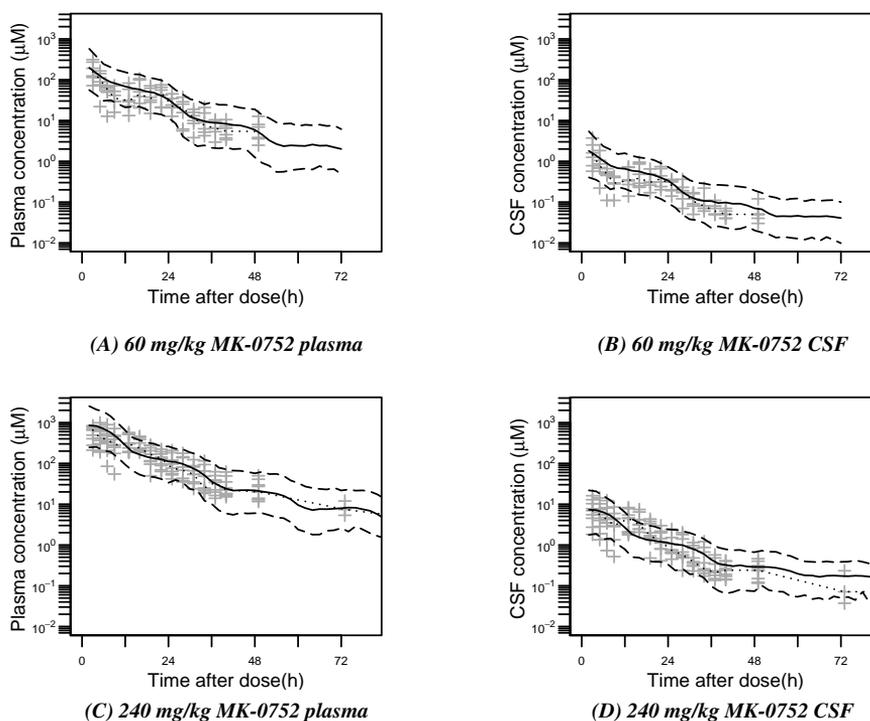
Figure S5.2: Visual predictive check of plasma **(left panels)** *and CSF* **(right panels)** *concentration time profile of MK-0752 in the rhesus with 90% confidence interval.* The rhesus were administrated with 60 mg/kg (A) (B) and 240 mg/kg (C) (D) MK-0752. Observation sample size: *Study 1*: n=16 for plasma and CSF per dose (60 and 240 mg/kg) from 6 monkeys collected over 2 days. *Study 2*: n=21 for plasma and CSF from 6 dose 240 mg/kg treated monkeys collected over 10 days. In the figure, the first 3 treatment days of study 2 are depicted.

Plus-symbols represent observed measurements. Dotted line corresponds to the median observed profile. Solid lines show the median simulated profiles. The longs-dashed lines correspond to the 90% prediction intervals obtained from 1000 individual simulated profiles.

References

1. Shou, M., *et al.* Population pharmacokinetic modeling for enterohepatic recirculation in Rhesus monkey. Eur J Pharm Sci. 2005;26 (2):151–61.

SUPPLEMENTAL MATERIAL (2)

Study differences in Aβ baseline levels

Baseline data of Aβ40 and Aβ42 from the two GS inhibitor studies (study 1 and 2) and the BACE1 inhibitor study (study 3) is depicted in Fig. S5.3A and S5.3B, respectively, together with additional baseline data which was included in the analysis from study A and B. A large between-study variability in the baseline data was observed.

There was overlap in the rhesus monkey individuals included in the studies. Half of the subjects included in the GS inhibitor studies (study 1 and 2) was also used in the BACE1 inhibitor study (study 3) and study A.

In study time lines, Study B was run first, followed closely by study 1. Approximately 1 year later study 2 was conducted. Study A came next a few months later and lastly study 3 followed. No relationship between the age of the rhesus monkeys and the baseline level could be identified. As clock times were not available, a circadian rhythm in the combined baseline data could not be investigated.

(A) Aβ40   *(B) Aβ42*
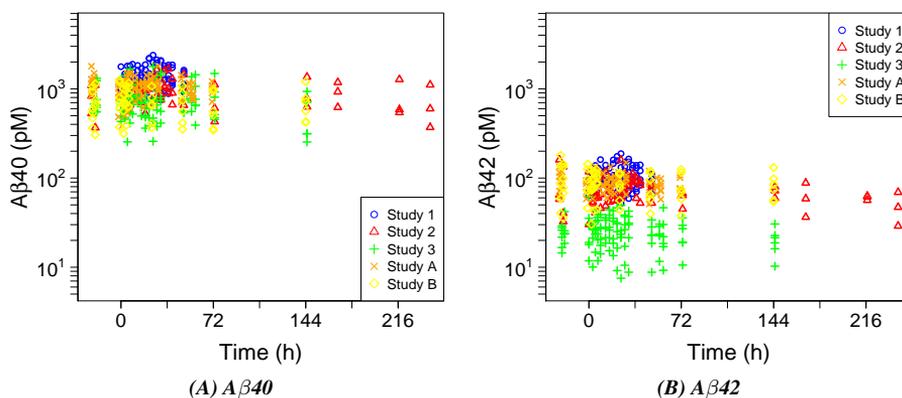
Figure S5.3: Study differences in baseline levels of Aβ40 (left) and Aβ42 (right).

SUPPLEMENTAL MATERIAL (3)

Study differences in ratio Aβ42:Aβ40

The ratio Aβ42:Aβ40 from the two GS inhibitor studies (study 1 and 2) and the BACE1 inhibitor study (study 3) is depicted in Fig. S5.4A, S5.4B and S5.4C, respectively. BACE1 inhibition resulted in a bigger change in the ratio, compared to GS inhibition, with the investigated dosages.

(A) Study 1

(B) Study 2

(C) Study 3
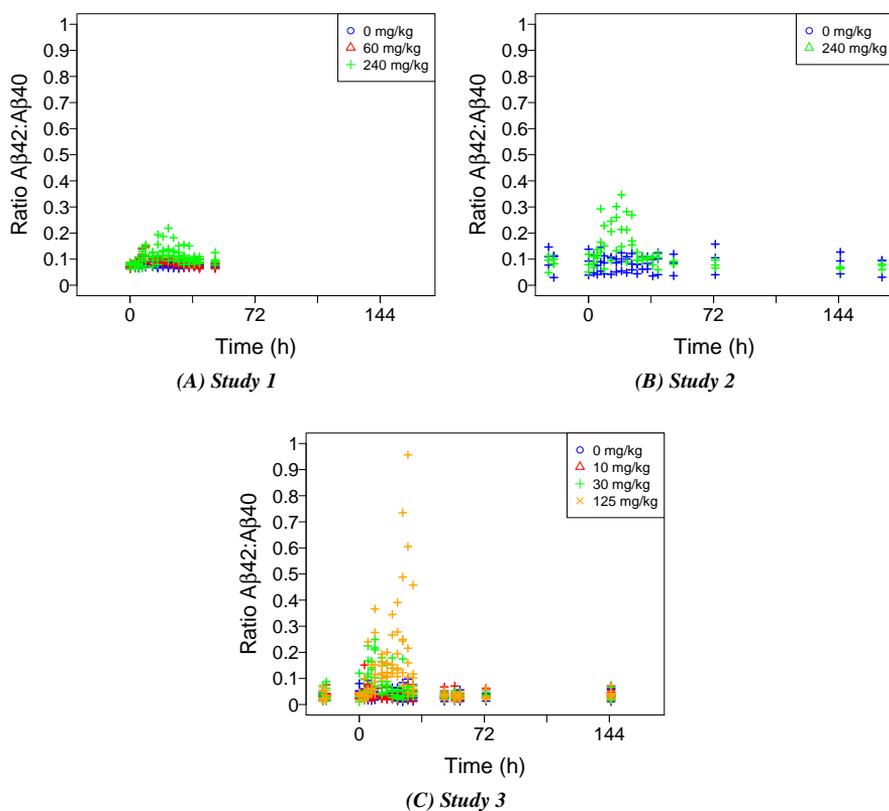
Figure S5.4: Study differences in the ratio Aβ42:Aβ40.
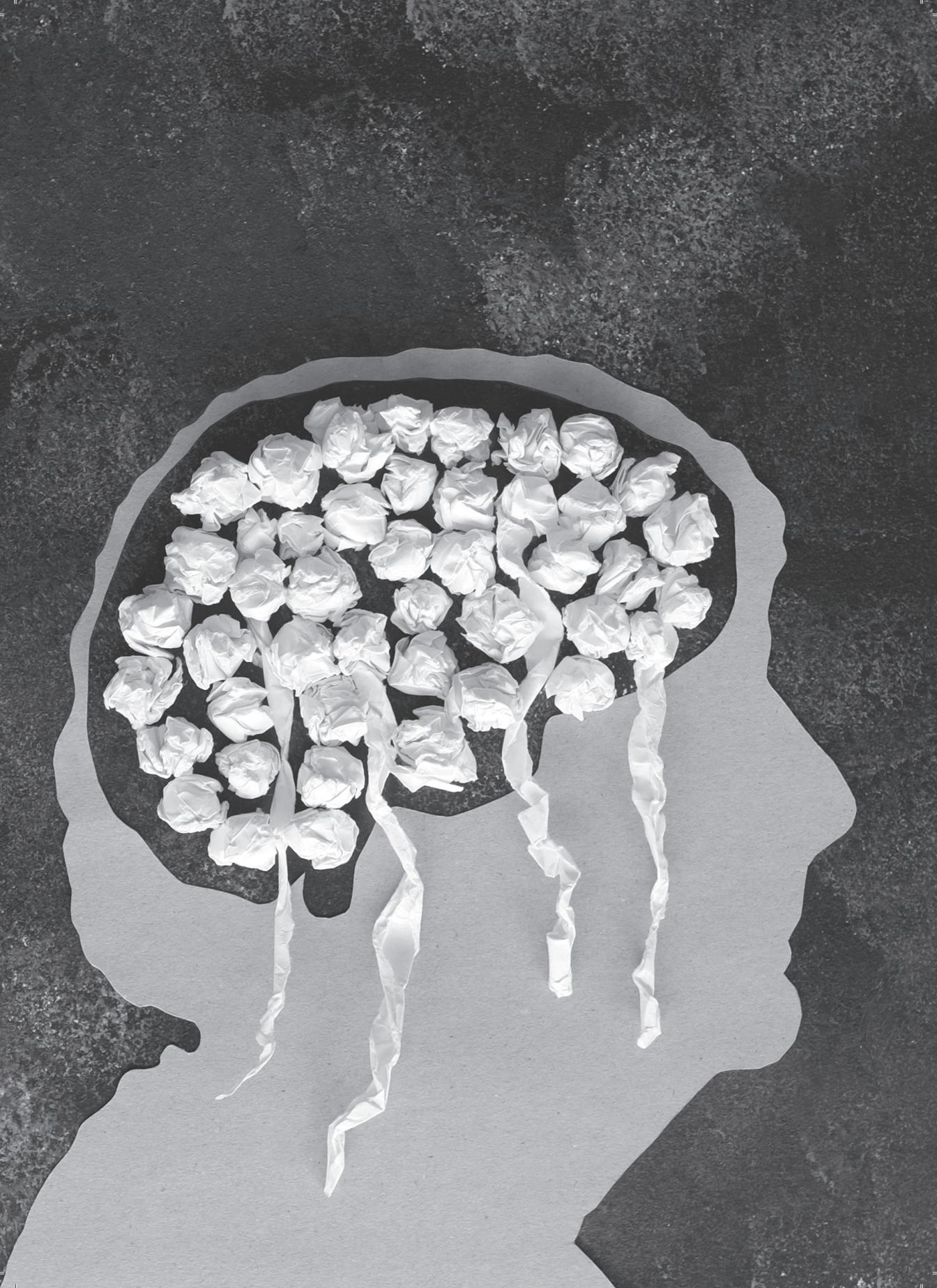
Section III

Application of a systems pharmacology model to characterize oligomer modulation following secretase inhibition
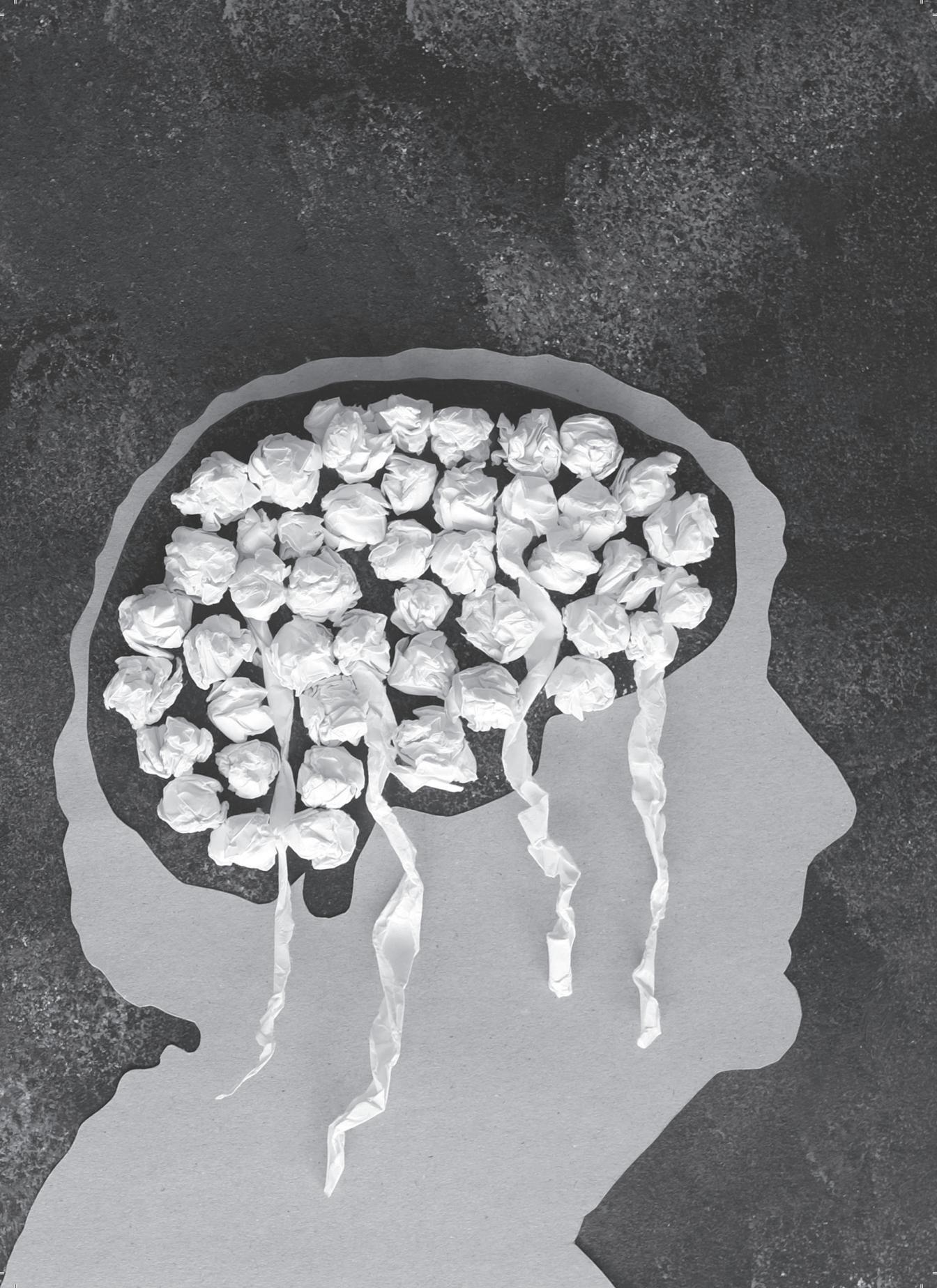
Chapter 6

Systems pharmacology analysis of the Aβ oligomer response following γ-secretase inhibition: Evidence for second-order kinetics of Aβ42 oligomerization

E.M.T. van Maanen, T.J. van Steeg, J. Kalinina, M.S. Michener, M.J. Savage, M.E. Kennedy, J.A. Stone, M. Danhof

Abstract

Toxic soluble $A\beta$ oligomers ($A\beta_O$) are considered to be the primary drivers of the neu-rodegeneration in Alzheimer's Disease (AD). Here, for the first time, the effect of BACE1 inhibition on the time course of the changes in $A\beta_O$ is determined. Administration of the BACE1 inhibitor MBi-5 (30 or 125 mg/kg) resulted in a reduction of $A\beta_O$ concentrations. The amyloid precursor protein (APP) metabolite (sAPPβ, sAPPα, $A\beta40$, $A\beta42$, $A\beta38$) and $A\beta_O$ responses in CSF from cisterna-magna-ported rhesus monkeys was analysed on the basis of a recently established systems pharmacology model of the APP pathway.

The changes in $A\beta_O$ were linked to the dynamics of the precursor $A\beta42$: There was no contribution from the precursors $A\beta40$ and $A\beta38$ to the $A\beta_O$ pool. $A\beta42$ oligomerization was characterized to be a second-order process. Decreases in monomeric $A\beta42$ responses following from BACE1 inhibition were partially compensated by dissociation of $A\beta_O$. The model gave an accurate description of the 6 biomarkers. The systems pharmacology analysis provided insights into $A\beta_O$ reduction after treatment with a BACE1 inhibitor, and supports the hypothesis that $A\beta42$ is the $A\beta$ species prone to oligomerization. Simulations visualized that 30% reduction of the $A\beta42$ monomeric level reduced $A\beta_O$ by more than half.

Introduction

According to the amyloid hypothesis, proteolytic processing of amyloid precursor protein (APP) to form the amyloid-β (Aβ) peptides plays a central role in the pathophysiology of Alzheimer's Disease (AD)[1,2]. Aβ levels are increased early in the disease process, while patients remain clinically asymptomatic, forming toxic soluble Aβ oligomers (Aβ_O) and plaques. Aβ_O are considered to be a primary driver of the neurodegeneration in AD brain[3].

Aβ is the final product of proteolytic cleavage of the transmembrane APP in the amyloidogenic pathway and is assumed to be a precursor of Aβ_O. In the APP processing and clearance pathways, APP is cleaved sequentially by β-secretase 1 (BACE1) and γ-secretase[4]. BACE1 cleavage of APP releases the N-terminal secreted fragment soluble β-amyloid precursor protein (sAPPβ) and C99, a C-terminal fragment which remains membrane bound. C99 is subsequently cleaved by γ-secretase, creating Aβ peptides of different amino acid chain lengths, of which the most common have 38, 40 or 42 amino acids (Aβ38, Aβ40, or Aβ42, respectively)[5]. A third secretase, α-secretase cleaves APP within the Aβ sequence generating non-amyloidogenic soluble sAPPα and precluding Aβ generation[6].

Aβ appears to aggregate into at least three different states: Aβ_O, which are soluble disordered clusters, protofibrils, which are prefibrilar insoluble high molecular weight Aβ_O (50-1500 kDa) comprising spherical, annular, and curvilinear assemblies, and fibrils, which are long, many-chain highly structured β-sheet-like aggregates[7,8,9]. Aβ is believed to co-exist with Aβ_O, protofibrils and fibrils at equilibrium[10]. The pathway by which normal monomeric forms of Aβ become fibrils is still uncertain[11].

One of the main therapeutic strategies for AD is to reduce Aβ in the central nervous system and thereby, theoretically, preventing all downstream pathological processes. Potential therapies include inhibition of the secretases responsible for its production (BACE1 or γ-secretase inhibitors). The effect of inhibiting Aβ production on Aβ_Os is not fully understood.

Several studies on the pharmacokinetics (PK) and the pharmacodynamics (PD) of BACE1 and γ-secretase inhibitors have been reported[12,13,14,15,16,17]. Such models focus primarily on the drug effect on Aβ40 and/or Aβ42 dynamics. A quantitative characterization of the drug effects on Aβ_O is still lacking.

The drug effects on the individual attributes of the APP pathway are difficult to predict, because it involves a complicated biological network. In order to develop a model that

fully characterized the drug effects on Aβ monomeric and oligomeric levels, its important to consider the interactions between APP metabolites.

Systems pharmacology provides a mathematical framework for integrating understanding of biochemical/pathological pathways with basic principles of PK and PD. Recently, a systems pharmacology model of the APP processing pathway was developed to characterize APP metabolite (sAPPβ, sAPPα, Aβ40, Aβ42) responses to BACE1 inhibition [18]. Throughout the article the name 'β-APP model' is used to refer this model. Using information from monomeric Aβ species, an Aβ42 oligomer pool was identified in the β-APP model. It is of interest to know if the Aβ_O response to BACE1 inhibition was correctly derived from Aβ monomeric responses. This would verify monomeric Aβ as good predictor of Aβ_O response to Aβ production inhibition. To this end, Aβ_O measurements need to be compared to model predicted Aβ_O levels.

In the current crossover study in cisterna-magna-ported rhesus monkeys the effects of a BACE1 inhibitor (MBi-5; 30, 125 mg/kg) on the CSF concentrations of six biomarkers (sAPPβ, Aβ40, Aβ42, Aβ38, Aβ_O, sAPPα) were determined. Aβ_O concentrations in CSF were quantified using a novel two-site ELISA assay [19]. The time course of the changes in the concentration of all biomarkers were simultaneously analysed with the β-APP model. This analysis yielded predictions of the effect of MBi-5 on the Aβ_O concentrations (the oligomer pool). Next, these model predictions were compared to measured Aβ_O concentrations. Finally, the existing model was extended to include also the effect on Aβ_O concentrations. Specifically, the objectives of this investigation were fourfold: (i) to compare model predicted Aβ_O from the recently reportedβ-APP model with observations of Aβ_O; (ii) to characterize Aβ_O dynamics following BACE1 inhibition; (iii) to confirm that Aβ_O dissociates to restore the equilibrium between Aβ monomers and Aβ_O, following secretase inhibition; (iv) to investigate the relationships of Aβ40, Aβ42 and Aβ38 monomers with the Aβ_O pool.

Materials and Methods

Animals

All animal studies were reviewed and approved by the MSD Institutional Animal Care and Use Committee. The NIH Guide to the care and use of Laboratory Animals and the Animal Welfare act were followed in the conduct of the animal studies (Institute of Laboratory Animal Resources, National Research Council, 1996). The CMP rhesus monkey model was reported by Gilberto et al. [20]. The rhesus monkeys are chronically

implanted with catheters in the cisterna magna, facilitating repeated sampling of CSF and plasma in conscious rhesus monkeys. These rhesus monkeys were individually housed and captive-bred in a closed colony.

In this study, six male animals, weighing between 8.6 kg and 11.8 kg (mean, 9.7 kg), age at 9 years to 13 years (mean, 11 years) at time of the study were included.

Drug administration and sampling

Information on the effect of BACE1 on sAPPα, sAPPβ, Aβ40, Aβ42, Aβ38 and Aβ_O was obtained following a single oral administration of MBi-5 at 30, 125 mg/kg (5 mL/kg) or vehicle (0.4% methylcellulose) in a four-way full crossover study.

Plasma and CSF drug concentrations were collected at 0 (predose) and 3, 5, 7, 9, 13, 14.5, 16, 19, 22, 25, 28, 31, 49, 55, 58, 73 and 96 h postdose, resulting in 18 plasma and CSF PK samples for each monkey per treatment group. 2 mL of blood and 1 mL of CSF were collected at each time point. The concentration of MBi-5 in the plasma and CSF samples was determined using LC-MS/MS. The concentrations of sAPPα, sAPPβ, Aβ40, Aβ42, Aβ38 and Aβ_O were determined from CSF samples, collected at the same time points as PK samples, by established and validated ELISA-based assays (Meso Scale Diagnostics), giving 18 measurements of each biomarker for each monkey per treatment. The two-site ELISA assay used for Aβ_O measurement was previously described by Savage et al.[19].

PK-PD analysis

The PK and PD data were analysed with a non-linear mixed effects modelling approach utilizing the software package NONMEM (version 7.2.0[21]). In this approach, structural (fixed) effects and both intra- and interindividual variability are taken into account. Typical values of structural model parameters (population parameters, which define the average value for a parameter in a population) (θ), the variance and covariance of the interindividual variability (ω^2) and the variance of the residual error (σ^2) are estimated.

The models were compiled using Compaq Visual Fortran (version 6.6, Compaq Computer Corporation, Houston, Texas, USA) and executed on a PC equipped with an an Intel QuadCore (Intel® Core^{TM} i7 CPU860, 2.80 GHz, 3.24 GB RAM). Data management and model assessment was done using the statistical software package S-PLUS for Windows (version 8.0 Professional, Insightful Corp., Seattle, USA).

The best models were chosen based on the analysis of their obtained minimum value of the objective function (defined as minus twice the log-likelihood), the precision of

parameter estimates, and visual inspection of goodness-of-fit plots. A more detailed description of the modelling procedure was described in van Maanen et al.[18].

To evaluate the performance of the model a visual predictive check (VPC) was performed in which the median and the 90% inter-quantile range of the data simulated with the final parameter estimates were plotted together with the observations. A validated result would have close resemblance of median observed and predicted line with 90% of the observations that fall within the 90% prediction interval.

Model description

The systems model of the APP processing pathway was developed by sequential analysis of PK and PD data following administration of MBi-5. The PK model of MBi-5 was based on simultaneous analysis of plasma and CSF PK data. The PK model of MBi-5 has been reported elsewhere by van Maanen et al.[18].

The PK model adequately described the plasma and CSF concentration time profiles of MBi-5, respectively, thus the model could serve as input for PD model analysis.

The interrelationships of the absolute amounts of APP metabolite responses to BACE1 inhibition were described recently using a comprehensive systems model of the APP processing pathway[18], the so-called β-APP model. To describe the effect of the BACE1 inhibitor on Aβ38, the model had to be extended. Also, the oligomerization of Aβ was changed to a second order process.

The biomarker response profiles of MBi-5 measured in CSF were adequately described by the β-O-APP model containing compartments for seven variables: APP, sAPPβ, sAPPα, Aβ40, Aβ38, Aβ42 and Aβ_{O} (Fig. 6.2). The production of APP was believed to be zero order, i.e. a constant production of APP. It was assumed that there is no alternative proteolytic enzyme cleaving full length APP other than α-secretase and BACE1. As both sAPPβ and C99 are products of APP cleavage by BACE1, sAPPβ and C99 were presumed to follow the same kinetics and therefore sAPPβ could be used in the model as surrogate precursor for Aβ. The production of sAPPα, sAPPβ and Aβ were assumed to be first order, i.e. dependent on the concentration of its precursor. The interaction between APP, sAPPβ, sAPPα, Aβ40, Aβ38, Aβ42 and Aβ_{O} is described by Eq. 6.1 - Eq. 6.7:

$$\frac{d}{dt}APP = Rin_{APP} - (Rin\beta \times EFF + Rin\alpha) \times APP \tag{6.1}$$

$$\frac{d}{dt} sAPP\alpha = Rin\alpha \times APP - Rout_a \times sAPP\alpha \tag{6.2}$$

$$\frac{d}{dt} sAPP\beta = Rin\beta \times EFF \times APP - (Kin_{40} + Kin_{42} + Kin_{38}) \times sAPP\beta \tag{6.3}$$

$$\frac{d}{dt} A\beta_{40} = Kin_{40} \times sAPP\beta - Kout \times A\beta_{40} \tag{6.4}$$

$$\frac{d}{dt} A\beta_{38} = Kin_{38} \times sAPP\beta - Kout * A\beta_{38} \tag{6.5}$$

$$\frac{d}{dt} A\beta_{42} = Kin_{42} \times sAPP\beta - Kout_{42} \times A\beta_{42} - Kpl \times (A\beta_{42})^{ALPH}$$
$$+ Krev \times A\beta_O / \left(\frac{MW_{A\beta42}}{1000} \times Factor_{oligo} \right) \tag{6.6}$$

$$\frac{d}{dt} A\beta_O = Kpl \times (A\beta_{42})^{ALPH} \times \frac{MW_{A\beta42}}{1000} \times Factor_{oligo} - Krev \times A\beta_O \tag{6.7}$$

The exchange between the $A\beta_O$ pool and the $A\beta42$ compartment is described by Eq. 6.6 and Eq. 6.7, where *ALPH* is the power of the concentration of $A\beta42$, *Factor_{oligo}* is the conversion factor on $A\beta_O$ and $MW_{A\beta42}$ is the molecular weight of $A\beta42$. *Krev* and *Kpl* are the dissociation rate and higher-order $A\beta42$ oligomerization rate constant, respectively, which are dependent on the baseline values of $A\beta42$ and the $A\beta_O$ pool ($A\beta42_{base}$ and $A\beta_{Obase}$, resp.) according to Eq. 6.8:

$$Krev = \frac{Kpl \times (A\beta_{42base})^{ALPH} \times \frac{MW_{AB42}}{1000} \times Factor_{oligo}}{A\beta_{Obase}} \tag{6.8}$$

The rate of change of APP with respect to time in the presence of the inhibitor is described by Eq. 6.1, in which the BACE1 cleavage inhibition is incorporated by the factor *EFF*.

EFF is the degree of inhibition caused by MBi-5, expressed as shown in Eq. 6.9.

$$EFF = 1 - \frac{C_{\text{target}}^{\text{GAM}} \times Imax}{C_{\text{target}}^{\text{GAM}} + IC50^{\text{GAM}}} \tag{6.9}$$

Where C_{target} is the target site concentration of MBi-5 , *IC50* the C_{target} that results in 50% inhibition of BACE1, *Imax* is the maximum response and *GAM* is the Hill coefficient. C_{target} was derived from the PK model as:

$$C_{\text{target}} = C_{\text{plasma}} \times \frac{AUC_{\text{CSF}}}{AUC_{\text{plasma}}} \tag{6.10}$$

Where AUC_{CSF} and AUC_{plasma} are the areas under the CSF and plasma concentration time curves, respectively. C_{target} is assumed to be in steady state with C_{plasma}.

It is assumed that the system is in steady state (SS) when no treatment is given *(EFF=1)*. These steady state conditions were used to derive part of the system parameters. From SS and Eq. 6.1 it follows that the source of APP *(Rin$_{\text{APP}}$)* is:

$$Rin_{APP} = Rout_a \times sAPP\alpha_{base} + (Kin_{40} + Kin_{42} + Kin_{38}) \times sAPP\beta_{base} \tag{6.11}$$

Where APP_{base} is the baseline level of APP, which is assumed to be equal to the sum of the baseline levels of sAPPα and sAPPβ.All alternate pathways are represented by the terms for α-secretase.

Using SS conditions and Eq. 6.2 the sAPPα formation rate (*Rinα*), equivalent to the α-secretase cleavage step, can be derived:

$$Rin\alpha = Rout_a \times \frac{sAPP\alpha_{base}}{APP_{base}} \tag{6.12}$$

Where sAPPα$_{\text{base}}$ is the baseline level of sAPPα.

The sAPPβ formation rate (*Rinβ*), equivalent to the BACE1 cleavage step, follows from SS and Eq. 6.3:

$$Rin\beta = (Kin_{40} + Kin_{42} + Kin_{38}) \times \frac{sAPP\beta_{base}}{APP_{base}} \tag{6.13}$$

Where *sAPPβ*_{base} is the baseline level of sAPPβ.

Using SS conditions and Eq. 6.4, 6.6 and 6.5, respectively, the formation rates of Aβ40 (*Kin40*), Aβ42 (*Kin42*) and Aβ38 (*Kin38*), equivalent to γ-secretase cleavage steps, can be calculated:

$$Kin_{40} = Kin_{42} \times \frac{A\beta 40_{base}}{A\beta 42_{base}} \tag{6.14}$$

$$Kin_{42} = Kout \times \frac{A\beta 42_{base}}{sAPP\beta_{base}} \tag{6.15}$$

$$Kin_{38} = Kin_{42} \times \frac{A\beta 38_{base}}{A\beta 42_{base}} \tag{6.16}$$

Where $A\beta 40_{base}$, $A\beta 42_{base}$ and $A\beta 38_{base}$ are the baseline levels of Aβ40, Aβ42 and Aβ38, receptively. sAPPβ_{base} is the baseline level of sAPPβ, used here as surrogate for the baseline level of C99.

The model structure includes six transit compartments (Fig. 6.2), one for each biomarker measured in CSF (sAPPα, sAPPβ, Aβ40, Aβ42, Aβ38, Aβ$_O$), to account for transport from the target site in the brain to CSF. These transit processes are described, in general, by Eq. 6.17:

$$\frac{d}{dt} xAx_{CSF} = Ktr * (xAx - xAx_{CSF}) \tag{6.17}$$

Where *Kt* is the transit rate for the particular particular APP metabolite xAx (*KtAP* for sAPPα and sAPPβ and *KtAB* for Aβ40, Aβ42, Aβ38 and Aβ$_O$).

Results

Within-study comparison

The performance of the recently reported β-APP model [18] was assessed using a 'within-study comparison': model parameter values were optimized using the current study data and then $A\beta_O$ was predicted and compared to the observed concentrations of $A\beta_O$ in the present study. The rationale for this analysis is that different methodologies were used for the quantitation of the PD biomarkers in the current study compared to the previous study [18]. Consequently, biomarker baseline levels and ratios changed (see Supplemental Material). When using the β-APP model and parameter values, the difference in prediction of $A\beta_O$ and data may be caused by methodology differences or model misspecification. It is impossible to distinguish the two from each other. In the 'within-study comparison', the difference in prediction of $A\beta_O$ and data must be related to model misspecification and the model can be optimized accordingly.

Comparison of model predicted versus observed $A\beta_O$ concentration profiles

The β-APP model parameters were optimized on a subset of the current data, using only the biomarker data of sAPPβ, sAPPα, Aβ40 and Aβ42. Compared to the results obtained in the previous study, the estimates of the Aβ degradation rate *(Kout)* was significantly lower and transit rate for sAPPα and sAPPβ from brain to CSF *(KtrAP)* was significantly higher (*Kout*: 0.94 h^{-1} (95% CI, 0.689-1.19) and 0.304 h^{-1} (95% CI, 0.198-0.41) in previous and current study, respectively; *KtAP*: 0.0985 (95% CI, 0.0931-0.104) and 0.127 (95% CI, 0.111-0.143) in previous and current study, respectively). The IC50 of the BACE1 inhibitor MBi-5 did not change significantly.

Using the parameter values, optimized for the current study data, the CSF $A\beta_O$ response data in the current study was predicted. For this, similar to the compartment "Observed CSF Aβ42", the compartment "Observed CSF $A\beta_O$" was added to the model, which represents the transport of $A\beta_O$ from brain-to-csf (Figure 6.2). The prediction of the onset of the $A\beta_O$ response to BACE1 inhibition was slow relative to the observations (Figure 6.1). Likewise, the maximum response was also underpredicted.

A conversion factor was included to account for different units of Aβ monomers and $A\beta_O$

It is to be noted that the concentrations of Aβ monomers were expressed in pM and $A\beta_O$ concentrations were expressed in pg/mL. Therefore, a conversion factor needed

to be included in the model, which has a relationship with the molecular weight of the oligomers and other processes involved (e.g. differences in distribution volume). The conversion factor is implemented in the differential equations describing Aβ42 (Eq. 6.6) and Aβ_O (Eq. 6.7). Based on visual inspection, this factor was initially set to 0.05 for the prediction discussed above and later optimized to be 0.0178.

(A) placebo
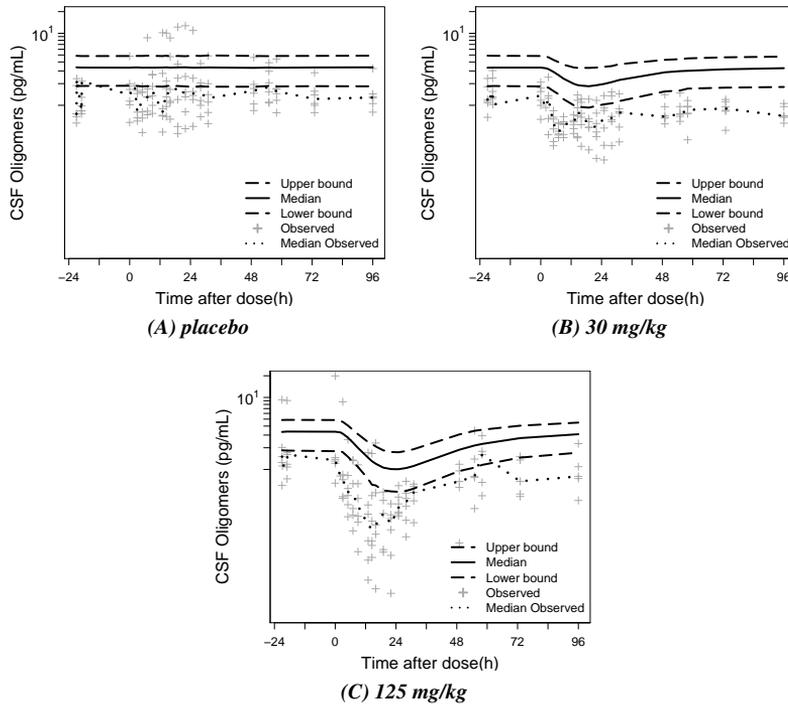
(B) 30 mg/kg

(C) 125 mg/kg

Figure 6.1: Prediction of Aβ_O response vs. time profile of placebo (A), 30 mg/kg (B) and 125 mg/kg (C) MBi-5 in the rhesus monkeys with 90% confidence interval.
Predictions were performed with the model structure presented in van Maanen et al. [18], with parameter values optimized on the current study data (*within-study comparison*). Observation sample size: n=108 for each APP metabolite from 6 monkeys collected over 4 days.
Plus-symbols represent observed measurements. Dotted line corresponds to the median observed profile. Solid lines show the median predicted profiles. The long-dashed lines correspond to the 90% prediction intervals obtained from 1000 individual simulated profiles.

The systems model was extended to describe Aβ38 response

The APP systems model was optimized, based on simultaneous analysis of sAPPβ, sAPPα, Aβ40, Aβ42, Aβ38 and Aβ$_O$ response data for BACE1 inhibition. Modifications were made to the β-APP model structure by adding extra compartments to describe Aβ38 dynamics and brain-to-csf transport, as shown in the schematic of the extended, so-called β-O-APP model, in Figure 6.2.

The differential equation representing Aβ38 dynamics in the β-O-APP model is Eq. 6.5. The same Aβ degradation rate *(Kout)* was identified for each Aβ isoform (Aβ40,

Figure 6.2: Schematic of β-O-APP model.
The model comprised thirteen compartments: Seven biomarker compartments in brain *(yellow circles)* and six transit compartments from brain to CSF *(white circles)*. Six biomarkers were measured in CSF (sAPPα, sAPPβ, Aβ40 ,Aβ42, Aβ38 and Aβ$_O$), indicated by the blue boxes. The drug effect *(EFF)* inhibited *Rinβ*. As driver of biomarker response C_{target} was used, which was derived from the PK model[18]. sAPPβ was used in the model structure as a surrogate substrate for C99 in the γ-secretase cleavage step[18]. Model extensions compared to the β-APP model presented in van Maanen et al. [18] are indicated with the green shaded area.
APP: Aβ-precursor protein; *Aβ*: amyloid-β-peptide; C_{target}: drug concentration target site; *Kin$_{38}$*: Aβ38 formation rate; *Kin$_{40}$*: Aβ40 formation rate; *Kin$_{42}$*: Aβ42 formation rate; *Kout*: Aβ38, Aβ40 and Aβ42 degradation rate; *Krev*: Oligomer dissociation rate; *KtAP*: transit rate sAPPα and sAPPβ from brain to CSF; *Kpl*: Oligomerization rate; *KtAB*: transit rate Aβ from brain to CSF; *KtAB$_O$*: transit rate Aβ$_O$ from brain to CSF; *RinAPP*: source of APP; *Rinα*: sAPPα formation rate; *Rinβ*: sAPPβ formation rate; *Routa*: sAPPα degradation rate.

Aβ42, Aβ38). Further, the transit rate for brain-to-CSF transport *(KtAB)* did not differ for Aβ38 compared to Aβ40 and Aβ42. Different formation rates were implemented for each one of the Aβ species. The formation rates of Aβ40, Aβ42 and Aβ38 were calculated according to Eqs. 6.14-6.16. The highest formation rate was found for *Kin*$_{40}$ (1.29 h^{-1}), followed by *Kin*$_{38}$ (0.380 h^{-1}) and than *Kin*$_{42}$ (0.0993 h^{-1}).

Aβ42 only contributor to Aβ_{O} pool

After extension of the model for Aβ38, the contribution of Aβ40, Aβ38 and Aβ42 to the oligomer pool was investigated. These Aβ species were evaluated both as single contributors as combined sources of Aβ for the oligomer pool, by including oligomerization rates for each Aβ. Aβ42 was identified as the only contributor to the oligomer pool.

Aβ oligomerization is a second-order process

The dependence of the Aβ_{O} concentration on the Aβ42 concentration was investigated. The oligomerization was identified to be a higher order process, with an order of 1.81 (95% CI, 1.33-2.29), indicating that its rate is proportional to the $\sim$2nd power of the concentration of monomeric species and that the oligomerization can only occur when two Aβ42 peptides interact. The difference in absolute oligomer response following a 1st, 1.81 and $2nd$ order oligomerization process is visualized in Figure 6.3. This plot illustrates that the order of the oligomerization process affects not only the onset of the oligomer response, but also the maximum effect.

The second-order Aβ oligomerization means that a relatively larger change from baseline for Aβ_{O} compared to monomeric Aβ species is obtained following BACE1 inhibition, as is depicted in Figure 6.5B.

To better understand the relationship between Aβ42 and Aβ_{O} response, the change of baseline for Aβ42 was plotted against the change of baseline for Aβ_{O} (Figure 6.4). This plot exhibits a hysteresis loop between Aβ42 and Aβ_{O} effects, when followed over time.

Thus, the same Aβ42 concentration corresponds to two different magnitudes of Aβ_{O} effects depending on the temporal sequence in which the effect is measured (e.g. 30% reduction in Aβ42 and 11% or 57% reduction in Aβ_{O} following 125 mg/kg MBi-5). The reason is because the maximum Aβ42 response was achieved before the maximum of Aβ_{O} response (Figure 6.5A).
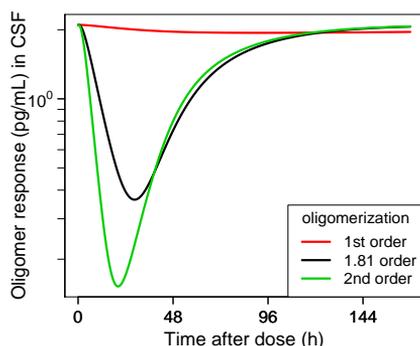
Figure 6.3: Illustration of the difference in absolute oligomer response following a 1st, 1.81 and 2nd order oligomerization process. The oligomer response was simulated after a single dose of 125 mg MBi-5, using the typical parameter estimates.
1st order: red solid line; *1.81 order:* black solid line; *2nd order:* green solid line.
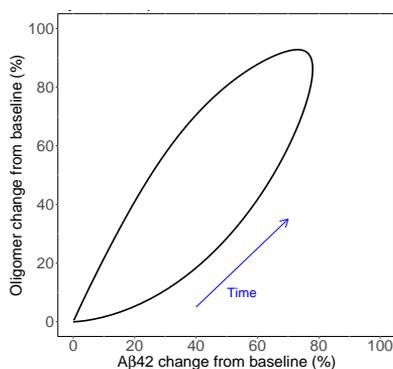
Figure 6.4: Illustration of the relationship between response of $A\beta42$ and $A\beta_O$. The $A\beta_O$ and $A\beta42$ response was simulated after a single dose of 125 mg MBi-5, using the typical parameter estimates.

The β-O-APP model described APP metabolite and $A\beta_O$ responses to BACE1 inhibition

Figures 6.6-6.8 show the model description of each APP metabolite and $A\beta_O$ for each dose group. In general, an adequate description of the biomarker responses was obtained across dose groups. A slight underprediction was observed for sAPPβ response at dose 125 mg/kg (Figure 6.8B) and overprediction of the $A\beta_O$ baseline (Figure 6.6F).

The β-O-APP model was used to simulate the biomarker interrelationships in CSF
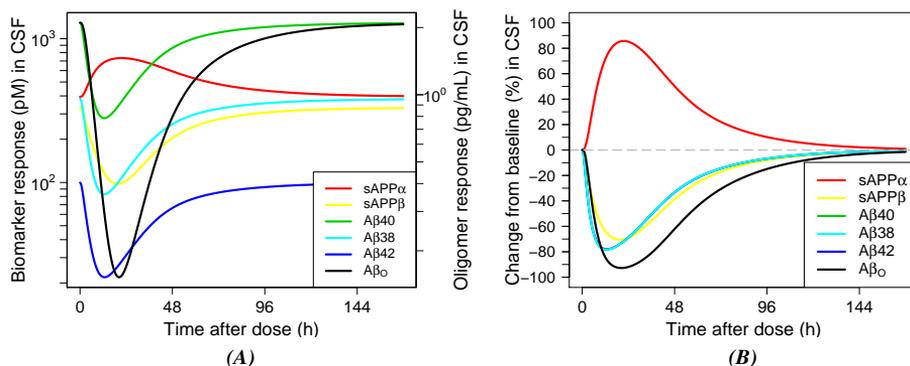
Figure 6.5: Simulation absolute biomarker responses (A) and biomarker change from baseline (%) (B). The biomarker responses were simulated after a single dose of 125 mg MBi-5, using the typical parameter estimates.
sAPPα red solid line; *sAPPβ* yellow solid line; *Aβ40* green solid line; *Aβ38* light blue solid line; *Aβ42* dark blue solid line; $A\beta_O$ black solid line.

after BACE1 inhibition (Figure 6.5A), illustrating that the biomarker maximum responses in CSF appear at different time sequence. Also, the response profiles of Aβ40, Aβ42 and Aβ38 were similar, albeit at different concentration levels. When visualizing the change from baseline for these Aβ species, the profiles were overlapping (Figure 6.5B).

Model parameters

The population parameters and intra- and interanimal variability, optimized for the current study population, are presented in Table 6.1. The random-effects model structure was optimized by comparing the results of models with interanimal variability on different parameters. The final model included interanimal variability for the baselines of sAPPβ, sAPPα and Aβ, modelled as lognormally distributed parameters. The same interanimal variability was included for the baselines of Aβ38, Aβ40 and Aβ42, as these are products of the same cleavage step. For each APP metabolite (sAPPβ, sAPPα, Aβ40, Aβ42, Aβ38, $A\beta_O$) separately, a proportional error was used to describe the random residual variability.

The parameter estimate of the IC50 was not significantly different from recently reported: in the recent analysis an IC50 of 0.0269 μM (95% CI, 0.0154–0.0384) was found [18]; in the current analysis an IC50 of 0.0322 μM (95% CI, 0.0214-0.043) was identified.

Table 6.1: Population parameter estimates including coefficient of variation (CV%)

PARAMETER	DESCRIPTION	VALUE	UNIT	CV%
Structural parameters				
$sAPP\beta_{base}$	baseline sAPPβ	332	pM	24.9
$A\beta38_{base}$	baseline Aβ38	381	pM	13.2
$A\beta40_{base}$	baseline Aβ40	1290	pM	7.18
$A\beta42_{base}$	baseline Aβ42	99.6	pM	10.3
$sAPP\alpha_{base}$	baseline sAPPα	395	pM	17.5
Kout	degradation rate Aβ40, Aβ42, Aβ38	0.321	h^{-1}	14.5
$Rout_a$	degradation rate sAPPα	1.18	h^{-1}	13.6
KtAP	transit rate sAPPα and sAPPβ	0.138	h^{-1}	5.68
$KtAB^a$	transit rate Aβ	10	h^{-1}	
$Imax^a$	maximal inhibition (Imax)	1		
IC_{50}	median inhibition concentration	0.0322	μM	17.1
GAM	Hill coefficient	0.749		10.3
Kpl	second-order oligomerization rate constant	6.59e-4	$pM^{-1}\,h^{-1}$	10.3
$A\beta_{O\,base}$	baseline $A\beta_O$	2.1	pg/mL	13.8
$ALPH^a$	Power of the concentration of Aβ42	2		
$Factor_{oligo}$	Conversion factor on $A\beta_O$	0.0178		45.8
Interanimal variability				
ω^2_{BSAPb} [b]	Interanimal variability sAPPβ baseline	0.26		30.4
ω^2_{BSAPa} [b]	Interanimal variability sAPPα baseline	0.145		30.3
ω^2_{AB} [b]	Interanimal variability Aβ	0.103		39.8
Residual error				
$\sigma^2_{A\beta40}$ [c]	Residual variability Aβ40	0.078		12.1
$\sigma^2_{A\beta42}$ [c]	Residual variability Aβ42	0.0576		19.8
$\sigma^2_{sAPP\beta}$ [c]	Residual variability sAPPβ	0.0971		26
$\sigma^2_{sAPP\alpha}$ [c]	Residual variability sAPPα	0.0486		23.3
σ^2_{oligo} [c]	Residual variability $A\beta_O$	1.14		20.7
$\sigma^2_{A\beta38}$ [c]	Residual variability Aβ38	0.0711		19.5

[a] Fixed.

[b] Interanimal variability is assumed to follow a normal distribution with mean zero and variance ω^2.

[c] Residual variability is assumed to follow a normal distribution with mean zero and variance σ^2.

(A) sAPPα

(B) sAPPβ

(C) Aβ38

(D) Aβ40

(E) Aβ42

(F) AβO
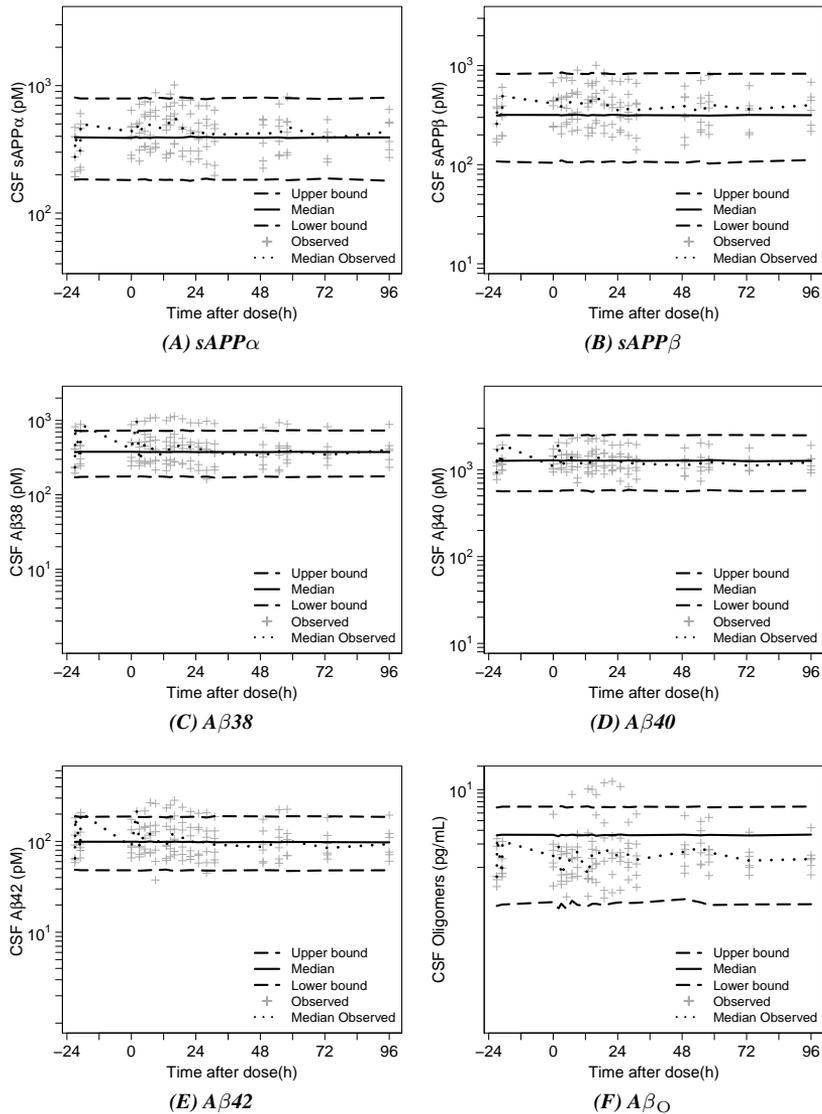
Figure 6.6: Placebo. Visual predictive check of biomarker response vs. time profile of placebo in the rhesus with 90% confidence interval. Predictions were performed with extended model ((A), (B), (C), (D), (E), (F)). Observation sample size: n=108 for each APP metabolite from 6 monkeys collected over 4 days.

Plus-symbols represent observed measurements. Dotted blue line corresponds to the median observed profile. Solid lines show the median simulated profiles. The long-dashed lines correspond to the 90% prediction intervals obtained from 1000 individual simulated profiles.

(A) sAPPα

(B) sAPPβ

(C) Aβ38

(D) Aβ40

(E) Aβ42

(F) Aβ$_O$
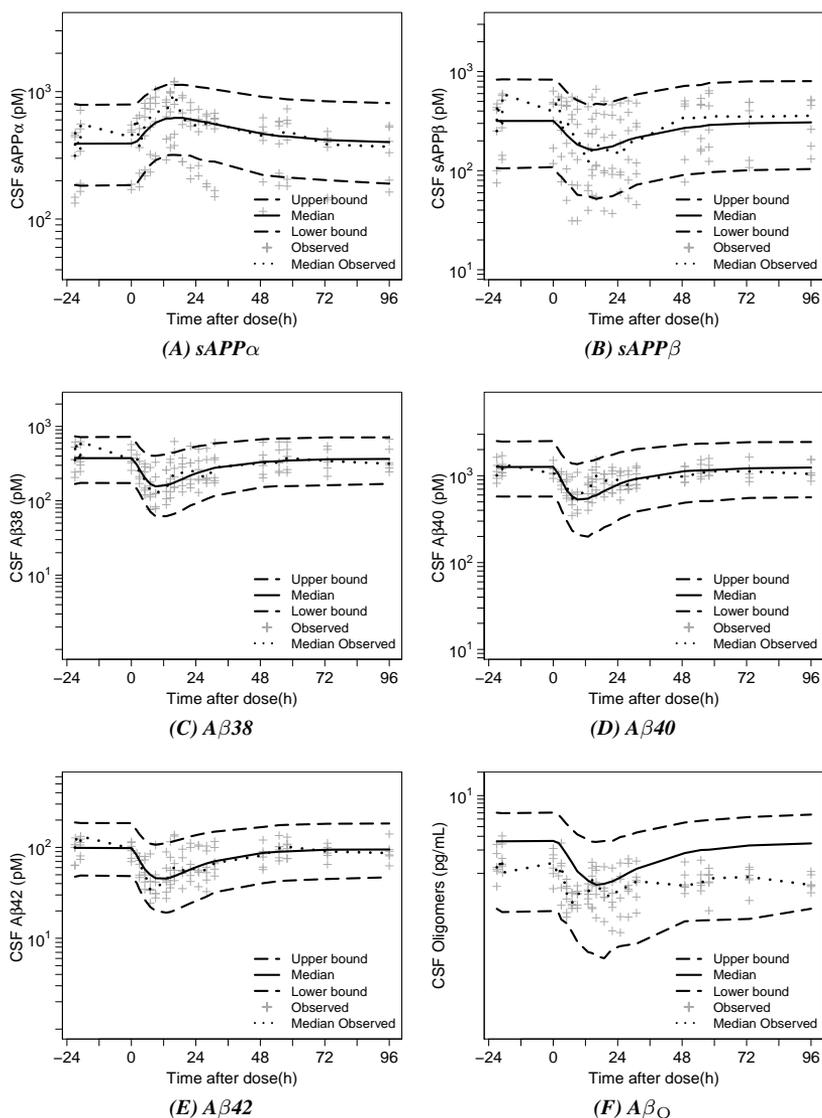
Figure 6.7: Dose 30 mg/kg. Visual predictive check of biomarker response **vs.** *time profile of MBi-5 in the rhesus with 90% confidence interval.* Predictions were performed with model with extended model ((A), (B),(C), (D), (E),(F)). Observation sample size: n=108 for each APP metabolite from 6 monkeys collected over 4 days.

Plus-symbols represent observed measurements. Dotted blue line corresponds to the median observed profile. Solid lines show the median simulated profiles. The long-dashed lines correspond to the 90% prediction intervals obtained from 1000 individual simulated profiles.

185
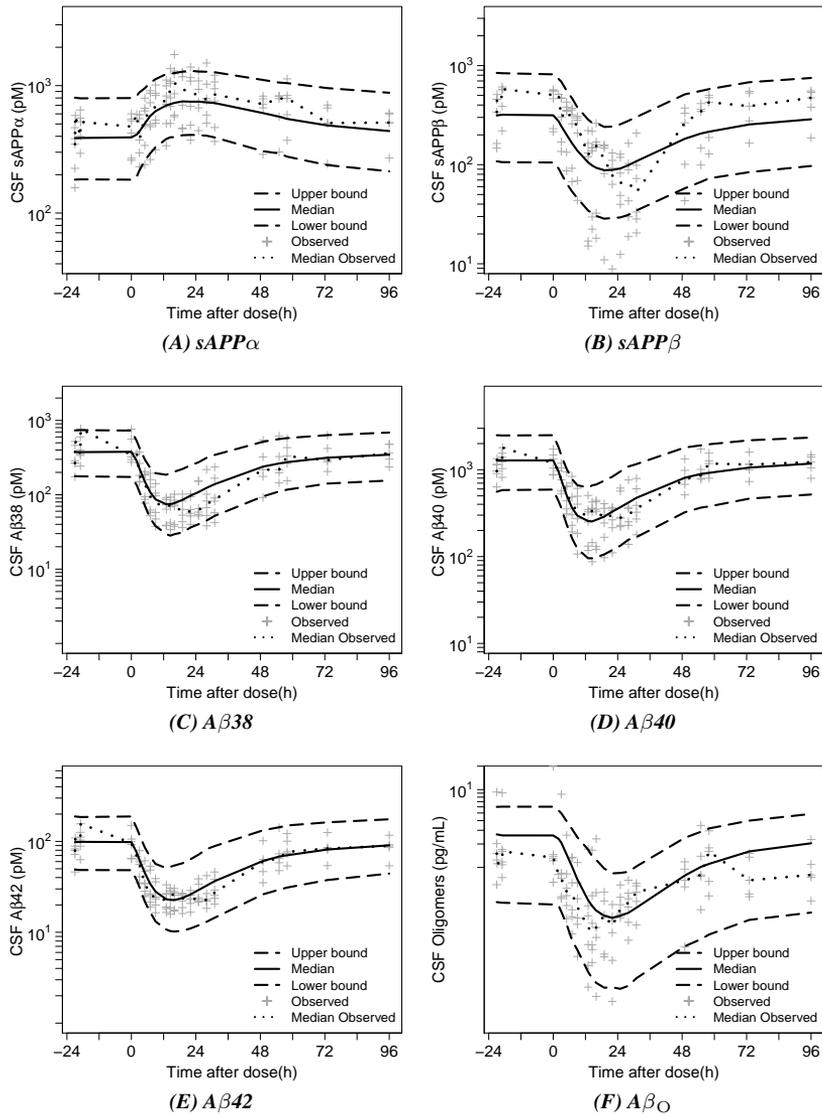
Figure 6.8: Dose 125 mg/kg. Visual predictive check of biomarker response vs. time profile of MBi-5 in the rhesus with 90% confidence interval. Predictions were performed with extended model ((A), (B),(C), (D), (E),(F)). Observation sample size: n=108 for each APP metabolite from 6 monkeys collected over 4 days.

Plus-symbols represent observed measurements. Dotted blue line corresponds to the median observed profile. Solid lines show the median simulated profiles. The long-dashed lines correspond to the 90% prediction intervals obtained from 1000 individual simulated profiles.

Discussion

Soluble Aβ_O are believed to be responsible for the neurodegeneration or toxicity to brain tissue observed in AD. To optimize therapeutic intervention targeting Aβ production with the aim to reduce Aβ_O burden, it is important to understand and quantify the PD effects on Aβ_O. In that respect, it is imperative to consider the behaviour of the APP system as a whole.

The recently reported APP systems model[18], the β-APP model, was extended to include Aβ38 dynamics and describe Aβ_O response data from a novel assay. The so-called β-O-APP model successfully captured sAPPβ and sAPPα concentration behaviour, Aβ monomeric (Aβ38, Aβ40, Aβ42) and oligomeric concentrations and the interactions between these species.

Aβ oligomerization was a second order process, indicating that the concentration of Aβ directly affects the rate of the reaction. Specifically, doubling the concentration of Aβ would quadruple the rate of the oligomerization. The half-life of the oligomerization process is dependent on the initial Aβ concentration. The second-order kinetics of Aβ oligomerization means that a relatively higher change from baseline for Aβ_O compared to monomeric Aβ species is obtained following BACE1 inhibition. e.g. 30% reduction in Aβ42 yields a 50% reduction in Aβ_O following 125 mg/kg MBi-5. By reducing Aβ_O levels, neuropathological alterations underlying AD may be slowed down or stopped. As such, Aβ production inhibition is a potential disease modifying therapy.

The β-O-APP model also contains expressions to account for the fact that decreases in monomeric Aβ42 response resulting from BACE1 inhibition is partially compensated by reverse dissociation of Aβ_Os. Aβ_Os appear to dissociate in order to restore the balance between Aβ monomers and Aβ_O. This supports the belief that Aβ co-exist with Aβ_O in equilibrium and that Aβ_O formation is reversible to a certain extent[10]. As amyloid plaques and fibrils might exist in equilibrium with Aβ oligomeric forms, reducing Aβ_O levels through Aβ production inhibition may bring down higher ordered forms as well. Takamura et al.[22] reported that antibodies raised against Aβ_O reduced plaques in conjunction with Aβ_O.

Our analysis indicated that of the measured Aβ species (Aβ38,Aβ40,Aβ42) Aβ42 was the only major contributor to the oligomer pool. This is in line with the findings that Aβ42 is the dominant Aβ species in plaques and fibrils[23,24,25]. Further, Garai and Frieden[26] reported greater *in vitro* oligomerization propensity of Aβ42 compared to Aβ40, using a fluorescent assay with tetramethylrhodamine-labelled Aβ. Aβ42 is very self-aggregating,

while $A\beta40$ may actually be anti-amyloidogenic[2,27]. The additional two amino acids on the C-terminus of $A\beta42$ makes the peptide more hydrophobic and significantly more rigid than $A\beta40$ and susceptible to aggregation. The increased rigidity promotes entropy-driven aggregation. The high hydrophobicity of $A\beta42$ pushes for aggregation to reduce exposure of the hydrophobic tail[28].

Recently, $A\beta_O$ were predicted to decrease in response to BACE1 inhibition, which was at that time derived indirectly on the basis of an analysis monomeric $A\beta$ response data. In the current analysis, the decrease in $A\beta_O$ concentrations following BACE1 inhibition was confirmed. The within-study comparison that was used to compare model predicted versus observed $A\beta_O$ indicated that the onset of the $A\beta_O$ response was predicted to be slower and the predicted maximum response was lower than observed.

The addition of the parameter $Factor_{olig}$ made it possible to account for differences in units of the quantification assays of monomeric $A\beta$ and $A\beta_O$. This parameter has a relationship with the size of the oligomers and other process involved. A lower apparent volume of distribution of $A\beta_O$ compared to $A\beta$ monomers would be expected, if the measured $A\beta_O$s are high-molecular weight species. This would then be reflected in $Factor_{orig}$. The measured $A\beta_O$s were a mixture of $A\beta_O$ with different number if $A\beta$ monomers incorporated, of which the distribution was unknown. If, for simplicity, it is assumed that $Factor_{orig}$ only has a relationship with $A\beta_O$ size, it is defined as one divided by the number of subunits of $A\beta42$ in $A\beta_O$. This would indicate that, on average, the measured $A\beta_O$s contain 56 subunits of $A\beta$. This is close to the reported size of larger amyloid oligomers of 30-50 protein molecules[29].

It was not possible to use the parameter estimates from the β-APP model in the current analysis, as different biomarker assays were used to determine APP metabolite concentrations. In principle, identified system parameters are attributed to the biological system and may not change from one analysis to another[30]. However, in practice, due to experimental variation system parameters may shift. Then, it is important to understand what is measured and to realize what experimental design aspects might be different as well as those that are kept the same. With respect to the development of a system model, standardization of biomarker assays for data collection will be beneficial.

The β-APP model was extended to describe $A\beta38$, in addition to $A\beta40$ and $A\beta42$ dynamics. Different formation rates were found for these $A\beta$ species. Ranking the formation rates from high to low these rank: $A\beta40$, $A\beta38$, $A\beta42$. This is consistent with the composition of $A\beta$ species reported for human CSF, in which $A\beta40$ is the dominant isoform, and the concentration of $A\beta42$ was much lower than $A\beta40$ and $A\beta38$

concentrations[31].

Unwanted protein aggregation, such as that of Aβ in AD, is generally believed to involve aggregation in a non-native state. In the case of amyloidogenic proteins, the starting reactant is the monomeric form of the protein and the product of the protein aggregation is aggregated protein fibrils. The intermediate species that are formed along the way are still uncertain. Various approaches to determine protein aggregation kinetics and understand the underlying mechanism have been reported in literature and were reviewed by Morris et al.[11]. These were based on *in situ* and *ex situ* aggregation kinetics studies. Lomakin et al.[32] investigated the fibrillation of Aβ40, by following its aggregation using quasi-elastic light scattering *in vitro*. They proposed a critical protein concentration above which stepwise protein aggregation occurs: (i) monomers, (ii) micelles, (iii) nuclei, (iv) fibrils. The fiber elongation rate was proposed to be proportional to the Aβ40 monomer concentration, i.e. a first order process. This cannot be directly compared to the higher order Aβ42 oligomerization identified in the current analysis. As Aβ42 is more prone to aggregation than Aβ40 *(vide supra)*, the results reported by Lomakin et al.[32] might have been different for Aβ42 under the same experimental conditions. Moreover, *in vitro* conditions for aggregation are less complex than *in vivo*, where processes as production, elimination, deposition and fibrillization of Aβ monomers are in dynamic equilibrium.

Conclusions & Perspectives

The findings reported herein indicate that the use of systems pharmacology modelling can be a very useful tool when investigating drug effects on attributes of a complicated biological network. The β-O-APP model was able to integrate information from an Aβ$_O$ assay with the PK and APP metabolites concentration measurements in response to BACE1 inhibition. This yielded important information about the relationship between monomeric Aβ species and Aβ$_O$s: (1) Oligomerization was a higher order process. This means that a relatively larger change from baseline for Aβ$_O$ compared to monomeric Aβ species is obtained following BACE1 inhibition; (2) Aβ$_O$s decreased in response to BACE1 inhibition; (3) Of the measured Aβ species Aβ42 was the only major contributor to the oligomer pool.

The β-O-APP model brings us closer to optimizing the therapeutic intervention to reduce Aβ$_O$ burden. In a follow-up analysis, the potential reduction of the putatively neurotoxic Aβ$_O$ pool following γ-secretase inhibition will be investigated. Potential differences in effects on Aβ$_O$ levels after treatment with a BACE1 *versus* a γ-secretase inhibitor will be evaluated. To this end, data following treatment with the γ-secretase inhibitor

MK-0752 from the current study will be added to further inform the model (**Chapter 7**).

References

1. Di Carlo, M., Giacomazza, D., & San Biagio, P.L. Alzheimer's disease: biological aspects, therapeutic perspectives and diagnostic tools. J physics Condens matter an Inst Phys J. 2012;24(24):244102.

2. Selkoe, D.J. & Hardy, J. The amyloid hypothesis of Alzheimer's disease at 25 years. EMBO Mol Med. 2016;8(6):595–608.

3. Klein, W.L. Synaptotoxic amyloid-β oligomers: a molecular basis for the cause, diagnosis, and treatment of Alzheimer's disease? J Alzheimer's Dis. 2013;33:S49–S65.

4. Esler, W.P. & Wolfe, M.S. A portrait of Alzheimer secretases - New features and familiar faces. Science. 2001;293(5534): 1449–54.

5. Wiltfang, J., *et al.* Higly conserved and disease-specific patterns of carboxyterminally truncated Aβ peptides 1-37/38/39 in addition to 1-40/42 in Alzheimer's disease and in patients with chronic neuroinflammation. J Neurochem. 2002;81(3):481–496.

6. Lichtenthaler, S.F. Alpha-secretase in Alzheimer's disease: Molecular identity, regulation and therapeutic potential. J Neurochem. 2011;116(1):10–21.

7. Grüning, C.S.R., *et al.* The off-rate of monomers dissociating from amyloid-β protofibrils. J Biol Chem. 2013;288(52): 37104–11.

8. Schmit, J.D., Ghosh, K., & Dill, K. What Drives Amyloid Molecules To Assemble into Oligomers and Fibrils? Biophys J. 2011;100(2):450–458.

9. Cerasoli, E., Ryadnov, M.G., & Austen, B.M. The elusive nature and diagnostics of misfolded Aβ oligomers. Front Chem. 2015;3:17.

10. Benilova, I., Karran, E., & De Strooper, B. The toxic Aβ oligomer and Alzheimer's disease: an emperor in need of clothes. Nat Neurosci. 2012;15(3):349–357.

11. Morris, A.M., Watzky, M.A., & Finke, R.G. Protein aggregation kinetics, mechanism, and curve-fitting: a review of the literature. Biochim Biophys Acta. 2009;1794(3):375–97.

12. Lu, Y., *et al.* Cerebrospinal fluid amyloid-β (Aβ) as an effect biomarker for brain Aβ lowering verified by quantitative preclinical analyses. J Pharmacol Exp Ther. 2012;342 (2):366–75.

13. Lu, Y., *et al.* Cerebrospinal fluid β-amyloid turnover in the mouse, dog, monkey and human evaluated by systematic quantitative analyses. Neurodegener Dis. 2013;12(1): 36–50.

14. Parkinson, J., *et al.* Modeling of age-dependent amyloid accumulation and γ-secretase inhibition of soluble and insoluble Aβ in a transgenic mouse model of amyloid deposition. Pharmacol Res Perspect. 2013;1 (2):e00012.

15. Janson, J., *et al.* Population PKPD modeling of BACE1 inhibitor-induced reduction in Aβ levels in vivo and correlation to in vitro potency in primary cortical neurons from

mouse and guinea pig. Pharm Res. 2014;31(3):670–83.

16. Das, R., *et al.* Modeling effect of a γ-secretase inhibitor on amyloid-β dynamics reveals significant role of an amyloid clearance mechanism. Bull Math Biol. 2011;73(1):230–47.

17. Niva, C., Parkinson, J., Olsson, F., van Schaick, E., Lundkvist, J., & Visser, S.a.G. Has inhibition of Aβ production adequately been tested as therapeutic approach in mild AD? A model-based meta-analysis of γ-secretase inhibitor data. Eur J Clin Pharmacol. 2013;69(6):1247–60.

18. van Maanen, E.M.T., *et al.* Systems pharmacology analysis of the amyloid cascade after β-secretase inhibition enables the identification of an Aβ42 oligomer pool. J Pharmacol Exp Ther. 2016;357(1):205–16.

19. Savage, M.J., *et al.* A sensitive Aβ oligomer assay discriminates Alzheimer's and aged control cerebrospinal fluid. J Neurosci. 2014;34(8):2884–97.

20. Gilberto, D.B., *et al.* An alternative method of chronic cerebrospinal fluid collection via the cisterna magna in conscious rhesus monkeys. Contemp Top Lab Anim Sci. 2003;42(4):53–59.

21. Bauer, R.J. 2011 NONMEM users guide. Introduction to NONMEM 7.2.0 Technical report;ICON Development Solutions, Ellicott City, MD.

22. Takamura, A., *et al.* Sortilin is required for toxic action of Aβ oligomers (AβOs): Extracellular AβOs trigger apoptosis, and intraneuronal AβOs impair degradation pathways. Life Sci. 2012;91(23-24):1177–1186.

23. Iwatsubo, T., Odaka, A., Suzuki, N., Mizusawa, H., Nukina, N., & Ihara, Y. Visualization of Aβ42(43) and Aβ40 in senile plaques with end-specific Aβ monoclonals: evidence that an initially deposited species is Aβ42(43). Neuron. 1994;13(1):45–53.

24. Gu, L., Tran, J., Jiang, L., & Guo, Z. A new structural model of Alzheimer's Aβ42 fibrils based on electron paramagnetic resonance data and Rosetta modeling. J Struct Biol. 2016;194(1):61–67.

25. Economou, N.J., *et al.* Amyloid β-Protein Assembly and Alzheimer's Disease: Dodecamers of Aβ42, but Not of Aβ40, Seed Fibril Formation. J Am Chem Soc. 2016;138(6):1772–1775.

26. Garai, K. & Frieden, C. Quantitative analysis of the time course of Aβ oligomerization and subsequent growth steps using tetramethylrhodamine-labeled Aβ. Proc Natl Acad Sci U S A. 2013;110(9):3321–6.

27. Kim, J., *et al.* Aβ40 Inhibits Amyloid Deposition In Vivo. J Neurosci. 2007;27(3):627–633.

28. Yan, Y. & Wang, C. Aβ42 is More Rigid than Aβ40 at the C Terminus: Implications for Aβ Aggregation and Toxicity. J Mol Biol. 2006;364(5):853–862.

29. Breydo, L. & Uversky, V.N. Structural, morphological, and functional diversity of amyloid oligomers. FEBS Lett. 2015;589(19):2640–2648.

30. Dingemanse, J., Danhof, M., & Breimer, D.D. Pharmacokinetic-pharmacodynamic modeling of CNS drug effects: An overview. Pharmacol Ther. 1988;38(1):1–52.

31. Janelidze, S., *et al.* CSF Aβ42/Aβ40 and Aβ42/Aβ38 ratios: better diagnostic markers of Alzheimer disease. Ann Clin Transl Neurol. 2016;3(3):154–65.

32. Lomakin, a., Chung, D.S., Benedek, G.B., Kirschner, D.a., & Teplow, D.B. On the nucleation and growth of amyloid beta-protein fibrils: detection of nuclei and quantitation of rate constants.. Proc Natl Acad Sci U S A. 1996;93(3):1125–1129.

Chapter 6

Supplemental Material

**E.M.T. van Maanen, T.J. van Steeg, J. Kalinina, M.S. Michener, M.J. Savage, M.E. Kennedy,
J.A. Stone, M. Danhof**

SUPPLEMENTAL MATERIAL

Study differences

The response data of Aβ40, Aβ42, sAPPβ and sAPPα from the recent BACE1 inhibitor study[1] (hereinafter referred to as study 1) and the current BACE1 inhibitor study (hereinafter referred to as study 2) following a dose of 125 mg/kg MBi-5 is depicted in Supplemental Figure S6.1. A large between-study variability in the data was observed. This is also apparent from the plots of the ratios of Aβ42:Aβ40 (Supplemental Figure S6.2A), Aβ40:sAPPβ (Supplemental Figure S6.2B) and sAPPβ:sAPPα (Supplemental Figure S6.2C) in each study. There was no overlap in the rhesus monkey individuals included in studies 1 and 2.

References

1. van Maanen, E.M.T., *et al.* Systems Pharmacology Analysis of the Amyloid Cascade after β-Secretase Inhibition Enables the Identification of an Aβ42 Oligomer Pool. J Pharmacol Exp Ther. 2016;357(1):205–16.
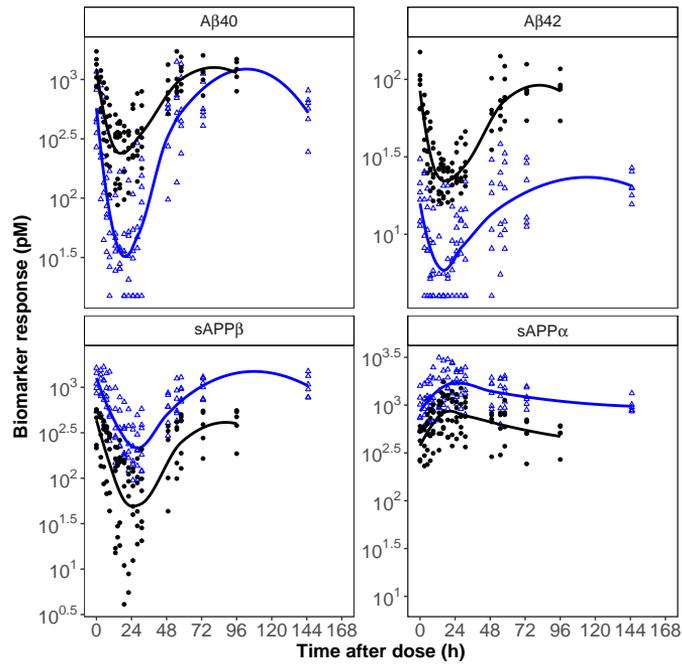
Figure S6.1: Study differences in absolute concentrations of biomarkers.
Study 1: blue line and symbols; Study2: black line and symbols; Lines are smoothers.

(A) Ratio Aβ42:Aβ40

(B) Ratio Aβ40:sAPPβ

(C) Ratio sAPPβ:sAPPα
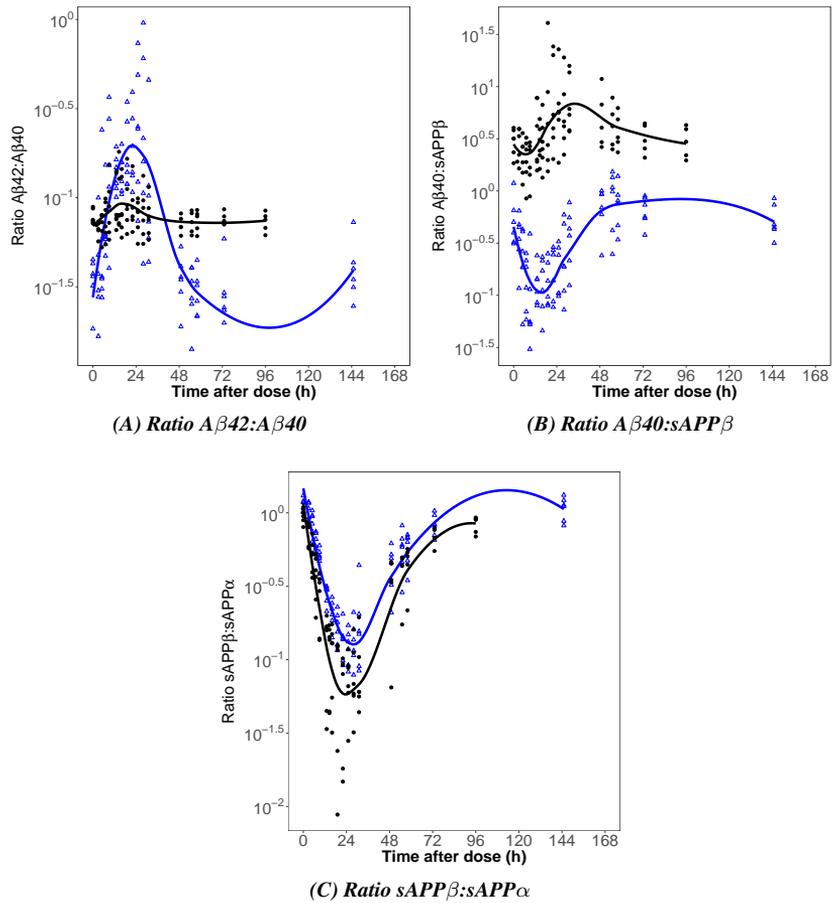
Figure S6.2: Study differences in ratios of biomarkers.
Study 1: blue line and symbols; Study2: black line and symbols; Lines are smoothers.
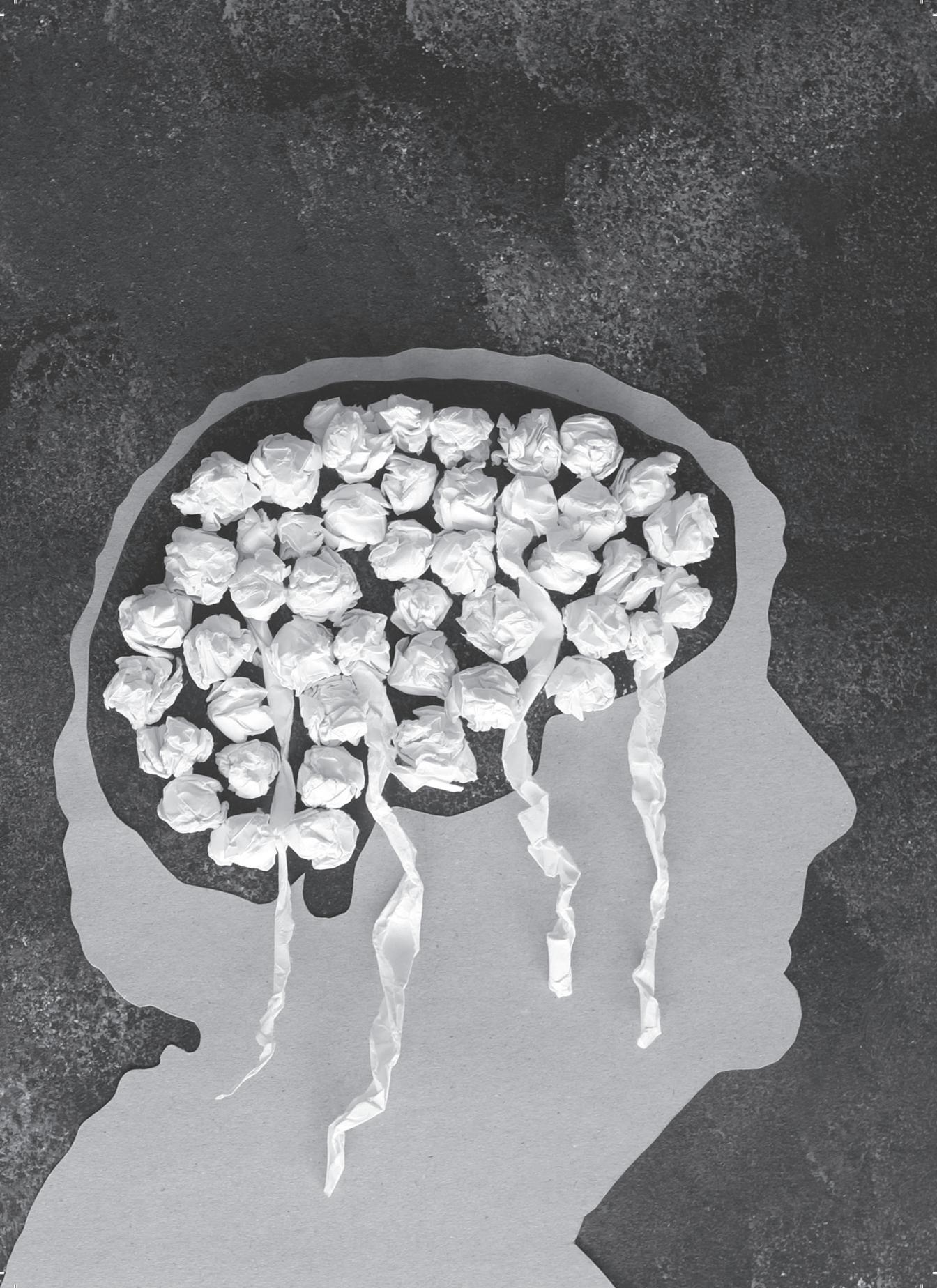
Chapter 7

A single systems pharmacology approach to
unravel Aβ oligomer modulation upon administration
of multiple APP cleavage inhibitors

E.M.T. van Maanen, T.J. van Steeg, J. Kalinina, M.S. Michener,
M.J. Savage, M.E. Kennedy, J.A. Stone, M. Danhof

Abstract

Accumulation of toxic soluble Aβ oligomers (Aβ_{O}) is the primary event driving the pathological changes in Alzheimer's Disease (AD). Inhibition of β-amyloid precursor protein (APP) cleavage enzymes has been proposed as an approach to reduce Aβ_{O} concentrations. Due to the complexity of the underlying biochemical network, the effects of these interventions on Aβ_{O} are difficult to predict.

The aim of this investigation was to develop a single systems pharmacology model to predict the change in Aβ_{O} following administration of inhibitors of multiple APP cleavage enzymes (i.e. β-secretase (BACE1) and γ-secretase (GS) inhibition). A novel systems pharmacology model, the β-γ-O-APP model, which is an extension of a previously proposed β-O-APP model, was successfully applied to describe the pharmacokinetics and the time course of the changes in APP metabolite (sAPPβ, sAPPα, Aβ42, Aβ40, Aβ38) and Aβ_{O} concentrations.

A differential effect of BACE1 versus GS inhibition on the APP metabolite profiles was observed, which was reflected in the ratio Aβ42:Aβ40:Aβ38. The analysis shows that this may be explained by stepwise successive cleavage of C99 by GS, wherein part of Aβ38 is converted from Aβ42. Both BACE1 and GS inhibition resulted in similar maximum reduction of the Aβ_{O} and monomeric Aβ. The β-γ-O-APP model suggests that GS inhibition may enhance the non-amyloidogenic processing of APP via homeostatic feedback exerted by C99. Understanding the mechanisms that underlie the APP processing pathway through the APP systems pharmacology model aids the optimization of therapeutic intervention to reduce Aβ_{O} burden.

Introduction

The amyloid cascade hypothesis for Alzheimer's Disease (AD) posits that the deposition of the amyloid peptides (Aβ) in the brain is a central event in the pathophysiology. Aβ s are elevated early in the disease, before clinical symptoms manifest and this leads to a series of pathophysiological changes[1]. The most toxic species of Aβ are soluble Aβ oligomers (Aβ_O), which are believed to be the initial drivers of neurodegeneration[2,3]

Aβ is the final product of proteolytic cleavage of the transmembrane β-amyloid precursor protein (APP) and the precursor of Aβ_O. In the amyloidogenic pathway, Aβ is produced by sequential cleavage of APP by β-secretase 1 (BACE1) and γ-secretase (GS)[4]. Cleavage by BACE1 creates the soluble β-amyloid precursor protein (sAPPβ) and C99, a C-terminal fragment which remains membrane bound. Aβ is derived from the GS cleavage of C99, generating Aβ peptides of various amino acid chain lengths, of which the most common are 38, 40 or 42 amino acids long (Aβ38, Aβ40, or Aβ42, respectively)[5]. An alternative pathway is driven by α-secretase cleavage, which generates the non-amyloidogenic soluble sAPPα and the C-terminal membrane-bound 83-amino acid fragment C83. This occurs within the Aβ sequence, and thus precludes Aβ generation[6].

Aβ peptide accumulates in stages into amyloid plaques. The Aβ peptides first form Aβ_O, which are soluble disordered clusters. Then, protofibrils are formed, which are prefibrillar insoluble high molecular weight Aβ_O (50-1500 kDa) consisting of spherical, annular, and curvilinear assemblies[7,8,9]. Next, chains of agglomerates called fibrils are generated, followed by an interwoven mass of fibrils called β-sheets and in the final stage plaques are developed[10].

Targeting Aβ_O may prove to be an effective treatment for AD by halting their accumulation and preventing their neurotoxic effect. One of the main therapeutic strategies for AD aims at Aβ reduction through inhibition of Aβ production. Due to the complexity of the underlying biochemical network, the effects of these interventions on the individual moieties of the APP processing pathways and Aβ_O are difficult to predict.

Systems pharmacology abstracts our understanding of biochemical/pathological pathways into mathematical constructs, in combination with the application of pharmacokinetic (PK) and pharmacodynamic (PD) principles. In this approach, the drug effect is considered to be the result of the interactions of the drug and the biological system.

Recently, we have proposed a systems pharmacology model of the APP processing pathway characterizing APP metabolite (sAPPα, sAPPα, Aβ40, Aβ42, Aβ38) and Aβ_O responses to BACE1 inhibition, the so called β-O-APP model[11]. In that inves-

tigation Aβ oligomerization was identified to display second order kinetics and Aβ42 was found to be the major contributor to the Aβ_O pool. This model was based on an analysis of the data of the effect of a BACE1 inhibitor from a 4-way crossover study in cisterna-magna-ported rhesus monkeys on the effects of a BACE1 (MBi-5) and a GS (MK-0752) inhibitor on the biomarker concentrations in CSF. In the current investigation, we have included the GS inhibitor response data from the same study and investigated differences in biomarker responses between BACE1 and GS inhibition.

In an earlier analysis with the β-γ-APP model, both BACE1 and GS inhibition were predicted to lower Aβ_O levels, which was at that point derived from monomeric Aβ dynamics[12]. The prediction suggested a lower oligomerization rate of Aβ42 after GS and BACE1 inhibition. Now, the effect of BACE1 and GS inhibition on the time course of the changes in Aβ_O measurements is determined and can be compared. Also, to our knowledge for the first time, sAPPβ and sAPPα levels following GS inhibition have been measured.

The objectives of this investigation were: (1) to extend a systems pharmacology model of the APP processing pathway, describing the effects of both BACE1 and GS inhibitors on its individual attributes and its interrelationships; (2) to elucidate the relationship between the Aβ_O and monomeric Aβ further, which is imperative to improve the prediction of therapeutic effects on Aβ; (3) to understand the difference in Aβ dynamics following BACE1 *versus* GS inhibition.

Materials and Methods

Animals

In this study, six male rhesus monkeys, weighing between 8.6 kg and 11.8 kg (mean, 9.7 kg), age at 9 years to 13 years (mean, 11 years) at time of the study were included. They were individually housed and captive-bred in a closed colony. The rhesus monkeys are chronically implanted with catheters in the cisterna magna, as described by Gilberto et al.[13]. This facilitated repeated sampling of CSF and plasma in conscious rhesus monkeys. All animal studies were reviewed and approved by the MSD Institutional Animal Care and Use Committee. The NIH Guide to the care and use of Laboratory Animals and the Animal Welfare act were followed in the conduct of the animal studies (Institute of Laboratory Animal Resources, National Research Council, 1996).

Drug administration and sampling

In a four-way full crossover study, a single oral dose of MBi-5 at 30 and 125 mg/kg, MK-0752 at 240 mg/kg (5 mL/kg) or vehicle (0.4% methylcellulose) was administered. Plasma and CSF drug concentrations were collected at 0 (predose) and 3, 5, 7, 9, 13, 14.5, 16, 19, 22, 25, 28, 31, 49, 55, 58, 73 and 96 h postdose, resulting in 18 plasma and CSF PK samples for each rhesus monkey per treatment group. 2 mL of blood and 1 mL of CSF were collected at each time point. The concentration of MBi-5 and MK-0752 in the plasma and CSF samples was determined using LC-MS/MS. The concentrations of sAPPα, sAPPβ, Aβ40, Aβ42, Aβ38 and Aβ_O were determined from CSF samples, collected at the same time points as PK samples, by established and validated ELISA-based assays (Meso Scale Diagnostics "sAPPα/sAPPβ Kit" (Catalog No. K15120E) and "Human (6E10) Abeta Triplex Assay" (Catalog No. K15148E)), giving 18 measurements of each biomarker for each monkey per treatment. To determine Aβ_O concentrations, a two-site ELISA assay was used, that was previously described by Savage et al. [14].

PK-PD analysis

A non-linear mixed effects modelling approach was used to analyze the PK and PD data. This approach takes structural (fixed) effects and both intra- and interindividual variability into account. Typical values of structural model parameters (population parameters, which define the average value for a parameter in a population) (θ), the variance and covariance of the interindividual variability (ω^2) and the variance of the residual error (σ^2) are estimated. The population approach described individual profiles relative to the overall population trend.

The β-γ-O-APP model was implemented in the software package NONMEM (version 7.2.0[15]). The models were compiled using Compaq Visual Fortran (version 6.6, Compaq Computer Corporation, Houston, Texas, USA) and executed on a PC equipped with an an Intel QuadCore (Intel® Core^{TM} i7 CPU860, 2.80 GHz, 3.24 GB RAM). Data management and model assessment was done using the statistical software package S-PLUS for Windows (version 8.0 Professional, Insightful Corp., Seattle, USA). Based on the analysis of their obtained minimum value of the objective function (defined as minus twice the log-likelihood), the precision of parameter estimates, and visual inspection of goodness-of-fit plots the best models were selected. A more detailed description of the modelling procedure was described in van Maanen et al. [16].

The performance of the β-γ-O-APP model was evaluated with a visual predictive check (VPC), in which the median and the 90% inter-quantile range of the data simulated

with the final parameter estimates were plotted together with the observations. A validated result would have close resemblance of median observed and predicted line with 90% of the observations that fall within the 90% prediction interval.

Berkeley Madonna[TM] version 8.3.18 (Macey and Oster, University of California, Berkeley) was used for simulations to illustrate the characteristics of the β-γ-O-APP model.

Model description

The APP systems pharmacology model was developed by sequential analysis of PK and PD data following administration of MBi-5 and MK-0752. The PK model of MBi-5 was based on simultaneous analysis of plasma and CSF PK data and has been described elsewhere by van Maanen et al.[16]. The PK model for MK-0752 was reported previously[17,12]. The PK models adequately described the plasma and CSF concentration time profiles of MBi-5 and MK-0752, respectively, thus the models could serve as input for PD model analysis.

The biomarker response profiles of MBi-5 and MK-0752 measured in CSF were adequately described by the β-γ-O-APP model containing compartments for eight moieties: APP, sAPPβ, sAPPα, C99, Aβ40, Aβ42, Aβ38 and Aβ_O (Fig. 7.1). APP production was assumed to be constant and described by a zero order input rate Rin_{APP}. The production of the APP metabolites was assumed to be first order, i.e. dependent on its precursor concentration. The interaction between APP and its metabolites (sAPPβ, sAPPα, C99, Aβ40, Aβ42 and Aβ38) and Aβ_O is described by Eq. 7.1 - Eq. 7.8:

$$\frac{d}{dt} APP = Rin_{APP} - \left(Rin\beta \times EFFB + Rin\alpha \times \left(\frac{C99}{C99_{base}} \right)^{FP} \right) \times APP$$

(7.1)

$$\frac{d}{dt} sAPP\alpha = Rin\alpha \times \left(\frac{C99}{C99_{base}} \right)^{FP} \times APP - Rout_a \times sAPP\alpha$$

(7.2)

$$\frac{d}{dt} sAPP\beta = Rin\beta \times EFFB \times APP - Rout_b * sAPP\beta$$

(7.3)

$$\frac{d}{dt}C99 = Rin\beta \times EFFB \times APP$$
$$- (Kin_{40} + Kin_{42} + Kin_{38}) * EFFG * C99 - Kout_{99} * C99$$

$$(7.4)$$

$$\frac{d}{dt}A\beta_{40} = Kin_{40} \times EFFG \times C99 - Kout \times A\beta_{40} \tag{7.5}$$

$$\frac{d}{dt}A\beta_{42} = Kin_{42} \times EFFG \times C99 - Kout_{42} \times A\beta_{42}$$
$$- Kin_{382} \times EFFG \times A\beta_{42} - Kpl \times (A\beta_{42})^{ALPH} \tag{7.6}$$
$$+ Krev \times A\beta_O / \left(\frac{MW_{A\beta42}}{1000} \times Factor_{oligo} \right)$$

$$\frac{d}{dt}A\beta_{38} = Kin_{38} \times EFFG \times C99 + Kin_{382} \times EFFG \times A\beta_{42}$$
$$- Kout * A\beta_{38} \tag{7.7}$$

$$\frac{d}{dt}A\beta_O = Kpl \times (A\beta_{42})^{ALPH} \times \frac{MW_{A\beta42}}{1000} \times Factor_{oligo} - Krev \times A\beta_O \tag{7.8}$$

The rate of change of APP with respect to time in the presence of the BACE1 inhibitor is expressed by Eq. 7.1, in which the BACE1 cleavage inhibition is incorporated by the factor *EFFB*. The rate of change of C99 with respect to time in the presence of the GS inhibitor is described by Eq. 7.4, in which the GS cleavage inhibition is incorporated by the factor *EFFG*. *EFFB* and *EFFG* are the degrees of inhibition caused by MBi-5 and MK-0752, respectively. Generally, the degree of inhibition is described by a sigmoidal Imax function, as shown in Eq. 7.9.

$$EFF = 1 - \frac{C_{target}^{GAM} * Imax}{C_{target}^{GAM} + IC50^{GAM}} \tag{7.9}$$

Where C_{target} is the target site concentration of MBi-5 or MK-0752, respectively, *IC50* the C_{target} that results in 50% inhibition of BACE1 or GS, *Imax* is the maximum response and *GAM* is the Hill coefficient. C_{target} was derived from the respective PK models as:

$$C_{target} = C_{plasma} * \frac{AUC_{CSF}}{AUC_{plasma}} \tag{7.10}$$

Where AUC_{CSF} and AUC_{plasma} are the areas under the CSF and plasma concentration time curves, respectively. C_{target} is assumed to be at a level between C_{CSF} and C_{plasma}, following the same profile as C_{plasma}.

It is assumed that the system is in steady state (SS) when no treatment is given *(EFFB=1, EFFG=1)*. These steady state conditions were used to derive part of the system parameters. From SS and Eq. 7.1 it follows that the zero order input rate of APP *(Rin_{APP})* is:

$$Rin_{APP} = (Rin_\alpha + Rin_\beta) * APP_{base} \tag{7.11}$$

Where APP_{base} is the baseline level of APP, assumed to be equal to the sum of the baseline levels of sAPPα and sAPPβ, as all alternate pathways are represented by the terms for α-secretase.

Using SS conditions and Eq. 7.2 the sAPPα formation rate *(Rin_α)*, equivalent to the α-secretase cleavage step, can be derived:

$$Rin_\alpha = Rout_a \times \frac{sAPP\alpha_{base}}{APP_{base}} \tag{7.12}$$

Where $sAPP\alpha_{base}$ is the baseline level of sAPPα.

The sAPPβ and C99 formation rate *(Rin_β)*, equivalent to the BACE1 cleavage step, follows from SS conditions and Eq. 7.3:

$$Rin_\beta = Rout_b \times \frac{sAPP\beta_{base}}{APP_{base}} \tag{7.13}$$

Where $sAPP\beta_{base}$ is the baseline level of sAPPβ.

From Eq. 7.5 and SS, the Aβ degradation rate (*Kout*), is deduced:

$$Kout = Kin_{40} \times \frac{C99_{base}}{A\beta40_{base}} \tag{7.14}$$

Where $C99_{base}$ is the baseline level of C99.

From Eq. 7.4 and SS the baseline level of C99 can be derived:

$$C99_{base} = \frac{Rout_b \times sAPP\beta_{base} \times A\beta40_{base}}{Kin_{40} \times (A\beta40_{base} + A\beta38_{base} + A\beta42_{base}) + A\beta40_{base} \times Kout_{99}} \tag{7.15}$$

Using SS conditions 7.6, 7.7 and 7.15, respectively, the formation rates of Aβ42 (*Kin42*) and Aβ38 (*Kin38*), equivalent to γ-secretase cleavage steps, can be calculated:

$$Kin_{42} = \frac{(Kout + Kin_{382}) \times A\beta42_{base}}{C99_{base}} \tag{7.16}$$

$$Kin_{38} = \frac{Kout \times A\beta38_{base} - Kin_{382} \times A\beta42_{base}}{C99_{base}} \tag{7.17}$$

Where $A\beta42_{\text{base}}$ and $A\beta38_{\text{base}}$ are the baseline levels of Aβ42 and Aβ38, receptively.

The exchange between the Aβ_O pool and the Aβ42 compartment is described by Eq. 7.6 and Eq. 7.8, where *ALPH* is the power of the concentration of Aβ42, $Factor_{oligo}$ is the conversion factor on Aβ_O and $MW_{A\beta42}$ is the molecular weight of Aβ42. *Krev* and *Kpl* are the dissociation rate and higher-order Aβ42 oligomerization rate constant, respectively, which are dependent on the baseline values of Aβ42 and the Aβ_O pool (Aβ42$_{\text{base}}$ and Aβ_{Obase}, resp.) according to Eq. 7.18:

$$Krev = \frac{Kpl \times (A\beta_{42base})^{ALPH} \times \frac{MW_{AB42}}{1000} \times Factor_{oligo}}{A\beta_{Obase}} \tag{7.18}$$

The model structure includes six transit compartments (Fig. 7.1), one for each biomarker measured in CSF (sAPPα, sAPPβ, Aβ40, Aβ42, Aβ38, Aβ_O), to account for transport from the target site in the brain to CSF. These transit processes are described, in general, by Eq. 7.19:

$$\frac{d}{dt} xAx_{CSF} = Ktr * (xAx - xAx_{CSF}) \tag{7.19}$$

Where *Kt* is the transit rate for the particular particular APP metabolite xAx (*KtAP* for sAPPα and sAPPβ and *KtAB* for Aβ40, Aβ42, Aβ38 and Aβ$_O$).

Figure 7.1: Schematic of β-γ-O-APP model.
The model comprised fourteen compartments: Eight biomarker compartments in brain *(yellow circles)* and six transit compartments from brain to CSF *(white circles)*. Six biomarkers were measured in CSF (sAPPα, sAPPβ, Aβ40,Aβ42, Aβ38 and Aβ$_O$), indicated by the blue boxes. The drug effect of the BACE1 inhibitor *(BACEi EFF)* inhibited *Rinβ*. The drug effect of the GS inhibitor *(GSi EFF)* inhibited *Kin$_{40}$*, *Kin$_{40}$*, *Kin$_{38}$* and *Kin$_{382}$*. As driver of biomarker response C_{target} was used, which was derived from the PK models of the BACE1 inhibitor [16] and GS inhibitor [12], respectively. The red arrow indicates the homeostatic feedback on α-secretase through the action of C99. Model extensions compared to the β-O-APP model are indicated with the green shaded area.
APP: Aβ-precursor protein; *Aβ*: amyloid-β-peptide; C_{target}: drug concentration target site; *Kin$_{38}$*: Aβ38 formation rate from C99; *Kin$_{382}$*: Aβ38 formation rate from Aβ42; *Kin$_{40}$*: Aβ40 formation rate; *Kin$_{42}$*: Aβ42 formation rate; *Kout*: Aβ38, Aβ40 and Aβ42 degradation rate; *Kout$_{C99}$*: C99 degradation rate; *Krev*: Oligomer dissociation rate; *KtAP*: transit rate sAPPα and sAPPβ from brain to CSF; *Kpl*: Oligomerization rate; *KtAB*: transit rate Aβ from brain to CSF; *KtAB$_O$*: transit rate Aβ$_O$ from brain to CSF; *RinAPP*: source of APP; *Rinβ*: sAPPβ formation rate; *Rinα*: sAPPα formation rate; *Routb*: sAPPβ degradation rate; *Routa*: sAPPα degradation rate.

Results

APP systems pharmacology model

A systems pharmacology model, incorporating the PK of MBi-5 and MK-0752, CSF APP metabolite (Aβ38, Aβ40, Aβ42, sAPPα and sAPPβ) concentrations and Aβ_O measurements was developed to quantify APP metabolite and Aβ_O responses to BACE1 and GS inhibition in monkeys. The model, named the β-γ-O-APP model, is schematically presented in Fig. 7.1. The model included terms to describe the production and elimination of each APP metabolite. The oligomerization of Aβ42 was described by higher order kinetics[11].

The drug effect of MBi-5 was incorporated in the model as blocking sAPPβ and C99 production, equivalent to the BACE1 cleavage step. The drug effect of MK-0752 was implemented as blocking Aβ production, corresponding to the GS cleavage step. Both drug effects where described by an Imax function[12].

Part of Aβ38 is converted from Aβ42

A difference in the ratios of Aβ42, Aβ40 and Aβ38 over total Aβ (Aβ38+Aβ40+Aβ42) following BACE1 versus GS inhibition was found (see Supplemental Material). This was described by extending the β-γ-O-APP model to account for subsequent GS cleavage of part of Aβ42 to Aβ38 (Equation 7.7). This cleavage step is inhibited by the GS inhibitor, but not blocked if BACE1 is inhibited.

MK-0752 exposure increased sAPPα

A slight decrease in sAPPβ and increase of sAPPα concentrations, as well as a change in the ratio sAPPβ:sAPPα was observed in response to GS inhibition (see Supplemental Material). This could be described by implementing a homeostatic feedback loop in the model structure regulated by C99: The increase in C99 relative to baseline C99 after GS inhibition stimulates α-secretase processing of APP (Equation 7.2). Then, as result of substrate competition, BACE1 processing of APP relatively decreases resulting in a slight decline of sAPPβ following GS inhibition. The strength of this homeostatic feedback action was quantified by the feedback parameter *FP*, that was estimated to be 0.438, which was significantly different from zero (when there would be no feedback).

Aβ production inhibition decreased Aβ$_O$

Both BACE1 and GS inhibition reduced the Aβ$_O$ levels, which was adequately described by the APP systems model (Figs. 7.3F, 7.4F and 7.5F, respectively). Note that Aβ monomers were measured in pM and Aβ$_O$ were expressed in pg/mL. For this reason, a conversion factor needed to be included in the model, which was discussed recently[11]. A similar maximum reduction of Aβ$_O$ concentration of 89% was obtained after treatment with 125 mg/kg MBi-5 and 240 mg/kg MK-0752. However, GS inhibition had a more prolonged pharmacological effect on Aβ$_O$ levels compared to BACE1 inhibition.

Model parameters

The analysis of the variability of model parameters due to interanimal variation resulted in a random-effects structure including interanimal variability for the baselines of sAPPβ, sAPPα, Aβ38, Aβ40, Aβ42 and Aβ$_O$, with the same random-effect parameter used for Aβ40 and Aβ42 (Table 7.2). All were included as exponential in nature, which reflects lognormal distributions of the individual parameters.

It was not possible to obtain a successful completion of the Covariance Step in NONMEM using the model including interanimal variability. Furthermore, because of long model minimization times it was not feasible to perform a bootstrap to obtain parameter precision. Therefore, the precision of the model parameters from the model without interanimal variability is reported in Table 7.1, which was adequate.

To take caution against over parameterization of the model, the formation rate constant of Aβ40 *Kin*$_{40}$ was fixed to the value from the β-O-APP model[11].

When estimated, the Hill coefficients of the concentration response relationships of MBi-5 and MK-0752 were not significantly different from 1. Therefore, the sigmoid-Imax concentration response relationships could be simplified to Imax relationships by fixing the Hill coefficients to 1. For MBi-5, a potency (IC50) of 0.0251 μM (95% CI, 0.02-0.0302) was identified, which was similar to the previously reported IC50 of 0.0256 μM (95% CI, 0.0137–0.0375) from another CMP rhesus study[16], and is also near the *in vitro* inhibition constant (Ki) of 10 nM for MBi-5 inhibition of purified BACE1 and the IC50 of 24 nM for inhibition of Aβ production in intact cells[18]. An IC50 of 0.0468 μM (95% CI, 0.0154–0.0782) was identified for MK-0752 . This value was 10 fold lower than reported earlier for CMP rhesus monkeys[12] and also 10 fold lower than the brain IC50 of MK-0752 in guinea-pigs of 440 nM[19].

Table 7.1: Population parameter estimates including coefficient of variation (CV%)

PARAMETER	DESCRIPTION	VALUE	UNIT	CV%
Structural parameters				
$sAPP\beta_{base}$	baseline sAPPβ	382	pM	17
$A\beta 38_{base}$	baseline Aβ38	411	pM	16
$A\beta 40_{base}$	baseline Aβ40	1330	pM	10.5
$A\beta 42_{base}$	baseline Aβ42	107	pM	12.1
$sAPP\alpha_{base}$	baseline sAPPα	457	pM	13.3
Kin_{40}[a]	formation rate Aβ40	1.29	h^{-1}	
Kin_{382}	Aβ38 formation rate from Aβ42	0.162	h^{-1}	17.5
$Rout_a$	degradation rate sAPPα	1.11	h^{-1}	12.7
$Rout_b$	degradation rate sAPPβ	1.46	h^{-1}	11.8
$Kout_{99}$	degradation rate C99	0.496	h^{-1}	34.9
KtAP	transit rate sAPPα and sAPPβ	0.122	h^{-1}	3.09
KtAB[a]	transit rate Aβ	10	h^{-1}	
ImaxB[a]	maximal inhibition (Imax) MBi-5	1		
$IC_{50}B$	median inhibition concentration MBi-5	0.0251	μM	10.4
GAMB[a]	Hill coefficient MBi-5	1		
ImaxG[a]	maximal inhibition (Imax) MK-0752	1		
$IC_{50}G$	median inhibition concentration MK-0752	0.0468	μM	34.2
GAMG[a]	Hill coefficient MK-0752	1		
Kpl	oligomerization rate	5.46e-4	$pM^{-1}\,h^{-1}$	40.1
$A\beta_{Obase}$	baseline Aβ_O	2.03	pg/mL	13.6
ALPH[a]	order oligomerization	2		
FP	feedback parameter	0.496		20.8
$Factor_{oligo}$	conversion factor on oligomers	0.00994		20.6
Residual error				
$\sigma^2_{A\beta 40}$[b]	Residual variability Aβ40	0.157		21.5
$\sigma^2_{A\beta 42}$[b]	Residual variability Aβ42	0.146		26.9
$\sigma^2_{sAPP\beta}$[b]	Residual variability sAPPβ	0.269		42.8
$\sigma^2_{sAPP\alpha}$[b]	Residual variability sAPPα	0.175		34.9
σ^2_{oligo}[b]	Residual variability Aβ_O	1.01		18.2
$\sigma^2_{A\beta 38}$[b]	Residual variability Aβ38	0.247		27.1

[a] Fixed.

[b] Residual variability is assumed to follow a normal distribution with mean zero and variance σ^2.

Table 7.2: Population parameter estimates

PARAMETER	DESCRIPTION	VALUE	UNIT
Structural parameters			
$sAPP\beta_{base}$	baseline sAPPβ	349	pM
$A\beta38_{base}$	baseline Aβ38	373	pM
$A\beta40_{base}$	baseline Aβ40	1250	pM
$A\beta42_{base}$	baseline Aβ42	98	pM
$sAPP\alpha_{base}$	baseline sAPPα	423	pM
Kin_{40}[a]	formation rate Aβ40	1.29	h^{-1}
Kin_{382}	Aβ38 formation rate from Aβ42	0.145	h^{-1}
$Rout_a$	degradation rate sAPPα	1.08	h^{-1}
$Rout_b$	degradation rate sAPPβ	1.54	h^{-1}
$Kout_{99}$	degradation rate C99	0.386	h^{-1}
KtAP	transit rate sAPPα and sAPPβ	0.129	h^{-1}
KtAB[a]	transit rate Aβ	10	h^{-1}
ImaxB[a]	maximal inhibition (Imax) MBi-5	1	
$IC_{50}B$	median inhibition concentration MBi-5	0.0255	μM
GAMB[a]	Hill coefficient MBi-5	1	
ImaxG[a]	maximal inhibition (Imax) MK-0752	1	
$IC_{50}G$	median inhibition concentration MK-0752	0.0488	μM
GAMG[a]	Hill coefficient MK-0752	1	
Kpl	oligomerization rate	6.45e-4	$pM^{-1}\,h^{-1}$
$A\beta_{O\,base}$	baseline Aβ_O	1.75	pg/mL
ALPH[a]	order oligomerization	2	
FP	feedback parameter	0.438	
$Factor_{oligo}$	conversion factor on oligomers	0.00667	
Interanimal variability			
ω^2_{BSAPb}[b]	Interanimal variability sAPPβ baseline	0.194	
ω^2_{BSAPa}[b]	Interanimal variability sAPPα baseline	0.105	
$\omega^2_{AB4.}$[b]	Interanimal variability Aβ40 and Aβ42	0.0681	
ω^2_{AB38}[b]	Interanimal variability Aβ38	0.119	
ω^2_{ABO}[b]	Interanimal variability Aβ_O	0.116	
Residual error			
$\sigma^2_{A\beta40}$[c]	Residual variability Aβ40	0.117	
$\sigma^2_{A\beta42}$[c]	Residual variability Aβ42	0.0705	
$\sigma^2_{sAPP\beta}$[c]	Residual variability sAPPβ	0.109	
$\sigma^2_{sAPP\alpha}$[c]	Residual variability sAPPα	0.0783	
σ^2_{oligo}[c]	Residual variability Aβ_O	0.785	
$\sigma^2_{A\beta38}$[c]	Residual variability Aβ38	0.0934	

[a] Fixed.

[b] Interanimal variability is assumed to follow a normal distribution with mean zero and variance ω^2.

[c] Residual variability is assumed to follow a normal distribution with mean zero and variance σ^2.
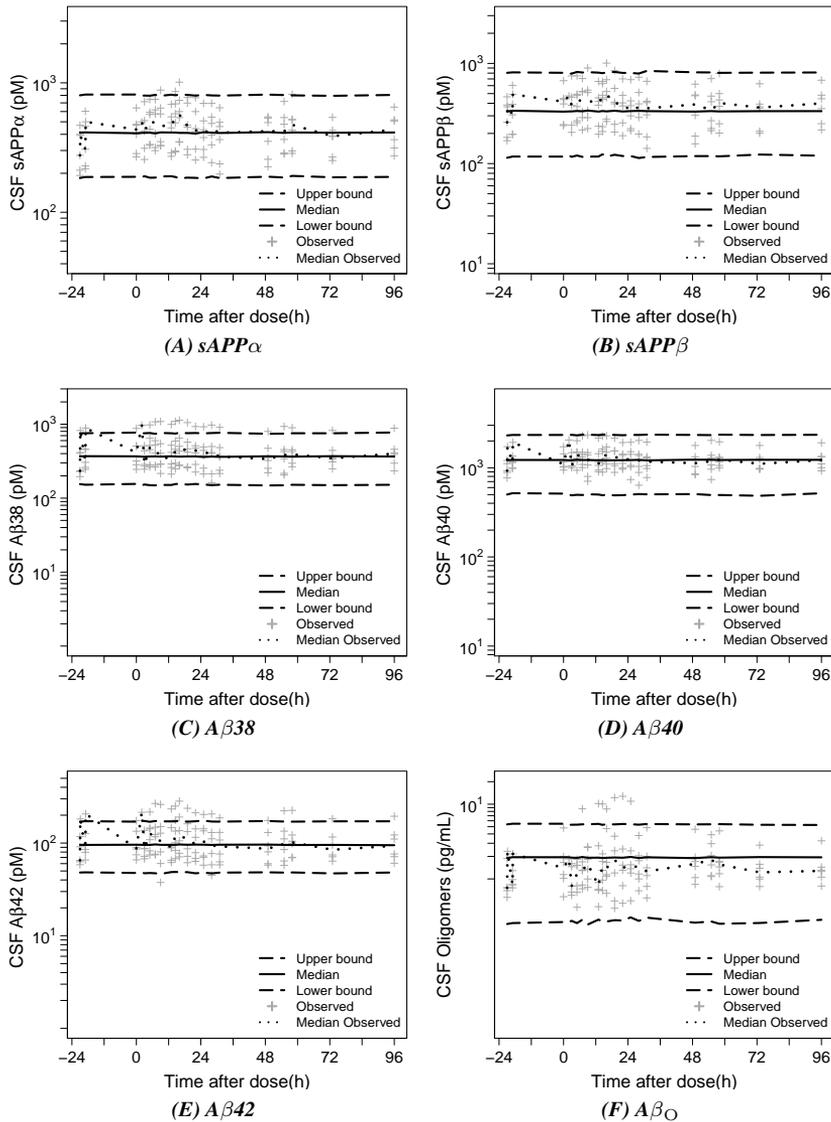
Figure 7.2: Placebo. Visual predictive check of biomarker response vs. time profile of placebo in the rhesus with 90% confidence interval. Predictions were performed with extended model ((A), (B), (C), (D), (E), (F)). Observation sample size: n=108 for each APP metabolite from 6 monkeys collected over 4 days.

Plus-symbols represent observed measurements. Dotted blue line corresponds to the median observed profile. Solid lines show the median simulated profiles. The long-dashed lines correspond to the 90% prediction intervals obtained from 1000 individual simulated profiles.

(A) sAPPα

(B) sAPPβ

(C) Aβ38

(D) Aβ40

(E) Aβ42

(F) AβO
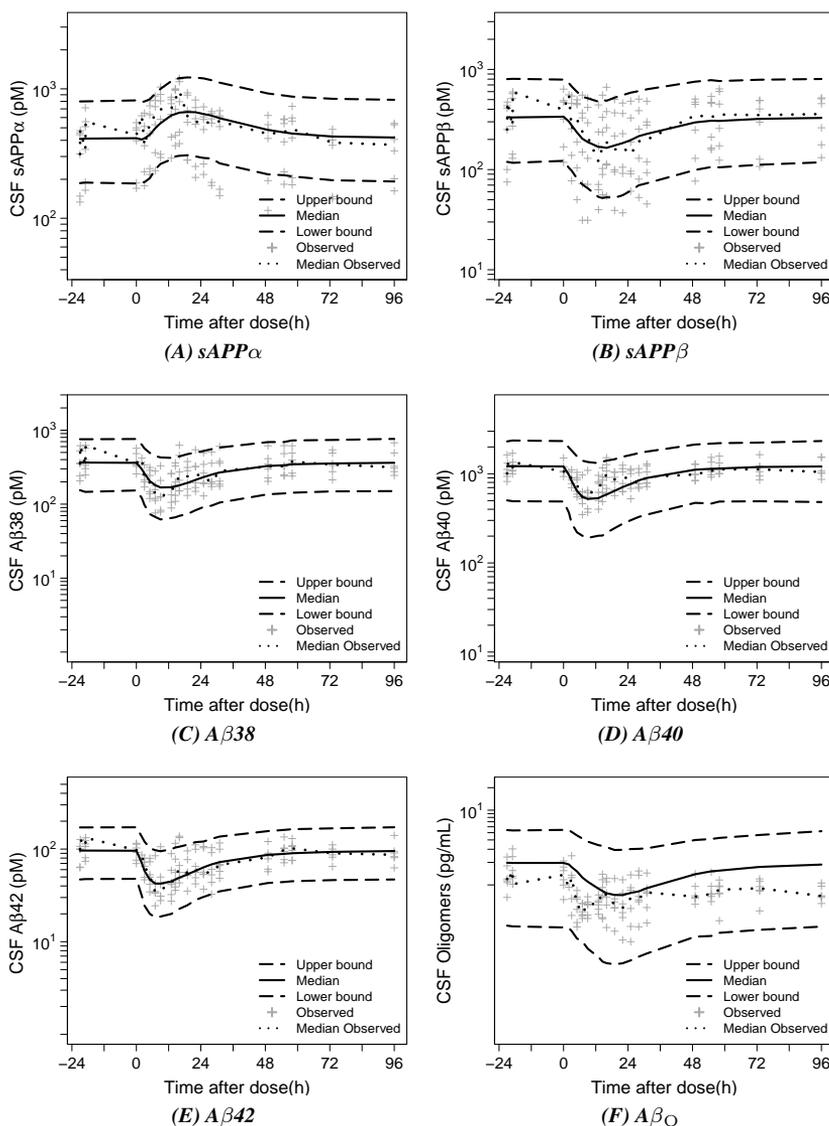
Figure 7.3: Dose 30 mg/kg MBi-5. Visual predictive check of biomarker response vs. time profile of MBi-5 in the rhesus with 90% confidence interval. Predictions were performed with model with extended model ((A), (B),(C), (D), (E),(F)). Observation sample size: n=108 for each APP metabolite from 6 monkeys collected over 4 days.

Plus-symbols represent observed measurements. Dotted blue line corresponds to the median observed profile. Solid lines show the median simulated profiles. The long-dashed lines correspond to the 90% prediction intervals obtained from 1000 individual simulated profiles.
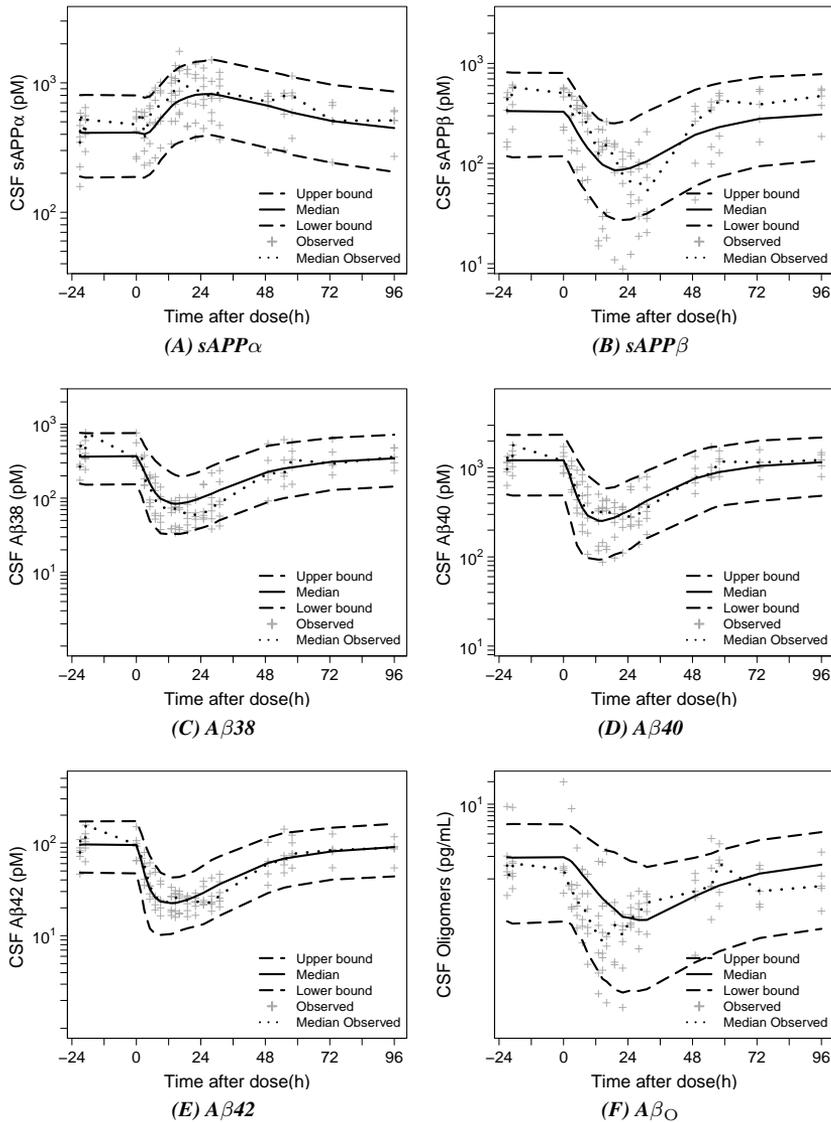
Figure 7.4: Dose 125 mg/kg MBi-5. Visual predictive check of biomarker response* vs. *time profile of MBi-5 in the rhesus with 90% confidence interval. Predictions were performed with extended model ((A), (B),(C), (D), (E),(F)). Observation sample size: n=108 for each APP metabolite from 6 monkeys collected over 4 days.

Plus-symbols represent observed measurements. Dotted blue line corresponds to the median observed profile. Solid lines show the median simulated profiles. The long-dashed lines correspond to the 90% prediction intervals obtained from 1000 individual simulated profiles.

218

(A) sAPPα

(B) sAPPβ

(C) Aβ38

(D) Aβ40

(E) Aβ42

(F) AβO
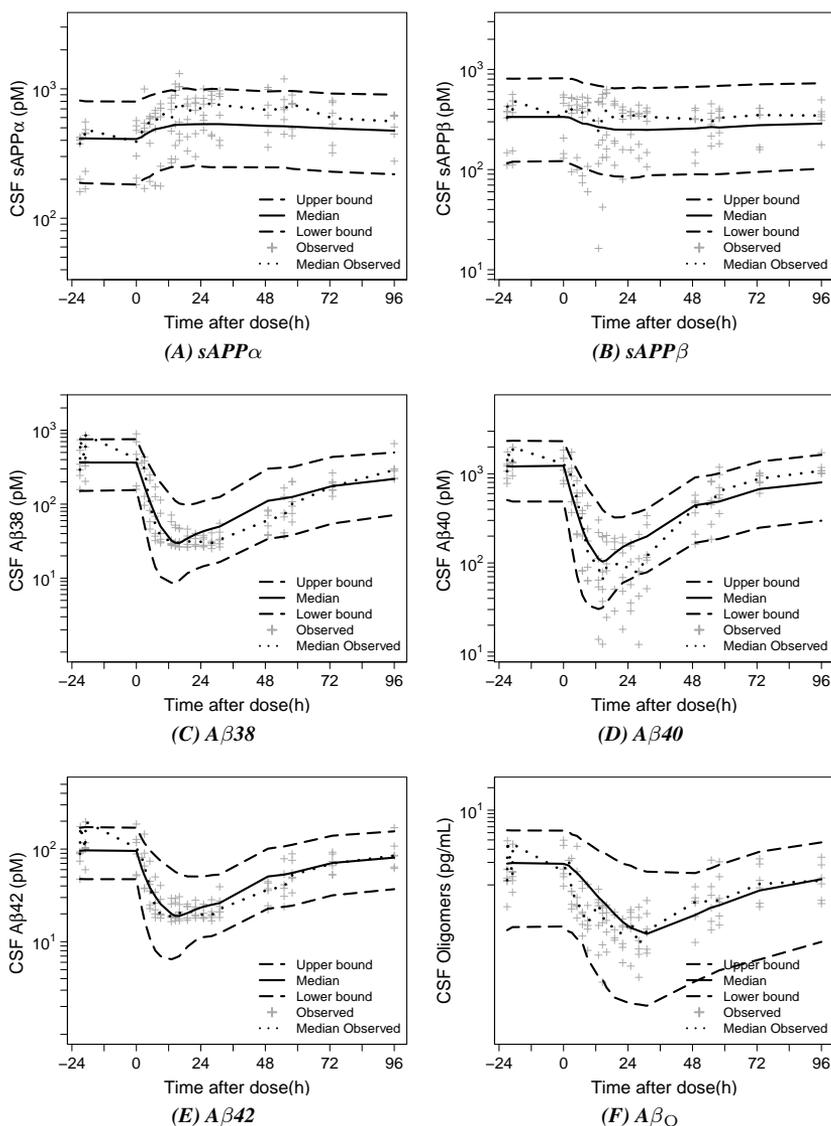
Figure 7.5: Dose 240 mg/kg MK-0752. Visual predictive check of biomarker response* vs. *time profile of MK-0752 in the rhesus with 90% confidence interval. Predictions were performed with extended model ((A), (B),(C), (D), (E),(F)). Observation sample size: n=108 for each APP metabolite from 6 monkeys collected over 4 days.

Plus-symbols represent observed measurements. Dotted blue line corresponds to the median observed profile. Solid lines show the median simulated profiles. The long-dashed lines correspond to the 90% prediction intervals obtained from 1000 individual simulated profiles.

β-γ-O-APP model described all biomarker responses

The β-γ-O-APP model simultaneously described APP metabolite and Aβ_O responses to both BACE1 and GS inhibition. In general, the data were adequately captured across biomarkers for both MBi-5 (Figs. 7.2, 7.3, 7.4) and MK-0752 (Fig. 7.5) treatment. The description of the Aβ responses after MBi-5 treatment was marginally improved compared to the description obtained with the β-O-APP model[11]. The raise in sAPPα after GS inhibition was slightly underpredicted (Fig. 7.5A).

β-γ-O-APP model predicts APP metabolites interrelations

The β-γ-O-APP model could be used to predict APP metabolites interrelations and responses to BACE1 and GS inhibition and foresee the response of APP and C99 in brain (Fig. 7.6).

APP increases after inhibition of BACE1 (Fig. 7.6A), as result of the blocked BACE1 pathway. APP is then shunted down the α-secretase pathway, resulting in an upsurge of sAPPα product. The sAPPβ level reduces after BACE1 inhibition, as it is a direct product of BACE1 cleavage of APP. The increase in sAPPα and decrease in sAPPβ results in a decline in the ratio of sAPPβ:sAPPα and net rise in the sum of sAPPα and sAPPβ (Fig. 7.6E). The C99 level is predicted to decline after BACE1 inhibition. The loss of C99 after BACE1 inhibition results in reduced Aβ levels.

After GS inhibition APP slightly reduces due to the increased α-secretase processing of APP (Fig. 7.6B). As a result of substrate competition sAPPβ also slightly declines. The accumulation of C99 through GS inhibition stimulates the α-secretase pathway, resulting in an upswing of sAPPα levels and changing the ratio of sAPPβ:sAPPα and net sum of sAPPα and sAPPβ (Fig. 7.6F).

Both BACE1 and GS inhibition lower the monomeric Aβ concentrations (Fig. 7.6C, 7.6D), though the respective inhibition results in different Aβ ratios (Fig. 7.6E, 7.6F). Both BACE1 and GS inhibition reduce the Aβ_O level, although the effect is more prolonged after GS inhibition.

The diurnal oscillations observed in the simulated biomarker responses after GS inhibition are induced by the enterohepatic recirculation which MK-0752 exhibits[12][17].

(A) 125 mg/kg MBi-5

(B) 240 mg/kg MK-0752

(C) 125 mg/kg MBi-5

(D) 240 mg/kg MK-0752

(E) 125 mg/kg MBi-5
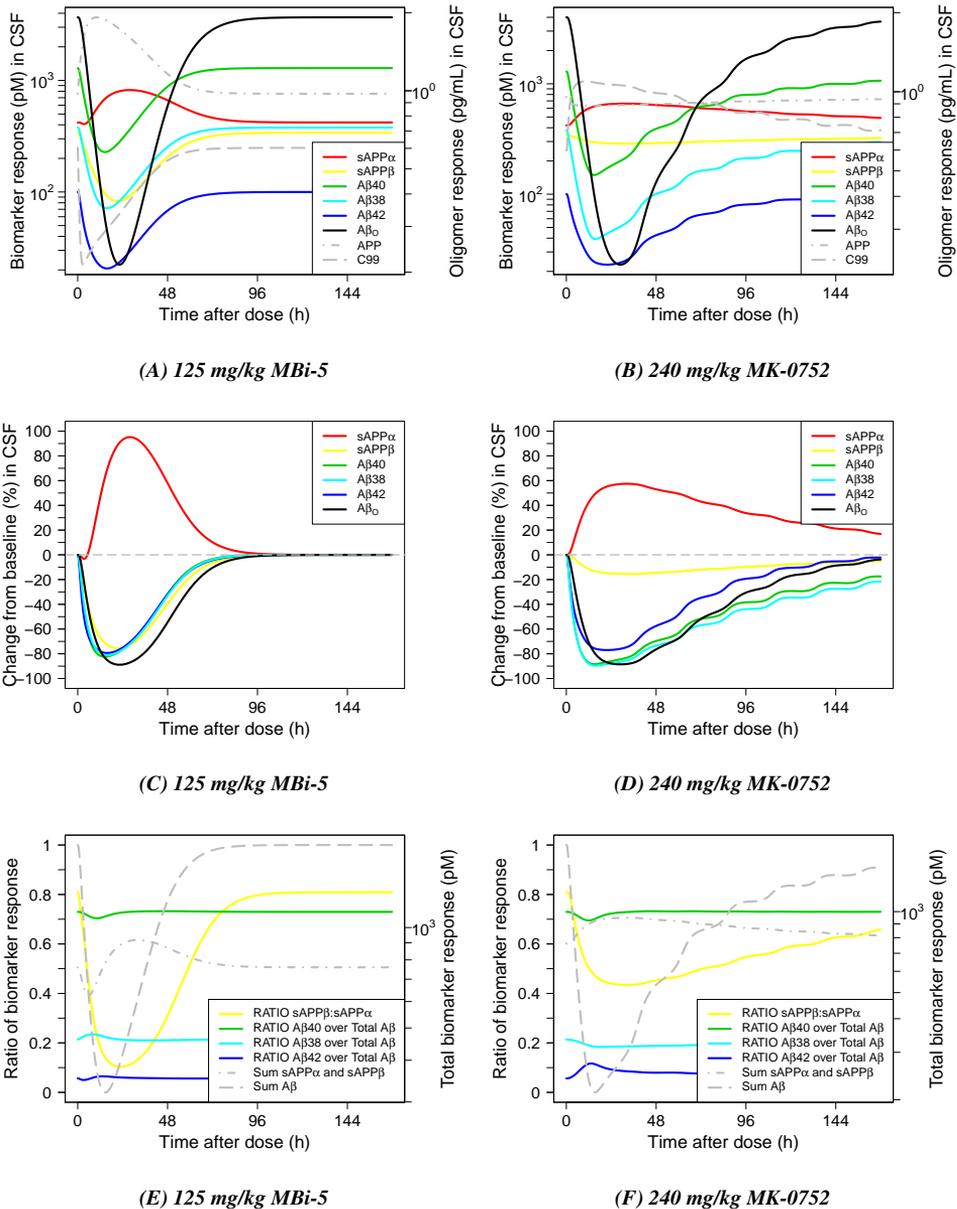
(F) 240 mg/kg MK-0752

Figure 7.6: Simulation absolute biomarker responses ((A), (B)), biomarker change from baseline (%) ((C), (D)) and biomarker ratios ((E), (F)) using the β-γ-O-APP model. The biomarker responses were simulated after a single dose of 125 mg/kg MBi-5 *(left)* and 240 mg/kg MK-0752 *(right)*, using the typical parameter estimates.

sAPPα red solid line; *sAPPβ* yellow solid line; *Aβ40* green solid line; *Aβ38* light blue solid line; *Aβ42* dark blue solid line; *Aβ*$_O$ black solid line; *C99* grey dot-dashed line; *APP* grey dashed line.

Discussion

One of the main therapeutic strategies is to delay AD onset and progression is reducing $A\beta$ aggregation through the decrease of $A\beta$ monomeric levels by means of $A\beta$ production inhibition. Therefore, the dynamics of $A\beta_O$ after $A\beta$ production inhibition needs to be elucidated. The β-γ-O-APP model described APP metabolites (sAPPβ, sAPPα, $A\beta38$, $A\beta40$, $A\beta42$) and $A\beta_O$ responses and their interrelations after GS and BACE1 inhibition successfully.

The reduction of $A\beta_O$ concentration after inhibition of BACE1 with 125 mg/kg MBi-5 was equivalent to the $A\beta_O$ decline obtained after 240 mg/kg MK-0752. The pharmacological effect of GS inhibition was prolonged by the enterohepatic recirculation of MK-0752. The enterohepatic recirculation of MK-0752 was previously discussed by Shou et al. [17].

The simultaneous analysis of BACE1 and GS inhibitor $A\beta$ response data revealed a shift in the relative formation of $A\beta38$, $A\beta40$ and $A\beta42$ after GS blockage. This was explained by stepwise successive cleavage of C99 by GS, in which part of $A\beta38$ is converted from $A\beta42$. This pathway is blocked after GS, but not after BACE1 inhibition. Matsumura et al. [20] reported that most of $A\beta38$ is converted from $A\beta42$ and $A\beta43$. Our results indicate that almost a third of $A\beta38$ originates from $A\beta42$ cleavage.

sAPPβ and sAPPα are upstream in the APP pathway of the GS cleavage path. To our surprise, sAPPα increased in response to GS inhibition. This could be characterized by a homeostatic feedback loop regulated by C99, where an increase in C99 via GS inhibition stimulates α-secretase processing of APP. This suggests that an increase of membrane bound C99 may affect cellular control of APP α-secretase cleavage or alter APP trafficking to the cell surface, directly or through α-secretase, therefore increasing α-secretase cleavage at the plasma membrane. Enhanced processing of APP by α-secretase after GS inhibition has also been observed in *in vitro* experiments performed in model cell lines reported by Siegenthaler et al. [21]. They suggested that GS activity could influence α-secretase levels or activity. However, the regulation of the activity of α-secretase is not fully understood [6,22].

The observed increase in sAPPα generation was accompanied by a modest reduction of sAPPβ after GS inhibition. This is due to less full-length APP remaining as substrate for BACE1 when α-secretase cleavage is raised. The idea of substrate competition for APP between α-secretase and BACE1 is well accepted [6]. However, here the decrease in sAPPβ is not as strong as would be expected purely based on substrate competition

following the upsurge of α-secretase activity. That is why the model underpredicted the raise in sAPPα. There appears to be an increase in the sum of sAPPβ and sAPPα after GS inhibition (see Supplemental Material, Figure S7.2A). This suggests an increase in production of APP. There may be an autoregulation mechanism of APP production, induced by GS inhibition, compensating for the loss of sAPPβ as result of α-secretase stimulation. This was investigated during model development, and there were indications that including autoregulation of APP would improve the description of the data. However, with the current data, the process of autoregulation could not be characterized adequately. Further investigation is warranted.

Because α-secretase cleaves APP within the Aβ sequence, pharmacological activation of α-secretase, and thereby reducing Aβ production may be a therapeutic intervention in AD. Further, sAPPα plays a role in neuroprotection and is downregulated in familial and sporadic AD patients[22].

Tian et al.[23] proposed a feedback mechanism initiated by the α-secretase cleavage path, in which Aβ production is lowered by increased C83 which negatively modulate GS activity. sAPPα and C83 are products of the same cleavage step by α-secretase. The model predicted increased C83 concentrations as result of BACE1 and GS inhibition. Therefore, this inhibitory effect on GS through C83 is expected to occur after both BACE1 and GS inhibition. The feedback mechanism as proposed by Tian was investigated in the β-γ-O-APP model, but could not be distinguished from the interaction of the inhibitors on the system as both work to lower Aβ levels.

In a series of investigations we have explored the development of a systems pharmacology model for the APP processing pathway. In the first of these investigations, a systems pharmacology model was developed of the APP processing pathway based on CSF concentrations of APP metabolites (Aβ40, Aβ42, sAPPβ, sAPPα) after exposure to the BACE1 inhibitor MBi-5 in CMP rhesus monkeys[16]. With this so called β-APP model, Aβ_O were predicted to reduce after BACE1 inhibition, which was informed from monomeric Aβ species.

In the second investigation, the systems model was validated using tracer kinetic data (fraction labeled sAPPα, fraction labeled sAPPβ and fraction labeled total Aβ). This β-13C-APP model accounted for the tracer $^{13}_6$C-Leucine dynamics throughout the systems model[24]. In the third investigation, separate descriptions to characterize the sequential cleavage steps of APP by BACE1 and GS were included in the systems model. This was based on the simultaneous investigation of APP metabolite response data from dedicated studies for the BACE1 inhibitor MBi-5 (Aβ40, Aβ42, sAPPβ, sAPPα) and

the GS inhibitor MK-0752 (Aβ40, Aβ42), respectively [12]. The investigation with this β-γ-APP model implied a difference in Aβ dynamics after BACE1 versus GS inhibition, which was reflected in a different Aβ40 formation rate constant. Further, the model based prediction of Aβ_O suggested a lower oligomerization rate of Aβ42 after GS then after BACE1 inhibition. However, in that investigation, the difference in Aβ dynamics between BACE1 *versus* GS inhibition could not be separated from study differences.

In the fourth investigation the β-APP model was extended to describe the effect of an additional Aβ isoform (Aβ38) and capture Aβ_O response measurements. This β-O-APP model, was based on simultaneous analysis of CSF APP metabolites (Aβ38, Aβ40, Aβ42, sAPPβ, sAPPα) and Aβ_O concentration measurements after MBi-5 exposure [11]. In this investigation, Aβ oligomerization was characterized to be a second order process. Further, Aβ42 was identified to be the Aβ species that drives the Aβ oligomerization

In the current, and hence fifth investigation, the β-O-APP model was extended to describe the effect of BACE1 and GS inhibition on the APP pathway simultaneously and capture Aβ_O response data to both inhibitors. With the current analysis, the β-γ-APP model could advance further, as information on the sAPPβ, sAPPα, Aβ38, and Aβ_O response data to GS inhibition could be added. Further, seeing the cross-over study design of the current study using both inhibitors, true differences could be separated from study differences. In the current analysis, no differences in systems parameters after BACE1 versus GS inhibition could be identified, which indicated a correct simultaneous characterization of the inhibitor-system interactions. Also, the Hill coefficients shifted to unity, which is the theoretical value for a simple receptor-target interaction, indicating that the β-γ-O-APP model provided a more accurate representation of the inhibitors interaction with the system.

Conclusions & Perspectives

The current and prior series of investigations illustrate that systems pharmacology modelling is work in progress and that various processes in the biological network have to be considered. With each turning, the APP systems model is progressed and biological insights are gained or questions raised that can get the model to an improved or more advanced state.

Here, the β-γ-O-APP model revealed a feedback mechanism by downstream components on a upstream path: blockage of the GS cleavage path promotes the non-amyloidogenic processing of APP by homeostatic feedback, proposed to be exerted

by C99. In addition, the stepwise successive cleavage of C99 by GS, wherein part of Aβ38 is converted from Aβ42 was characterized by the model. Furthermore, the effects of Aβ production inhibition on Aβ_O concentrations were quantified.

A next step in the advancement of the APP systems model could be the extension of the model to include higher order agglomerated species, such as fibrils. It would be of interest to know if Aβ production inhibition can bring down the fibril concentrations as well, which may dissociate to Aβ_O to restore the balance between these species.

To further evaluate the proposed feedback mechanism, sAPP (sAPPβ and sAPPα) data following a dose range of the GS inhibitor may be informative. Also, sAPP response measurements after an α-secretase stimulator could provide information on a possible autoregulation mechanism of APP production.

The developed β-γ-O-APP model can be used to perform simulations to investigate other interventions, such as inhibition of Aβ oligomerization or Aβ clearance enhancers.

References

1. Jack, C.R. & Holtzman, D.M. Biomarker modeling of Alzheimer's disease. Neuron. 2013;80(6):1347–1358.

2. Klein, W.L. Synaptotoxic amyloid-β oligomers: a molecular basis for the cause, diagnosis, and treatment of Alzheimer's disease? J Alzheimer's Dis. 2013;33:S49–S65.

3. Sengupta, U., Nilson, A.N., & Kayed, R. The Role of Amyloid-β Oligomers in Toxicity, Propagation, and Immunotherapy. EBioMedicine. 2016;6:42–49.

4. Esler, W.P. & Wolfe, M.S. A portrait of Alzheimer secretases - New features and familiar faces. Science. 2001;293(5534): 1449–54.

5. Wiltfang, J., *et al.* Higly conserved and disease-specific patterns of carboxyterminally truncated Aβ peptides 1-37/38/39 in addition to 1-40/42 in Alzheimer's disease and in patients with chronic neuroinflammation. J Neurochem. 2002;81(3):481–496.

6. Lichtenthaler, S.F. Alpha-secretase in Alzheimer's disease: Molecular identity, regulation and therapeutic potential. J Neurochem. 2011;116(1):10–21.

7. Grüning, C.S.R., *et al.* The off-rate of monomers dissociating from amyloid-β protofibrils. J Biol Chem. 2013;288(52): 37104–11.

8. Schmit, J.D., Ghosh, K., & Dill, K. What Drives Amyloid Molecules To Assemble into Oligomers and Fibrils? Biophys J. 2011;100(2):450–458.

9. Cerasoli, E., Ryadnov, M.G., & Austen, B.M. The elusive nature and diagnostics of misfolded Aβ oligomers. Front Chem. 2015;3:17.

10. Takahashi, R.H., Nagao, T., & Gouras, G.K. Plaque formation and the intraneuronal accumulation of β-amyloid in Alzheimer's disease. Pathol Int. 2017;67(4):185–193.

11. van Maanen, E.M., *et al.* Systems pharmacology analysis of the Aβ oligomer response following β-secretase inhibition: Evidence for second-order kinetics of Aβ42 oligomerization. Prep. 2017.

12. van Maanen, E.M., *et al.* Extending a systems model of the APP pathway: Separation of β- and γ-secretase sequential cleavage steps of APP. Submitted. 2017.

13. Gilberto, D.B., *et al.* An alternative method of chronic cerebrospinal fluid collection via the cisterna magna in conscious rhesus monkeys. Contemp Top Lab Anim Sci. 2003;42 (4):53–59.

14. Savage, M.J., *et al.* A sensitive Aβ oligomer assay discriminates Alzheimer's and aged control cerebrospinal fluid. J Neurosci. 2014;34(8):2884–97.

15. Bauer, R.J. 2011 NONMEM users guide. Introduction to NONMEM 7.2.0 Technical report;ICON Development Solutions, Ellicott City, MD.

16. van Maanen, E.M.T., *et al.* Systems pharmacology analysis of the amyloid cascade after β-secretase inhibition enables the identifica-

tion of an Aβ42 oligomer pool. J Pharmacol Exp Ther. 2016;357(1):205–16.

17. Shou, M., *et al.* Population pharmacokinetic modeling for enterohepatic recirculation in Rhesus monkey. Eur J Pharm Sci. 2005;26 (2):151–61.

18. Dobrowolska, J.A., *et al.* Diurnal patterns of soluble amyloid precursor protein metabolites in the human central nervous system. PLoS One. 2014;9(3):e89998.

19. Cook, J.J., *et al.* Acute γ-secretase inhibition of nonhuman primate CNS shifts amyloid precursor protein (APP) metabolism from amyloid-β production to alternative APP fragments without amyloid-β rebound. J Neurosci. 2010;30(19):6743–50.

20. Matsumura, N., *et al.* γ-Secretase associated with lipid rafts: multiple interactive pathways in the stepwise processing of β-

carboxyl-terminal fragment. J Biol Chem. 2014;289(8):5109–21.

21. Siegenthaler, B., Bali, J., & Rajendran, L. γ-Secretase regulates the α-secretase cleavage of the Alzheimer's disease, amyloid precursor protein. Matters. 2016;pages 1–7.

22. Vingtdeux, V. & Marambaud, P. Identification and biology of α-secretase. J Neurochem. 2012;120 (Suppl. 1):34–45.

23. Tian, Y., Crump, C.J., & Li, Y.M. Dual Role of α-Secretase Cleavage in the Regulation of γ-Secretase Activity for Amyloid Production. J Biol Chem. 2010;285(42): 32549–32556.

24. Van Maanen, E.M., *et al.* Integrating tracer kinetic data into a systems pharmacology model of the amyloid precursor pathway - effect of a β-secretase inhibitor. Prep. 2017.

Chapter 7

Supplemental Material

E.M.T. van Maanen, T.J. van Steeg, J. Kalinina, M.S. Michener, M.J. Savage, M.E. Kennedy, J.A. Stone, M. Danhof

SUPPLEMENTAL MATERIAL

Differences in Aβ ratios after BACE1 *versus* GS inhibition
The sum of Aβ38, Aβ40 and Aβ40 in the treatment arms of the cross-over study is presented in Fig. S7.1A. Both BACE1 and GS inhibition resulted in a reduction of total Aβ. The ratios of Aβ38, Aβ40 and Aβ40 over total Aβ is depicted in Fig. S7.1B. GS inhibition resulted in a bigger change in the ratios of each Aβ species over total, compared to BACE1 inhibition, with the investigated dosages. The difference is most pronounced for the ratio Aβ42 over total Aβ.

Differences in the sum and ratio of sAPPβ and sAPPα after BACE1 *versus* GS inhibition
The sum of sAPPβ and sAPPα and the ratio of sAPPβ over sAPPα in the treatment arms of the cross-over study is depicted in Fig. S7.2A and S7.2B, respectively. Both BACE1 and GS inhibition reduce the ratio of sAPPβ over sAPPα.
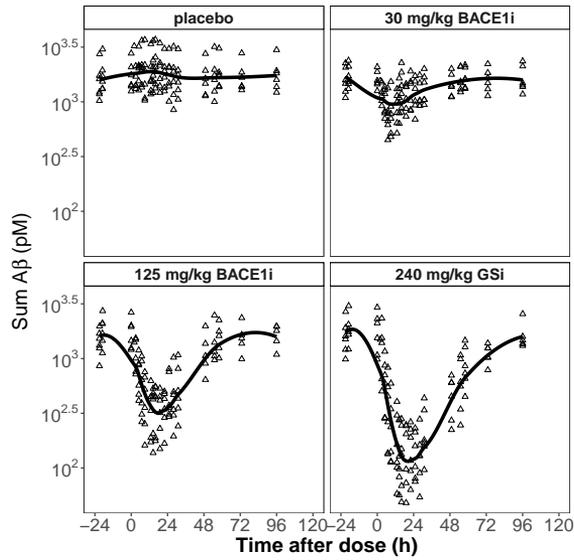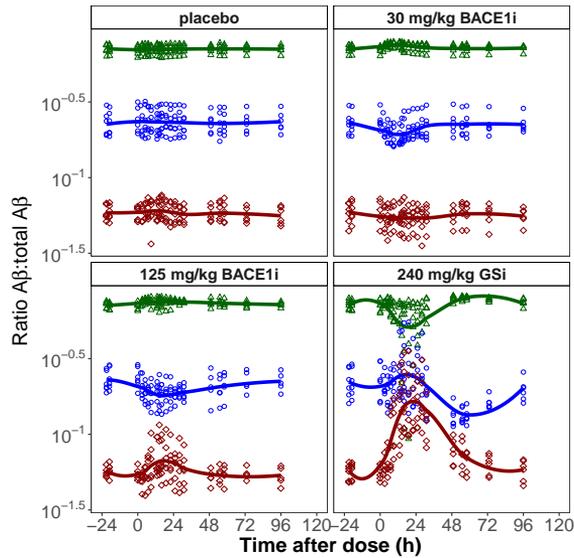
(A) Sum of Aβ

(B) Ratio of Aβ

Figure S7.1: Observed differences in the treatment arms of the sum of Aβ38, Aβ40 and Aβ42 (A) and the ratio of each Aβ species over total Aβ (B). The lines are smoothers through the observed data.

Black: sum of Aβ; *Green*: ratio Aβ40 over total Aβ; *Blue:* ratio Aβ38 over total Aβ; *Red:* ratio Aβ42 over total Aβ.
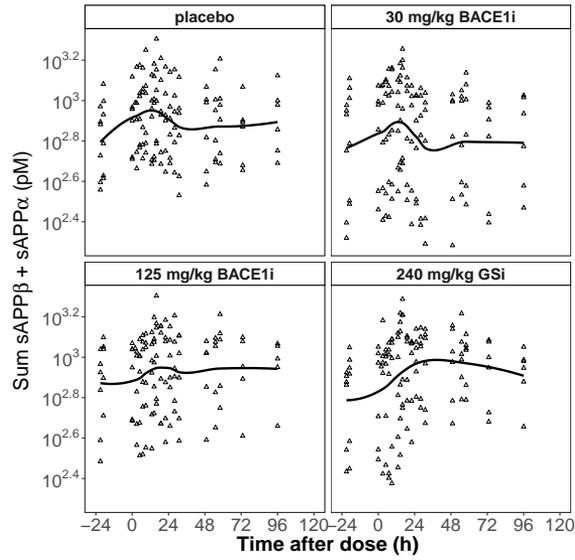
(A) Sum of sAPPβ and sAPPα
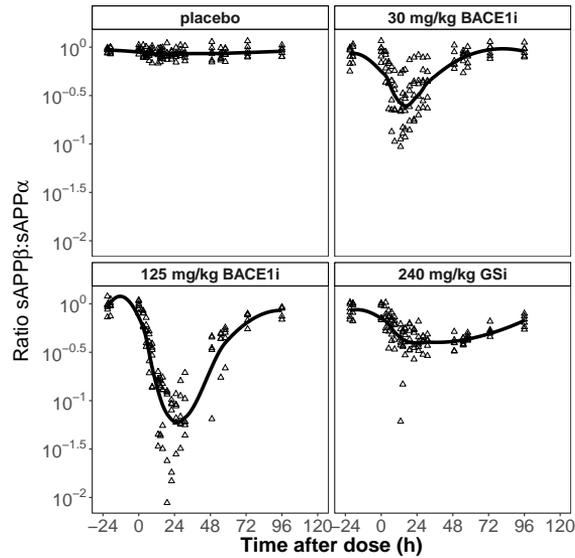
(B) Ratio sAPPβ:sAPPα

Figure S7.2: Observed differences in the treatment arms of the sum of sAPPα and sAPPβ (A) and the ratio of sAPPβ over sAPPα (B). The lines are smoothers through the observed data.
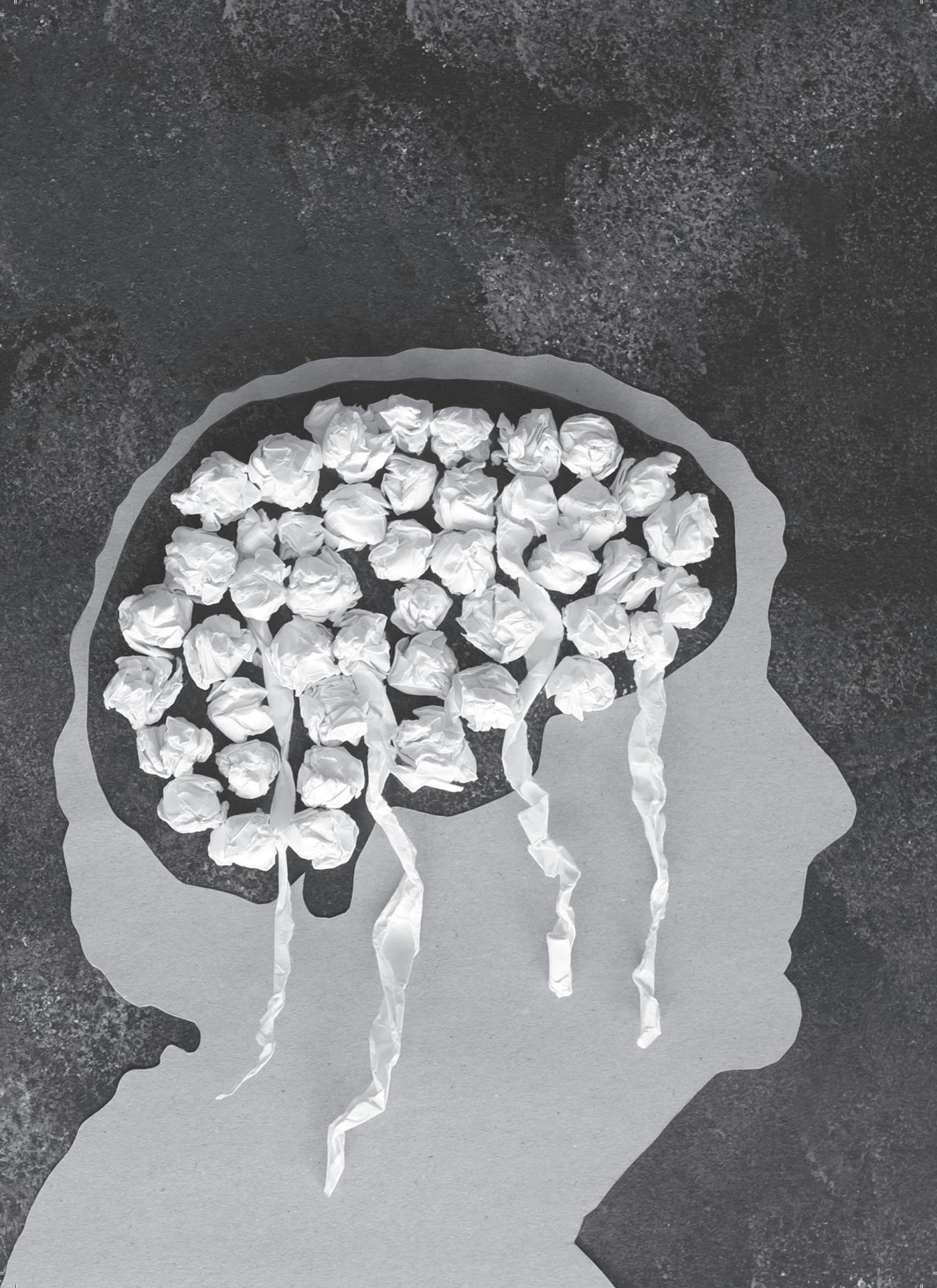
Section IV

Systems pharmacology of the amyloid cascade

Summary, conclusions & perspectives
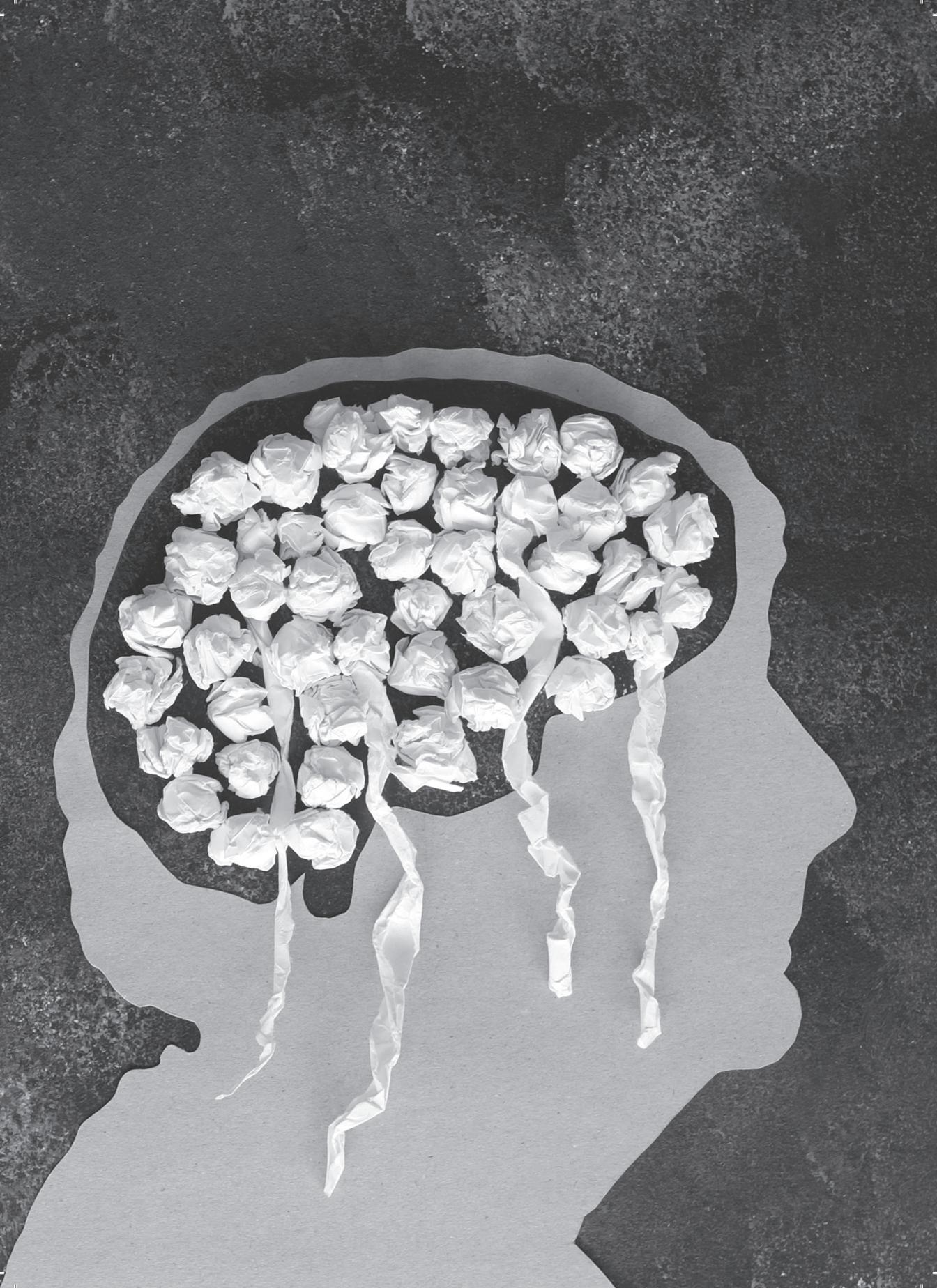
Chapter 8

Systems pharmacology of the amyloid precursor
protein pathway in Alzheimer's disease

Conclusions & perspectives

Introduction and objectives

The leading cause of cellular dysfunction in neurodegenerative diseases is the accumulation of protein aggregates inside or outside of neurons. These aggregates are phenotypically different but biochemically similar across neurodegenerative diseases suggesting a conserved molecular mechanism of pathogenesis. This is consistent with the observation that neurodegenerative disorders as Alzheimer's disease (AD), Parkinson's disease (PD), Huntington's disease (HD) and motor disorders such as amyotrophic lateral sclerosis (ALS) present the same pattern of progression of neuronal death, nervous system deterioration and cognitive impairment. Presumably these pathological changes are driven by an error in protein conformation followed by abnormal aggregation to form pathogenic assemblies ranging from small oligomers to large amyloid masses. The amyloid cascade hypothesis of AD provides a framework for protein misfolding neurodegenerative diseases.

AD is presently incurable, as the loss of neurons is irreversible and none of the currently available treatments attenuates the progression of the pathological cascade. According to the amyloid hypothesis, proteolytic processing of amyloid precursor protein (APP) to form the amyloid-beta ($A\beta$) peptides plays a central role in the pathophysiology of AD. $A\beta$ levels are increased early in the disease process, forming toxic soluble $A\beta$ oligomers ($A\beta_O$) and plaques. $A\beta_O$ are considered to be a primary driver of the neurodegeneration in AD brain. In the APP processing and clearance pathways, APP is cleaved sequentially by β-secretase (BACE1) and γ-secretase (GS) to produce $A\beta$.

The drug effects on the individual attributes of the APP pathway are difficult to predict, because of the complexity of the underlying biochemical network that governs the formation and elimination of the individual components. As a consequence also, the effect on $A\beta_O$s and on the $A\beta$ equilibrium after inhibiting $A\beta$ production or enhancing $A\beta$ clearance is largely unknown. A systems pharmacology modelling approach, describing the interactions in the underlying biochemical network, will provide a mechanistic understanding of the behaviour of the APP pathway, enabling the prediction of therapeutic effects on $A\beta$ and indirectly also on $A\beta_O$ concentrations (**Chapter 2**).

The objectives of the investigations described in this thesis were: (1) To establish a systems pharmacology model to describe in a strictly quantitative manner the biochemical network of APP processing; (2) to predict and evaluate the effect of $A\beta$ production inhibitors, acting at different sequences in the APP processing pathway, on $A\beta_O$ concentrations; (3) to explore other therapeutic strategies which may aid the reduction of

$A\beta_O$ burden.

Development of a systems pharmacology model to predict the oligomer response following secretase inhibition

The effects of $A\beta$ production inhibitors were characterized in conscious cisterna-magna-ported (CMP) rhesus monkeys. In these CMP rhesus monkeys a permanent catheter was implanted into the cisterna-magna enabling repeated sampling of cerebrospinal fluid (CSF) collection in conscious monkeys (Figure 8.1)[1]. With this animal model, detailed studies on the pharmacokinetics (PK) and pharmacodynamics (PD) of potential APP modifying drugs in the central nervous system can be performed, which is difficult to achieve in humans.

Table 8.1: Summary overview model structures

Model	Inhibitors	Included biomarkers	Chapter
β-APP model	BACE1i (MBi-5)	sAPPβ, sAPPα, Aβ40, Aβ42	3
β-13C-APP model	BACE1i (MBi-5)	sAPPβ, sAPPα, Aβ40, Aβ42, **fraction labeled Aβ, fraction labeled sAPPα, fraction labeled sAPPβ**	4
β-γ-APP model	BACE1i (MBi-5)	sAPPβ, sAPPα, Aβ40, Aβ42	5
	GSi (MK-0752)	**Aβ40, Aβ42**	
β-O-APP model	BACE1i (MBi-5)	sAPPβ, sAPPα, Aβ40, Aβ42, **Aβ38, Aβ_O**	6
β-γ-O-APP model	BACE1i (MBi-5)	sAPPβ, sAPPα, Aβ40, Aβ42, Aβ38, Aβ_O	7
	GSi (MK-0752)	**sAPPβ, sAPP**α, Aβ40, Aβ42, **Aβ38, Aβ_O**	

In a series of investigations, we have developed a systems pharmacology model for the APP processing pathway. The various steps in the development of this model are summarized in Table 8.1 and presented in Figure 8.2-Figure 8.6. First, we established a systems pharmacology model of the APP processing pathway to characterize the influence of BACE1 inhibition on the concentrations of the APP metabolites sAPPβ, sAPPα, Aβ40, Aβ42 (Figure 8.2) (**Chapter 3**). In this so called β-APP model, the effect of the BACE1 inhibitor MBi-5 was described by inhibition of the formation of sAPPβ out of APP, where sAPPβ was used as surrogate of C99, to drive the Aβ formation. This analysis showed that upon BACE1 inhibition the concentration of the metabolite sAPPα increased
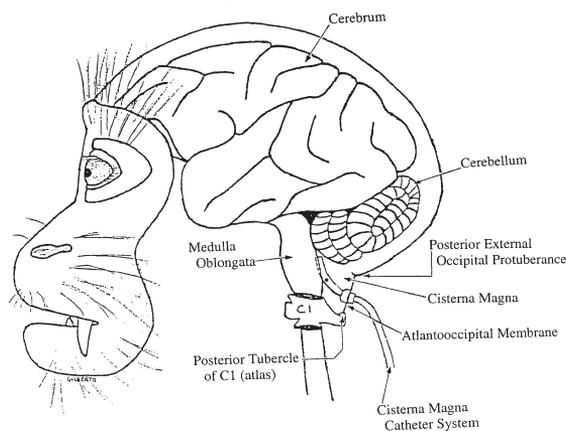
Figure 8.1: Schematic of lateral view of implant placement in rhesus monkey head.
The rhesus monkeys were surgically implemented with a catheter system which was placed 1.0 cm into the cisterna, facilitating direct access to CSF outflow from the cisterna magna. The catheter was attached to a titanium port placed subcutaneously between the shoulder blades to allow easy access for sampling CSF in a conscious, chaired rhesus monkey. Figure from Gilberto et al. [1].

and while the concentrations of the metabolites $A\beta40$, $A\beta42$ and $sAPP\beta$ decreased in a dose-proportional manner. Analysis of the changes in the monomeric $A\beta$ species with the β-APP model enabled prediction of a reduction of the putative neurotoxic $A\beta_O$ pool. Also, the findings indicated that decreases in monomeric $A\beta$ responses resulting from BACE1 inhibition were partially compensated for by dissociation of $A\beta_O$.

The next step in the model development was the interfacing of the β-APP model with tracer kinetic data obtained with the so-called stable-isotope-labeling kinetics (SILK) protocol (**Chapter 4**). The SILK protocol was originally used to quantify differences in the $A\beta$ kinetics between patients with AD and their cognitively normal controls. Here the SILK protocol was applied for the first time to examine the effect of BACE1 inhibition on the fraction labelled $A\beta$, fraction labelled $sAPP\alpha$ and fraction labelled $sAPP\beta$ after $^{13}C_6$-Leucine infusion, which was started at 1 hour after the administration of MBi-5. Interfacing of the tracer kinetic data with the β-APP model yielded the next version of the systems pharmacology model of the APP pathway, the β-13C-APP model (Figure 8.3).

The β-13C-APP model distinguished labelled and unlabelled species and also separated steps in the biotransformation and the distribution of APP peptides to CSF. This improved the understanding of the dose-proportionality of the effect on the fraction labelled $sAPP\beta$ and the lack of such a dose-proportional response in fraction labelled

sAPPα. A disconnect between Aβ response measurements that were obtained with the data from the enzyme-linked immunosorbent assay (ELISA) and SILK was found, that may be explained by on the one hand the formation of an unknown APP fragment with differing kinetics or, on the other hand an unknown process that influenced the result of the SILK assay. In the modelling this effect was accounted for by inclusion of the model component FactorX.

A limitation of the β-APP model was that the influence of γ-secretase cleavage step could not be separated from an effect on sAPPβ elimination. Therefore, in **Chapter 5** the β-APP model was extended to describe Aβ40 and Aβ42 response to GS inhibition. This led to the third version of the model, the β-γ-APP model, which contains separate descriptions to characterize the sequential cleavage steps of APP by BACE1 and GS while the elimination of sAPPβ is described by a separate parameter (Figure 8.4). The β-γ-APP model was identified on the basis of a simultaneous analysis of APP metabolite response data following the administration of the BACE1 inhibitor MBi-5 (1 study; effects on the metabolites Aβ40, Aβ42, sAPPβ and sAPPα) and the GS inhibitor MK-0752 (2 studies; effects on Aβ40 and Aβ42), respectively. This analysis revealed a difference in Aβ dynamics after BACE1 versus GS inhibition, which was reflected in a different value of the Aβ40 formation rate constant. Further, the model based prediction of Aβ_O suggested a lower oligomerization rate of Aβ42 after GS then after BACE1 inhibition. Unfortunately, in this investigation, the identified differences in Aβ dynamics after BACE1 or GS inhibition could not be separated from study differences, as levels of CSF biomarkers can vary between studies *(vide infra)*.

Application of the systems pharmacology model to characterize oligomer modulation following secretase inhibition

In the previous studies we have obtained indirect information on the formation of Aβ_O, through the analysis of the effects of secretase inhibitors on the monomeric species. This was necessary, because no direct measurements of the Aβ_O were available. In this respect it should be realized that it is extremely difficult to measure the low concentrations of the Aβ species[2,3]. In the meantime however an assay had become available for direct measurement of Aβ_O[4]. It was therefore of great interest to compare the model based prediction of Aβ_O response to BACE1 and GS inhibition with the observed Aβ_O response measurements. In the fourth study therefore the effects of MBi-5 and MK-0752 on the CSF concentrations of five APP metabolites (sAPPβ, sAPPα, Aβ40, Aβ42, Aβ38)

and Aβ_O were determined. The study was designed in a 4-way full crossover design. The APP systems model was extended to describe the effect of BACE1 inhibition on an additional Aβ isoform (Aβ38) and to capture Aβ_O response measurements (**Chapter 6**; β-O-APP model). The model was advanced further to describe GS inhibitor response data (sAPPβ, sAPPα, Aβ40, Aβ42, Aβ38, Aβ_O), which ultimately led to the β-γ-O-APP model (**Chapter 7**).

Before analysing the data on the basis of the β-O-APP model, a subset of the data (the effects on the peptides sAPPβ, sAPPα, Aβ40 and Aβ42) was analysed on the basis of the original β-APP model. This was necessary, because due to changes in the sample pre-treatment and the analytical methodology the absolute values of the concentrations in these studies differed from those in previous investigations, leading to different values of the model parameters. Using a within-study comparison, it was shown that the onset and maximum observed Aβ_O response was underpredicted by the β-APP model. As a next step therefore, the monomeric Aβ (Aβ38, Aβ40, Aβ42) and Aβ_O response measurements were incorporated in the fourth version of the model (Figure 8.5). This analysis showed that the Aβ oligomerization follows second order kinetics. Furthermore, the model also provided evidence that dissociation of Aβ_O, restoring the balance with Aβ monomers (homeostatic adaptation), contributes to the ultimate treatment effect. This analysis also showed that, of the various peptides, Aβ42 is the main monomeric Aβ species that drives the Aβ oligomerization, which is in line with the general belief that Aβ42 is the Aβ species prone to toxic aggregation.

In **Chapter 7**, the β-O-APP model was extended to simultaneously describe the effect of BACE1 and GS inhibition and to capture Aβ_O response data to inhibitors of both enzymes (Figure 8.6). In the β-γ-O-APP model the sequential cleavage steps by BACE1 and GS were described separately, in a manner that is similar to the β-γ-APP model. With this analysis, information on the sAPPβ, sAPPα, Aβ38, and Aβ_O response to GS inhibition was included. Quite unexpectedly, this revealed that upstream of the GS cleavage step in the APP pathway, changes in sAPPβ and sAPPα concentrations in response to GS inhibition were present. The systems analysis of the decrease of sAPPβ and the increase of sAPPα in response to GS inhibition revealed a homeostatic feedback loop regulated via C99: the increase in C99 following GS inhibition stimulated α-secretase processing of APP.

A difference in the ratio Aβ42:Aβ40:Aβ38 between BACE1 versus GS inhibition was found, which was explained by stepwise successive cleavage of C99 by GS, wherein part of Aβ38 is converted from Aβ42. Further, due to the cross-over study design using both
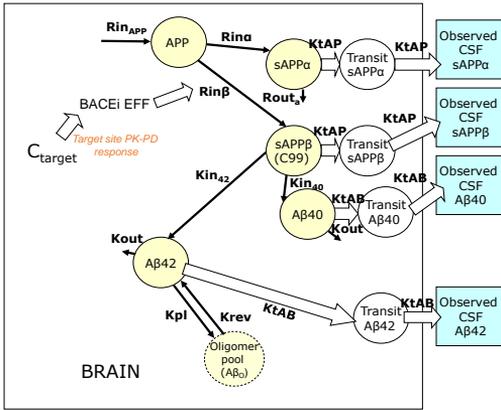
Figure 8.2: *β-APP model (Chpt. 3).*
The model comprised nine compartments: Five biomarker compartments in brain *(yellow circles)* and four transit compartments from brain to CSF *(white circles)*. Four biomarkers were measured in CSF (sAPPα, sAPPβ, Aβ40 and Aβ42), indicated by the blue boxes. The model included an $A\beta_O$ compartment *(dashed circle)*. The drug effect of the BACE1 inhibitor *(EFF)* inhibited *Rinβ*. sAPPβ was used in the model structure as a surrogate substrate of C99 in the γ-secretase cleavage step.
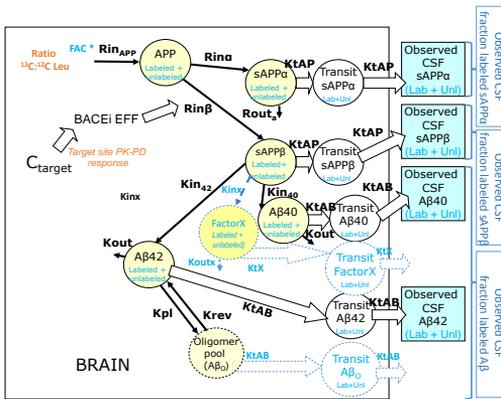
Figure 8.3: *β-13C-APP model (Chpt. 4).*
The model comprised two times thirteen compartments: Six biomarker compartments in brain *(yellow circles)*, one oligomer compartment and six transit compartments from brain to CSF *(white circles)*, wherein each compartment was duplicated to track labeled and unlabeled species. Seven biomarkers were measured in CSF (sAPPα, sAPPβ, Aβ40 and Aβ42 (ELISA); fraction labeled sAPPα, fraction labeled sAPPβ and fraction labeled total Aβ (SILK)).The drug effect *(EFF)* inhibited *Rinβ*. sAPPβ was used in the model structure as a surrogate substrate for C99 in the γ-secretase cleavage step. The tracer PK model of label enrichment of the Leucine pool informed label incorporation into the APP pathway. Model extensions compared to the β-APP model are indicated in blue.
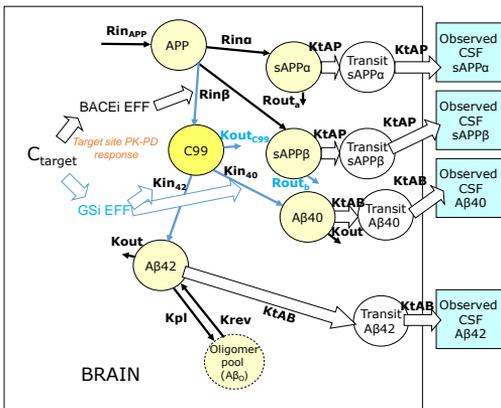
Figure 8.4: *β-γ-APP model (Chpt. 5).*
The model comprised eleven compartments: Six biomarker compartments in brain *(yellow)*, one oligomer pool *(blank dashed)* and four transit compartments from brain to CSF *(blank)*. Four biomarkers were measured in CSF (sAPPα, sAPPβ, Aβ40 and Aβ42), indicated by the blue boxes. The model included a C99 compartment, which was not present in the β-APP model. Model extensions compared to the β-APP model are indicated in blue. The drug effect of the BACE1 inhibitor *(BACEi EFF)* inhibited *Rinβ*. The drug effect of the GS inhibitor *(GSi EFF)* inhibited Kin_{42} and Kin_{40}.

Figure 8.5: *β-O-APP model (Chpt. 6).*
The model comprised thirteen compartments: Seven biomarker compartments in brain *(yellow circles)* and six transit compartments from brain to CSF *(white circles)*. Six biomarkers were measured in CSF (sAPPα, sAPPβ, Aβ40, Aβ42, Aβ38 and Aβ$_O$), indicated by the blue boxes. The drug effect of the BACE1 inhibitor *(EFF)* inhibited *Rinβ*. sAPPβ was used in the model structure as a surrogate substrate for C99 in the γ-secretase cleavage step. Model extensions compared to the β-APP model are indicated in blue.

Figure 8.6: *β-γ-O-APP model (Chpt. 7.*
The model comprised fourteen compartments: Eight biomarker compartments in brain *(yellow circles)* and six transit compartments from brain to CSF *(white circles)*. Six biomarkers were measured in CSF (sAPPα, sAPPβ, Aβ40, Aβ42, Aβ38 and Aβ$_O$), indicated by the blue boxes. The drug effect of the BACE1 inhibitor *(BACEi EFF)* inhibited *Rinβ*. The drug effect of the GS inhibitor *(GSi EFF)* inhibited Kin_{40}, Kin_{40}, Kin_{38} and Kin_{382}. The tick blue arrow indicates the homeostatic feedback on α-secretase through the action of C99. Model extensions compared to the β-O-APP model are indicated in blue.

Figure 8.2 - Figure 8.6:

Advancement of the systems pharmacology model in a series of models (β-APP model (Figure 8.2), β-13C-APP model (Figure 8.3), β-γ-APP model (Figure 8.4), β-O-APP model (Figure 8.5), β-γ-O-APP model (Figure 8.6) to characterize drug effects on the APP pathway. As driver of biomarker responses C_{target} was used in all models, which was derived from the PK models of the BACE1 inhibitor and GS inhibitor, respectively.

APP: Aβ -precursor protein; *Aβ* : amyloid-β-peptide; C_{target}: drug concentration target site; Kin_{38}: Aβ38 formation rate from C99; Kin_{382}: Aβ38 formation rate from Aβ42; Kin_{40}: Aβ40 formation rate; Kin_{42}: Aβ 42 formation rate; Kin_x: FactorX formation rate; *Kout*: Aβ38, Aβ40 and Aβ42 degradation rate; $Kout_{C99}$: C99 degradation rate; *Koutx*: FactorX degradation rate; *Krev*: Oligomer dissociation rate; *KtAP*: transit rate sAPPα and sAPPβ from brain to CSF; *Kpl*: Oligomerization rate; *KtAβ* : transit rate Aβ from brain to CSF; *KtAβ $_O$*: transit rate Aβ$_O$ from brain to CSF; *KtX*: transit rate FactorX from brain to CSF; *RinAPP*: source of APP; *Rinβ*: sAPPβ formation rate; *Rinα*: sAPPα formation rate; *Routb*: sAPPβ degradation rate; *Routa*: sAPPα degradation rate.

245

inhibitors, variation between studies could be accounted for, revealing the true differences in the systems behaviour. Identical values of the systems parameters after BACE1 versus GS inhibition were obtained. Specifically, the lower value of the oligomerization rate constant after GS inhibition that had been observed after the analysis on the basis of the β-γ-APP model could now be explained by the fact that that model did not account for stepwise successive cleavage of C99 by GS.

Identical values of the system specific parameters were observed for the two different interventions (BACE1 versus GS inhibition). This confirms that a true system specific model characterizing the interactions in the APP biochemical network has been obtained. The structure of the final systems pharmacology model of the APP pathway, the so called β-γ-O-APP model, is depicted in Figure 8.6.

In conclusion, a systems pharmacology model of APP processing has been developed which constitutes a basis for the prediction of the influence of therapeutic interventions on the exposure to $A\beta_O$. The systems pharmacology model is based on a network structure. Specific features of the model are i) the $A\beta_O$ formation is a second-order process, ii) the treatment effect is influenced by $A\beta_O$ dissociation restoring the equilibrium with $A\beta$ monomers and iii) GS inhibition can trigger a homeostatic feedback mechanism promoting the non-amyloidogenic pathway.

Extrapolation of the systems APP model from rhesus monkeys to humans – some preliminary results

An important question is how the model of the APP pathway in monkeys could be adapted to predict, in a quantitative manner the effects of drugs targeting the APP pathway in humans. Here we present some preliminary results of the interspecies scaling of BACE1 inhibition between rhesus monkeys and humans. In this context, first the APP pathway homology of rhesus monkeys to humans is discussed. Next, the considerations in the interspecies translation of drug effects in the β-γ-O-APP model are outlined. Finally, the systems APP model is used to predict CSF response data in humans after BACE1 inhibition.

APP is highly conserved between humans and rhesus monkeys[5]. The 695 amino acid isoform of APP (APP_{695}) is completely homologous between humans and rhesus monkeys, whereas the common longer isoform APP_{770} differs in only four amino acids[6]. APP is quite exceptional in having across mammals a totally conserved length and a very high degree of interspecies sequence identity, indicating that the proteolytic processing is

important for the physiological APP function[7]. BACE1, GS and α-secretase sequences are also highly similar between humans and rhesus monkeys with respectively a 99%, 97% and 99% match in amino acids (NCBI homoloGene). Quantitative ELISAs have shown that the concentrations of cerebral $A\beta$ are comparable in patients with AD and aged rhesus monkeys[8]. However, binding assays with radiolabelled Pittsburgh Compound B have shown significant differences in the ligand affinity for $A\beta$ rich cortical extracts from aged nonhuman primates compared to patients with AD. This may be explained by differences in the $A\beta$ aggregates or endogenous cofactors[6]. With the selective $A\beta$ oligomer ELISA assay that was used in the current rhesus studies, oligomers could also be quantified in human CSF[4].

The β-γ-O-APP model consists of eight linked turnover equations for APP, C99, sAPPα, sAPPβ, $A\beta$38, $A\beta$40, $A\beta$42 and $A\beta_O$. The values of physiological turnover rate constants in species other than rhesus monkeys can in principle be predicted based on allometric scaling principles[9]. Therefore, allometric scaling principles were applied to scale the values of the first order rate constants $Rin\beta$ and $Rin\alpha$ from rhesus monkeys to humans on the basis of body weight using the allometric exponent of -0.25 (Eq. 8.1)[10]. The baseline values of APP, C99, sAPPα, sAPPβ, $A\beta$38, $A\beta$40, $A\beta$42 and $A\beta_O$ are considered species independent and were therefore not scaled. The feedback parameter (FP) was dependent on the baseline C99, which is the same in both species. Therefore, FP was also not scaled. This means that intrinsically the values of the zero-order production rate of APP are scaled (Eq. 8.2 and 8.3).

$$R_{human} = R_{rhesus} \cdot \left(\frac{BW_{human}}{BW_{rhesus}} \right)^{-0.25} \tag{8.1}$$

$$\frac{d}{dt} APP = Rin_{APP} - \left(Rin\beta + Rin\alpha \times \left(\frac{C99}{C99_{base}} \right)^{FP} \right) \times APP \tag{8.2}$$

$$Rin_{APP} = (Rin_\alpha + Rin_\beta) * APP_{base} \tag{8.3}$$

Because of the linkage of the turnover equations in the model, other parameters of the model ($Rout_a$, $Rout_b$, Kin_{40}, Kin_{42}, Kin_{38}, Kin_{382}, $Kout_{99}$, $Kout$, Kpl, $Krev$) are also intrinsically scaled. However, due the linkage of the turnover equations and derived

parameters, the allometric scaling of the system of equations is cancelled out and the values of the system parameters remain unchanged. For the herein reported prediction of APP metabolite responses in human, the values of the system parameters were therefore kept the same as established in rhesus monkey.

Another factor that needs to be taken into account in the scaling is the fact that in the rhesus monkey CSF samples were taken from the cisterna magna, whereas in humans CSF is obtained by a lumbar puncture. A transit compartment model, consisting of a series of transit compartments, was included to account for the delay between the cisterna magna and lumbar CSF biomarker responses, in manner that is similar as previously reported by Kleijn et al. [11]. Thus to translate the β-γ-O-APP model from rhesus monkey to human the following assumptions were made:

(1) APP processing pathway is identical in humans and rhesus monkeys. It is assumed that the identified homeostatic feedback mechanism applies also in humans.

(2) Values of the system parameters are the same in rhesus monkeys and humans.

(3) Values of the drug effect parameters (Imax, IC50) are similar across species.

(4) The delay between the cisterna magna and lumbar CSF biomarker responses can be described by a series of transit compartments.

To evaluate if the β-γ-O-APP model can be translated from rhesus monkeys to humans, with the above mentioned assumptions, the human predictions for the BACE1 inhibitor verubecestat (MK8931) were compared to experimentally determined values that had been reported in the literature [12]. The population PK parameters of verubecestat [13] and reported IC50 in healthy subjects [12] were used to predict the response of the APP metabolites (Aβ40, Aβ42, Aβ38, sAPPβ, sAPPα) and Aβ_O in healthy non-elderly subjects and AD patients. System and drug parameters were assumed to be the same for healthy subjects and AD patients, although this is a simplification of the likely non-homogeneous systems conditions during disease. An empirical drift model component was used to correct for the upward drift in CSF concentrations over the sampling period observed in healthy subjects (see Supplemental Material).

The model adequately predicted the response of Aβ40, Aβ42 and sAPPβ after a single dose in healthy volunteers (Figure 8.7 *left panels*). After 14 days of once-daily dosing of verubecestat in healthy volunteers, the response of Aβ40, Aβ42 and sAPPβ for the highest dose groups was slightly underpredicted (Figure 8.7 *middle panels*). In AD, the

model yielded a reasonable prediction of the observed biomarker response after 7 days of once-daily dosing (Figure 8.7 *right panels*).

The model predicted a decrease in the human $A\beta_O$ concentrations in CSF at the lumbar region (Figure 8.8 *middle row*). After a single 100 mg dose of verubecestat in healthy volunteers an 84% reduction in the predicted concentration of $A\beta_O$ was observed. This value is close to the 94% reduction at day 7 following repeated administration of once daily doses in the range of 40-150mg that was predicted by the model.

These simulations show that the translated model holds promise for use in the dose selection for clinical trials and to determine what dose level is needed to reach a predefined target % reduction in $A\beta_O$ concentrations. When clinical $A\beta_O$ concentration data from $A\beta$ production inhibitors would become available, the proposed model for the interspecies extrapolation could be verified.
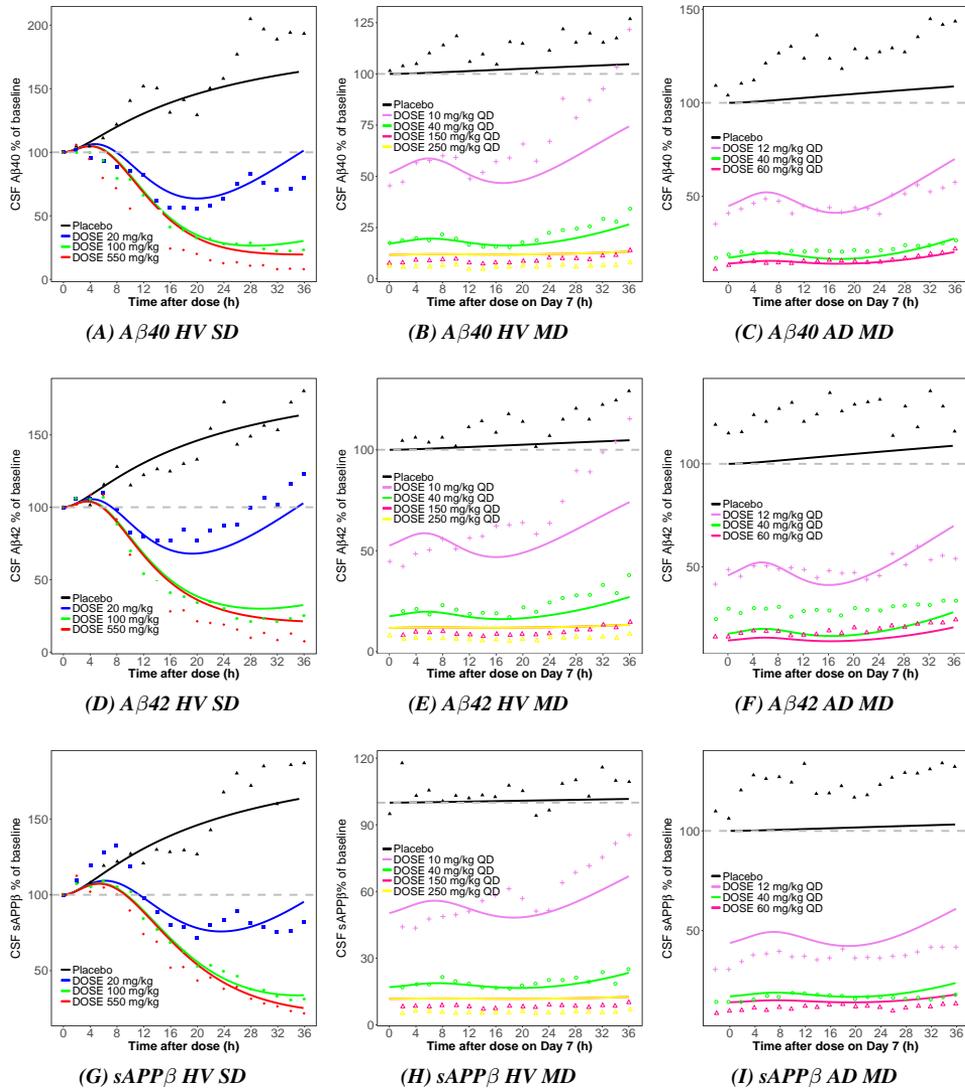
***Figure 8.7: Model based prediction of verubecestat effects on CSF Aβ40, Aβ42 and
sAPPβ after a single dose (SD) in healthy volunteers (HV)* (left)*, multiple dose (MD) in HV*
(middle) *and MD in AD patients* (right)*.** Predictions are expressed as percentage relative to
baseline. Symbols represent the median of observed percentage relative to baseline.
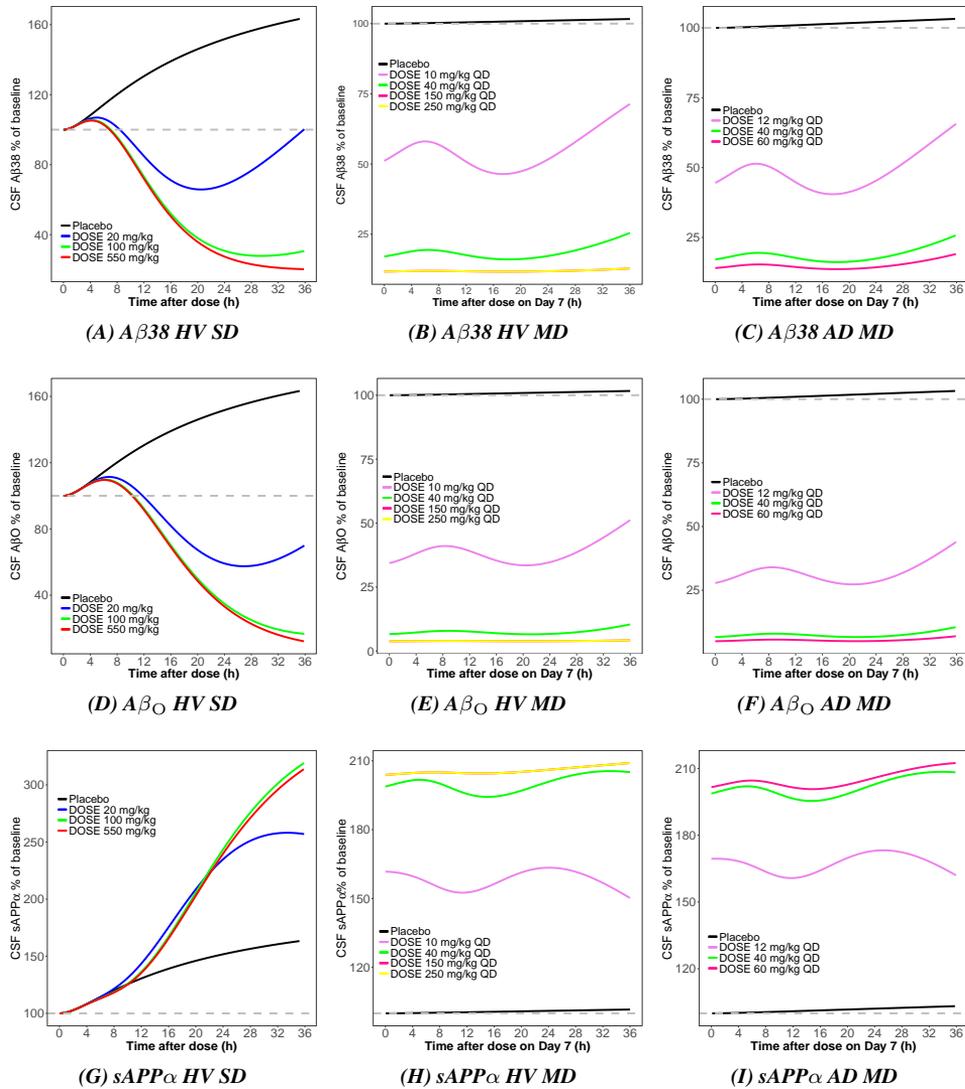
***Figure 8.8: Model based prediction of verubecestat effects on CSF Aβ38, Aβ_O and sAPPα after a single dose (SD) in healthy volunteers (HV) (left), multiple dose (MD) in HV (middle)** and MD in AD patients* (**right**)*.** Predictions are expressed as percentage relative to baseline. CSF Aβ38, Aβ_O and sAPPα were not measured in these studies.

Perspectives in clinical studies in AD

The systems pharmacology model of the APP pathway in monkeys can be of value in the design and development of therapeutic interventions for AD in many ways. Here we briefly discuss a number of potentially useful applications.

Optimization of clinical study designs

Assessment of disease severity and treatment effect in clinical trials in AD constitutes a major challenge, due the lack of meaningful biomarkers reflecting disease severity, or predicting treatment effect. Moreover, frequently highly invasive techniques such as repeated sampling of CSF must be applied to obtain meaningful data. As a result, there is little room to optimize study protocols experimentally. Here we propose that modelling and simulation offers an informative approach to the optimization of the designs of clinical trials on the effects of novel drugs following single dose and repeated administration. This is exemplified in the optimization of the so-called SILK protocol. A number of years ago the protocol has been developed to determine kinetics of low-abundance proteins such as Aβ[14]. In this protocol, a primed bolus of ^{13}C$_6$-Leucine is infused intravenously, at 2 mg/kg over 10 minutes, followed by 2 mg/kg/hours continuous infusion for 9 hours. The proportion of synthesized and secreted Aβ labelled with ^{13}C$_6$-Leucine at amino acid 17 and 34 is measured, and the fraction of labelled Aβ in CSF is monitored for a number of hours after the end of the infusion[14]. As was mentioned earlier, the method has been successfully applied to assess differences in Aβ kinetics in cognitively normal persons versus symptomatic AD patients[15]. Recently, this SILK protocol has been used to assess the effect of drugs such as GS inhibitors on Aβ production[16]. Here, it is important to optimize the design of the SILK protocol, particularly in relation to the time of administration of the ^{13}C$_6$-Leucine infusion relative to the time of administration of the drug and the interpretation of the signal.

Our studies on the effects of MBi-5 on the APP pathway in monkeys, using chemical assays (ELISA) for the quantification of the peptides showed a clear dose dependency for the effect on all APP metabolites (**Chapter 4**). However, in the same study such a dose dependency was not detected by the SILK protocol for the fraction labelled sAPPα. For sAPPβ and Aβ the sensitivity to detect dose proportionality appears to depend on, among other factors, the timing of administration of the ^{13}C$_6$-Leucine infusion. An important question is how the design of the SILK protocol can be further optimized. Here, we use the β-13C-APP model to investigate in a series of simulations the effect of study design

features on the $^{13}C_6$-signal. These simulations focus specifically on i) the sensitivity to detect a treatment effect and ii) the possibility of identifying the exposure response relation. The details of the simulated scenarios are reported in the Supplemental Material.

These simulations showed that the timing of the $^{13}C_6$-Leucine infusion relative the drug dose and dose frequency affects the magnitude of the $^{13}C_6$-signal and the possibility to observe a dose proportionality in the signal. For the fraction labelled sAPPα signal, the protocol cannot be optimized further. This is caused by the fact that this APP metabolite is upstream of BACE1 inhibition. As a result of the inhibition of this enzyme unlabelled sAPPα accumulates, diluting the signal, independent of the timing of the $^{13}C_6$-Leucine infusion.

To investigate the effect of drugs, the SILK protocol should be optimized based on the best timing of the $^{13}C_6$-Leucine infusion for an endpoint which is closest to the target Aβ_O, which is fraction labelled Aβ. The optimal time of the $^{13}C_6$-leucine infusion depends on a number of factors, such as i) the PK of the drug under investigation, ii) the delay between the PK and BACE1 inhibition, iii) the delay between the kinetics of effects on Aβ relative to the kinetics of BACE1 inhibition and iv) the delay between start of $^{13}C_6$-Leucine infusion and sufficient enrichment at the target site. These factors can only be investigated simultaneously using an integrated model approach. Our simulations show that the greatest signal in terms of clear dose proportionality in fraction labelled Aβ is obtained when the $^{13}C_6$-Leucine infusion starts immediately after administration of the BACE1 inhibitor. The signal is already diminished when $^{13}C_6$-Leucine infusion starts at 1 hour post drug dose.

Early diagnosis

Initiating treatment early in the course of the disease is likely to be important when the aim is to slow or alter disease progression. The early diagnosis of preclinical AD is challenging, because patients do not display any symptoms presumably as result of a large resilience in the functioning of the biological system (**Chapter 2**). An important question is whether, and if so how, metabolites of the APP pathway might serve as biomarkers for the early detection of AD. It is well established that metabolite concentrations in CSF can reflect some of the pathophysiological changes that occur in the brain [17]. According to amyloid cascade hypothesis, the first step in the pathological cascade is accumulation of Aβ (Figure 2.3). CSF Aβ has therefore potential as a biomarker for (early) diagnosis and may provide clue of preclinical AD [18].

The development of biomarkers for the early detection of AD that are predictive of

preclinical AD constitutes a major challenge for a variety of reasons. First, the quantitation of metabolites of the APP pathway in CSF is technically difficult. As a result the reported values of CSF concentrations of Aβ can vary between different research centres and laboratories. This has led to a large initiative for the standardization of pre-analytical aspects of CSF biomarkers: The "Alzheimer's Association Cerebrospinal Fluid (CSF) Quality Control Program" brings together laboratories across the globe with the aim of standardizing the measurement of potential Alzheimer's biomarkers[19]. There has also been intensive research of aggregate-based biomarkers, including Aβ_O in CSF. However, to date, no biomarkers have been identified that can reliably diagnose AD in the early disease stage in an individual patient[20,21].

Second, due to the resilience in the biological system, changes in biomarkers may not be observed until advanced stages of the disease. An intriguing question is whether the sensitivity could be enhanced on the basis of a challenge test, analogous to the use of the glucose tolerance test for the detection of glucose intolerance as a precursor of type II diabetes mellitus[22]. For the APP pathway, the system could be challenged by the administration of a modulator such as a secretase inhibitor. The design of such a challenge test could be optimized on the basis of the systems pharmacology model of the APP network. Furthermore, the model-based analysis of the system response could yield estimates of system parameters that may serve as novel biomarkers which are indicative for the disease severity, and possibly predictive of the treatment response to APP modulating drugs.

Personalized treatment solutions

In most of the clinical trials in AD the molecular heterogeneity of the disease has not been taken into account. Because of such heterogeneity of AD, treatment may need to be stratified as, dependent on the genotype, response to potentially disease modifying therapeutics such as secretase inhibitors and Aβ clearance enhancers may be different.

In recent years important progress has been made in delineating genetic factors in the pathophysiology of AD related to changes in APP processing. Familial AD mutations in APP and in the presenilin genes PS-2 and PS-2 and at-risk gene polymorphisms responsible for late-onset AD all point to a unambiguous and early role of Aβ in the pathogenesis of AD[23,24,25]. In early-onset AD genetic variations were found on the APP gene as well as in the presenilin genes PS1 and PS2, encoding for the catalytic subunit of GS, causing altered APP processing[26,27,28]. In sporadic, late-onset AD the epsilon4 allele of the apolipoprotein E gene (APOE) was identified as a major risk factor contributing

to the pathogenesis of AD in about 20% of the cases[29,25]. Mechanistically, this can be understood by the fact that APOE is involved in the clearance and the aggregation of the $A\beta$ peptide.

The current general thinking is that susceptibility for late-onset AD involves various genetic risk factors, as up to 60%-80% of the late-onset AD is genetically determined[27,30]. The genetic heterogeneity of the disease is high, and a large number of genetic risk factors, with relatively low penetrance but high prevalence must be involved. Also, genes with a modest contribution to the risk of AD may operate interactively[24]. A few risk factors, supporting the amyloid hypothesis, are discussed in the Supplemental Material. It is important that genetic information is considered in future clinical trials with drugs acting at the APP pathway.

The genetic information may be utilized in various ways. Firstly, this may hint to system parameters that need to be adjusted to describe the disease state. Secondly, an individual's genetic susceptibility may serve as a preselection criterion for further diagnostic tests as well as personalized treatment of interventions targeting the APP pathway.

Prediction of the long term treatment effect

Future treatments for AD are likely to be interventions that modify the progression of the disease[17]. Demonstration of a drug effect on disease progression is notoriously difficult due to the slow progression of the disease and the typically wide inter-individual variation in the rate of progression. An additional complicating factor is that the statistical techniques that are applied in the evaluation of clinical trials (such as analysis of variance) are not valid in the case of a chronically progressive disease. Moreover, they do not differentiate between symptomatic and disease modifying effects. To meet these challenges, the concept of disease progression analysis has been introduced[31,32]. Disease progression analysis utilizes regression models to estimate the rate of disease progression. Using a simple linear regression model and the Alzheimer Disease Assessment Scale – Cognition subscale (ADAS-Cog) score as a pharmacodynamic endpoint it was found that AD progresses at a rate of 8.2 units per year[33].

It remains to be determined however whether disease severity progresses linearly with time. Here it is of interest that the rate of progression was slower at earlier stages of the disease[34]. Moreover, the ADAS-Cog score can only be used as a disease status marker when cognitive changes have commenced. Therefore, in the early phases of the disease and for the design of pre-emptive studies other biomarkers and a more complex disease

progression model are needed. To overcome these and other complexities, the concept of disease systems analysis has been introduced as a mechanistic alternative to disease progression analysis Post et al. [35].

In "disease systems analysis" the disease progression is modelled on the basis of a cascade of turnover models to describe the biomarker responses. This opens the possibility to connect changes in biomarker responses at the early stages of the disease to changes in behavioural endpoints (i.e. rating scales such as the ADAS-Cog score) at later stages. The systems pharmacology models that have been introduced in this thesis are based on the same concept of cascading turnover models and constitute therefore a basis for disease systems analysis models in AD. These models can be extended to comprise also the effects on further downstream biomarkers. The next biomarker to become abnormal is amyloid-PET, reflecting accumulation of cortical $A\beta$ fibrils, followed by CSF tau, indicative for neurofibrillary tangles (NFT), followed by biomarkers for neurodegeneration (fluorodeoxyglucose [FDG]-PET and structural magnetic resonance imaging [MRI]). Cognitive impairment is the last event in the progression of the disease (2.3). New biomarkers to measure disease progression in AD may became available over the years.

To integrate these biomarkers in a disease systems model, the correlations between these biomarkers need to be considered, firstly, between the biochemical markers CSF $A\beta$ and tau, secondly between fluid and imaging biomarkers, and ultimately with ADAS-Cog scores. Most of these correlations are investigated in clinical-autopsy correlation studies. In order to be able to capture disease progression longitudinal data in the same subjects are needed. However, this type of data in the same subjects is rare and new initiatives are needed in this respect. One of the first initiatives currently ongoing is the 'Alzheimer's Disease Neuroimaging Initiative' (ADNI). The ADNI is studying the rate of cognition decline, change is brain structures and fluid biomarkers among volunteers over 55 years, who are healthy, as well as those who have been diagnosed with mild dementia due to AD.

Alternative interventions targeting the APP pathway

We have developed a systems pharmacology model of the APP pathway on the basis of $A\beta$ production inhibitors (BACE1 and GS inhibition) and quantified their effects on $A\beta_O$. In theory, to reduce $A\beta$ burden the functioning of the APP pathway can be modified in many different ways: (1) inhibition of $A\beta$ production; (2) enhancement of $A\beta$ clearance;

(3) blocking $A\beta_O$ toxicity through interactions with the $A\beta_O$ target site.

Until now, clinical trials of $A\beta$ production inhibitors (i.e. BACE1 and GS inhibitors) could not demonstrate clinical efficacy at tolerated doses in patients[36,37,38]. Moreover, the anti-$A\beta$ monoclonal antibodies, developed to enhance $A\beta$ clearance, bapineuzumab (Pfizer Inc.) and solanezumab (Eli Lilly & Co.) could not demonstrate efficacy in AD patients large Phase III clinical trials[39,40]. In general, for amyloid-targeted therapy there is now a tendency to move towards clinical trials with prodromal AD or in subjects at preclinical stage of familial hereditary AD variants.

The primary endpoints for efficacy in the clinical AD studies were measures of cognitive performance by changes in ADAS-Cog score and in the AD Cooperative Study – Activities of Daily Living (ADCS-ADL) score. There are several possible explanations for the lack of efficacy. A particularly important question is whether target engagement as reflected in the exposure to $A\beta_O$ has been achieved. The β-γ-O-APP model could be used to predict this.

In this section, the β-γ-O-APP model is used to perform simulations to investigate interventions targeting the APP pathway. The behaviour of the individual moieties of the β-γ-O-APP model was evaluated by simulating the responses after $A\beta$ production inhibition (BACE1 or GS inhibition) and by triggering the system with a hypothetical compound enhancing $A\beta$ clearance (Figure 8.9). The hypothetical $A\beta$ clearance enhancer was assumed to have similar PK properties as the BACE1 inhibitor. An Emax concentration effect relationship was simulated assuming a maximal increase of the $A\beta$ clearance rate constant (Kout) by 5 fold.The simulation showed that the effect of the $A\beta$ clearance enhancer yielded less reduction in $A\beta_O$ concentration (83.4%) than production inhibition (86.8% and 87.4% for BACE1 and GS inhibitor, respectively). Furthermore, $A\beta$ clearance enhancement does not affect APP, sAPPβ, C99 and sAPPα concentrations.

The β-γ-O-APP model offers the opportunity to investigate the net system's responses to combined intervention acting at different targets. Therefore, the system was triggered by combined administration of two compounds: a combination of a BACE1 and GS inhibitor, a combination of a GS inhibitor and $A\beta$ clearance enhancer and a combination of a BACE1 inhibitor and $A\beta$ clearance enhancer (Figure 8.10). The effects of the different treatments were assumed to be additive and no PK interactions were taken into consideration.

Combined administration of MBi-5 and MK-0752 would further reduce $A\beta$ monomers and $A\beta_O$ concentrations compared to monotherapy: a reduction of 97% in $A\beta_O$ was achieved with combined administration. Combining two drugs with similar action ($A\beta$ production inhibition), provided less reduction in $A\beta_O$ concentrations than a combination

of GS inhibition and Aβ clearance enhancement (98.5%), although differences are small. These simulations showed an additive response on Aβ_O concentrations of combined intervention. Further pharmacodynamic drug interaction studies may be required to investigate a possible synergistic effect, in which response surface analysis may be used to elucidate the drug interactions fully[41].

A promising strategy seems to be the prevention of toxicological effects by preventing the interaction of toxic Aβ_O species with target receptors. Such novel therapies pharmacologically compete with Aβ_O with critical receptor targets, thereby preventing synapse loss and improving memory. An example of such receptor targets are the sigma-2/PGRMC1 receptors that mediate Aβ_O binding to the synaptic puncta on neurons[42]. One such candidate compound targeting these receptors is the small molecule therapeutic CT1812 (Cognition Therapeutics, Inc.), which is in clinical testing in AD patients. Adding information from CT1812 study data would provide the opportunity to extend the β-γ-O-APP model with a receptor interaction model component for Aβ_O-receptor interactions. Then, it would be of interest to investigate what happens to the Aβ equilibrium when Aβ_O concentrations rise as result of receptor blockage. The increase of Aβ_O in the brain may lead to redistribution of Aβ_O into the CSF and more effective elimination. Or it could lead to the undesirable effect of increased fibril formation. In that respect, extension of the model to describe the higher ordered agglomerated species as fibrils and plaques would be essential. For an effective suppression of the Aβ_O concentrations and it's toxic effects if probably necessary to use rational combinations of drugs targeting multiple targets in the system. Once the β-γ-O-APP model is extended, the combined intervention of an Aβ production inhibitor and prevention of the interaction of Aβ_O species with it's receptor target can be investigated such that therapy may be optimized.

The APP systems pharmacology model can bring us closer to optimizing the therapeutic intervention to reduce oligomer burden in AD. This thesis shows that systems pharmacology models provide a powerful tool for integrated analysis of biology and pharmacology to assess system-drug interactions that is difficult to study in other ways. Further, the model constitutes the basis for the development of a disease systems model for AD to investigate the effect of disease modifying treatments on disease progression. Because of a common pathological principle, this approach can also be applied to other protein misfolding neurodegenerative disease such as PD, HD and ALS. An ultimate objective would be to combine disease system models to investigate common pathological paths as well as disease-specific signatures in protein misfolding neurodegenerative diseases.
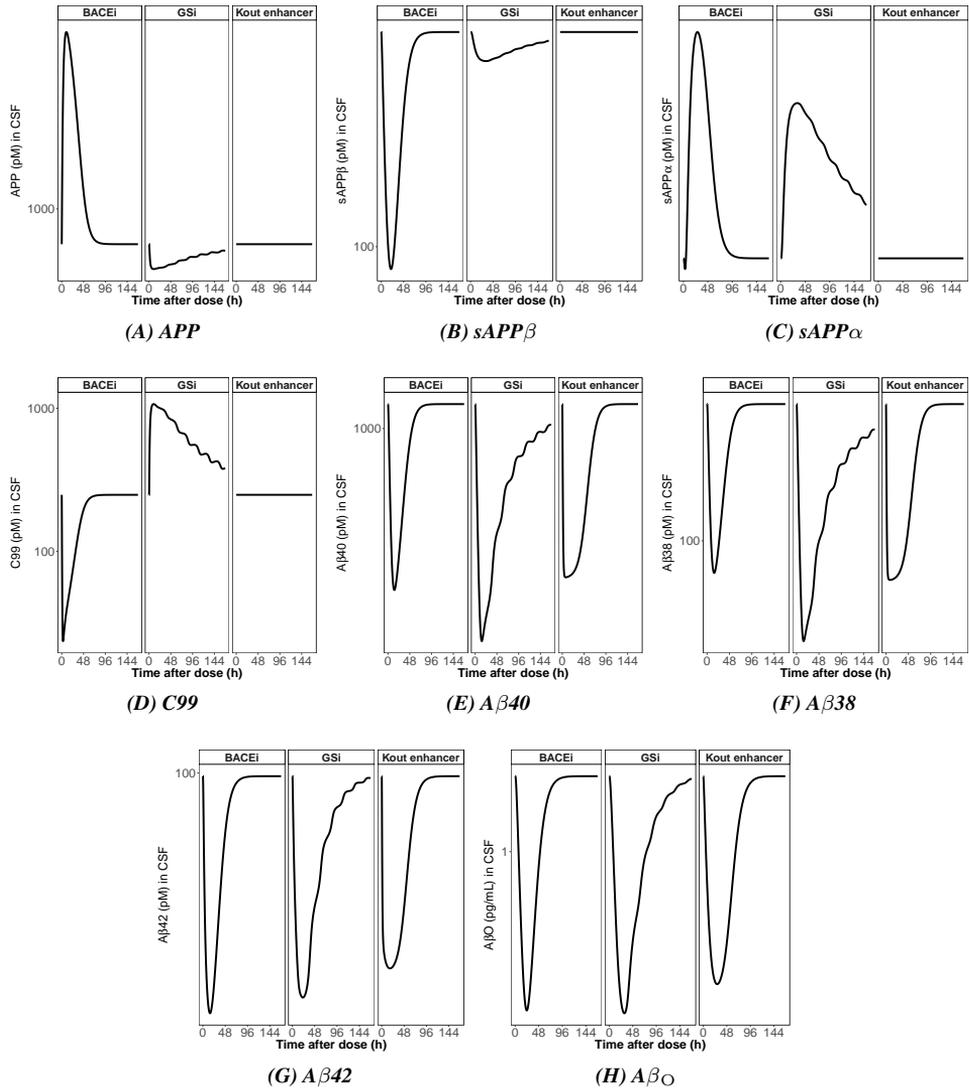
Figure 8.9: Different moieties of β-γ-O-APP model in response to 125 mg/kg MBi-5 (left panels), 240 mg/kg MK-0752 (middle panels) and hypothetical compound (Aβ clearance enhancer) (right panels).

(A) APP

(B) sAPPβ

(C) sAPPα

(D) C99

(E) Aβ40

(F) Aβ38

(G) Aβ42

(H) Aβ_O
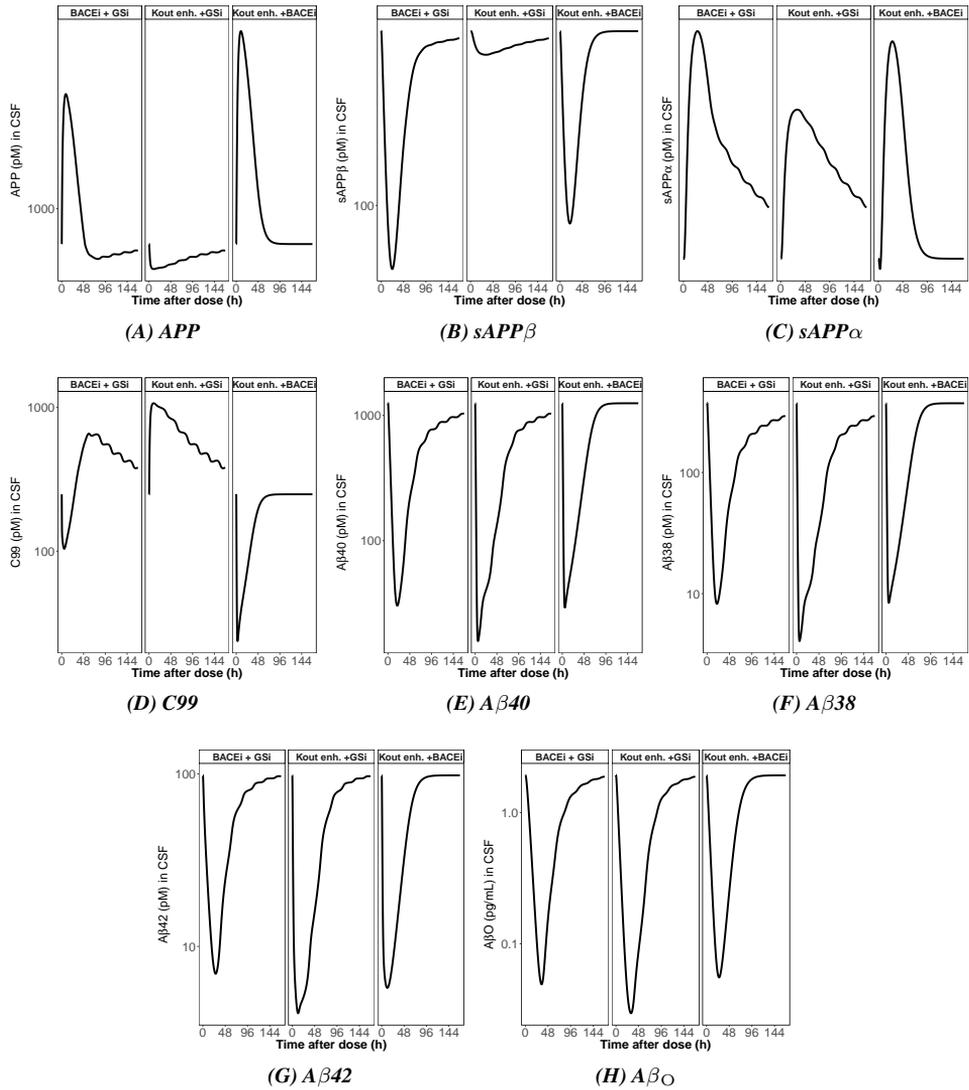
Figure 8.10: Different moieties of β-γ-O-APP model in response to combination of 125 mg/kg MBi-5 and 240 mg/kg MK-0752 (left panels), the combination of 240 mg/kg MK-0752 and hypothetical compound (Aβ clearance enhancer) (middle panels) and the combination of 125 mg/kg MBi-5 and hypothetical compound (Aβ clearance enhancer) (right panels).

References

1. Gilberto, D.B., *et al.* An alternative method of chronic cerebrospinal fluid collection via the cisterna magna in conscious rhesus monkeys. Contemp Top Lab Anim Sci. 2003;42 (4):53–59.

2. Ogata, Y., Charlesworth, M.C., & Muddiman, D.C. Evaluation of protein depletion methods for the analysis of total-, phospho- and glycoproteins in lumbar cerebrospinal fluid. J Proteome Res. 2005;4(3):837–845.

3. Mikkonen, S., Jacksen, J., Roeraade, J., Thormann, W., & Emmer, A. Microfluidic Isoelectric Focusing of Amyloid Beta Peptides Followed by Micropillar-Matrix-Assisted Laser Desorption Ionization-Mass Spectrometry. Anal Chem. 2016;88(20): 10044–10051.

4. Savage, M.J., *et al.* A sensitive Aβ oligomer assay discriminates Alzheimer's and aged control cerebrospinal fluid. J Neurosci. 2014;34(8):2884–97.

5. Podlisny, M.B., Tolan, D.R., & Selkoe, D.J. Homology of the amyloid beta protein precursor in monkey and human supports a primate model for beta amyloidosis in Alzheimer's disease. Am J Pathol. 1991;138 (6):1423–1435.

6. Heuer, E., Rosen, R.F., Cintron, A., & Walker, L.C. Nonhuman primate models of Alzheimer-like cerebral proteopathy. Curr Pharm Des. 2012;18(8):1159–1169.

7. Franco, R., Navarro, G., E, M.P., & Moreno, E. Amyloid Beta Precursor Protein: Proper Credit for the Basic Biochemical Properties of the Most Studied Protein in the 21st Century*. J Neurol Neurol Disord. 2014;1(1): 1–6.

8. Rosen, R.F., Walker, L.C., & Iii, H.L. PIB binding in aged primate brain: Enrichment of high-affinity sites in humans with Alzheimer's disease 2012;32(2):223–234.

9. Mager, D.E., Woo, S., & Jusko, W.J. Scaling Pharmacodynamics from In Vitro and Preclinical Animal Studies to Humans. Drug Metab Pharmacokinet. 2009;24(1):16–24.

10. Stevens, J., *et al.* Mechanism-based PK-PD model for the prolactin biological system response following an acute dopamine inhibition challenge: quantitative extrapolation to humans. J Pharmacokinet Pharmacodyn. 2012;39(5):463–77.

11. Kleijn, H.J., *et al.* Development and Application of a Semi-Mechanistic Model for Modulation of Amyloid-β in Cerebrospinal Fluid after Inhibition of γ-secretase. Poster Present PAGE, Athens, Greece. 2011.

12. Kennedy, M.E., *et al.* The BACE1 inhibitor verubecestat (MK-8931) reduces CNS β-amyloid in animal models and in Alzheimers disease patients. Sci Transl Med. 2016;8(363):363ra150–363ra150.

13. Ma, L., *et al.* Population pharmacokinetic modeling of the novel BACE inhibitor MK-8931 following single and multiple dose administration in healthy subjects. Poster Sess Present AAIC. 2012;pages P1–229.

14. Bateman, R.J., Munsell, L.Y., Chen, X., Holtzman, D.M., & Yarasheski, K.E. Stable

isotope labeling tandem mass spectrometry (SILT) to quantify protein production and clearance rates. J Am Soc Mass Spectrom. 2007;18(6):997–1006.

15. Mawuenyega, K.G., *et al.* Decreased clearance of CNS beta-amyloid in Alzheimer's disease.. Science. 2010;330(6012):1774.

16. Bateman, R.J., *et al.* A gamma-secretase inhibitor decreases amyloid-beta production in the central nervous system. Ann Neurol. 2010;66(1):48–54.

17. Lleó, A., *et al.* Cerebrospinal fluid biomarkers in trials for Alzheimer and Parkinson diseases. Nat Rev Neurol. 2015;11:41–55.

18. Anoop, A., Singh, P.K., Jacob, R.S., & Maji, S.K. CSF Biomarkers for Alzheimer's Disease Diagnosis.. Int J Alzheimers Dis. 2010;2010(Table 1):1–12.

19. Mattsson, N., Andreasson, U., & Persson, S. The Alzheimer's Association external quality control program for cerebrospinal fluid biomarkers. NIH Public Access. 2013;7(4): 386–395.

20. Giacomelli, C., Daniele, S., & Martini, C. Potential biomarkers and novel pharmacological targets in protein aggregation-related neurodegenerative diseases. Biochem Pharmacol. 2017;131:1–15.

21. Hölttä, M., *et al.* Evaluating amyloid-β oligomers in cerebrospinal fluid as a biomarker for Alzheimer's disease.. PLoS One. 2013;8(6):e66381.

22. Unwin, N., Shaw, J., Zimmet, P., & Alberti, K.G. Impaired glucose tolerance and impaired fasting glycaemia: The current status on definition and intervention. Diabet Med. 2002;19(9):708–723.

23. Bilousova, T., *et al.* Synaptic Amyloid-β Oligomers Precede p-Tau and Differentiate High Pathology Control Cases. Am J Pathol. 2016;186(1):185–198.

24. Campion, D., Pottier, C., Nicolas, G., Le Guennec, K., & Rovelet-Lecrux, A. Alzheimer disease: modeling an Aβ-centered biological network. Mol Psychiatry. 2016;21(7):861–871.

25. Nicolas, G., Charbonnier, C., & Campion, D. From common to rare variants: The genetic component of Alzheimer disease. Hum Hered. 2017;81(3):129–141.

26. Chávez-Gutiérrez, L., *et al.* The mechanism of γ-Secretase dysfunction in familial Alzheimer disease. EMBO J. 2012;31(10): 2261–74.

27. Bertram, L., Lill, C.M., & Tanzi, R.E. The genetics of alzheimer disease: Back to the future. Neuron. 2010;68(2):270–281.

28. Veugelen, S., Saito, T., Saido, T.C., Chávez-Gutiérrez, L., & De Strooper, B. Familial Alzheimer's Disease Mutations in Presenilin Generate Amyloidogenic Aβ Peptide Seeds. Neuron. 2016;90(2):410–416.

29. Bertram, L., McQueen, M.B., Mullin, K., Blacker, D., & Tanzi, R.E. Systematic meta-analyses of Alzheimer disease genetic association studies: the AlzGene database. Nat Genet. 2007;39(1):17–23.

30. Gatz, M., *et al.* Role of genes and environments for explaining Alzheimer disease.. Arch Gen Psychiatry. 2006;63(2):168–174.

31. Holford, N. Disease progression and neuroscience. J Pharmacokinet Pharmacodyn. 2013;40(3):369–376.

32. Holford, N. Clinical pharmacology = disease progression + drug action. Br J Clin Pharmacol. 2015;79(1):18–27.

33. Yesavage, J.A., Poulsen, S.L., Sheikh, J., & Tanke, E. Rates of change of common measures of impairment in senile dementia of the Alzheimer's type. Psychopharmacol.Bull.. 1988;24(0048-5764):531–534.

34. Samtani, M.N., *et al.* An improved model for disease progression in patients from the Alzheimer's disease neuroimaging initiative.. J Clin Pharmacol. 2012;52(5):629–44.

35. Post, T.M., Freijer, J.I., DeJongh, J., & Danhof, M. Disease system analysis: Basic disease progression models in degenerative disease. Pharm Res. 2005;22(7):1038–1049.

36. Toyn, J. What lessons can be learned from failed Alzheimer's disease trials? Expert Rev Clin Pharmacol. 2015;8(3):1–3.

37. Kennedy, M.E., *et al.* The BACE1 inhibitor verubecestat (MK-8931) reduces CNS β-amyloid in animal models and in Alzheimers disease patients. Sci Transl Med. 2016;8(363):363ra150–363ra150.

38. Hawkes, N. Merck ends trial of potential Alzheimer's drug verubecestat. Bmj. 2017;845:j845.

39. Panza, F., Logroscino, G., Imbimbo, B.P., & Solfrizzi, V. Is there still any hope for amyloid-based immunotherapy for Alzheimer's disease? Curr Opin Psychiatry. 2014;27(2):128–137.

40. Panza, F., *et al.* Emerging drugs to reduce abnormal β-amyloid protein in Alzheimer's disease patients. Expert Opin Emerg Drugs. 2016;21(4):377–391.

41. Jonker, D.M., Visser, S.A., Van Der Graaf, P.H., Voskuyl, R.A., & Danhof, M. Towards a mechanism-based analysis of pharmacodynamic drug-drug interactions in vivo. Pharmacol Ther. 2005;106(1):1–18.

42. Izzo, N.J., *et al.* Alzheimer's therapeutics targeting amyloid beta 1-42 oligomers I: Abeta 42 oligomer binding to specific neuronal receptors is displaced by drug candidates that improve cognitive deficits. PLoS One. 2014;9(11):27–29.

Chapter 8

Supplemental Material

Supplement to

Systems pharmacology of the amyloid precursor protein pathway in Alzheimer's disease
- Conclusions & perspectives

SUPPLEMENTAL MATERIAL

Perspectives in clinical studies in AD - Drift behaviour

In the reported human studies on verubecestat[1], observed lumbar CSF concentrations increased over the sampling period of 36 hours (Figure S8.1). It may be related to the transport to the lumbar region or an artefact of repeated sampling from lumbar region[2] and on the volume removed relative to the total CSF in spine. This drift behaviour is subjected to between-study variation, as result of differences in study procedures and how the lumbar samples were drawn. If this drift is not accounted for in the model, the drug effect may be underpredicted. Therefore, the drift was predicted by an empirical drift model component, similar to the drift model reported by Kleijn et al.[3].
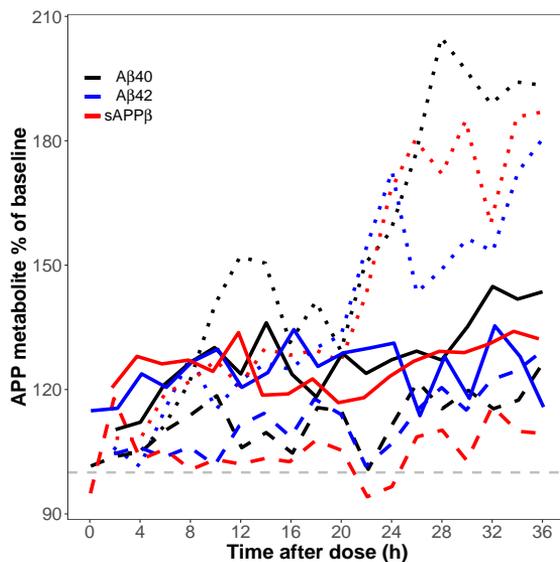
Figure S8.1: Comparison observed CSF concentrations of Aβ40 (black), Aβ42 (blue), and sAPPβ (red) after last placebo administration over the 36-hour sampling period for healthy volunteers after single dose (dashed line), once-daily doses for 14 days (long-dashed line) and for AD patients after once-daily doses for 7 days (solid line).

Optimization of clinical study designs - **Simulation scenarios**

The β-13C-APP model was used to investigate the effect of study design features on the 13C signal (Chapter 8). The simulated scenarios are presented in Table S8.1.

Table S8.1: Simulation scenarios

Scenario	Investigation objective	MBi-5 dose (mg/kg)	$^{13}C_6$-Leu administration timing[a]	Figure
A	Effect of time of administration of $^{13}C_6$-Leu primed infusion relative to the time of administration of MBi-5	125 single dose (SD)	0, 2, 4, 6, 8, 10 or 12 h post SD	S8.2
B	Effect on the dose proportionality of MBi-5 with $^{13}C_6$-Leu primed infusion at various time points following the administration of MBi-5	SD 1, 5, 10, 30, 60, 90, 125	1, 6 or 12 h post SD	S8.3
C	Effect on $^{13}C_6$-signal upon repeated dosing of MBi-5	0, 10, 30, 125 once daily (OD) for 5 days	1 h post last dose	S8.4
D	Effect on the dose proportionality in the $^{13}C_6$-signal upon repeated dosing of a dose range of MBi-5 OD with $^{13}C_6$-Leu primed infusions started 1 h after drug dose on various days	0, 10, 30, 125 mg/kg OD for 5 days	1 h after drug dose on day 1, 2, 3, 4 or 5	S8.5

[a] relative to MBi-5 dose

Optimization of clinical study designs- **Simulation results**

Simulation on scenario A showed that the timing of $^{13}C_6$-Leu primed infusion has an influence on the magnitude of the $^{13}C_6$-signal as reflected in the fraction labelled Aβ, fraction labelled sAPPα and fraction labelled sAPPβ (Figure S8.2). For fraction labelled Aβ and fraction labelled sAPPβ the highest signal was obtained when starting the infusion 12 hours post drug dose, whereas for fraction labelled sAPPα the signal is maximal when the infusion starts at the same time as drug dose.

Simulations of scenario B indicated that for the low MBi-5 dose levels ($<$30 mg/kg), increase of $^{13}C_6$-Leucine infusion start time relative to the administration of the drug results in a loss of dose proportionality. For sAPPα dose proportionality was not evident at 1 hour post drug and this was worsened at 6 and 12 hours post drug. For sAPPβ, the dose proportionality of the $^{13}C_6$-signal diminished with increasing $^{13}C_6$-Leucine infusion post drug start time, in particular after low MBi-5 doses ($<$30 mg/kg) (Figure S8.3).

Simulations of scenario C showed that the dose dependency in the $^{13}C_6$-signal was absent after once daily administration of MBi-5 during 5 days, while a dose dependent response was predicted in the absolute protein concentrations (Figure S8.4).

Scenario D illustrated that the $^{13}C_6$-signal in fraction labelled Aβ diminished with time when dosed once daily (Figure S8.5).

(A) Fraction labeled Aβ   *(B) Fraction labeled sAPPα*   *(C) Fraction labeled sAPPβ*
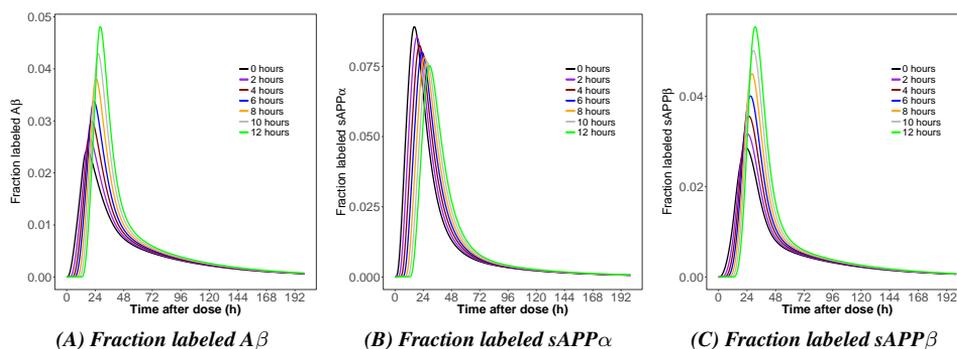
Figure S8.2: Simulation tracer kinetic profiles (fraction labeled Aβ (A), fraction labeled sAPPα (B), fraction labeled sAPPβ (C)) with the β-13C-APP model.
Simulation scenario A: The start time of the $^{13}C_6$-Leucine infusion relative to the MBi-5 administration (125 mg/kg dose) is varied from 0 up to 12 hours post drug.

(A) Fraction labeled Aβ (1h)   *(B) Fraction labeled Aβ (6h)*   *(C) Fraction labeled Aβ (12h)*

(D) Fraction labeled sAPPα (1h)   *(E) Fraction labeled sAPPα (6h)*   *(F) Fraction labeled sAPPα (12h)*

(G) Fraction labeled sAPPβ (1h)   *(H) Fraction labeled sAPPβ (6h)*   *(I) Fraction labeled sAPPβ (12h)*
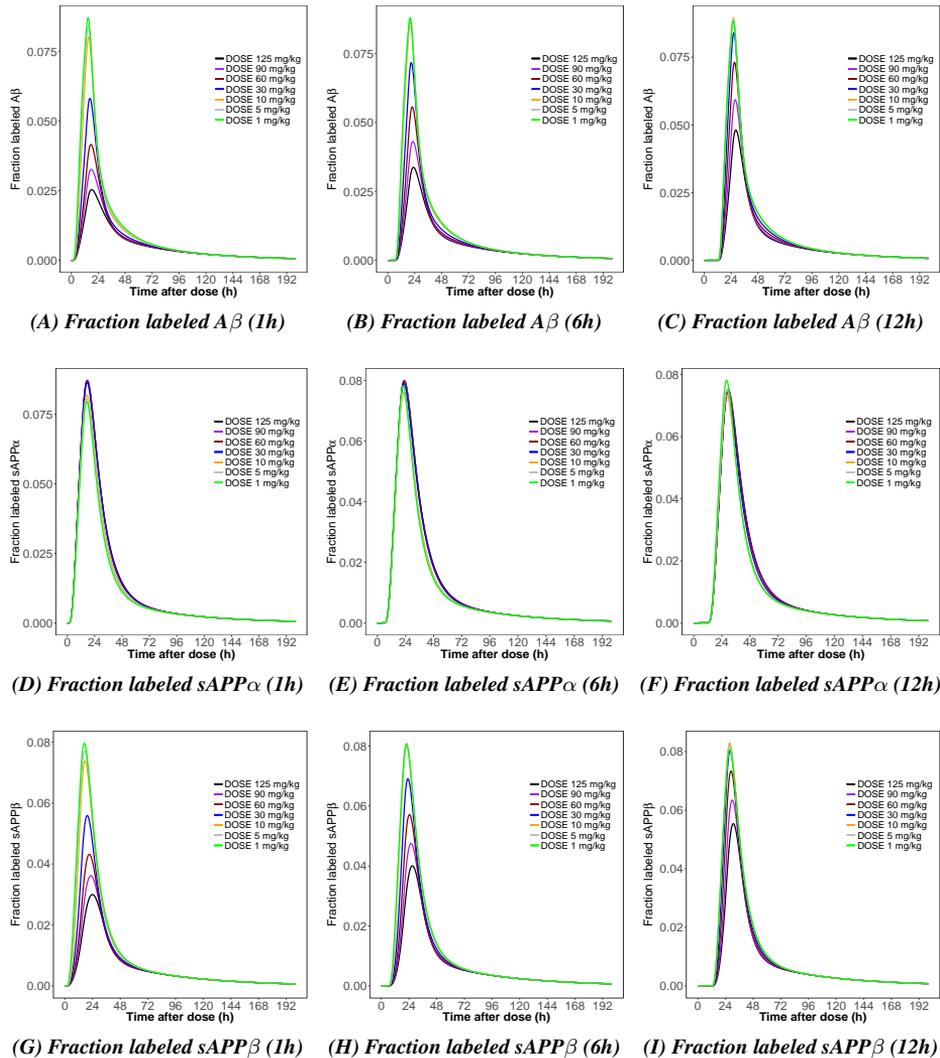
Figure S8.3: Simulation tracer kinetic profiles with the β-13C-APP model.
Simulation scenario B: The start time of the $^{13}C_6$-Leucine infusion relative to the MBi-5 administration is varied (1, 6 and 12 hours post drug) and a dose range of MBi-5 (1 up to 125 mg/kg) is simulated.
Top panels: fraction labeled Aβ; *Middle panels:* fraction labeled sAPPα; *Bottom panels:* fraction labeled sAPPβ.

(A) Total Aβ *(B) sAPPα* *(C) sAPPβ*

(D) Fraction labeled Aβ *(E) Fraction labeled sAPPα* *(F) Fraction labeled sAPPβ*
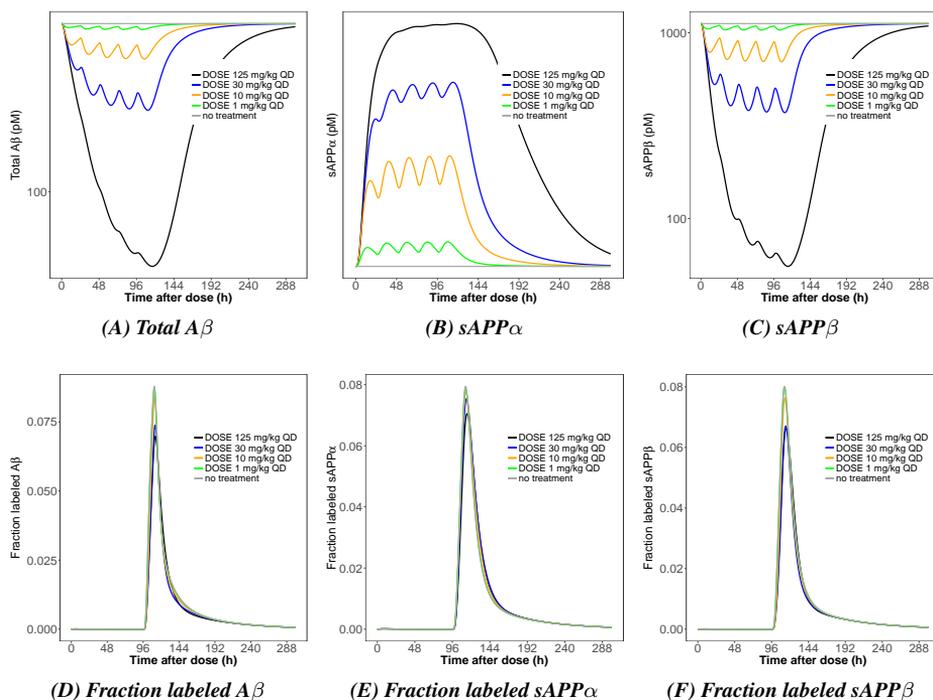
Figure S8.4: Simulation absolute protein concentrations and tracer kinetic profiles of APP metabolites with the β-13C-APP model.

Simulation scenario C: Once daily dosing MBi-5 for 5 days, varying MBi-5 dose (0, 10, 30, 125 mg/kg). The start time of the $^{13}C_6$-Leucine infusion relative to the MBi-5 administration is fixed to 1h after last dose.

Top panels: Absolute protein concentrations; *Bottom panels:* tracer kinetic profiles.
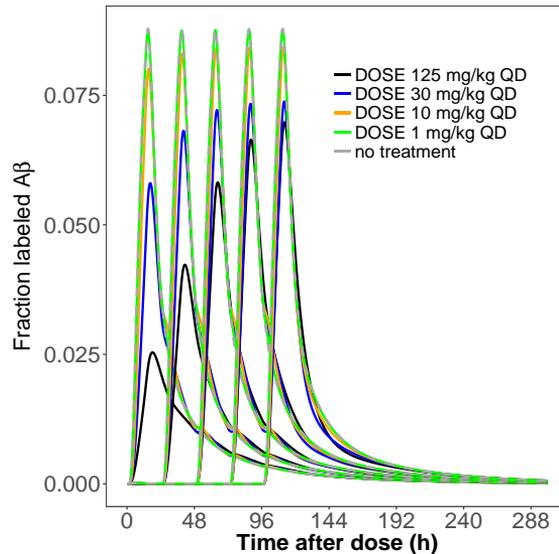
Figure S8.5: Simulation tracer kinetic profiles of Aβ with the β-13C-APP model.
Simulation scenario D: Once daily dosing MBi-5 for 5 days, varying MBi-5 dose (0, 10, 30, 125 mg/kg). The start time of the $^{13}C_6$-Leucine infusion relative to the MBi-5 administration is 1 hour after MBi-5 dose on day 1, 2, 3, 4 and 5.

Personalized treatment solutions- **Examples of genetic risk factors**

The Triggering Receptor Expressed On Myeloid Cells 2 (TREM2) variant p.R47H and p.A673T APP variant have been associated with AD risk or protection. TREM2 is expresses on microglial cells and has a role in regulating the response of the innate immune system to Aβ pathology and facilitating Aβ phagocytosis[4]. It binds to anionic lipids that interact with Aβ fibrils and apoliproteins, such as APOE. The p.R47H TREM2 variant weakens microglial detection of these lipids, thereby decreasing Aβ clearance. The APP p.A673T variant is close to the BACE1 cleavage site, making APP a less favourable substrate for the β-cleavage path[5].

Association analyses at the gene level have revealed that the loss-of-function in the sortilin related receptor 1 (SORL1) and ATP-binding cassette transporter A7 (Aβ CA7) genes are a moderate risk factor of AD. The SORL1 encodes a cargo protein which can bind APP and direct its processing to non-amyloidogenic pathways. It can also bind Aβ peptide and direct it to the lysosome, leading to its degradation[6]. Loss-of-function

of SORL1 has been linked with increased late onset AD risk[5]. Several rare variants in Aβ CA7 have been identified as risk factors of late onset AD, although its precise role in AD pathogenesis is not well understood. Aβ CA7 is primarily expressed in microglial cells and has a lipid transport function. It may be involved in Aβ clearance or production as Aβ CA7 knockout mice showed an increase in amyloid plaques[6,5,7].

References

1. Kennedy, M.E., *et al.* The BACE1 inhibitor verubecestat (MK-8931) reduces CNS β-amyloid in animal models and in Alzheimers disease patients. Sci Transl Med. 2016;8 (363):363ra150–363ra150.

2. Lucey, B.P., *et al.* An integrated multi-study analysis of intra-subject variability in cerebrospinal fluid amyloid-β concentrations collected by lumbar puncture and in-dwelling lumbar catheter. Alzheimers Res Ther. 2015;7(1):53.

3. Kleijn, H.J., *et al.* Development and Application of a Semi-Mechanistic Model for Modulation of Amyloid-β in Cerebrospinal Fluid after Inhibition of γ-secretase. Poster Present PAGE, Athens, Greece. 2011.

4. Ulrich, J.D., Ulland, T.K., Colonna, M., & Holtzman, D.M. Elucidating the Role of TREM2 in Alzheimer's Disease. Neuron. 2017;94(2):237–248.

5. Nicolas, G., Charbonnier, C., & Campion, D. From common to rare variants: The genetic component of Alzheimer disease. Hum Hered. 2017;81(3):129–141.

6. Campion, D., Pottier, C., Nicolas, G., Le Guennec, K., & Rovelet-Lecrux, A. Alzheimer disease: modeling an Aβ-centered biological network. Mol Psychiatry. 2016;21 (7):861–871.

7. Kunkle, B.W., *et al.* Targeted sequencing of ABCA7 identifies splicing, stop-gain and intronic risk variants for Alzheimer disease. Neurosci Lett. 2017;649:124–129.

Synopsis in Dutch

Samenvatting in het Nederlands van het proefschrift:

    "Systems pharmacology of the amyloid cascade

    Unfolding oligomer modulation in Alzheimer's disease"

Veel neurodegeneratieve ziekten, zoals de ziekte van Alzheimer (ZvA), de ziekte van Parkinson (ZvP) en de ziekte van Huntington (ZvH), en motorische aandoeningen als amyotrofe laterale sclerose (ALS) zijn geassocieerd met de misvouwing van een ziekte specifiek eiwit. Deze aandoeningen laten een vergelijkbaar patroon van neuronale afsterving, achteruitgang van het zenuwstelsel en cognitieve stoornissen zien. De cellulaire disfunctie wordt veroorzaakt door accumulatie van eiwit-aggregaten binnen of buiten neuronen. De pathologische veranderingen worden gedreven door de abnormale ophoping van het misgevouwen eiwit. Dit leidt tot de vorming van eiwit-aggregaten variërend van kleine oligomeren tot geordende vezels en grote amyloïde massa's. Vanwege de overeenkomsten tussen de verschillende eiwit-misvouwing gerelateerde neurodegeneratieve ziekten, biedt de 'amyloïde-cascade-hypothese' van de ZvA een kader voor de bestudering van eiwit-misvouwing neurodegeneratieve ziekten.

Volgens de amyloïde-cascade-hypothese initieert de accumulatie van de beta-amyloïd ($A\beta$) peptiden de cascade van pathologische processen van de ZvA. Vroeg in het ziekteproces, voordat klinische symptomen optreden, is er een toename van de $A\beta$ concentraties, wat leidt tot de vorming van giftige oplosbare $A\beta$ oligomeren ($A\beta_O$). De neurodegeneratie in de hersenen bij de ZvA wordt primair aangedreven door deze $A\beta_O$s. Vooralsnog is er geen farmacologische behandeling beschikbaar die de progressie van de pathologische cascade bij de ontwikkeling van de ZvA stopt of vertraagt. Een van de belangrijkste therapeutische strategieën voor de ZvA is het verlagen van de $A\beta$ concentratie in het centrale zenuwstelsel (CZS), door ofwel de vermindering van de vorming van $A\beta$ of het versnellen van de afbraak van $A\beta$. Theoretisch kan de verlaging van de $A\beta$ concentratie in het CZS alle opvolgende pathologische processen voorkomen.

$A\beta$ is het eindproduct van de proteolytische opdeling van het 'transmembraan beta-amyloïd voorloper eiwit' (APP) door achtereenvolgens β-secretase (BACE1) en γ-secretase (GS). De effecten van geneesmiddelen op de afzonderlijke metabole routes van de afbraak van APP zijn moeilijk te voorspellen, omdat de vorming en de afbraak via een ingewikkeld biochemisch netwerk worden gereguleerd. Daarom is ook het effect van de vermindering van de vorming van $A\beta$ of verhoging van de klaring van $A\beta$ op de concentratie van $A\beta_O$ en op het $A\beta$ evenwicht moeilijk in strikt kwantitatieve zin te voorspellen.

In dit proefschrift werden wiskundige modellen ontwikkeld waarmee de afbraak en eliminatie van APP via de verschillende routes kan worden gekwantificeerd. Het onderliggende doel van dit onderzoek was om op een strikt kwantitatieve wijze het biochemische netwerk van de APP-omzetting te beschrijven, om vervolgens het effect van therapeutische interventies op de blootstelling aan $A\beta_O$ te voorspellen en te evalueren.

Hiertoe werd een 'systeem-farmacologie' benadering toegepast, waarmee de beschikbare kennis van de biologie en farmacologie van de systeemreacties wordt geïntegreerd (**Hoofdstuk 2**).

In een reeks onderzoeken werd een systeem-farmacologie model voor de omzettingen van APP via verschillende routes in het APP netwerk opgesteld, op basis van farmacokinetische en farmacodynamische data in rhesusapen. Deze rhesusapen waren voorzien van een katheter in de cisterna magna, waardoor herhaalde afname van cerebrospinale vloeistof (CSV) mogelijk was. Allereerst werd een systeem-farmacologie model opgesteld voor de afbraak van AAP via de routes die leiden tot de vorming van de metabolieten (sAPPβ, sAPPα, Aβ40, Aβ42) na een enkele toediening van de BACE1 remmer MBi-5 (**Hoofdstuk 3**; β-APP model). Na remming van het enzym BACE1 werd een dosis-afhankelijke daling van de concentraties van de metabolieten Aβ40, Aβ42 en sAPPβ gevonden, terwijl de concentratie van sAPPα werd verhoogd. Op basis van het ontwikkelde model werd voorspeld dat na BACE1 remming er een daling is van de concentratie van Aβ_Os en voorts dat deze dissociëren waardoor de afname van Aβ monomeren gedeeltelijk wordt gecompenseerd. Dit werd indirect afgeleid op basis van de analyse van de verandering in de concentraties van de Aβ monomeren; Er waren ten tijde van dit onderzoek geen directe metingen van Aβ_O beschikbaar.

Bij klinisch onderzoek naar de werking van stoffen die een effect hebben op het APP netwerk, wordt vaak gebruik gemaakt van een stabiele-isotoop-techniek, waarbij na toediening van Leucine gemerkt met het stabiele isotoop ^{13}C de ^{13}C-gemerkte fracties Aβ worden bepaald, volgens het zogenaamde 'Stabel Isotope Labeling Kinetics (SILK)' protocol. In het onderzoek dat is beschreven in **Hoofdstuk 3** werden de gegevens verkregen met het SILK protocol (de fracties ^{13}C-gemerkte sAPPβ, sAPPα en Aβ) gecombineerd met de absolute eiwitconcentratie metingen (**Hoofdstuk 4**; β-13C-APP model). Hierdoor werd een beter inzicht verkregen van enerzijds het gebrek aan dosis-evenredigheid in het effect van de BACE1-remmer op de fractie gelabeld sAPPα en anderzijds de aanwezigheid van zo'n dosis-proportionele respons in absolute sAPPα concentratie metingen. Verder werd er een discrepantie gevonden tussen de Aβ reacties die werden gemeten met ELISA en SILK. Deze discrepantie wordt mogelijk veroorzaakt door de aanwezigheid van een onbekend APP fragment met verschillende kinetiek of door de aanwezigheid van een onbekend proces dat de meting van de fractie gelabeld Aβ beïnvloedt.

De volgende stap in de ontwikkeling van het model was gericht op de afzonderlijke beschrijving van de achtereenvolgende APP splitsingsstappen door BACE1 en GS. Hiertoe werd in het derde onderzoek het β-APP model uitgebreid met de beschrijving van de

effecten van GS remming op Aβ40 en Aβ42 (**Hoofdstuk 5**; β-γ-APP model). Deze analyse was gebaseerd op de combinatie van APP-metaboliet-respons gegevens uit studies voor de BACE1-inhibitor MBi-5 (1 studie; metingen van Aβ40, Aβ42, sAPPβ en sAPPα) en de GS-remmer MK-0752 (2 studies; metingen van Aβ40, Aβ42). De analyse liet zien dat er een verschil is in Aβ dynamiek na BACE1 versus GS remming. Dit kwam tot uitdrukking in een andere waarde van de vormings-snelheidsconstante van Aβ40. Bovendien werd op basis van het model een lagere Aβ oligomerisatie snelheid na remming van BACE1, in vergelijking met de remming van GS gevonden. Het was in dit onderzoek echter niet mogelijk om de waargenomen verschillen in Aβ dynamiek na remming van BACE1 en remming van GS van studieverschillen te onderscheiden. Daaropvolgend hebben we de voorspellingen van de Aβ_O respons na remming van BACE1 en remming van GS remming, zoals verkregen op basis van het β-APP model (**Hoofdstuk 3**) vergeleken met directe waarnemingen van de Aβ_O respons die zijn verkregen met behulp van een nieuwe analytische techniek. Hiertoe werden in een viervoudig volledig cross-over studie ontwerp de effecten van MBi-5 en MK-0752 op de CSV concentraties van vijf APP-metabolieten (sAPPβ, sAPPα, Aβ40, Aβ42, Aβ38) en Aβ_O bepaald. Met deze studiegegevens werd het APP-systeemmodel op de volgende wijze aangevuld: (1) het β-APP model werd uitgebreid om de vorming van de Aβ isoform Aβ38 te karakteriseren en de Aβ_O respons metingen in reactie op BACE1 remming te beschrijven (**Hoofdstuk 6**; β-O-APP model); (2) het β-O-APP model werd vervolgens nog verder ontwikkeld om de respons gegevens na GS remming te beschrijven (op basis van de sAPPα, sAPPβ, Aβ40, Aβ42, Aβ38, Aβ_O responsen) (**Hoofdstuk 7**; β-γ-O-APP model).

In **Hoofdstuk 6** wordt het vierde onderzoek beschreven. Hierin werd de relatie tussen de oligomeerpoel in het β-APP model en de metingen van Aβ_O onderzocht en de relatie tussen de Aβ monomeren (Aβ40, Aβ42, Aβ38) en Aβ_O gekwantificeerd. Aβ42 werd geïdentificeerd als de Aβvariant die de Aβ oligomerisatie aandrijft. Dit is in overeenstemming met de algemene veronderstelling dat Aβ42 de Aβ-variant is die gevoelig is voor toxische aggregatie.

Vervolgens bleek dat Aβ oligomerisatie verloopt volgens een tweede-orde kinetisch proces. Dit betekent dat bij het remmen van Aβ productie, een relatief grotere verandering van Aβ_O ten opzichte van de basislijn wordt verkregen in vergelijking tot monomeren Aβ varianten. De dissociatie van Aβ_Os, om het evenwicht te herstellen met Aβ monomeren (homeostatische aanpassing), draagt ook bij aan het uiteindelijke geneesmiddeleffect.

In het vijfde onderzoek (**Hoofdstuk 7**) werd het β-O-APP model uitgebreid om

Aβ_O responsmetingen na remming van respectievelijk BACE1- en remming van GS gelijktijdig te beschrijven. Hiertoe werden in het β-γ-O-APP model de opeenvolgende APP splitsingsstappen door BACE1 en GS gescheiden, vergelijkbaar met de implementatie in het β-γ-APP model. In deze analyse werd informatie over de sAPPβ, sAPPα, Aβ38 en Aβ_O respons op remming van GS toegevoegd. Verrassend was dat stroomopwaarts in de APP vanaf de GS-splitsingsstap veranderingen in de concentraties van sAPPβ en sAPPα in reactie op de remming van GS werden waargenomen. Dit leidde tot de identificatie van een homeostatische terugkoppelingsmechanisme dat gereguleerd wordt via C99: de toename van C99 na GS remming stimuleerde α-secretase verwerking van APP.

Voorts werd na remming van GS een andere verhouding Aβ42:Aβ40:Aβ38 gevonden dan na remming van BACE1. Dit kon worden verklaard door de stapsgewijze en opeenvolgende splitsing van C99 door GS, waarbij een deel van Aβ38 wordt gevormd vanuit Aβ42. Door de studies met de remmers van respectievelijk BACE1 en GS volgens een cross-over design uit te voeren, was het mogelijk de daadwerkelijke verschillen in het systeemgedrag in reactie op BACE1 versus GS remming aan te tonen. De lagere oligomerisatie snelheid na GS remming die werd gevonden in vergelijking met de remming van BACE1 waargenomen in de analyse op basis van van het β-γ-APP model, kan worden verklaard door de incorporatie van de stapsgewijze en opeenvolgende splitsing van C99 door GS. In deze analyse waren de waarden van de systeemparameters na BACE1 en GS remming identiek, wat suggereert dat een fysiologisch correcte beschrijving van de processen in het APP biologische netwerk is verkregen.

Concluderend is er een systeem-farmacologie model van de APP verwerkings- en klaringsroutes ontwikkeld. Dit model levert belangrijke kwantitatieve informatie over de routes van de verwerking van APP: (i) Aβ-oligomerisatie is een tweede-orde proces; (ii) Aβ_O dissociëren om het evenwicht te herstellen met Aβ monomeren, wat het uiteindelijke geneesmiddeleneffect beïnvloedt; (iii) Aβ42 is de enige belangrijke Aβ monomeren variant die bijdraagt aan de oligomeerpoel; (iv) remming van GS stimuleert de niet-amyloidogene verwerking van APP door homeostatische terugkoppeling die door C99 wordt uitgeoefend.

Een belangrijke vraag is hoe het model van de APP-paden in rhesusapen aangepast moet worden, om de effecten van geneesmiddelen op de APP-paden in de mens op een kwantitatieve manier te voorspellen. In het laatste hoofdstuk van dit proefschrift (**Hoofdstuk 8**) werden enkele voorlopige resultaten van de vertaling van rhesusapen naar mensen van de effecten van de remming van BACE1 gepresenteerd. Om het β-γ-O-APP model van rhesusapen te vertalen naar de mens werd verondersteld dat de

waarden van de systeemparameters in rhesusapen en mensen identiek zijn. Verder werd de vertraging tussen de cisterna magna en de lumbale regio, waar CSV gemeten wordt in mensen, beschreven door een reeks transitcompartimenten. De respons van Aβ40, Aβ42 en sAPPβ na een enkele dosis van de BACE1 remmer verubecestat (MK8931) bij gezonde vrijwilligers werd goed door het model voorspeld. Het model voorspelde na toediening van een enkele dosis van 100 mg dosis verubecestat een afname van 84% in de Aβ_O concentratie in de lumbale CSV bij de mens en een afname van 94% na herhaalde toediening gedurende 7 dagen in een dosering van 40 -150 mg.

Het APP-systeem-farmacologie model in rhesusapen kan op meerdere manieren van waarde zijn bij het ontwerpen en ontwikkelen van therapeutische interventies voor de ZvA, zoals werd besproken in **Hoofdstuk 8**. Ten eerste kan het model gebruikt worden om het SILK protocol te optimaliseren, met name met het oog op de beste timing van de $^{13}C_6$-Leucine infusie voor een eindpunt dat het dichtst bij het doel Aβ_O ligt. Daarbij is vooral het tijdstip van de toediening van de $^{13}C_6$-Leucine infusie ten opzichte van de toediening van het te onderzoeken farmacon van belang. Simulaties lieten zien dat de $^{13}C_6$-Leucine infusie het beste direct na de te onderzoeken stof kan worden toegediend.

Ten tweede kan het model worden gebruikt om een diagnostische test te ontwikkelen, vergelijkbaar met de glucosetolerantietest bij type 2 diabetes mellitus, met als doel in een vroeg stadium de ziekte van Alzheimer vast te stellen. Ten aanzien van de APP-paden kan het systeem dan worden geprikkeld door toediening van een secretase-remmer. Het model kan gebruikt worden om een dergelijke test te optimaliseren en systeemparameters te onderzoeken die kunnen dienen als nieuwe biomarkers, indicatief voor de ernst van de ziekte en eventueel voorspellend voor de behandelingsrespons op APP-modulerende geneesmiddelen.

Ten derde kan het model worden gebruikt in de ontwikkeling van op de individu-ele patiënt toegesneden behandeling. De genetische heterogeniteit van de ZvA is hoog. Afhankelijk van het genotype kan de reactie op potentieel ziekte modificerende therapeu-tica, zoals secretase-remmers verschillend zijn. De genetische informatie geeft mogelijk aanwijzingen welke systeemparameters aangepast moeten worden om de staat van de ziekte en op de individuele patient toegesneden interventies gericht op de APP-paden te beschrijven.

Ten vierde vormt het APP-systeem model de basis voor een ziekte-systeem anal-yse model van de ZvA, om ziekteprogressie en lange termijn behandelingseffecten te voorspellen. Hiertoe kan het model uitgebreid worden om ook de effecten op latere stroomafwaartse biomarkers te includeren, zoals amyloïd-PET, CSF-tau en biomarkers

voor neurodegeneratie als FDG-PET en MRI, alsmede gedrags-eindpunten (d.w.z. schaal-waarden zoals de ADAS-Cog score). Hierbij moet rekening gehouden worden met de correlaties tussen deze biomarkers, waarvoor longitudinale data in dezelfde individuen nodig zijn. Dergelijke data is momenteel zeldzaam.

Ten slotte, kan het β-γ-O-APP model gebruikt worden om simulaties uit te voeren om interventies te onderzoeken die gericht zijn op de APP-paden. Tot nog toe konden klinische studies van Aβ productie-remmers (d.w.z. BACE1 en GS remmers) geen klinische werkzaamheid aantonen bij getolereerde doses in patiënten. Er zijn verschillende mogelijke verklaringen voor het gebrek aan werkzaamheid. Hierbij is een belangrijke vraag of de doelstelling zoals weerspiegeld in de blootstelling aan Aβ_O is bereikt.

Het β-γ-O-APP model zou gebruikt kunnen worden om dit te voorspellen. Ook biedt het β-γ-O-APP model de mogelijkheid om de netto reacties van het systeem op gecombi-neerde interventies gericht op verschillende doelen in de APP-paden te onderzoeken. Een veelbelovende strategie lijkt de preventie van toxische effecten, door het voorkomen van de interacties van giftige Aβ_Os met doelreceptoren. Voor een effectieve onderdrukking van de Aβ_O concentraties en de toxische effecten is het waarschijnlijk noodzakelijk is om rationele combinaties van geneesmiddelen te gebruiken die zich op meerdere doelen in het systeem richten. Zodra het β-γ-O-APP model wordt uitgebreid met een receptor-interactie modelcomponent voor Aβ_O-receptor interacties, kan de gecombineerde interventie van een Aβ productie-remmer en preventie van de interactie van Aβ_Os met het receptor doelwit worden onderzocht, zodat therapie kan worden geoptimaliseerd.

Het APP-systeem-farmacologie model kan het optimaliseren van de therapeutische interventie om de oligomeer-last in de ZvA te verlagen dichterbij brengen. Dit proef-schrift illustreerde dat systeem-farmacologie modelering een krachtige aanpak is in de geïntegreerde analyse van biologie en farmacologie om systeem-geneesmiddel interacties te beoordelen. Vanwege een algemeen pathologisch principe kan deze benadering ook worden gebruikt voor andere eiwit-misvouwings gerelateerde neurodegeneratieve ziekten zoals ZvP, ZvH en ALS.

Nawoord

Als buitenpromovendus heb ik de afgelopen 4,5 jaar naast mijn werk bij LAP&P aan dit promotieonderzoek gewerkt. In dit nawoord wil ik iedereen bedanken die mij heeft gesteund en een bijdrage heeft geleverd in de totstandkoming van dit proefschrift.

Allereerst wil ik Merck (Whitehouse Station, NJ) bedanken voor de samenwerking. Julie Stone, I want to thank you for your cooperation, advice and insights throughout my work. I'm grateful to Mary Savage and Juliya Kalinina for giving me the opportunity to work with the oligomer data. It was of great value in taking the model one step further. My sincere appreciation to Matt Kennedy and Eric Parker for their critical comments on my manuscripts. Maria Michener, thank you for showing me the rhesus monkeys. It is good to know where the data is coming from.

Mijn co-promotor, Tamara, bedankt dat je je kennis en ervaring met me hebt gedeeld. Ik hoop nog veel met je te mogen samenwerken.

Henk-Jan, ik wil je graag bedanken voor de kans die ik bij LAP&P heb gekregen om dit onderzoek uit te voeren en mijn proefschrift te schrijven. Bedankt voor het vertrouwen.

Ik wil mijn collega's van LAP&P bedanken voor de getoonde interesse gedurende de afgelopen jaren. Joost, bedankt voor je feedback en de fijne gesprekken. Diana, bedankt voor je bijdrage aan het datamanagement.

Beste mamma, jij en pappa hebben me de mogelijkheden geboden om mijn eigen weg te gaan. En dan ligt er nu dit proefschrift. Ik weet dat pappa heel trots zou zijn.

Arnold, wij ondervonden dat het leven niet te plannen valt. Met de komst van Annemijn, ben jij een dag minder gaan werken, zodat ik door kon gaan. Lieve Arnold, heel veel dank voor je steun.

Promoveren naast het werk met een klein kind thuis was niet gelukt zonder de ondersteuning van de oppasoma's en de oppasopa; veel dank!

Annemijn, jouw glimlach is voor mij een bron van relativering en inspiratie. Mijn 'Boek' is nu af.

Op naar nieuwe uitdagingen!

Eline

List of Publications

van Maanen, E.M.T., van Steeg, T.J., Ahsman, M.J., Michener, M.S., Savage, M.J., Kennedy, M.E., Kleijn, H.J., Stone, J.A., Danhof, M. (2017). Extending a systems model of the APP pathway: Separation of β- and γ-secretase sequential cleavage steps of APP. *Submitted to JPET.*

van Maanen, E.M.T., van Steeg, T.J., Michener, M.S., Savage, M.J., Kennedy, M.E., Kleijn, H. J., Danhof, M. (2016). Systems Pharmacology Analysis of the Amyloid Cascade after β-Secretase Inhibition Enables the Identification of an Aβ42 Oligomer Pool. The Journal of Pharmacology and Experimental Therapeutics, 357(1), 205–16.

Datson N.A., Polman J.A., de Jonge R.T., van Boheemen P.T., **van Maanen E.M.T.**, Welten J., McEwen B.S., Meiland H.C., Meijer O.C.. Specific regulatory motifs predict glucocorticoid responsiveness of hippocampal gene expression. Endocrinology. 2011 Oct;152(10):3749-57.

Curriculum Vitae

Eline van Maanen was born in Hoogezand on April 27, 1978. In 1997 she obtained her "VWO" diploma at the OSG Nieuwediep in Den Helder. In 1998 she began to study Industrial Design Engineering at the Delft University of Technology. In 2002 she moved to study Life Science & Technology at the Delft University of Technology and Leiden University. During her masters, she performed her research internship at the Department of Medical Pharmacology at the Leiden/Amsterdam Center for Drug Research at Leiden University under the guidance of Dr. Onno Meijer. Her work was nominated for the S.E. de Jongh award. She did her masters business internship at LAP&P Consultants BV in Leiden. In 2008 she obtained her M.Sc. degree with the laureate *"cum laude"* (with honour) and the same year she joined LAP&P Consultants BV as a consultant. Besides the commercial work there, she started her PhD in 2013 under the guidance of Prof. Dr. M. Danhof (promoter), Dr. T.J. van Steeg (co-promoter) and Julie Stone (co-promoter). In 2013 she was invited to present her work in the session *"Can Systems Pharmacology Provide a Way Forward in the Search for Novel Treatments in Alzheimer's Disease?"* during the ACOP to Fort Lauderdale (USA) and in 2016 at the Computation Hub fall meeting (Leiden). Currently, she is working as a consultant at LAP&P Consultants BV.

Curriculum Vitae

Eline van Maanen werd op 27 april 1978 geboren te Hoogezand-Sappemeer. In 1997 behaalde zij het diploma VWO aan de OSG Nieuwediep te Den Helder. In 1998 begon zij aan de studie Industrieel Ontwerpen aan de Technische Universiteit Delft. In 2002 maakte zij de overstap naar de studie Life Science & Technology aan de Technische Universiteit Delft en Universiteit Leiden. In de master fase heeft zij haar onderzoeksstage gedaan bij de afdeling Medische Pharmacology van het Leiden/Amsterdam Center for Drug Research aan de Universiteit Leiden onder begeleiding van Dr. Onno Meijer. Haar werk was genomineerd voor de S.E. de Jongh-prijs. Haar master bedrijfsstage heeft zij gedaan bij LAP&P Consultants BV in Leiden. In 2008 haalde zij haar Master met het predikaat *cum laude* en in hetzelfde jaar begon zij als consultant bij LAP&P Consultants BV. Naast het commerciele werk daar, begon zij haar promotieonderzoek in 2013 onder begeleiding van Prof. Dr. M. Danhof (promotor), Dr. T.J. van Steeg (co-promotor) en Julie Stone (co-promotor). In 2013 werd zij uitgenodigd om haar werk te presenteren in de sessie *"Kan systeem farmacologie een weg voorwaarts bieden in het zoeken naar nieuwe behandelingen van de ziekte van Alzheimer?"* tijdens de ACoP te Fort Lauderdale (VS) en in 2016 tijdens de Computation Hub fall meeting (Leiden). Op dit moment is zij werkzaam als consultant bij LAP&P Consultants BV.

Abbreviations

$A\beta$	amyloid-β
$A\beta_O$	amyloid-β oligomer
AD	Alzheimer's Disease
ALPH	power of $A\beta42$ concentration
APP	β-amyloid precursor protein
BACE1	β-secretase
CI	confidence interval
CMP	cisterna magna ported
CSF	cerebrospinal fluid
C_{target}	drug concentration target site
C83	C-terminal membrane-bound 83-amino acid fragment
C99	C-terminal membrane-bound 99-amino acid fragment
ELISA	enzyme-linked immunosorbent assay
FAC	scale correction factor
FB	feedback parameter
GS	γ-secretase
IC_{50}	median inhibition concentration
Imax	maximum inhibition
Kin_{38}	$A\beta38$ formation rate constant
Kin_{382}	$A\beta38$ formation rate constant from $A\beta42$
Kin_{40}	$A\beta40$ formation rate constant
Kin_{42}	$A\beta42$ formation rate constant
Kout	$A\beta$ degradation rate constant
$Kout_{99}$	C99 degradation rate constant
Kpl	(second order) oligomerization rate constant
KtAB	transit rate constant $A\beta$ from brain to CSF
KtAP	transit rate constant sAPPα and sAPPβ from brain to CSF
Krev	$A\beta_O$ dissociation rate constant
LC-MS/MS	liquid chromatography tandem mass spectrometry
MTT	mean transit time
MW	molecular weight
PK	pharmacokinetic
PD	pharmacodynamic
RinAPP	zero order input rate constant for APP
Rinα	sAPPα formation rate constant
Rinβ	sAPPβ formation rate constant
Rout	sAPPβ degradation rate constant
Routa	sAPPα degradation rate constant
Routb	sAPPβ degradation rate constant
sAPPα	soluble APP alpha
sAPPβ	soluble APP beta
SILK	stable isotope labelling kinetics
TTR	tracer to tracee ratio
$^{12}C_6$-L	endogenous $^{12}C_6$ Leucine
$^{13}C_6$-L	$^{13}C_6$-labelled Leucine